AEROSOL FORMATION AND GROWTH IN LAMINAR FLOW

Thesis by

Andrew John Pesthy

In Partial Fulfillment of the Requirements

for the Degree of

Doctor of Philosophy

California Institute of Technology

Pasadena, California

1983

(Submitted April 16, 1982)

ACKNOWLEDGEMENT

I would like to thank Professors John H. Seinfeld and Richard C. Flagan for their patient guidance and valuable assistance. Much appreciation goes to Elton F. Daly for constructing experimental equipment, and to Concetto Geremia for his help in the laboratory project.

I express my special gratitude to Lenore Kerner who prepared the beautiful pages of text and to Phillip Dubé, Theresa Fall and to Wendy All for the many illustrations.

CONTENTS

Abstract		viii
Chapter 1.	Introduction	1
Chapter 2.	Relevance	2
Chapter 3.	Theory of the Laminar Flow Aerosol Generator	5
Chapter 4.	Experimental Apparatus and Technique	59
Chapter 5.	Experimental Results	71
Chapter 6.	Discussion and Conclusions	82
Appendix A.	Buoyancy Effects on the Velocity Profile	85
Appendix B.	The Effect of Coagulation	88
Appendix C.	The Role of the Kelvin Effect	90
Appendix D.	Particle Mass Flux Expression	92
Appendix E.	The Effect of Thermal Diffusion	95
Appendix F.	Fortran Source Code and Sample Output	99
Appendix G.	The Effect of a Growing Aerosol on the Rate of Homogeneous Nucleation of a Vapor	131
Symbols Used		147
References		152

LIST OF TABLES

Table 1.	Summary of Work on Aerosol Formation and Growth in Flowing Systems	3
Table 2.	Comparison of Classical and Lothe-Pound Theories of Homogeneous Nucleation	16
Table 3.	Numerical Comparison of Nucleation Rates Predicted for Dibutyl Phthalate by the Classical and Lothe-Pound Theories	17
Table 4.	Simulated Operating Conditions for the Cooled Laminar Flow Tube	28
Table 5.	Evaporator Outlet Concentrations	65
Table B.1.	Limiting Number Density at Several Radial Positions	89
Table C.1	Transition Diameter for the Kelvin Effect	91
Table E.1	Thermal Diffusion Coefficient for Dibutyl Phthalate in Air	98

LIST OF FIGURES

Figure 1. Schematic diagram of cooling section. Gas temperature and vapor mole fraction are uniform at z = 0. 6

Figure 2. Nucleation rate function and vapor mole fraction profiles in the vicinity of a growing aerosol particle, exaggerated for illustration. 19

Figure 3. Dimensionless temperature profile. Wall temperature profile is a linear transition as depicted in the inset. 29

Figure 4. Streamline trajectories in vapor composition-temperature profile without nucleation. Isopleths of critical nucleation rate indicated for the Lothe-Pound and classical nucleation theories. 30

Figure 5. Theoretical vapor mole fraction profiles for cooling section with classical nucleation theory, no seed aerosol. 32

Figure 6. Aerosol volume fraction predicted by classical nucleation theory, without seed aerosol. 33

Figure 7. Cup-mixed average aerosol volume distribution predicted by classical nucleation theory, without seed aerosol. Area under the curves is total aerosol volume. 35

Figure 8. Vapor mole fraction profiles predicted with Lothe-Pound theory, with initial seed aerosol concentrations of 0 and 10^8 cm^{-3}. $T_0' = 150°C$, $T_{Wf}' = 25°C$, $x_0 = 10^{-4}$. 37

Figure 9. Radial profiles of homogeneous nucleation rate predicted by Lothe-Pound theory, with initial seed aerosol concentrations of 0 and 10^8 cm^{-3}. Same conditions as in Figure 8. 38

Figure 10. Radial profiles of volume fraction for homogeneous aerosol predicted by Lothe-Pound theory with no seed aerosol. Same conditions as in Figure 8. 40

Figure 11. Radial profiles of volume fraction for homogeneous and seeded aerosol predicted by Lothe-Pound theory. Same conditions as in Figure 8. 41

Figure 12. Cup-mixed average aerosol volume distributions predicted by Lothe-Pound theory for initial seed aerosol concentrations of 0, 10^7 and 10^8 cm^{-3}. Seed aerosol is illustrated by the truncated peaks near $d_p = 0.3$ μm. Same conditions as in Figure 8. 43

Figure 13. Vapor sink function predicted by Lothe-Pound theory with no seed aerosol. Same conditions as in Figure 8. 44

Figure 14. Vapor sink function predicted by Lothe-Pound theory with initial seed aerosol concentration of 10^7 cm^{-3}. Same conditions as in Figure 8. 45

Figure 15. Vapor sink function predicted by Lothe-Pound theory with initial seed aerosol concentration of 10^8 cm^{-3}. Same conditions as in Figure 8. 46

Figure 16. Homogeneous nucleation function predicted by Lothe-Pound theory for several values of inlet temperature. $x_o = 10^{-4}$, and dewpoint is 101°C. 48

Figure 17. Overall mass balance on condensing species and aerosol volume fraction predicted with Lothe-Pound theory as a function of inlet temperature with no seed aerosol. Same conditions as in Figure 16. 49

Figure 18. Cup-mixed average total number concentration of homogeneous aerosol predicted with Lothe-Pound theory with no seed aerosol. Dashed line shows average neglecting wall layer of aerosol, $r > 0.9$. Same conditions as in Figure 16. 50

Figure 19. Cup-mixed number average homogeneous aerosol diameter predicted with Lothe-Pound theory with no seed aerosol. Dashed line shows average neglecting wall layer of aerosol, $r > 0.9$. Same conditions as in Figure 16. 51

Figure 20. Vapor mole fraction profiles without seed aerosol predicted with Lothe-Pound nucleation theory for several initial values of mole fraction. $T_o' = 150°C$. 53

Figure 21. Profiles of homogeneous nucleation rate predicted by Lothe-Pound theory without seed aerosol, for several values of initial mole fraction. Same conditions as in Figure 20. 54

Figure 22. Cup-mixed average homogeneous aerosol number concentration without seed aerosol, predicted by Lothe-Pound theory. Same conditions as in Figure 20. 56

Figure 23. Cup-mixed average homogeneous aerosol volume distributions for several values of initial mole fraction, with no seed aerosol. Diameter of critical nucleus is indicated. Same conditions as in Figure 20. 57

Figure 24. Overall mass balance on condensing species for Lothe-Pound theory, with no seed aerosol. Same conditions as in Figure 20. 58

Figure 25. Schematic diagram of experimental apparatus. 60

Figure 26. Detail of hot zone, depicted without thermal insulation. 61

Figure 27. Detail of cool zone. 63

Figure 28. Typical wall temperature profiles. 66

Figure 29. Fifty percent cutoff diameters for the Sierra impactor. 68

Figure 30a. Cumulative particle volume distributions from Sierra impactor data at four flow rates specified. Flow rate before dilution was 1.5 ℓ/min, $T_o' = 189°C$, and $x_o = 9.35 \times 10^{-5}$. 69

Figure 30b. Particle volume distribution from cumulative distribution of (a). 69

Figure 31. Measured particle volume distributions at several initial temperatures. Flow rate before dilution was 2.9 ℓ/min, $x_o = 9.1 \times 10^{-5}$ and impactor flow rates were 1.4, 2.0, 2.8 and 4.0 ℓ/min. 72

Figure 32. Number average particle diameter from ——theory, and - - - Sierra impactor data. 73

Figure 33. Average total aerosol volume fraction from theory and Sierra impactor data. — — — Maximum, corresponding to initial vapor, ——theory, ◬ data of Figure 32 and ⊙ other data. 75

Figure 34. Theoretical profiles of uncondensed vapor in the experimental apparatus. For the indicated values of T_o', isopleths are given for $x = 0.10x_o$. 76

Figure 35. Average particle volume distributions from Sierra impactor data at several initial vapor mole fractions. 78

Figure 36. Dibutyl phthalate mass balance from theory and Sierra impactor data, $T_o' = 192°C$. 79

Figure 37. Dependence of aerosol volume fraction on flow rate. Flow rates before dilution: ——— 2.9 ℓ/min, - - - 1.5 ℓ/min, ----- 1.5 ℓ/min. 80

Figure A.1. Velocity profile in cooled tube. Profiles are shown for: — — — No buoyancy forces, and ———Buoyancy induced by temperature profile of $T = 1-r^2$ with $T_o' = 150°C$, $T_{wf}' = 25°C$, flow rate = 3 ℓ/min and $Gr/Re \cong 243$. 87

Figure D.1. Particle growth mass flux for dibutyl phthalate at 125°C normalized by flux obtained from kinetic theory. Shown are: ——— Modified Sitarski-Nowakowski expression with $\lambda = 1.18 \times 10^{-2}$ μm (Eq. [D.4]), and — — — Fuchs-Sutugin interpolation formula with $\lambda = 5.04 \times 10^{-2}$ μm (Eq. [D.6]) 94

Abstract

A detailed theoretical analysis of aerosol nucleation and growth in laminar flow, including the important aspects of mass and energy transfer and aerosol size distribution dynamics, is presented. Simulations of dibutyl phthalate aerosol formation and growth in a laminar flow cooled tube, in the presence and absence of seed particles, are carried out using the classical and Lothe-Pound theories of homogeneous nucleation. The competition between new particle formation and vapor growth onto seed particles is explored in detail. The mathematical model is compared to experimental measurements of aerosol volume distribution and dibutyl phthalate mass balance for a laminar flow cooled tube without seed particles. The model with Lothe-Pound theory shows fair agreement with the mass balance data, but overpredicts the total aerosol number concentration by four orders of magnitude.

Chapter 1

INTRODUCTION

Aerosol formation and growth in laminar flow is studied theoretically and experimentally in a setting closely resembling the classic Graetz problem. The specific problem treated here is related in Chapter 2 to the general problem of aerosol formation and growth in flowing systems. This work studies cooling-induced aerosol formation and growth in a well characterized parabolic pipe flow with specified wall temperature. In Chapter 3, the theory of the laminar tube flow aerosol generator is developed and the numerical model is used to examine the detailed operational characteristics of one such device. In this device, described in Chapter 4, dilute dibutyl phthalate in air is cooled to supersaturation, without seed particles, creating aerosol by homogeneous nucleation and growth. Although not applicable to the experiment, the model can incorporate the presence of foreign seed particles, monomer source by chemical reaction, and effects of latent heating from condensational particle growth. The model is also easily adapted to other geometries and flow velocity profiles. The experimental results are compared to the model predictions in Chapter 5. Chapter 6 discusses the results in detail and offers suggestions for future work.

Chapter 2

RELEVANCE

Understanding the fundamental mechanisms of aerosol nucleation and growth has long been a central problem in aerosol science. Such understanding has important implications in characterizing and controlling fine particle emissions from combustion systems and in elucidating the dynamic processes governing the formation and growth of atmospheric aerosols. In simulating atmospheric aerosol dynamics, for example, it is desired to predict the rate of new particle formation as a function of the rate of generation of condensable vapor by gas phase chemical reactions. Predicting rates of new particle formation in the atmosphere requires consideration of the effect of both preexisting particles and newly formed growing particles on the vapor and cluster concentrations in the system (1-4).

Simultaneous homogeneous nucleation and heterogeneous condensation can be conveniently studied in a laminar tube flow in which an inert carrier gas containing a condensable vapor with or without seed particles is rapidly cooled. Numerous studies of aerosol formation in steady tube flow have been carried out (Table 1). Most of the investigations have been directed towards producing an aerosol of minimal polydispersity. The designs of the devices, generally incorporate a feed of foreign nuclei, with conditions chosen to minimize the occurrence of homogeneous nucleation. Although not shown in Table 1, the continuous flow condensation nuclei counter has many characteristics similar to the laminar flow aerosol generators.

The object of this work is to provide a detailed theoretical analysis of aerosol nucleation and growth in laminar flow, including the important aspects of mass and energy transfer and aerosol size distribution dynamics. The analysis will enable the prediction of the aerosol size distributions obtained in such devices as a function of wall cooling rates, inlet conditions, and the presence or absence of a seed aerosol.

Table 1. Summary of Work on Aerosol Formation and Growth in Flowing Systems

Investigator	System Studied	Results
La Mer et al. (5)	Heated dibutyl phthalate vapors with or without foreign nuclei were sent up a cooled chimney where aerosol formed.	Production of monodisperse aerosol (diam. < 0.01 to 0.15 μm). Condensational growth to five times initial size could be controlled quantitatively, permitting accurate measurement of small aerosols. H_2SO_4 is not preferred for this.
Matijević et al. (6)	Heated linolenic acid vapors were condensed on AgCl nuclei.	Self-nucleated aerosols were more polydisperse than foreign-nucleated aerosols.
Matijević et al. (7)	Heated octanoic acid vapors were condensed on AgCl nuclei, although aerosols could be generated without such foreign nuclei.	Used light scattering methods to determine flow rate-output relationships of the aerosol generator.
Okada et al. (8)	Heated dioctyl phthalate vapors condensed on spark-produced gold nuclei in an air-cooled chimney.	Generated aerosol with diam. ∿ 0.3 - 1 μm with logarithmic standard deviation of 0.08 - 0.12 μm.
Huang et al. (9)	Linolenic acid vapors in helium condensed on AgCl or NaCl nuclei.	Demonstrated stable aerosol generator.
Nicolaon et al. (11-13)	Dibutyl phthalate vaporized in a tube coated by a falling film of DBP. AgCl or NaCl nuclei-laden helium was the carrier medium. Nucleation occurred in an air-cooled tube.	Measurement of generated aerosol distribution by light scattering.

Table 1. Summary of Work on Aerosol Formation and Growth in Flowing Systems (Continued)

Investigator	System Studied	Results
Shahriari and Goodrich (10)	Dibutyl phthalate vaporized in a tube coated by DBP-soaked blotter paper. NaCl nuclei-laden nitrogen was the carrier gas. Nucleation occurred after a reheater section in a freely exposed jet.	Growth kinetics were explained by a kinetic theory collision hypothesis and diffusion hypothesis. The accommodation coefficient was unity.
Nicolaon and Kerker (14)	Same system as Nicolaon et al. (11-13), but with a heated intermediate temperature zone during cooling.	Characterization of aerosol generator.
Davis and Liao (15)	Modified Sinclair-La Mer generated with seeded dibutyl phthalate particles in downward flow. Theoretical treatment neglected vapor losses to the wall.	For nuclei concentrations of 1.2×10^7 cm^{-3}, an aerosol of approximately 0.3 μm diameter was predicted.
Chang and Davis (16)	Atomization of 10% emulsion of dioctyl phthalate in water flowed to a storage flask.	Showed ability to measure droplet sizes by light scattering.
Carroz et al. (17)	Nitrates of Al, Fe, Cr, Mg, Zn, and Cd, and $(CH_3)_2Si(OC_2H_5)_2$ and $VOSO_4$ were dissolved in flammable solvent (ethanol, methanol) and burned.	Measured aerosol with Whitby and Royco aerosol analyzers, and electron microscope photographic analysis.

Chapter 3

THEORY OF THE LAMINAR FLOW AEROSOL GENERATOR

A schematic diagram of the laminar flow aerosol generator is shown in Figure 1. The mathematical model describing the system is based on the appropriate steady state mass, energy, and momentum conservation laws. It is assumed that the formation and growth of aerosol does not disturb the laminar velocity profile of the gas.

3.1 Governing Equaitions

The velocity profile is obtained from solving the Navier-Stokes equation, the applicable form of which is

$$0 = -\frac{\partial p'}{\partial z'} + \frac{1}{r'}\frac{\partial}{\partial r'}\left(r'\mu\frac{\partial v_z}{\partial r'}\right) + g\left(\frac{\partial \rho_g}{\partial T'}\right)_{p'}(T' - \overline{T}') \qquad [1]$$

where the viscosity μ is, in general, a function of radial position r' due to its temperature dependence. For cooled gas flow downward, the viscosity reduction near the wall and buoyancy forces produce an effect of flattening the velocity profile as compared to the standard parabolic profile with constant temperature. A sample velocity profile is calculated in Appendix A. This deviation from the parabolic velocity profile is not expected to cause significant changes in the aerosol production because the aerosol formation and growth time constants are very much smaller than those associated with the flow relaxation. Consequently, we assume the gas velocity profile is parabolic. The relationship between axial position and effective residence time along a streamline is simply

$$t' = \frac{z'}{v_z(r')} \qquad [2]$$

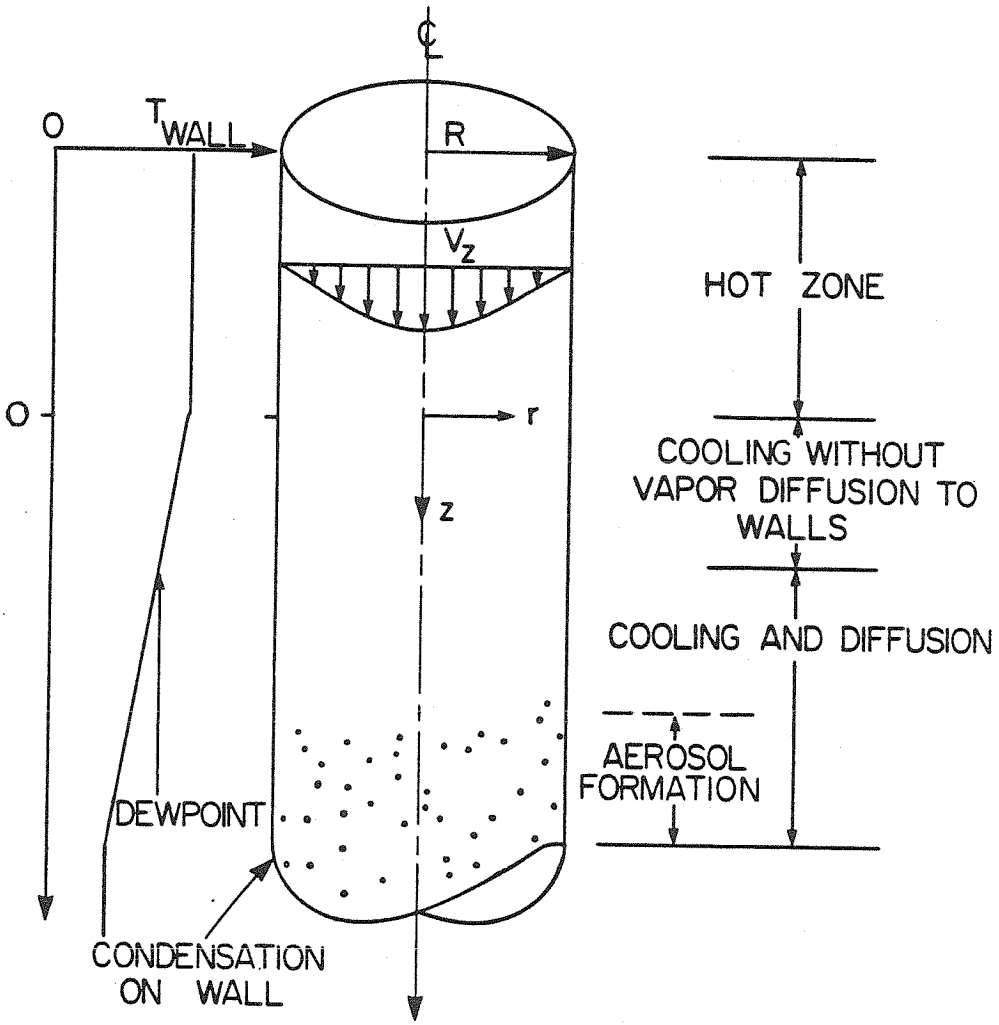

Figure 1. Schematic diagram of cooling section. Gas temperature and vapor mole fraction are uniform at z = 0.

The energy and vapor conservation equations are

$$v_z(r') \frac{\partial T'}{\partial z'} - \frac{\alpha}{r'} \frac{\partial}{\partial r'} \left(r' \frac{\partial T'}{\partial r'} \right) = \left(\frac{\Delta H_v}{C_p} \right) S_v(r',z') \qquad [3]$$

$$v_z(r') \frac{\partial x}{\partial z'} - \frac{D}{r'} \frac{\partial}{\partial r'} \left(r' \frac{\partial x}{\partial r'} \right) = - S_v(r',z') \qquad [4]$$

where physical properties have been assumed constant at their values at ambient temperature and pressure and where the rate of loss of vapor to aerosol formation and growth is represented as a homogeneous sink in Eq. [4] of magnitude $S_v(r',z')$. Axial conduction and diffusion have been neglected, an assumption which is valid when Péclet numbers for both transport processes are much greater than unity.

Boundary conditions for Eqs. [3] and [4] are

$$T'(r',0) = T'_o \qquad [5]$$

$$x(r',0) = x_o \qquad [6]$$

$$T'(R,z') = T'_w(z') \qquad [7]$$

$$x(R,z') = \min \{x_o, x^{sat}(T'_w(z'))\} \qquad [8]$$

$$\frac{\partial T'}{\partial r'} = 0 \qquad r' = 0 \qquad [9]$$

$$\frac{\partial x}{\partial r'} = 0 \qquad r' = 0 \qquad [10]$$

where T'_o is the gas temperature at the entrance to the cooled section, x_o is the mole fraction of vapor in the entering gas, $T'_w(z')$ is the wall temperature, and x^{sat} is the saturation vapor mole fraction.

The aerosol phase is described by a general dynamic equation for size distribution along each laminar streamline assuming no Brownian diffusion of particles. Aerosol coagulation has been neglected; this assumption is not always valid but the effect of coagulation may be estimated later (Appendix B). The aerosol phase is represented by the size distribution function $n'(v',r',z')$,

defined such that n'dv' is the number of particles in the particle volume range [v',v'+dv'] at position (r',z'). The aerosol volume fraction ϕ' is related to the size distribution function by

$$\phi' = \int_{v'^*}^{\infty} v'n' \, dv' \qquad [11]$$

where v'* is the volume of the critical nucleus.

Considering nucleation and growth processes only, and representing residence time along a streamline by Eq. [2], the population balance on a streamline leads to

$$\frac{\partial n'}{\partial t'} + \frac{\partial}{\partial v'}(n' \, I) = J'\delta(v'-v'^*) \qquad [12]$$

where J' is the rate of homogeneous nucleation, and I(v',t') = dv'/dt', is the rate of change of the volume of a particle of volume v' by vapor condensation, the so-called growth law. The initial condition for Eq. [12] is

$$n'(v',0) = N_s'\delta(v'-v_s'^*) \qquad [13]$$

where N_s' is the number density of seed aerosol of volume $v_s'^*$. For conditions of pure gas feed, $N_s' = 0$. The boundary value of the size distribution function at v'=v'* is derived from Eq. [12], assuming that no particles exist smaller than v'*. Integrating Eq. [12] from v' = 0 to v' = v'*+dv', and assuming n'(v') = 0 for v' < v'*,

$$\frac{\partial}{\partial t'} \int_0^{v'^*+dv'} n' \, dv' + n'(v'^*+dv',t')I(v'^*+dv',t') = J'(t') \qquad [14]$$

The first term of Eq. [14] is the time rate of change of the differential number of particles in the size range [v'*,v'*+dv']. This term is well behaved and

goes to zero as we take the limit $dv' \to 0$, giving the boundary condition for n',

$$n'(v'^*,t') = \frac{J'(t')}{I(v'^*,t')} \qquad [15]$$

Assuming that the Kelvin effect is negligible (Appendix C), the steady state growth law I(v',t') along a streamline is expressible as a separable function,

$$\frac{dv'}{dt'} = \theta(t')\nu(v') \qquad [16]$$

where the function $\theta(t')$ describes the diffusional driving forces, and $\nu(v')$ relates growth rate to size.

Specification of the right-hand side of Eq. [16] requires a general expression for the mass flux of vapor molecules to a particle of volume v' over the range of particle sizes from the free molecule to continuum regimes. The mass flux expressions considered in this work are discussed in Appendix D. The specific form of Eq. [16] employed is

$$\frac{dv'}{dt'} = 2\pi D\lambda \frac{c}{c_d} (x-x^{sat})Kn^{-1}F(Kn) \qquad [17]$$

where the Knudsen number $Kn = 2\lambda/d_p$ is related to particle volume by $v' = (4\pi/3)\lambda^3 Kn^{-3}$ and F(Kn) is defined in Appendix D.

3.2 Dimensionless Form

To place the foregoing equations in dimensionless form we define

$$T = \frac{T'-T'_{w_f}}{T'_o-T'_{w_f}} \qquad T_w = \frac{T'_w-T'_{w_f}}{T'_o-T'_{w_f}}$$

$$X = \frac{x-x_{w_f}}{x_o-x_{w_f}} \qquad X^{sat} = \frac{x^{sat}-x_{w_f}}{x_o-x_{w_f}}$$

$$t = \frac{Dt'}{R^2} \qquad r = r'/R \qquad Le = \frac{\alpha}{D} \qquad z = \frac{z'}{R}(Pe)^{-1}$$

$$\Phi = \frac{R^2}{D} \frac{1}{x_o-x_{w_f}} S_v$$

$$\beta = \frac{\Delta H_v}{C_p}\left(\frac{x_o - x_{w_f}}{T'_o - T'_{w_f}}\right)$$

$$\gamma = 10^{-4}\,\frac{\lambda}{R}\ \text{cm}\ \mu\text{m}^{-1}$$

$$J = \frac{\gamma R^5}{D} J'$$

$$n = \gamma\lambda^3 R^3 n'$$

$$N = \gamma R^3 N' \qquad N_s = \gamma R^3 N'_s$$

$$\phi = \gamma\lambda^{-3} R^3 \phi'$$

$$v = v'\lambda^{-3} \qquad v_s = v'_s\lambda^{-3}$$

$$v^* = v'^*\lambda^{-3} \qquad v^*_s = v'^*_s\lambda^{-3}$$

The energy and mass conservation equations become, in dimensionless form,

$$(1-r^2)\frac{\partial T}{\partial z} - \text{Le}\,\frac{1}{r}\frac{\partial}{\partial r}\left(r\frac{\partial T}{\partial r}\right) = \beta\Phi \qquad [18]$$

$$(1-r^2)\frac{\partial X}{\partial z} - \frac{1}{r}\frac{\partial}{\partial r}\left(r\frac{\partial X}{\partial r}\right) = -\Phi \qquad [19]$$

with boundary conditions,

$$T(r,0) = 1 \qquad [20]$$

$$X(r,0) = 1 \qquad [21]$$

$$T(1,z) = T_w(z) \qquad [22]$$

$$X(1,z) = \min\{1, X^{sat}(T_w(z))\} \qquad [23]$$

$$\frac{\partial T}{\partial r} = 0 \qquad r = 0 \qquad [24]$$

$$\frac{\partial X}{\partial r} = 0 \qquad r = 0 \qquad [25]$$

The aerosol growth law, Eq. [17], becomes

$$-\frac{d\,Kn}{dt} = \Lambda(X - X^{sat})Kn^3\,F(Kn) \qquad [26]$$

where $\Lambda = (c/c_d)(x_o - x_{w_f})\gamma^{-2}$, the ratio of the characteristic time for radial diffusion of vapor to the characteristic time for particle growth. The growth law [26] can be integrated along a streamline to calculate the Knudsen number of a particle at axial position z whose formation originated at $\hat{z}$,

$$\frac{\Lambda}{1-r^2}\int_{\hat{z}}^{z}[X(r,\zeta) - X^{sat}(r,\zeta)]d\zeta \;=\; \int_{Kn^*}^{Kn(r,z,\hat{z},Kn^*)} \frac{-dKn}{Kn^3F(Kn)} \qquad [27]$$

Eq. [27] applies to the growth of seed aerosol as well as to the growth of homogeneously formed nuclei.

Eqs. [12],[13] and [15] are solved by the method of characteristics using Eq. [17] for the growth law. The result, in dimensionless form, is

$$n(r,z,v) = \frac{J(r,\hat{z}\,(z,v))}{4\pi\Lambda[X(r,\hat{z}\,(z,v))-X^{sat}(r,\hat{z}\,(z,v))]Kn^{-1}(v)F(Kn(v))}$$

$$+ \quad N_s\delta(v-v_s(r,z)) \qquad [28]$$

where $\hat{z}$ is defined by Eq. [27], and v_s is determined from Eq. [27] with $\hat{z} = 0$ and $Kn^* = Kn^*_s$.

The aerosol vapor sink function S_v is calculated by substituting Eqs. [28] and [11] into the relation connecting the vapor sink and the rate of change of the aerosol volume fraction,

$$S_v = \frac{c_d}{c}\frac{d\phi'}{dt'} \qquad [29]$$

The dimensionless result is

$$\Phi = 4\pi[X(r,z)-X^{sat}(r,z)]\left\{\int_0^z J(\zeta)Kn^{-1}(z,\zeta)F(Kn(z,\zeta))\,\frac{d\zeta}{1-r^2}\right.$$

$$\left. + N_sKn^{-1}(z,0)F(Kn(z,0))\right\} + \frac{4\pi J(z)}{3\Lambda Kn^{*3}} \qquad [30]$$

The first two terms on the right hand side of Eq. [30] represent vapor sinks by the growth of homogeneously nucleated aerosol and seed particles. The

third term accounts for the vapor loss due to the formation of critical nuclei by homogeneous nucleation. This last term is generally negligible when compared to the first two.

3.3 Solution of the Energy and Mass Conservation Equations

The solutions of the energy and mass conservation equations can be expressed in terms of a Green's function $G(r,z;\rho,\zeta)$ as

$$T(r,z) = \int_0^1 \left[G(r,\mathrm{Le}\ z;\rho,0) - \int_0^z T_w(\zeta) \frac{\partial}{\partial z} G(r,\mathrm{Le}\ z;\rho,\mathrm{Le}\ \zeta)d\zeta \right] \rho(1-\rho^2)d\rho$$

$$+ \mathrm{Le}^{-1}\beta \int_0^z \int_0^1 \rho\Phi(\rho,\zeta)G(r,\mathrm{Le}\ z;\rho,\mathrm{Le}\ \zeta)d\rho d\zeta \qquad [31]$$

$$X(r,z) = \int_0^1 \left[G(r,\ z;\ \rho,\ 0) - \int_0^z X_w(\zeta) \frac{\partial}{\partial z} G(r,z;\rho,\zeta)d\zeta \right] \rho(1-\rho^2)d\rho$$

$$- \int_0^z \int_0^1 \rho\Phi(\rho,\zeta)G(r,z;\rho,\zeta)\ d\rho d\zeta \qquad [32]$$

where

$$G(r,z;\rho,\zeta) = \sum_j \frac{\psi_j(r)\psi_j(\rho)}{\| \psi_j \|^2} e^{-\lambda_j^2(z-\zeta)} \qquad [33]$$

and ψ_j are the eigenfunctions of the Sturm-Liouville problem,

$$\frac{d}{dr}\left(r \frac{d\psi}{dr} \right) + \lambda^2 r(1-r^2)\psi = 0 \qquad [34]$$

$$\frac{d\psi}{dr} = 0 \qquad r = 0 \qquad [35]$$

$$\psi = 0 \qquad r = 1 \qquad [36]$$

with the norm defined by

$$\| \psi_j \|^2 = \int_0^1 r(1-r^2)\psi_j^2(r)\ dr \qquad [37]$$

For many practical conditions, such as that to be considered shortly involving dibutyl phthalate, $\beta << 1$. Therefore, the latent heat released upon vapor condensation is negligble when compared with convection and conduction, and the last terms on the right hand side of Eqs. [18] and [31] may be neglected. The solution of the energy equation, Eq. [31], is then uncoupled from that for the vapor conservation equation and can be evaluated directly from Eq. [31]. The dimensionless vapor sink Φ is a function of both X and T and thus Eq. [32] must be used iteratively to determine X. Once X and T have been calculated over the volume of the tube, the nucleation rate can be determined everywhere and used in Eqs. [27] and [28] to obtain the aerosol size distribution as a function of location.

The Green's function $G(r,z;\rho,\zeta)$ must be calculated over a suitably chosen grid. Physically, G is the steady state solution to the diffusion equation in the laminar flow tube with homogeneous boundary conditions for 2π units of mass per unit time injected uniformly over the circle of radius ρ at axial position ζ. This solution is not well behaved as $\rho \to 0$. However, the expressions in Eqs. [31] and [32] require only the group ρG. This well-behaved function physically represents the solution to the same problem, but with an injection of a unit mass per unit time per unit length of the circle at (ρ,ζ). It is thus straightforward to compute the discrete form of ρG numerically on a finite grid by integrating Eqs. [18] and [19] with the point source initial condition just described and homogeneous boundary conditions. Thus, the eigenfunctions ψ_j need not be calculated.

An efficient method of evaluating Eqs. [31] and [32] is to integrate the Green's function over the initial conditions at $z = 0$, stepping forward to $z = z_1$. The solutions at $z = z_1$ are then used as the initial condition from which the solutions are obtained at $z = z_2$. This process is continued down the length of the tube, storing the temperature and mole fraction at all r and z.

From this, the aerosol size distribution is obtained directly from Eq. [28] The marching solutions are given by

$$T(r_n,z_{m+1}) = T_w(z_{m+1}) + \sum_{j=1}^{N_r} [T(r_k,z_m) - T_w(z_{m+1})](1-r_j^2)G_1(r_n,r_j) + \beta\Phi(r_n,z_{m+1}) \frac{\Delta z}{1-r_n^2} \quad [38]$$

$$X(r_n,z_{m+1}) = X_w(z_{m+1}) + \sum_{j=1}^{N_r} [X(r_k,z_m) - X_w(z_{m+1})](1-r_j^2)G_2(r_n,r_j) + \Phi(r_n,z_{m+1}) \frac{\Delta z}{1-r_n^2} \quad [39]$$

where G_1 and G_2 are the finite-difference Green's function ρG evaluated at $(r_n,\text{Le}\ \Delta z;r_j,0)$ and $(r_n,\Delta z;r_j,0)$, respectively. Eqs. [38] and [39] require iteration with Eq. [30] because Φ is an implicit function of X. As noted earlier, when latent heating can be neglected, i.e. $\beta << 1$, no iteration is required to evaluate Eq. [38].

3.4 Homogeneous Nucleation Theories

The theory of the condenser requires an expression for the rate of formation of new particles by homogeneous nucleation, J'. Springer (18) has presented a review of current theories of homogeneous nucleation. While there are many modifications to the classical nucleation theory, only the Lothe-Pound theory shows a significant numerical difference. Therefore, two theories will be employed here, the classical theory of homogeneous nucleation and the Lothe-Pound theory. Both theories predict the formation rate of particles of critical nucleus size from a steady state pre-embryo cluster distribution derived from free energy considerations. Both theories include contributions from volume and surface free energies. The Lothe-Pound theory, in addition, includes translational, rotational and replacement free energy contributions.

Both the classical and Lothe-Pound nucleation theories can be expressed as

$$J' = c^* \kappa N^* \qquad [40]$$

where c^* is the rate of arrival and sticking of monomer, κ is the Zeldovich nonequilibrium factor, and N^* is the concentration of critical nuclei. Table 2 shows a comparison of the expressions involved in the two theories. Although the forms of the expressions for the nucleation rate are comparable, numerical values of the rate for dibutyl phthalate differ by 20 orders of magnitude. The difference in predicted nucleation rates for most monomer species between the two theories is similarly dramatic. Although Springer (18) notes that some species are better described by the classical theory, while others are better modeled by the Lothe-Pound theory, no systematic basis is observed by which the more relevant theory may be predicted a priori.

Table 3 compares numerical predictions of homogeneous nucleation rates by the classical theory and the Lothe-Pound theory, for dibutyl phthalate over a range of conditions typical in an aerosol generator. The Lothe-Pound theory consistently predicts nucleation rates of 18 to 20 orders of magnitude higher than the corresponding classical theory predictions.

Table 2. Comparison of Classical and Lothe-Pound Theories of Homogeneous Nucleation

	Classical theory	Lothe-Pound theory
Critical nucleus diameter d_p^*	$\frac{4\sigma V_\ell}{kT\ \ell nS}$	$\frac{4\sigma V_L}{kT\ \ell nS}\left(1 - \frac{6kT}{\pi\sigma d^{*2}_{p_{LP}}}\right)$ (a)
Arrival rate c*	$\zeta_c \frac{\pi d_p^{*2} p}{(2\pi mkT)^{1/2}}$	$\zeta_c \frac{\pi d^{*2}_{p_{LP}} p}{(2\pi mkT)^{1/2}}$
Zeldovich factor κ	$\left(\frac{\sigma}{kT}\right)^{1/2}\left(\frac{2V_\ell}{\pi d_p^{*2}}\right)$	$\left(\frac{\sigma}{kT}\right)^{1/2}\left(\frac{2V_\ell}{\pi d^{*2}_{p_{LP}}}\right)\left(1 - \frac{18kT}{\pi\sigma d^{*2}_{p_{LP}}}\right)^{1/2}$ (b)
Critical nucleus concentration N*	$\frac{p}{kT}\exp\left(-\frac{\pi\sigma d_p^{*2}}{3kT}\right)$	$\frac{1.1\times10^{-5}(\rho_\ell kT)^3\left(d^*_{p_{LP}}\right)^{12}}{h^6}\exp\left(-\frac{\pi\sigma d^{*2}_{p_{LP}}}{3kT}\right)$

[a] Expression is implicit for $d^*_{p_{LP}}$.

[b] The third factor is usually within a few percent of unity and is not included in the final rate expression in Springer (18).

Table 3. Numerical Comparison of Nucleation Rates Predicted for Dibutyl Phthalate by the Classical and Lothe-Pound Theories

T, °C	$x = 10^{-5}$ J', $cm^{-3}sec^{-1}$		T, °C	$x = 10^{-4}$ J', $cm^{-3}sec^{-1}$	
	Classical	Lothe-Pound		Classical	Lothe-Pound
40		$3x10^{-1}$	75		$1x10^{-5}$
35		$1x10^{6}$	70		$3x10^{4}$
30	$1x10^{-10}$	$4x10^{10}$	65	$2x10^{-10}$	$5x10^{10}$
25	$6x10^{-7}$	$8x10^{13}$	60	$1x10^{-5}$	$1x10^{15}$
20	$5x10^{-4}$	$3x10^{16}$	55	$4x10^{-2}$	$1x10^{18}$
			50	$2x10^{1}$	$2x10^{20}$
			45	$3x10^{3}$	$9x10^{21}$
			40	$1x10^{5}$	$2x10^{23}$

3.5 Calculation of Average Nucleation Rate

In the development we have followed, the local nucleation rate, $J'(r',z')$, is determined from the local temperature and vapor mole fraction. The local vapor mole fraction results from the solution of the vapor species conservation equation and includes the effect of vapor depletion by homogeneous nucleation (generally negligible) and by heterogeneous condensation of vapor on growing particles. Thus, as vapor is depleted by condensation on growing particles, the local nucleation rate can be expected to decrease, neglecting, of course, the effect of local temperature changes due to cooling.

There is, in fact, another effect that serves to decrease the local nucleation rate, one that has been elucidated by Pesthy et al. (19). There exist vapor concentration and temperature profiles in the immediate vicinity of a growing particle that extend from the background values far from the particle's surface to the values at the particle surface. Because of the vapor sink at the particle surface and the heat released by condensation, the vapor concentration and temperature profiles around the particle are such that the nucleation rate in the immediate vicinity of a particle is depressed below that existing at background conditions (see Figure 2).

We note from Figure 2 that the mole fraction profile around a growing particle extends from the local background value x_b to the value at the particle surface x_p. The local background value x_b is obtained from the solution of the vapor species conservation equation. The sink term in that equation automatically accounts for the mole fraction profile sketched in Figure 2. The nucleation rate predicted by the model in the present study is based on x_b rather than on the detailed mole fraction profile around each particle. Thus, it is necessary to assess the error inherent in approximating the actual spatially averaged nucleation rate by that evaluated at x_b. We now carry out such an assessment.

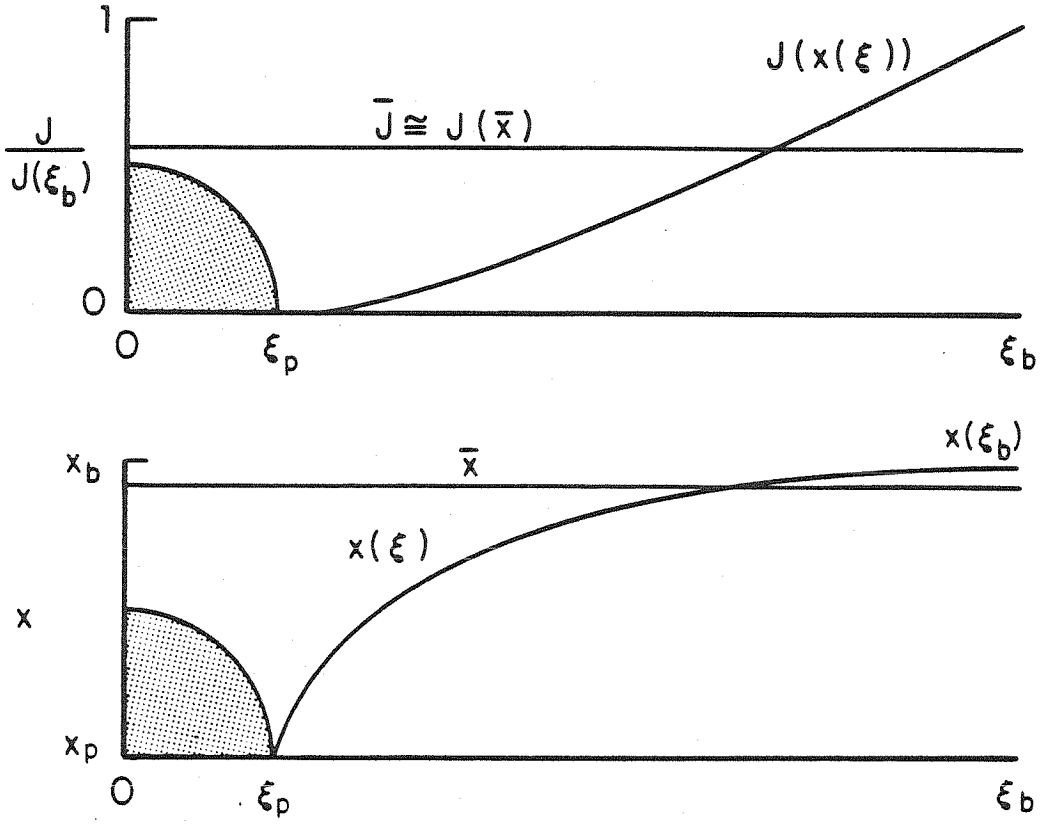

Figure 2. Nucleation rate function and vapor mole fraction profiles in the vicinity of a growing aerosol particle, exaggerated for illustration.

The spatially averaged nucleation rate occurring in a spherical region around a particle of radius ξ_p out to a radius ξ_b when $\xi_b >> \xi_p$ can be expressed as (primes are dropped for convenience; all quantities are dimensional)

$$\bar{J} = \frac{3}{4\pi\xi_b^3} \int_0^{\xi_b} 4\pi\xi^2 J(\xi)\, d\xi \qquad [41]$$

where $J(\xi)$ is the homogeneous nucleation rate at radial position ξ from the particle center, where the vapor mole fraction and temperature are $x(\xi)$ and $T(\xi)$, respectively. Eq. [41] can be rearranged as (19)

$$\frac{\bar{J}}{J_\infty} = 1 - \frac{3}{\xi_b^3} \int_0^{\xi_b} \frac{-\Delta J(\xi)}{J_\infty} \xi^2 d\xi \qquad [42]$$

where $J_\infty = J(\xi_b)$ is the homogeneous nucleation rate at the background conditions.

For dilute systems the contribution of latent heat release at the particle surface to ΔJ is small, and the dominant contribution to the integral of Eq. [42] arises from the region where ξ^2 is large but ΔJ is small. Thus, it is advantageous to treat mole fraction x as the integration variable and express Eq. [41] as

$$\bar{J} = \int_{x_p}^{x(\xi_b)} J(x) \left[\xi_b^3 \frac{dx}{d\xi^3} \right]^{-1} dx \qquad [43]$$

The Jacobian of the transformation may be interpreted as a distribution function of averaging volume in x-space. This distribution has a unit area if $x = 0$ within the volume of the aerosol particle, yielding

$$\bar{J} = \int_0^{x(\xi_b)} J(x) f(x) dx \qquad [44]$$

where

$$f(x) = \left[\xi_b^3 \frac{dx}{d\xi^3}\right]^{-1} \qquad 0 \le x \le x(\xi_b) \qquad [45]$$

After particle growth affects the background mole fraction in an aerosol system, the approximate mole fraction profile around a particle is (19)

$$x = x_p + (x_b - x_p)\left[\frac{1-\xi_p/\xi}{1-\xi_p/\xi_b}\right] \qquad \xi_p \le \xi \le \xi_b \qquad [46]$$

This profile can be substituted into Eq. [45] and algebraically inverted to give

$$f(x) = \frac{3\left(\frac{\xi_p}{\xi_b}\right)^3\left(1-\frac{\xi_p}{\xi_b}\right)}{x_b - x_p}\left[1 - \left(1 - \frac{\xi_p}{\xi_b}\right)\frac{x-x_p}{x_b-x_p}\right]^{-4} U(x-x_p)$$

$$+ 2\left(\frac{\xi_p}{\xi_b}\right)^3 \delta(x) \qquad 0 \le x \le x_b \qquad [47]$$

where U is the unit step function. A convenient averaging radius we will use is $\xi_b/\xi_p = \hat{\phi}^{1/3}$. (19)

The background concentration depends on the aerosol volume and macroscopic parameters affecting diffusional loss of monomer. For example, if monomer is depleted only by diffusion to growing particles, the background mole fraction is approximately given by (19)

$$x_b = x_p + (x_b(0) - x_p)\left(1 - \frac{\hat{\phi}}{\hat{\phi}_f}\right)\left[\frac{1-\hat{\phi}^{1/3}}{1-3/2\hat{\phi}^{1/3}}\right] \qquad [48]$$

where $x_b(0)$ is the initial background mole fraction, $\hat{\phi}$ is the aerosol volume fraction, and $\hat{\phi}_f$ is the ultimate aerosol volume fraction when all monomer has been condensed. Eq. [48] is valid only after $\hat{\phi} > (\hat{\phi}_f/2)^{3/2}$, so that the initial transients are not important and $x_b < x_b(0)$. If the monomer vapor is influenced by other sources or sinks, then Eq. [48] does not apply, and x_b must be determined by a species conservation equation as in the present case.

The local nucleation rate may be expanded in a Taylor series about a reference point given by the average mole fraction,

$$\bar{x} = \int_0^{x_b} x f(x)\, dx \qquad [49]$$

to give

$$J(x) = J(\bar{x}) + \left(\frac{\partial J}{\partial x}\right)_{\bar{x}} (x-\bar{x}) + \frac{1}{2}\left(\frac{\partial^2 J}{\partial x^2}\right)_{\bar{x}} (x-\bar{x})^2 + \cdots \qquad [50]$$

Using Eqs. [44] and [50], we obtain

$$\overline{J(x)} - J(\bar{x}) = \frac{1}{2}\left(\frac{\partial^2 J}{\partial x^2}\right)_{\bar{x}} (\overline{x^2}-\bar{x}^2) + \cdots \qquad [51]$$

Because the distribution f(x) is fairly sharp, the higher order terms of Eq. [51] are negligible.

Defining

$$\overline{x^2} = \int_0^{x_b} x^2 f(x)\, dx \qquad [52]$$

we obtain the difference $(\overline{x^2}-\bar{x}^2)$ to lowest orders of $\hat{\phi}$ as

$$\overline{x^2} - \bar{x}^2 \cong \frac{1}{4}\hat{\phi}^{2/3}(x_b-x_p)^2\left[1 + 2\hat{\phi}^{1/3}\left(1 + \frac{2x_p}{x_b-x_p}\right)\right] \qquad [53]$$

The variance, $\overline{x^2}-\bar{x}^2$, is always positive, and, for dilute systems, proportional to $\hat{\phi}^{2/3}$. Since all realistic models of homogeneous nucleation give $\partial^2 J/\partial x^2 > 0$, Eq. [51] predicts that the true average nucleation rate always exceeds the value of the nucleation rate evaluated at the average mole fraction.

Substituting Eq. [53] into Eq. [51] gives

$$\overline{J(x)} \cong J(\bar{x}) + \frac{1}{8}\left(\frac{\partial^2 J}{\partial x^2}\right)_{\bar{x}} (x_b - x_p)^2 \hat{\phi}^{2/3} \left[1 + 2\hat{\phi}^{1/3}\left(1 + \frac{2x_p}{x_b - x_p}\right)\right] \qquad [54]$$

From Eqs.[46] and [49], we obtain

$$\frac{x_b - \bar{x}}{x_b - x_p} \cong \frac{1}{2}\hat{\phi}^{1/3}\left[1 + \hat{\phi}^{1/3}\right] + \frac{x_p}{x_b - x_p}\hat{\phi} \qquad [55]$$

Eq. [50] may now be evaluated at x_b neglecting higher-order terms,

$$J(x_b) \cong J(\bar{x}) + \frac{1}{2}\left(\frac{\partial J}{\partial x}\right)_{\bar{x}} (x_b - x_p)\hat{\phi}^{1/3}\left[1 + \hat{\phi}^{1/3}\right]$$

$$+ \frac{1}{8}\left(\frac{\partial^2 J}{\partial x^2}\right)_{\bar{x}} (x_b - x_p)^2 \hat{\phi}^{2/3}\left[1 + \hat{\phi}^{1/3}\right]^2 \qquad [56]$$

The average nucleation rate is now

$$\overline{J(x)} \cong J(x_b) - \frac{1}{2}\left(\frac{\partial J}{\partial x}\right)_{\bar{x}} (x_b - x_p)\hat{\phi}^{1/3}\left[1 + \hat{\phi}^{1/3}\right]$$

$$+ \frac{1}{8}\left(\frac{\partial^2 J}{\partial x^2}\right)_{\bar{x}} (x_b - x_p)^2 \hat{\phi}\left[\frac{x_p}{x_b - x_p} - \hat{\phi}^{1/3}\right] \qquad [57]$$

An order of magnitude analysis of the difference between $\overline{J(x)}$ and $J(x_b)$ from Eq. [57] shows

$$\frac{\overline{J(x)}}{J(x_b)} = 1 - \frac{1}{2} O(1) O(\hat{\phi}^{1/3}) + \frac{1}{8} O(1) O(\hat{\phi}) O\left(\frac{x_p}{x_b} - \hat{\phi}^{1/3}\right) \qquad [58]$$

Since $\hat{\phi} << 1$ for dilute systems, the negative correction to $J(x_b)$ is at most a few percent. Therefore, the foregoing analysis confirms the validity of approximating the average homogeneous nucleation rate as $J(x_b)$.

3.6 Numerical Solution of the Governing Equations

Numerical calculations with the theoretical model are performed over a regular grid of points in (r,z) space. The iteration scheme and grid spacings in both coordinate directions are chosen to yield a reasonable solution accuracy. The model incorporates greatly differing time scales, presenting a stiff set of equations. The integral result of Eq. [27] allows the removal of some stiffness. The model of Eqs. [38] and [39] may be discretized on a scale of Δr and Δz characteristic of vapor diffusion and heat conduction if Eqs. [28] and [30] are properly discretized. The discrete solution to Eq. [12] using the characteristic of Eq. [27] is the discrete aerosol distribution,

$$n(r_n,z_m,v(r_n,z_m,z_i)) = \frac{J(r_n,z_i)\,\frac{\Delta z}{1-r_n^2} + N_s\delta_{i,1}}{[v(r_n,z_m,z_i)-v(r_n,z_m,z_{i-1})]} \qquad [59]$$

$$i = 1,2,\ldots,m$$

$$n = 1,2,\ldots, N_r$$

$$m = 1,2,\ldots, N_z$$

$$\delta_{i,1} = \begin{cases} 1 & i = 1 \\ 0 & i \neq 1 \end{cases}$$

and the discrete vapor sink, the finite-difference analog of Eq. [29], is

$$\Phi(r_n,z_m) = \frac{\phi(r_n,z_m)-\phi(r_n,z_{m-1})}{\Lambda}\;\frac{(1-r_n^2)}{\Delta z} \qquad [60]$$

Eq. [59] is the sum of two distributions. The first term of the numerator represents the number of new particles per unit volume formed at interval z_i on streamline r_n, and the second term represents the monodisperse seed particle concentration, present since z_1. Thus the total number concentration is

$$N(r_n,z_m) = \sum_{i=1}^{m} J(r_n,z_i) \frac{\Delta z}{1-r_n^2} + N_s \qquad [61]$$

and the total volume fraction is

$$\phi(r_n,z_m) = \sum_{i=1}^{m} v(r_n,z_m,z_i)J(r_n,z_i) \frac{\Delta z}{1-r_n^2}$$

$$+ N_s v_s(r_n,z_m) \qquad [62]$$

Note that the seed volume is only a special case of the general volume characteristic,

$$v_s(r_n,z_m) = v(r_n,z_m,z_1)$$

$$= \frac{4\pi}{3} Kn^{-3}(r_n,z_m,z_1,Kn_s^*) \qquad [63]$$

where Kn is solved from Eq. [27] after the left hand side of Eq. [27] is numerically integrated. Eqs. [27], [62] and [63] are combined with Eq. [60] to calculate the vapor sink term in the discretized model.

Once the discrete model incorporating Φ is calculated with Eqs. [38] and [39] and a modified regula falsi iteration scheme, the aerosol distribution, number concentration and volume fraction are calculated with the discrete Eqs. [59], [61] and [62]. The discrete number distribution is partitioned by the aerosol volume characteristic, $v(r_n,z_m,z_i)$, and is therefore resolved to an accuracy dependent on the streamline location and the z-interval of the numerical grid.

Meaningfully accurate solutions to Eqs. [38] and [39] are achieved when the difference in each dependent variable at consecutive z coordinates is small compared to the magnitude of that variable. Sufficiently fine resolution of the

aerosol distribution may require a still finer grid spacing in z. The region of low velocity and regions of high vapor sink rate exhibit the lowest accuracy. The appropriate choice of the z-step size may therefore depend on the boundary conditions, the nucleation rate and the inlet seed concentration. The streamline located one r-interval away from the wall has the lowest velocity and highest cooling rate, and is therefore the most convenient determinant of the z-interval. As such, the choice of the r-interval directly influences the choice of the z-interval. This relationship is fundamentally illustrated by the nature of Eqs. [31] and [32]. With these equations, numerical integration requires a grid in (r,z) fine enough to accurately represent the integrands. The plume-like nature of the diffusional Green's function is in part responsible for the interrelationship of the maximum r and z grid spacings.

The choice of the r-interval may be made first, determining the spatial resolution of the model. Intuitively, a lower limit to the r-interval may be specified by the mean distance between the particles of concentration N, or $\Delta r = N^{-1/3}$. Since the total aerosol concentration cannot be known a priori, several simulations with different Δr may be compared. It has been found from numerical solutions to pipe flow in a 17.3 mm I.D. tube that Δr of 0.05 of the tube radius (0.43 mm) is adequate for particle concentrations less than 10^9 cm^{-3}. Values of Δz used ranged from 1.25×10^{-4} to 5×10^{-4}. This limit of particle concentration includes all cases of negligible coagulation (Appendix B).

3.7 Simulation of Dibutyl Phthalate Aerosol Formation and Growth

We now examine the predictions of the theory developed above over a range of conditions chosen to reflect those of a laminar flow aerosol generator constructed in our laboratory, and generally typical of such devices (5,6,8,10,11). The variable having the greatest effect by far on the predicted behavior of the system is the choice of homogeneous nucleation theory. We choose to study the classical and Lothe-Pound nucleation theories because they predict greatly differing nucleation rates. All simulations are based on dibutyl phthalate as the condensable vapor. Table 4 shows the ranges of operating parameters used in the simulations.

To perform the simulation for dibutyl phthalate the following properties were selectd: saturation mole fraction function $x^{sat} = \exp(21.497 - \frac{11,497}{T})$ (20,21), surface tension, $\sigma_{DBP} = 33 - 0.8(T'-25°C)$ g sec^{-2} (12), the ratio of gaseous to liquid molar concentrations, $c/c_d = 0.011$ (at 25°C), molecular diffusivity, $D_{DBP} = 0.0282$ $cm^2 sec$ (20,21), and the critical Knudsen number, Kn*. The value of the Lewis number for this choice of D_{DBP} is Le = 7.74. We also note that the axial Péclet numbers for mass and heat transfer, Pe_z, based on tube diameter and a 3 ℓ/min flow rate have values of 700 and 170, respectively, validating the early assumption neglecting axial diffusion and heat conduction relative to convection.

Figure 3 shows dimensionless radial temperature profiles at four dimensionless axial distances. In all cases the wall temperature profile is taken as a linear transition from $T_w = 1$ to $T_w = 0$ over a distance of $z = 0.008$. The solution of the heat and mass transfer problems in the absence of aerosol formation is shown in Figure 4. This solution is realistic only to the position z where the first aerosol would form and begin to consume vapor by growth. At all points downstream from that position, distortion of the plotted streamlines would be

Table 4. Simulated Operating Conditions for the Cooled Laminar Flow Tube

Parameter Ranges and Conditions	Comments
$101°C \lesssim T_o' \lesssim 200°C$	Dewpoint = 101°C
	$x_o = 1 \times 10^{-4}$ held constant
$2 \times 10^{-5} \lesssim x_o \lesssim 2 \times 10^{-4}$	$T_o' = 150°C$ held constant
$0 \lesssim N_s' \lesssim 10^8\ cm^{-3}$	$x_o = 1 \times 10^{-4}$, $T_o' = 150°C$ } held constant

Note: The simulations assume a cooling zone fabricated from a standard 3/4 in. tube of 0.035 in. wall thickness (R = 0.864 cm), a linear wall temperature transition of 10 cm length, and a gas flow rate of 3 ℓ/min at 25°C. In all cases considered, $T_{w_f}' = 25°C$.

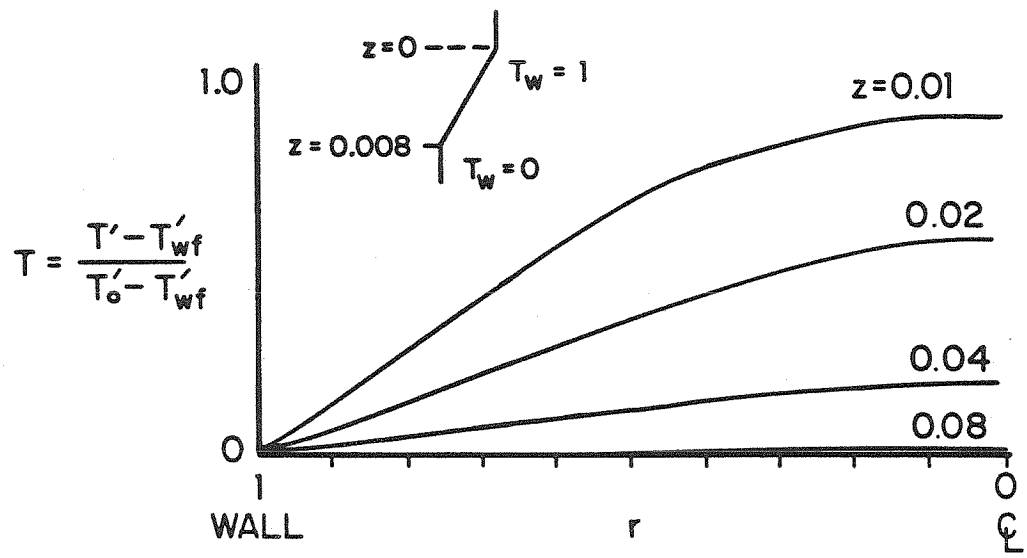

Figure 3. Dimensionless temperature profile. Wall temperature profile is a linear transition as depicted in the inset.

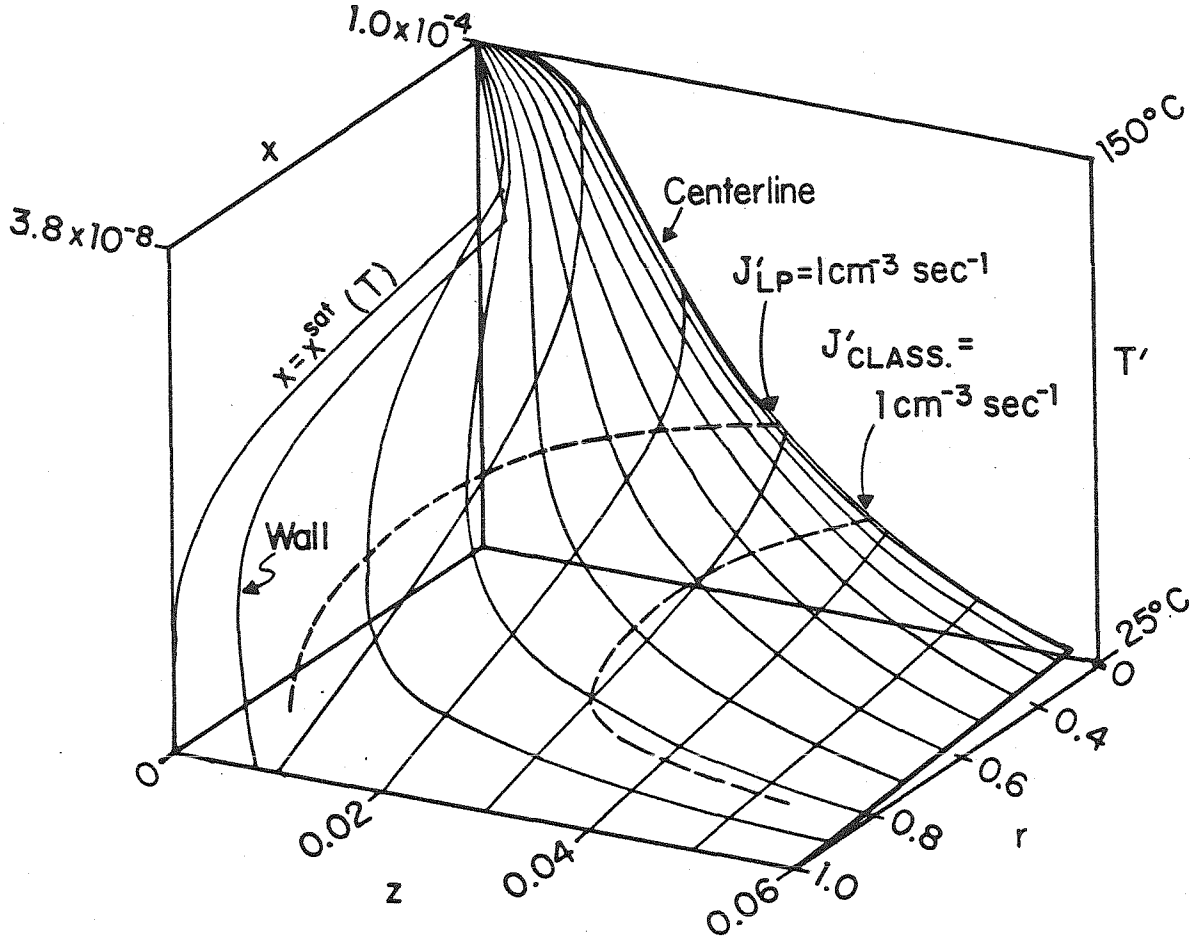

Figure 4. Streamline trajectories in vapor composition-temperature profile without nucleation. Isopleths of critical nucleation rate indicated for the Lothe-Pound and classical nucleation theories.

caused by the aerosol. Streamlines at ten radial positions are plotted to show temperature and vapor mole fraction as a function of z. The saturation curve is shown in the x,T plane. Streamlines near the wall reach saturation ratios greater than unity at the earliest axial positions. The highest saturation ratios are achieved late along the center streamline. Consequently, the isopleth of critical nucleation rate for the Lothe-Pound theory, lying nearer to the saturation curve than that for the classical theory, predicts aerosol formation to initiate near the wall. The classical theory predicts aerosol formation much later, initially nearer the centerline and never near the wall. By this late position, much of the monomer vapor is lost to wall condensation. Low wall losses are predicted for the Lothe-Pound theory owing to the insulating effect of particles forming early near the wall, whereas high wall losses are predicted by the classical theory.

These predictions of a model solution without aerosol are not realistic beyond the first appearance of aerosol, therefore the full simulations are now described.

Classical Nucleation Theory

The temperature profile is unaffected by latent heating for $\beta << 1$, or $\frac{\Delta H_v}{C_p}\left(\frac{x_o - x_{w_f}}{T'_o - T'_{w_f}}\right) << 1$. For dibutyl phthalate, and $T'_o = 150°C$, the above constraint becomes $x_o \leq 0.05$. The simulations lie well within this limit, and therefore Figure 3 is the correct temperature profile.

Figure 5 shows the vapor mole fraction profile without seed particles at nominal conditions used in Figure 4. The radial profile of aerosol volume fraction shown in Figure 6 reveals that by z = 0.18, little aerosol forms, and that only in the central region. By that point, the aerosol represents only

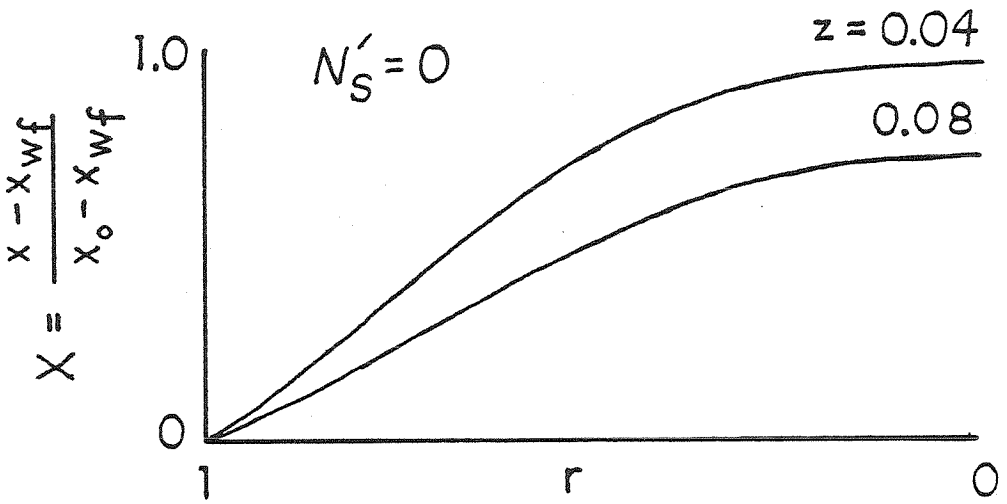

Figure 5. Theoretical vapor mole fraction profiles for cooling section with classical nucleation theory, no seed aerosol.

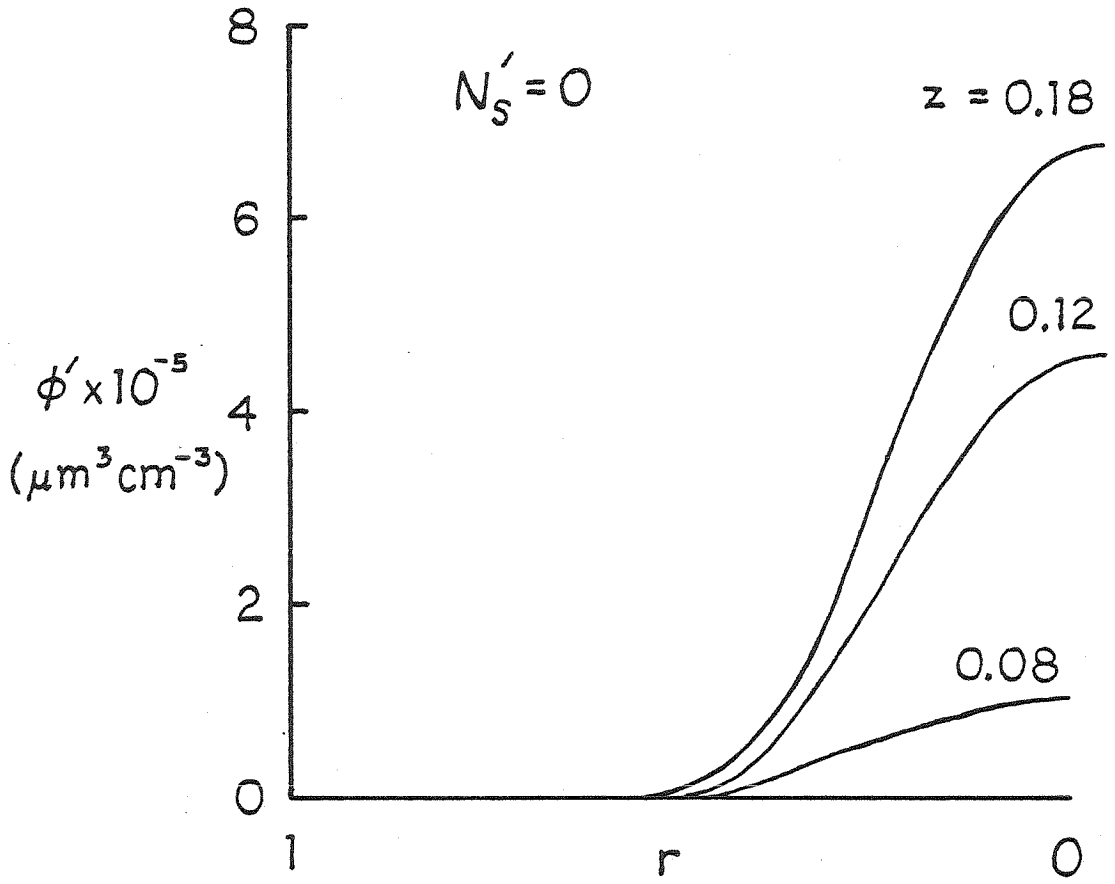

Figure 6. Aerosol volume fraction predicted by classical nucleation theory, without seed aerosol.

11 percent of the initial dibutyl phthalate, while 75 percent of the initial mass is lost to the wall by condensation. Figure 7 shows the cup-mixed average volume distribution of aerosol at z = 0.18. The number average particle size at z = 0.18 is 0.67 μm. The number density at the centerline is 4×10^6 cm^{-3}, and the average number density across the tube is 7×10^5 cm^{-3}. Very far downstream the particles will grow larger, but 80 percent of the vapor will ultimately be lost to the wall.

The general characteristics of high wall loss of vapor and late nucleation near the centerline are found for most operating conditions simulated with classical nucleation theory. Significant nucleation occurs only when the final wall temperature T'_{w_f} is well below 25°C or initial mole fraction x_o is a few percent. Neither of these extremes is typical for aerosol generators.

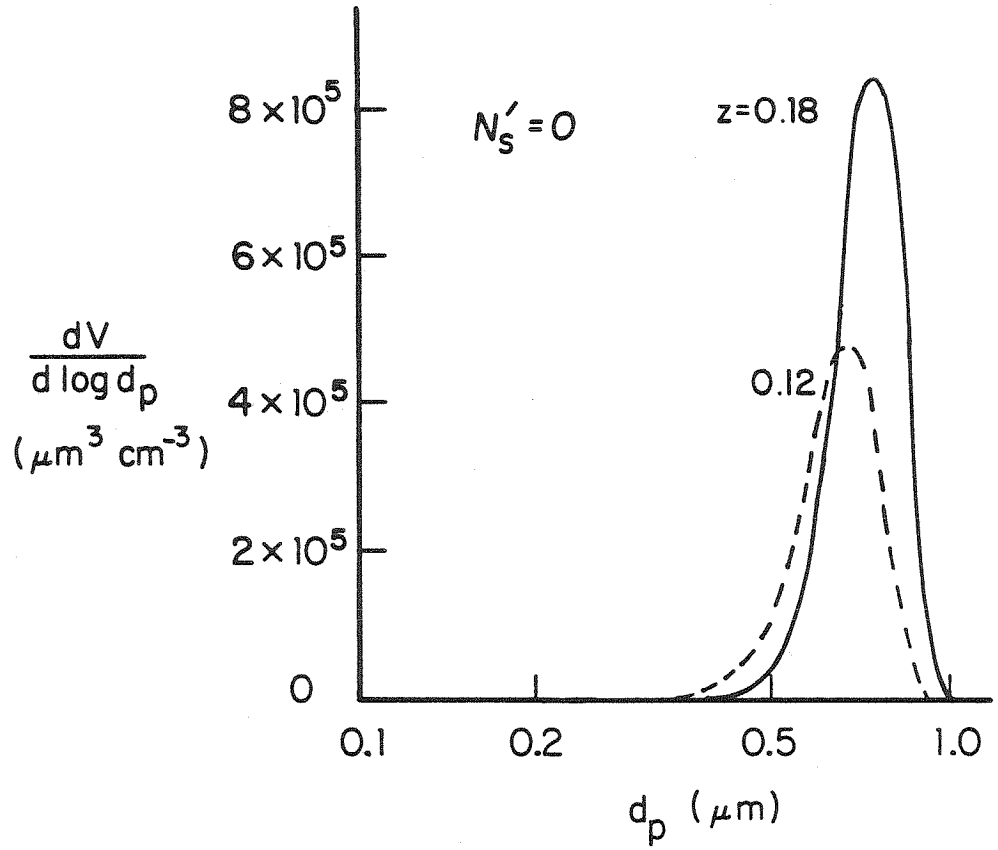

Figure 7. Cup-mixed average aerosol volume distribution predicted by classical nucleation theory, without seed aerosol. Area under the curves is total aerosol volume.

3.7.2 Lothe-Pound Nucleation Theory

1. Effect of seed aerosol

The mole fraction profiles for nominal conditions with and without seed aerosol are shown in Figure 8. The simulations with seed aerosol for $N_s' \leq 10^7$ cm^{-3} produce mole fraction profiles and new aerosol similar to the case without seed, with seed aerosol growth to approximately 0.28 μm diameter. Homogeneous nucleation without seed aerosol occurs as shown in Figure 9a. Nucleation rates in excess of 10^9 $cm^{-3}sec^{-1}$ occur initially near the wall. The zone of nucleation progresses toward the centerline while increasing in magnitude. Beyond $z = 0.03$, the nucleation pulse rapidly decays. For seed aerosol of $N_s' \leq 10^7$ cm^{-3}, homogeneous nucleation remains as significant as without seed. For $N_s' = 10^8$ cm^{-3}, Figure 9b shows that the initial pulse near the wall is two orders of magnitude smaller than without seed. The qualitative behavior of the nucleation zone downstream is similar but peaks at the centerline only late, $z = 0.045$, but with magnitude comparable to the case without seed.

The differences between the nucleation rates in Figures 9a and 9b are due to the presence of the seed aerosol. Before conditions of homogeneous nucleation can exist, the saturation ratio of a region must rise well above unity. Seed particles grow from the moment that the saturation ratio exceeds unity. This growth causes a subtle difference in the vapor concentration, producing a large negative effect on the homogeneous nucleation rate whose arrival follows the onset of seed growth. Figure 8 shows the vapor mole fraction profiles for $N_s' = 0$ and 10^8 cm^{-3}, revealing the subtle difference discussed above. Differences in the two simulations become more apparent for $z = 0.03$. The simulation with seed aerosol results in lower vapor concentrations due to

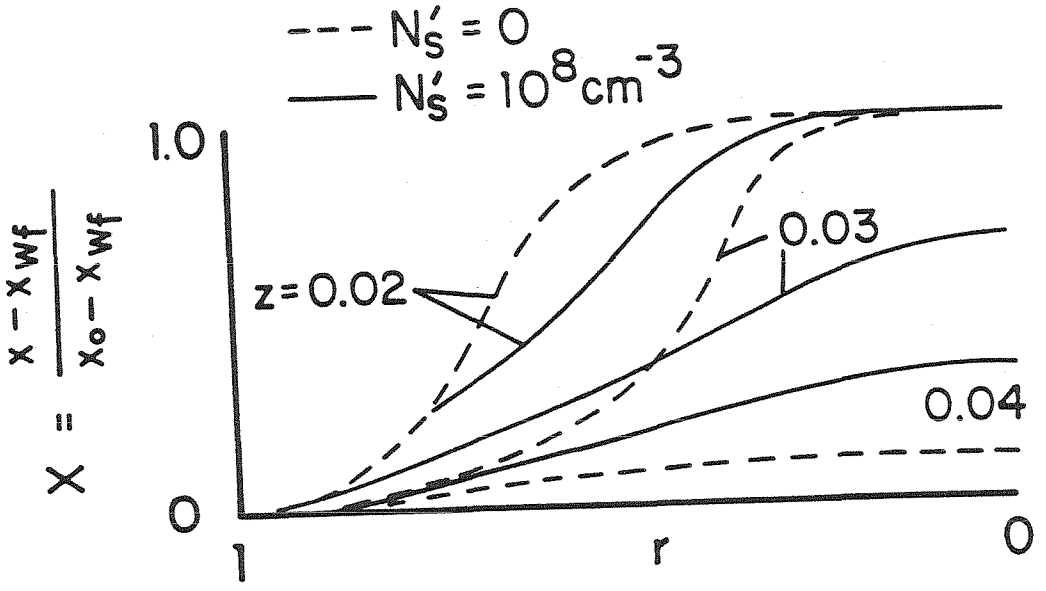

Figure 8. Vapor mole fraction profiles predicted with Lothe-Pound theory, with initial seed aerosol concentrations of 0 and 10^8 cm^{-3}. $T_o' = 150°C$, $T_{w_f}' = 25°C$, $x_o = 10^{-4}$.

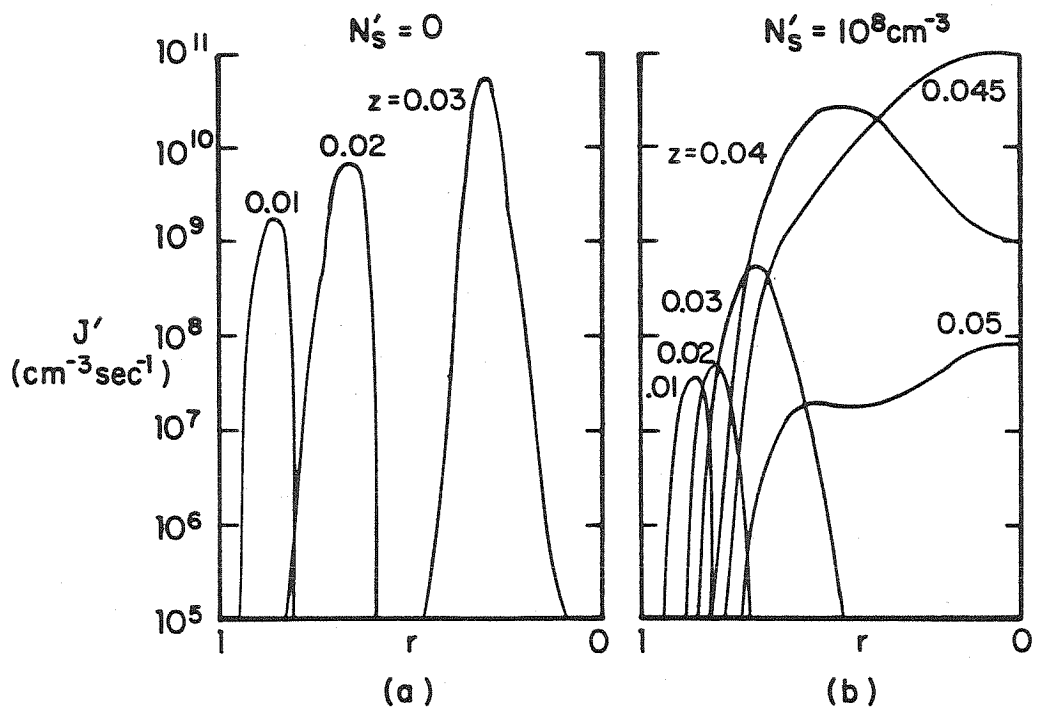

Figure 9. Radial profiles of homogeneous nucleation rate predicted by Lothe-Pound theory, with initial seed aerosol concentrations of 0 and 10^8 cm^{-3}. Same conditions as in Figure 8.

vapor consumed by growing seed aerosol. For $z > 0.03$, a reversal occurs in this trend. The reversal is seen first nearer the wall, then throughout. The case without seed aerosol produced more particles due to the absence of the seed aerosol and its accompanying quenching effect on homogeneous nucleation by vapor consumption. Vapor is more quickly consumed by the high number of homogeneously nucleated particles without seed present than by the combination of the lower homogeneously formed aerosol and seed aerosol. The peak in nucleation rate along the center streamline occurs later with seed than without seed but both peaks produce nucleation rates in excess of $10^{10} cm^{-3}$ sec^{-1}. Without seed, the peak occurs just after $z = 0.03$, while the centerline vapor concentration is still within a few percent of its original value and the temperature has dropped to about 34 percent of its original value. With seed, a similar nucleation rate occurs at a peak near $z = 0.045$ with only 26 percent of the original vapor concentration, but with $T = 0.15$.

The radial distribution of volume fraction for the simulation with $N_s' = 0$ is shown in Figure 10. The volume fraction corresponding to a parcel of inlet vapor condensed to aerosol without diffusional losses is $1.1 \times 10^6 \mu m^3$ cm^{-3}. For $r < 0.85$ the aerosol volume fraction is well below 10^6 μm^3 cm^{-3}, indicating losses of vapor by outward diffusion from the core. The initial burst of nucleation at $r \cong 0.9$ shows a volume fraction in excess of 10^6 μm^3 cm^{-3}, because this region of aerosol scavenged the vapor from the core region. The overall mass balance reveals a net wall loss of monomer vapor of 16 percent of the initial monomer mass flow at the tube inlet.

For the same simulation with seed aerosol of $N_s' = 10^8$ cm^{-3}, the radial distribution of volume fraction is shown in Figure 11. The contribution by homogeneously nucleated aerosol is less but still dominant near the wall. By $z = 0.06$, some homogeneous aerosol is found in the core region, but the seed

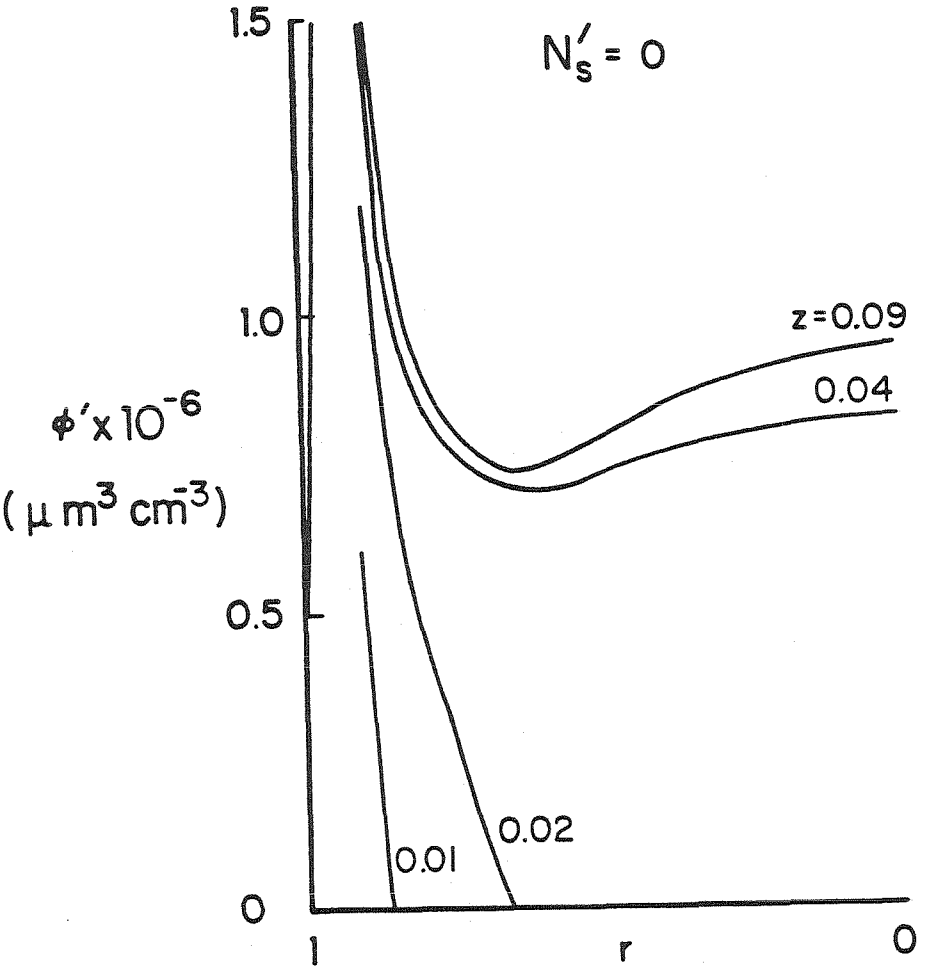

Figure 10. Radial profiles of volume fraction for homogeneous aerosol predicted by Lothe-Pound theory with no seed aerosol. Same conditions as in Figure 8.

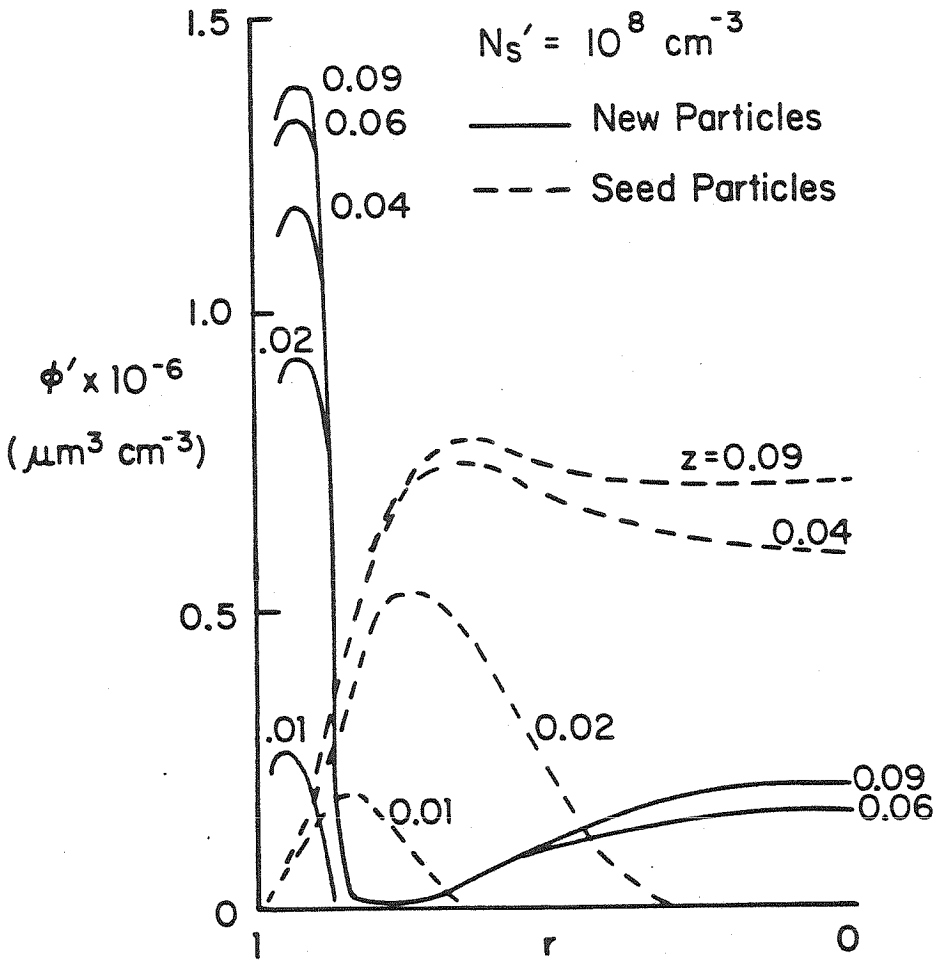

Figure 11. Radial profiles of volume fraction for homogeneous and seeded aerosol predicted by Lothe-Pound theory. Same conditions as in Figure 8.

aerosol dominates the core region. Due to the lesser influence of the aerosol near the wall in shielding vapor from diffusing to the wall from the core region, the net wall loss is 20 percent of the initial monomer mass flow at the tube inlet, slightly greater loss than in the case without seed aerosol.

Figure 12 shows the cup-mixed average volume distributions of aerosol at $z = 0.09$, after the aerosol has ceased to evolve. The volume distribution is shown for $N_s' = 10^8$ cm^{-3}, 10^7 cm^{-3}, and 0. The peaks near 0.1 μm diameter are the contributions by homogeneously nucleated aerosol, and the sharp peaks near 0.3 μm diameter are the seed aerosols. The seed concentration of 10^8 cm^{-3} appears to be a critical crossover point, a concentration beyond which new particle formation yields to seed growth. The bimodal distribution of homogeneously nucleated particles in the case of $N_s' = 10^8$ cm^{-3} arises from the mixing of aerosol near the wall with diameter near 0.1 μm with aerosol formed later in the core with diameter near 0.04 μm. The peaks due to seed aerosol are very narrow, fairly monodisperse. The size dispersity of the seed aerosol is due only to the radial diffusion of vapor.

Another function of interest is the vapor sink function which indicates the magnitude of the aerosol growth process. Figures 13-15 show the sink function for the same simulations described above. Figure 13 shows the case of no seed aerosol. The sink function possesses a peak which propagates away from the wall, proceeding down the length of the tube, until no further growth can occur. For $N_s' = 10^7$ cm^{-3}, Figure 14 shows similar peaks describing vapor depletion to growing homogeneously nucleated aerosol, but with smaller peaks preceding the large ones, due to seed aerosol growth. For $N_s' = 10^8$ cm^{-3}, the seed aerosol contribution clearly dominates the homogeneous aerosol contribution. At $z = 0.04$, the region near $r = 0.50$ shows the effect of a surge of new particles nucleating as seen in Figure 9b. At $z = 0.045$, the wave of new particles has

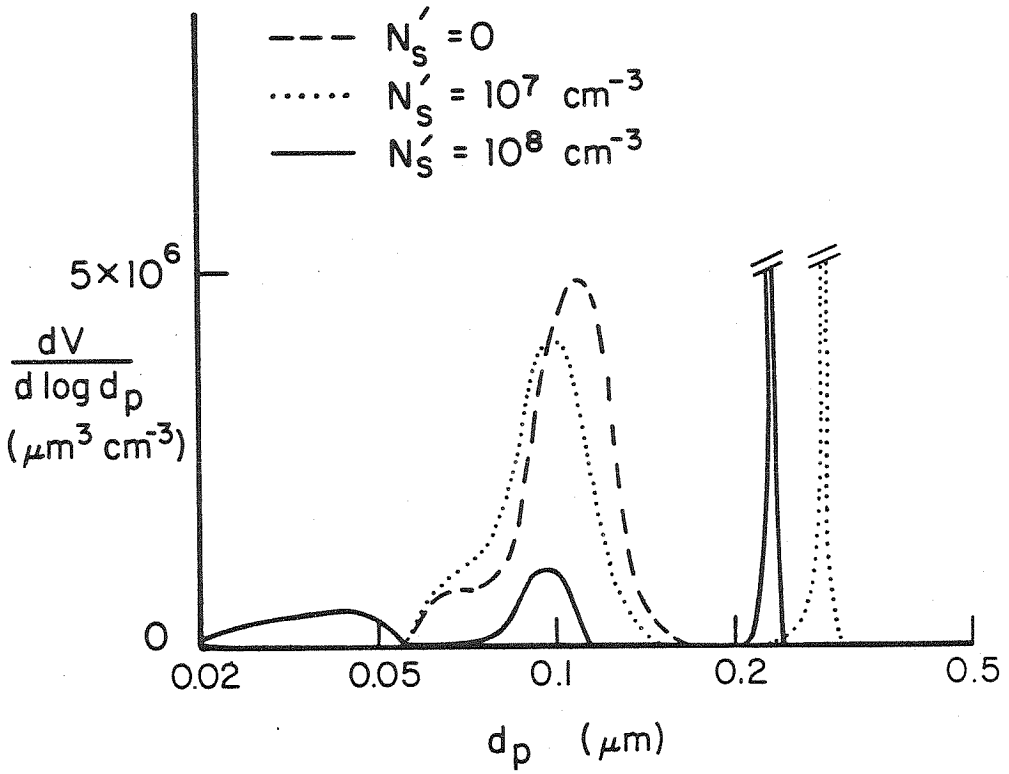

Figure 12. Cup-mixed average aerosol volume distributions predicted by Lothe-Pound theory for initial seed aerosol concentrations of 0, 10^7 and 10^8 cm^{-3}. Seed aerosol is illustrated by the truncated peaks near d_p = 0.3 μm. Same conditions as in Figure 8.

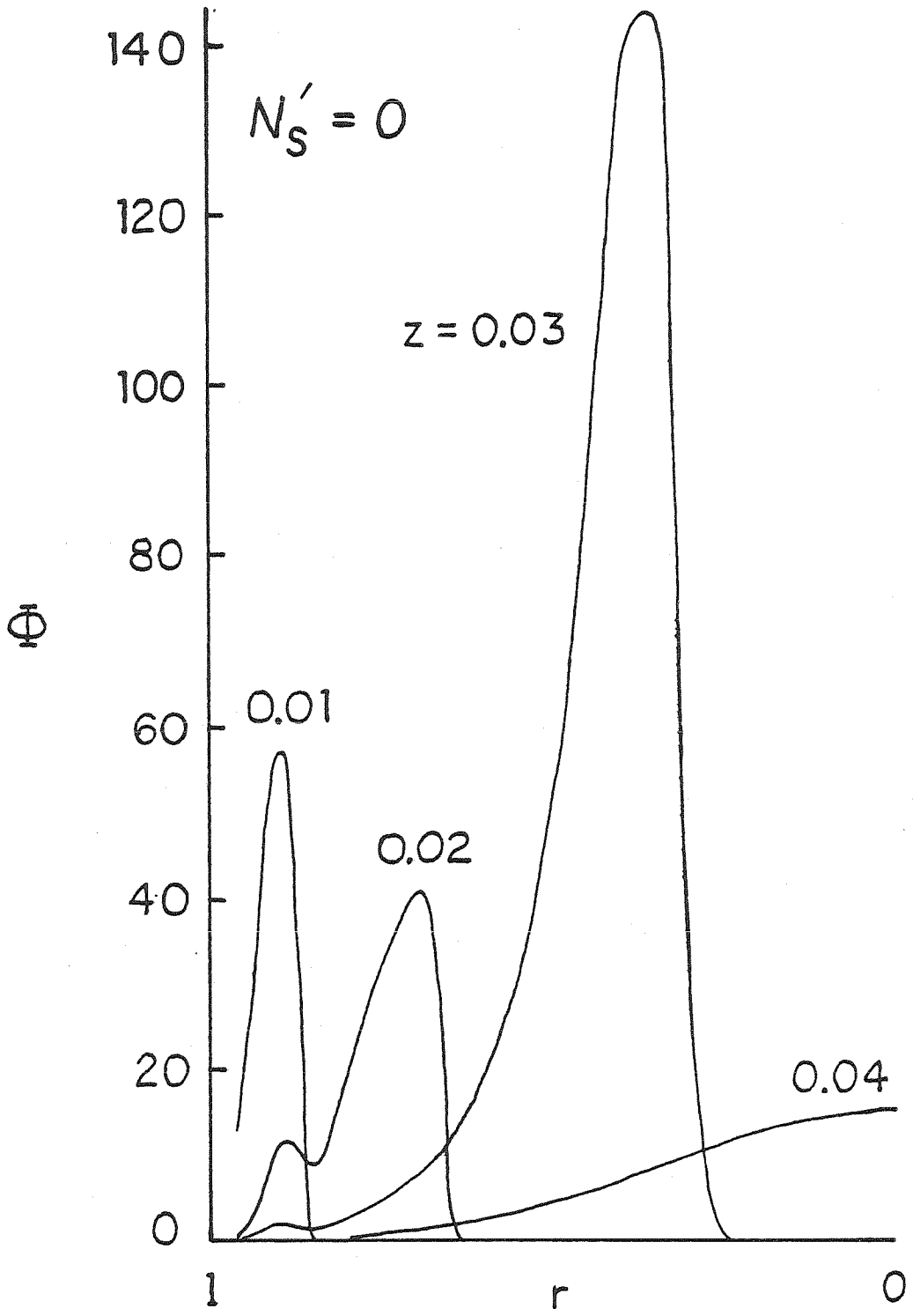

Figure 13. Vapor sink function predicted by Lothe-Pound theory with no seed aerosol. Same conditions as in Figure 8.

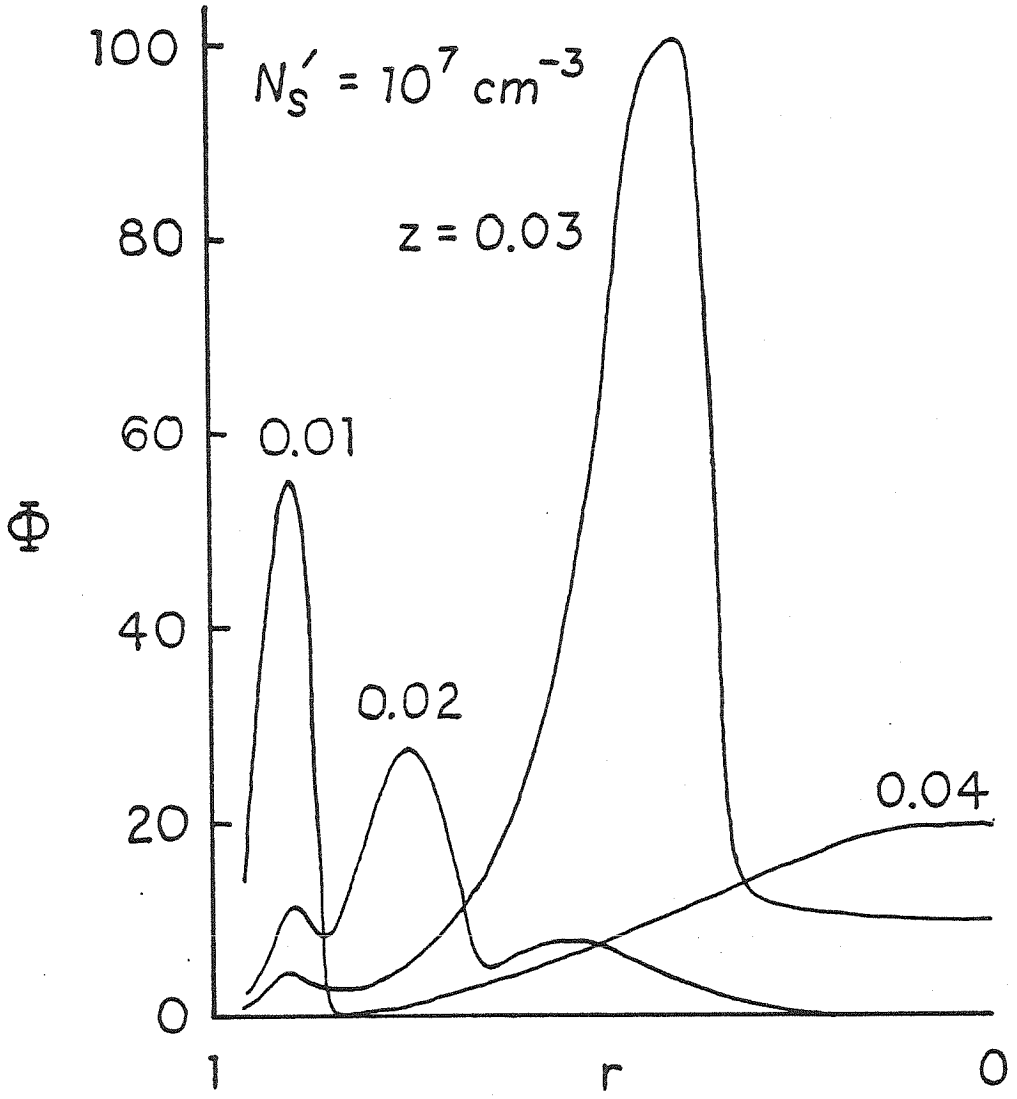

Figure 14. Vapor sink function predicted by Lothe-Pound theory with initial seed aerosol concentration of 10^7 cm^{-3}. Same conditions as in Figure 8.

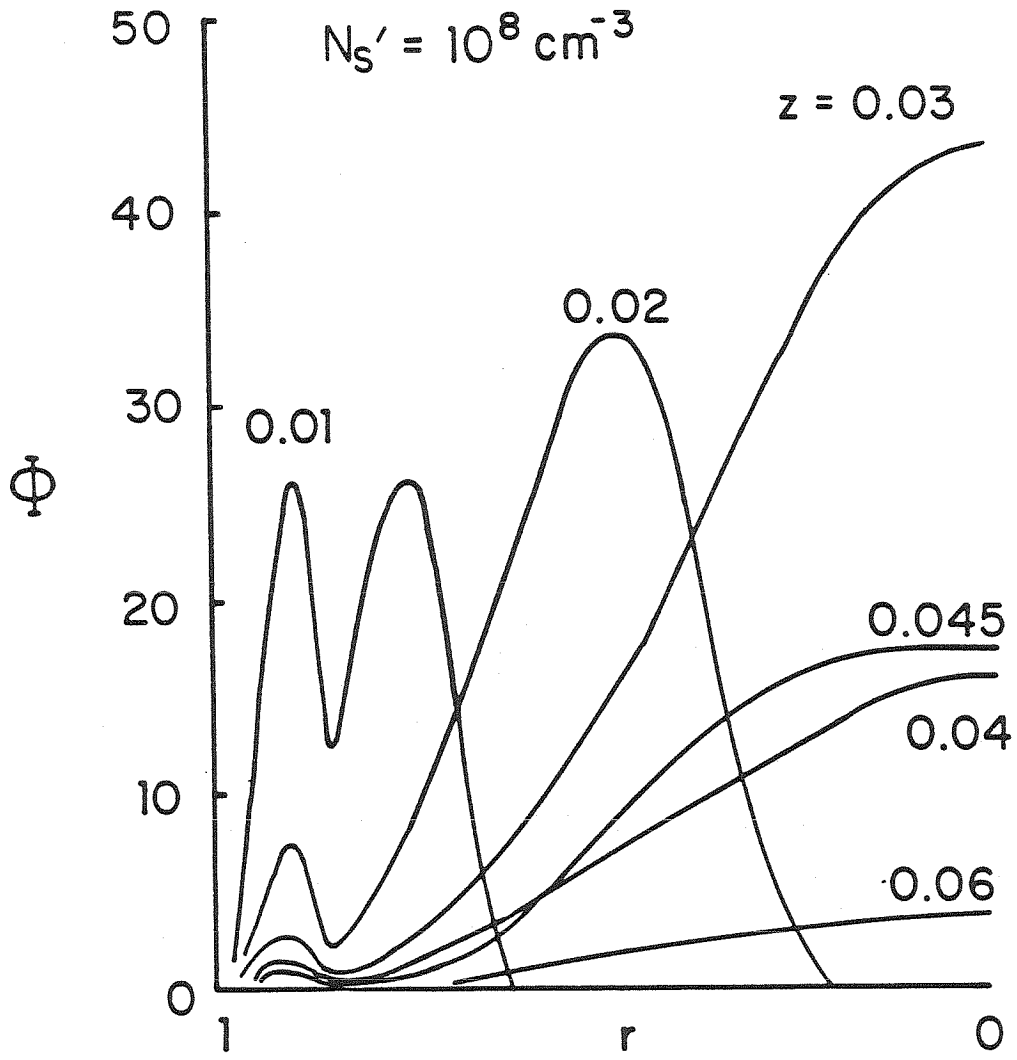

Figure 15. Vapor sink function predicted by Lothe-Pound theory with initial seed aerosol concentration of 10^8 cm^{-3}. Same conditions as in Figure 8.

reached the center, also seen in Figure 9b, and the sink function at the centerline in Figure 15 actually exceeds the value from z = 0.04. By z > 0.045 all activity is gradually slowing as vapor is consumed and new particles are no longer forming.

2. Effect of Initial Temperature

A series of simulations without seed aerosol were performed with an initial monomer vapor concentration of 10^{-4} and with T_o' varied from the dewpoint at 101°C to 200°C. In dimensionless coordinates, the temperature profile is that given in Figure 3, valid for no latent heating.

Figure 16 shows the Lothe-Pound nucleation rate for three cases of differing initial temperature. For higher initial temperatures, nucleation along core streamlines occurs later, and at higher rates, than for low initial temperatures. Two competing factors are responsible for the nucleation pulse that occurs along a streamline. While conductive cooling gives rise to an increasing rate of nucleation, depletion of monomer by diffusion to the wall and by the growth of particles that formed earlier along the streamline leads to a decreasing rate of nucleation. (For streamlines away from the immediate vicinity of the wall the loss of monomer to growing particles is by far the predominant sink of vapor.) The time required for the earliest particles to grow and deplete vapor sufficiently to quench nucleation depends on the initial vapor concentration and the initial nucleation rate. During this time, the maximum value of the nucleation rate achieved depends on the rate of cooling along the streamline. In Figure 16, the onset of nucleation occurs at comparable temperatures, but at different cooling rates. The highest cooling rate, for T_o' = 200°C, produces the highest nucleation rate before the growth of previously formed particles sufficiently reduces the vapor concentraition to quench nucleation.

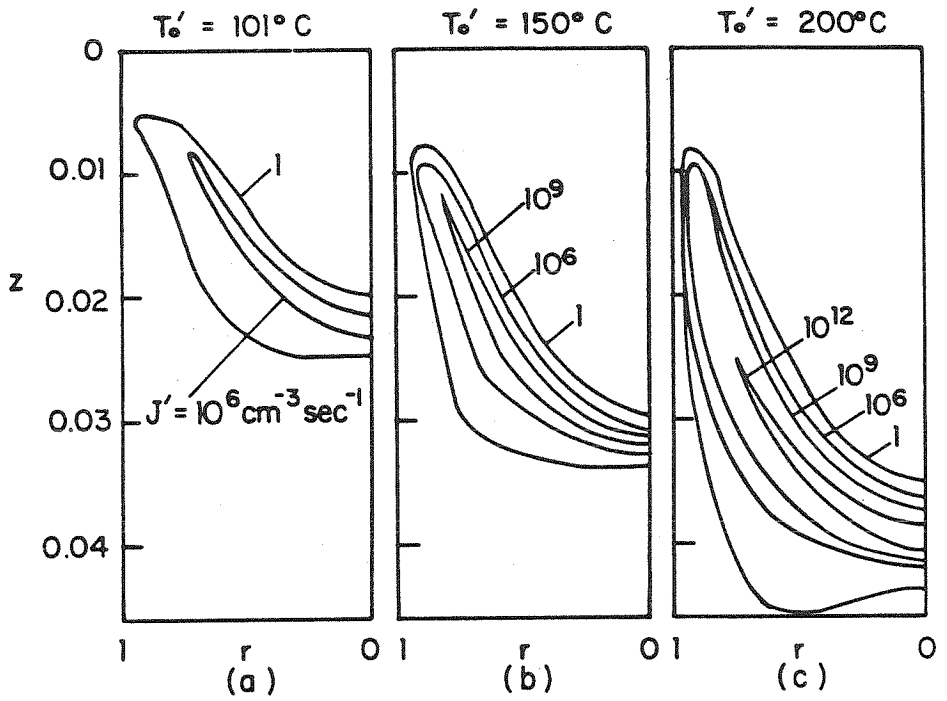

Figure 16. Homogeneous nucleation function predicted by Lothe-Pound theory for several values of inlet temperature. $x_0 = 10^{-4}$, and dewpoint is 101°C.

The average aerosol volume fraction and wall loss in shown in Figure 17. For higher T_o', less aerosol forms near the wall, and tends to form later, providing less insulation against vapor diffusion to the wall, resulting in more wall loss. Figures 18 and 19 show the average number concentration and number-average diameter of aerosol. For T_o' less than approximately 170°C, the dashed lines indicate the average number and diameter not counting the thin layer of fine particles formed by the first pulse of nucleation near the wall. The smooth trend of $\overline{N}'$ and $\overline{d_p}$ given with the dashed lines shows the effects of the cooling rate on the aerosol formed on the main core streamlines. For $T_o' \gtrsim 150°C$, coagulation may be significant and tend to decrease the number and increase the average diameter.

3. Effect of Initial Mole Fraction

Figure 20 shows the monomer mole fraction profiles for three simulations of varying x_o, with $T_o' = 150°C$, and $N_s' = 0$. Figure 20a precedes aerosol formation because of the low vapor concentration. This contrasts to Figures 20b and c with higher vapor concentrations and marked depression of the concentration profiles due to aerosol growth.

Figure 21 shows the Lothe-Pound nucleation function in these simulations. The dilute cases nucleate aerosol late in the axial coordinate, and primarily near the centerline. In the more concentrated vapor situations the high nucleation rate region shifts to the vicinity of the wall. In the dilute case, the region of nucleation is limited by diffusion of vapor to the wall. However, high nucleation rates are achieved in the tube core through the competing effects of much cooling and vapor loss. The cooling rate is small, with an associated slow rise in nucleation rate, but particle growth in the

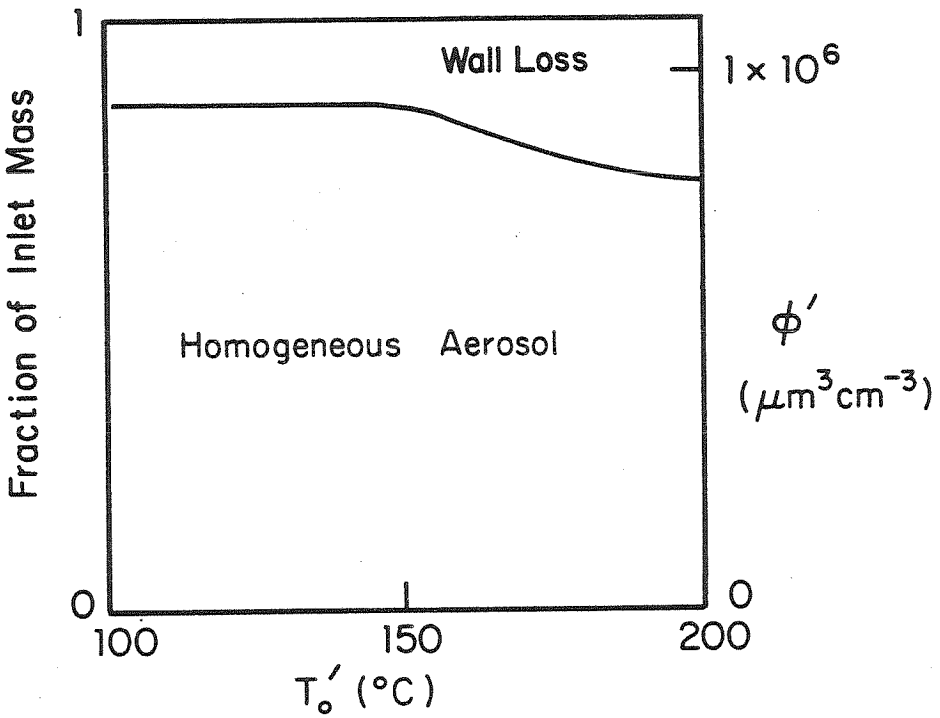

Figure 17. Overall mass balance on condensing species and aerosol volume fraction predicted with Lothe-Pound theory as a function of inlet temperature with no seed aerosol. Same conditions as in Figure 16.

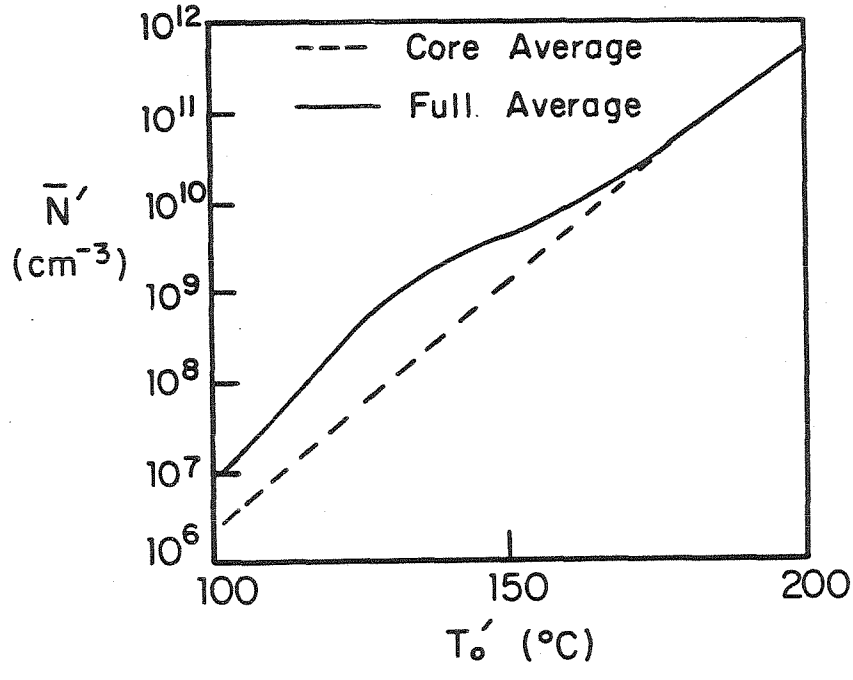

Figure 18. Cup-mixed average total number concentration of homogeneous aerosol predicted with Lothe-Pound theory with no seed aerosol. Dashed line shows average neglecting wall layer of aerosol, $r > 0.9$. Same conditions as in Figure 16.

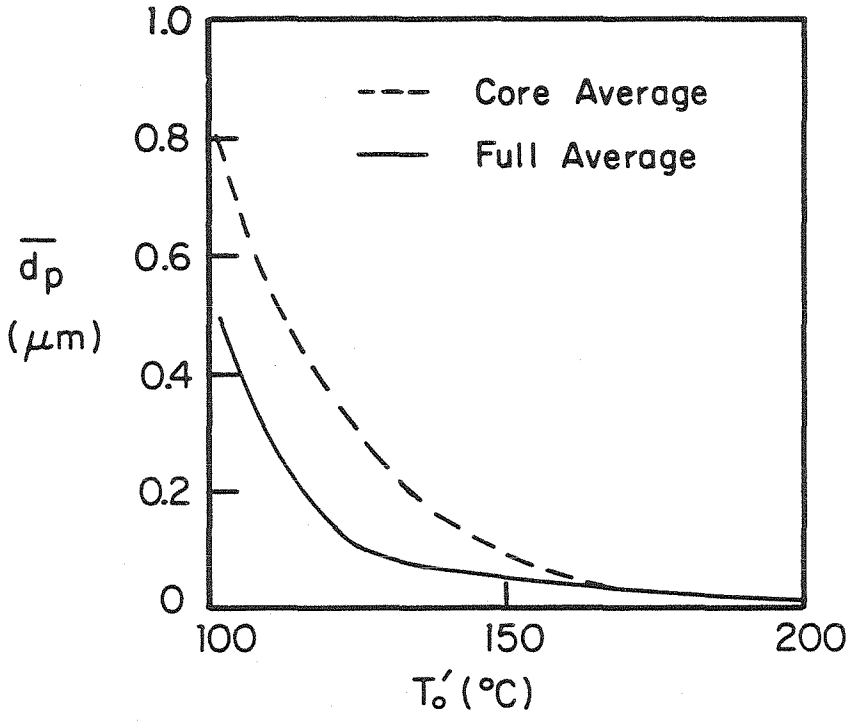

Figure 19. Cup-mixed number average homogeneous aerosol diameter predicted with Lothe-Pound theory with no seed aerosol. Dashed line shows average neglecting wall layer of aerosol, $r > 0.9$. Same conditions as in Figure 16.

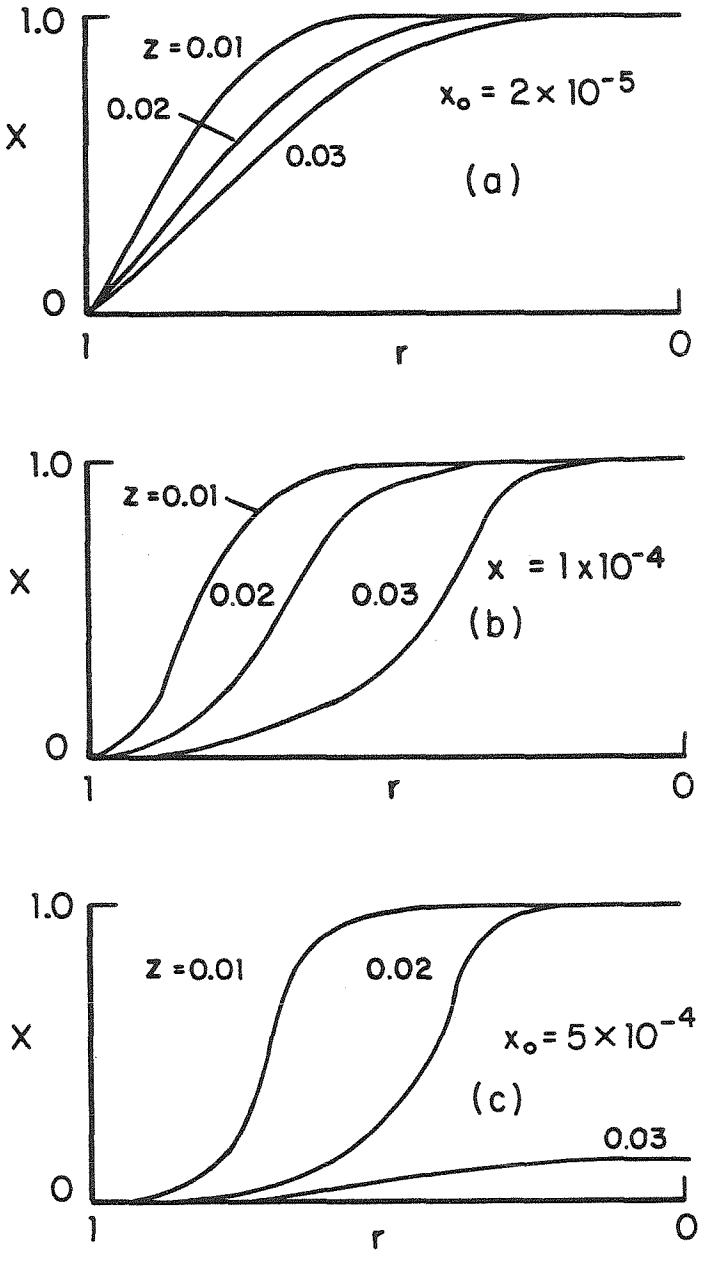

Figure 20. Vapor mole fraction profiles without seed aerosol predicted with Lothe-Pound nucleation theory for several initial values of mole fraction. $T_o' = 150°C$.

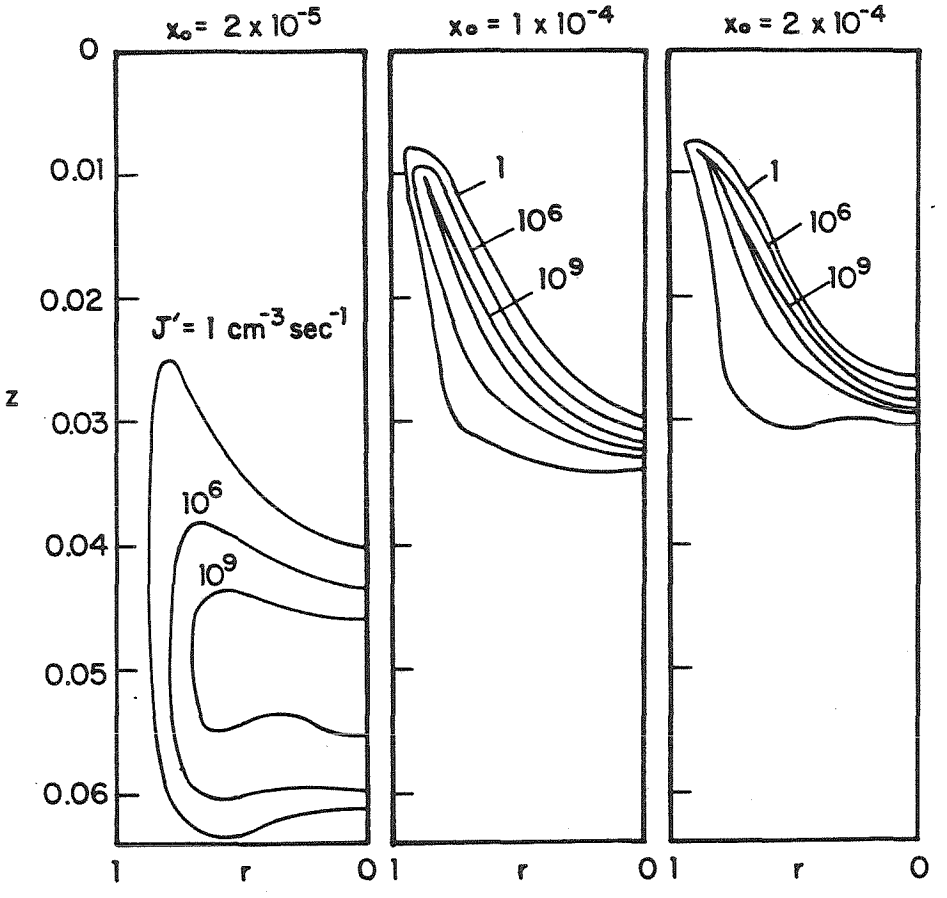

Figure 21. Profiles of homogeneous nucleation rate predicted by Lothe-Pound theory without seed aerosol, for several values of initial mole fraction. Same conditions as in Figure 20.

dilute vapor is slow enough to yield a relatively small vapor loss until much farther downstream. Therefore initially dilute vapor yields a longer nucleation pulse than initially higher vapor concentrations.

The resulting average number concentration of these simulations is shown in Figure 22. The general decreasing trend in $\bar{N}'$ as x_o increases is due to the greater vapor sink and consequential nucleation quenching for increasing x_o. The low deviation on the left side of Figure 22 is due to the absence of particle generation near the wall.

Figure 23 shows the average volume distributions of these simulations. While the total number was highest for the most dilute case, the volume fraction and average particle size are much less for that case. A systematic increase in both volume and average diameter is seen with increasing x_o. In the more concentrated vapor simulations, the aerosol in the wall region begins to show volume in a region of smaller particles, skewing the volume distribution for those cases. The critical nucleus size is indicated on the figure.

The aerosol in the wall region is responsible for shielding the flow stream from vapor loss to the wall. Therefore the simulations for $x_o \gtrsim 10^{-4}$ yield low wall losses, as shown in Figure 24. Below the transition point, the wall losses appear to depend linearly on the initial vapor concentration.

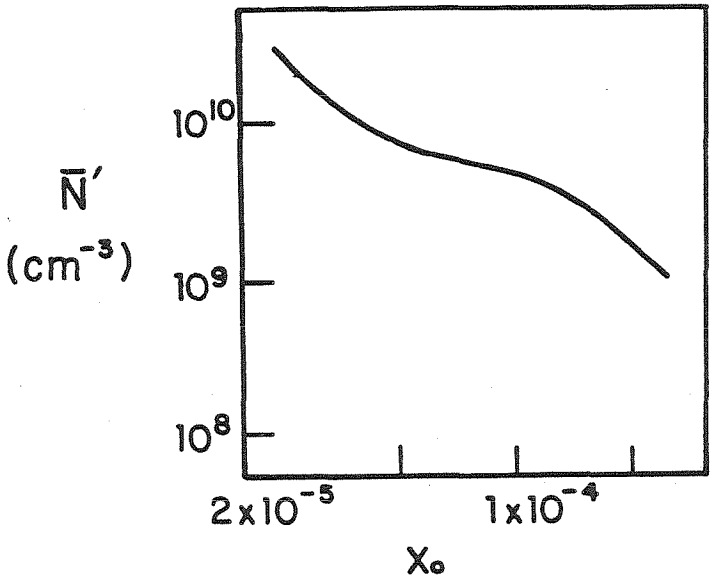

Figure 22. Cup-mixed average homogeneous aerosol number concentration without seed aerosol, predicted by Lothe-Pound theory. Same conditions as in Figure 20.

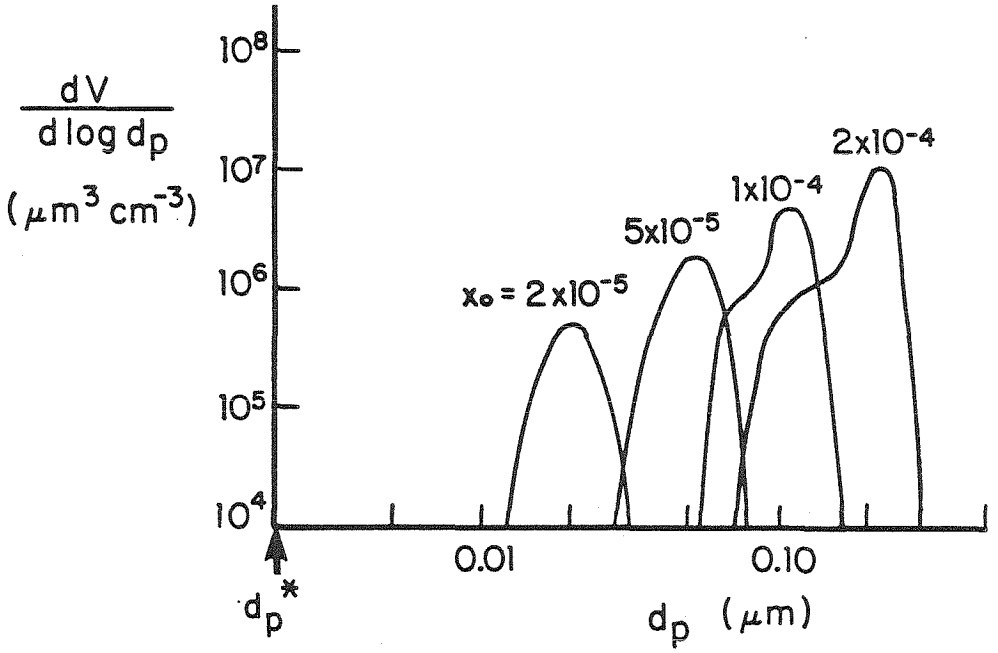

Figure 23. Cup-mixed average homogeneous aerosol volume distributions for several values of initial mole fraction, with no seed aerosol. Diameter of critical nucleus is indicated. Same conditions as in Figure 20.

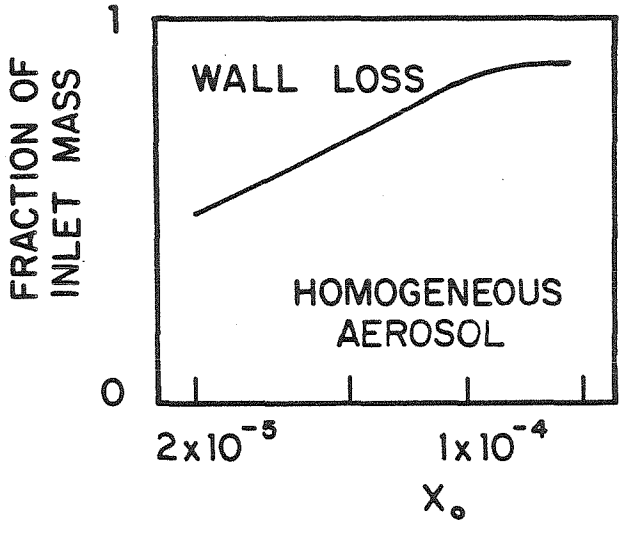

Figure 24. Overall mass balance on condensing species for Lothe-Pound theory, with no seed aerosol. Same conditions as in Figure 20.

Chapter 4

EXPERIMENTAL APPARATUS AND TECHNIQUE

The experimental system was designed to generate aerosol continuously in a well-characterized flow. In the basic configuration, a fully developed laminar pipe flow of a well mixed, isothermal, undersaturated condensable vapor is cooled by a sudden drop in wall temperature. Dibutyl phthalate was chosen as the condensing species because of its high boiling point, low diffusivity, and its common use in aerosol generators.

4.1 Laminar Flow Aerosol Generator

The laminar flow aerosol generator is illustrated in Figure 25. The laminar flow section is a 118 cm long stainless steel (type 316) tube with an inside diameter of 1.73 cm (3/4" O.D. x 0.035" wall). The aerosol generator is vertical with the heated inlet at the top in order to minimize buoyancy induced secondary flows. An aluminum honeycomb flow straightener is inserted about 10 cm from the entrance to the pipe. The hydrodynamic entry length is less than a few centimeters at the Reynolds numbers of interest ($Re < 250$), corresponding to flow rates of under 3 standard liters per minute. The upper end of the flow tube is wrapped with a heating tape and fiberglass pipe insulation (8.9 cm O.D.). Variable spacing of the heating tape, illustrated in Figure 26, was used to achieve a uniform wall temperature. Electrically insulated Chromel-Alumel thermocouples were cemented (Sauereisen No. 33 high-temperature cement) onto the outer surface of the tube at positions illustrated in Figure 26 to facilitate wall temperature profile measurement. At the maximum design flow rate of 3 ℓ/min the dimensionless length of the hot zone, z defined by Eq. [18], is

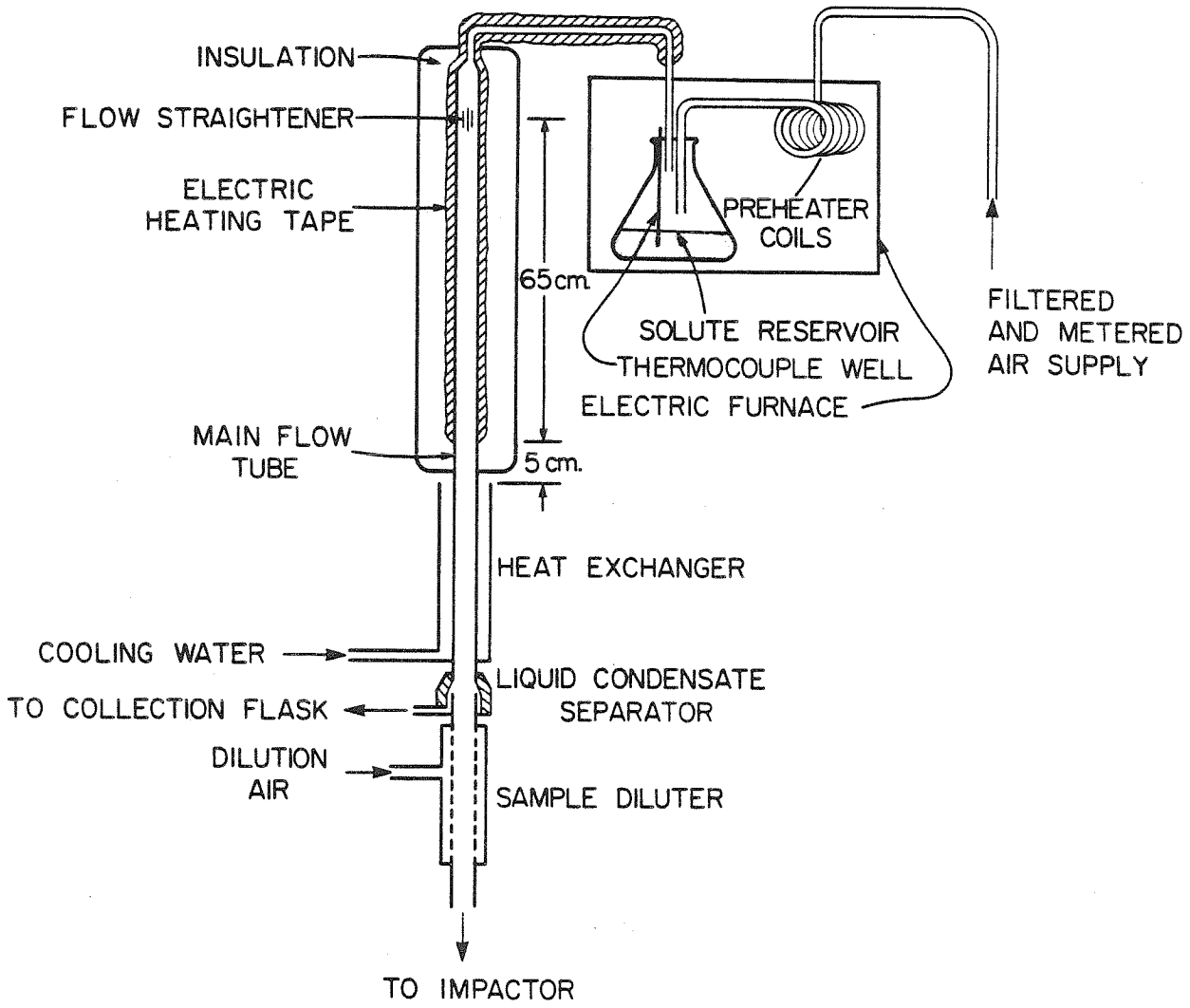

Figure 25. Schematic diagram of experimental apparatus.

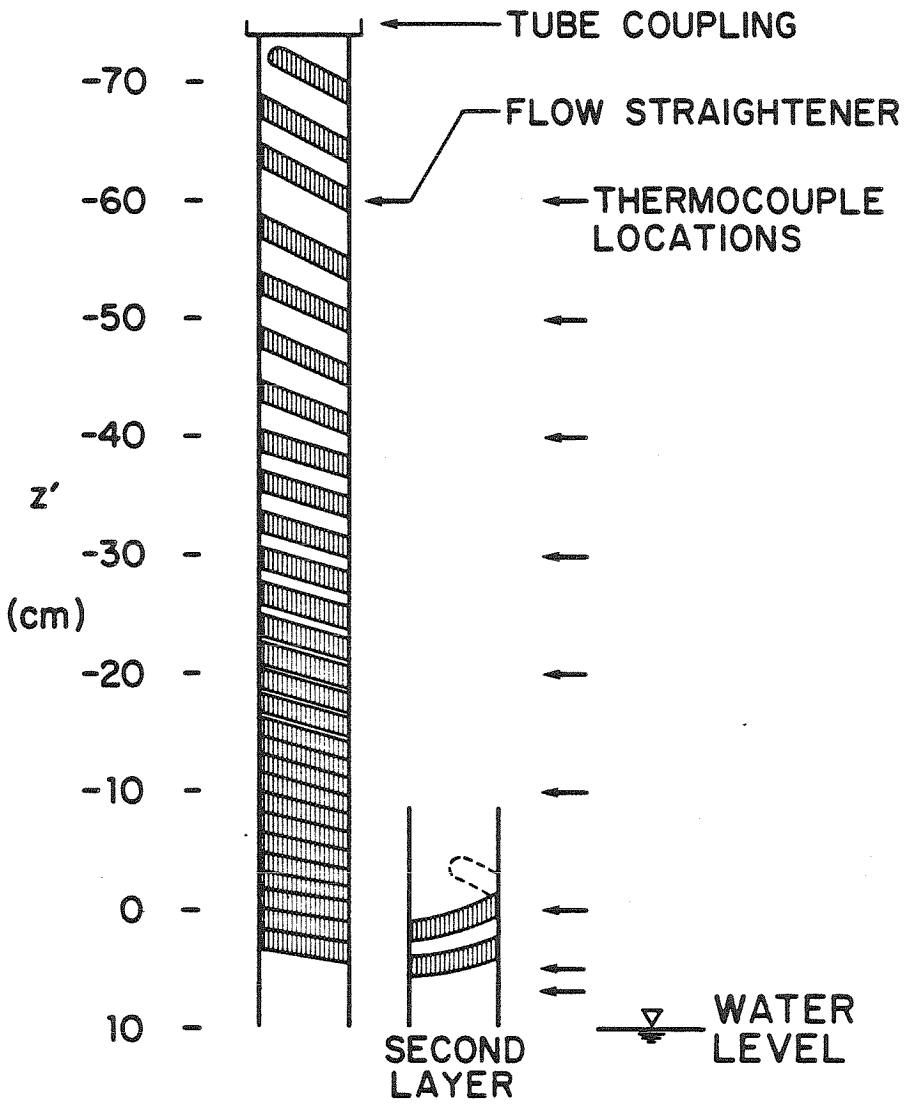

Figure 26. Detail of hot zone, depicted without thermal insulation.

$$z = \frac{65 \text{ cm}}{0.864 \text{ cm}} \frac{0.0282 \text{ cm}^2 \text{ sec}^{-1}}{2(0.864 \text{ cm})(21 \text{ cm sec}^{-1})} = 0.059$$

This length is adequate to reduce any thermal nonuniformities to less than 10 percent of their initial value. Thermal damping is greater at lower flow rates. As illustrated in Figure 27, flow tube cooling is achieved by a water jacket extending from z' = 10 cm to z' = 40 cm. This provides a uniform wall temperature of 25°C and removes most of the heat load of the gas stream.

Figure 25 also shows the auxiliary equipment which is necessary for the operation of the aerosol generator. This includes the vapor source, wall condensation separator, and sample dilutor.

The wall condensation separator is a 0.3 cm gap in the wall 5 cm below the end of the water jacket. As shown in Figure 27, the gap has edges at 45°C and is blocked to prevent gas flow. The sample dilutor is a porous stainless steel tube (1.9 cm I.D. x 15 cm, 10 μm pore size) with an external jacket to deliver metered air flow. For flow rates and dilution ratios of interest, the flow is laminar throughout the dilutor. A 15 cm length of Tygon tube (1.9 cm I.D.) connects the dilutor to the cascade impactor. A 0.64 cm hole in the side of the tube permits venting of sample flow for sampling a constant aerosol source at various flow rates.

The vapor source is a heated reservoir with constant surface area as illustrated in Figure 25. The laboratory air supply is regulated by a pressure regulator (Matheson 3473) and filtered (Gelman 12501-1, 0.45 μm pore size). The flow is metered and delivered to the evaporator oven with standard 1/4" copper tubing. Pure air, preheated in a 200 cm coiled tube, is

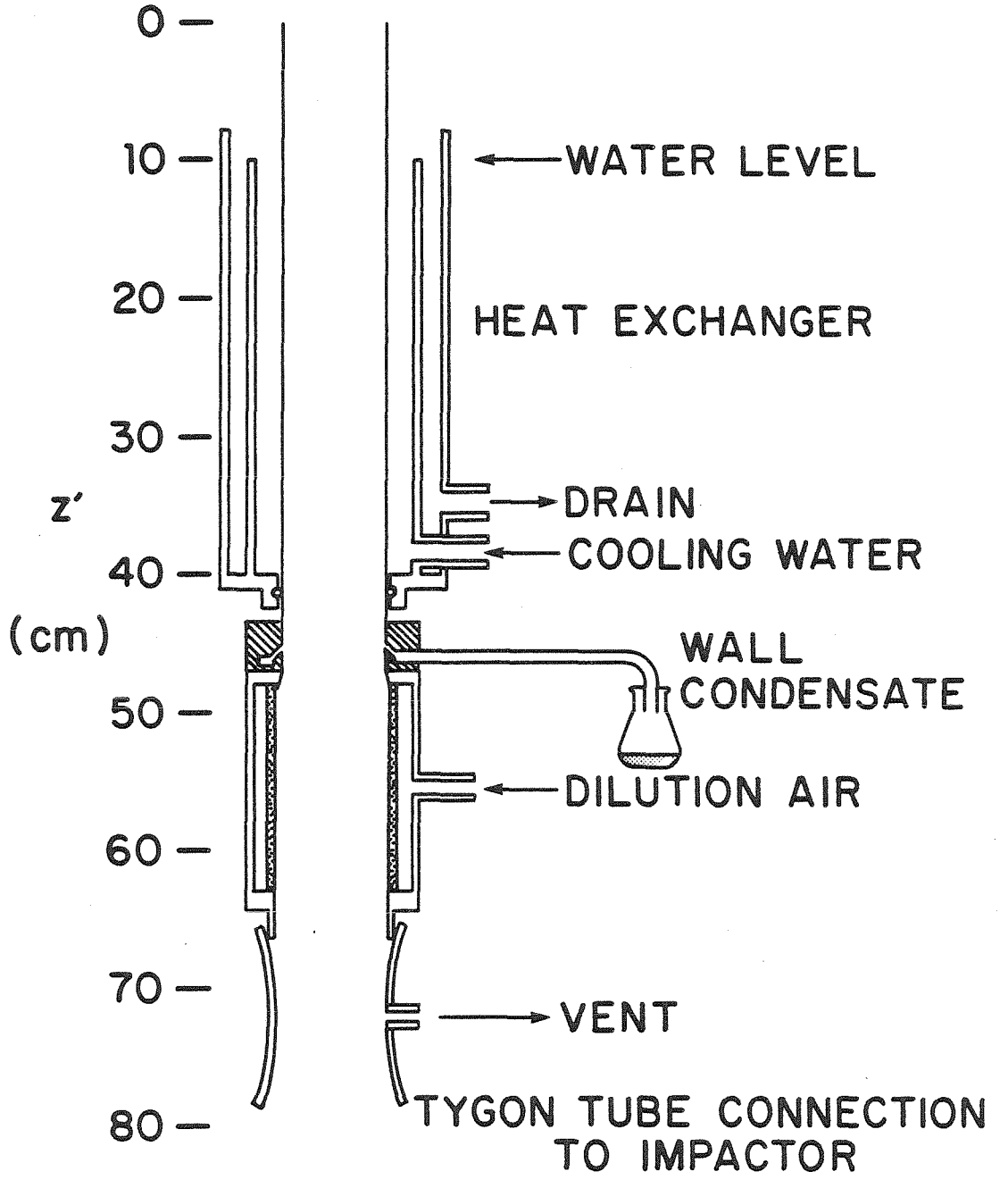

Figure 27. Detail of cool zone.

delivered to a 250 ml Erlenmeyer flask containing approximately 75 ml dibutyl phthalate. The flask is sealed with an aluminum head clamped with a greased Neoprene o-ring. In addition to inlet and outlet ports, a 0.48 cm sealed glass-tube thermocoupled well is mounted in the head, to facilitate temperature measurement at the liquid-gas interface. The evaporation rate was determined gravimetrically. The mass loss from the evaporation flask was determined after an extended period of operation, typically 10 hours. The measured vaporization rates of dibutyl phthalate are summarized in Table 5. If the mass transfer coefficient is a function of only the flow rate of the carrier gas, the evaporation rate may be assumed to be proportional to the saturation pressure at the interfacial temperature. For temperatures less than 120°C, the outlet vapor concentration was 45±5 percent of the saturation concentration.

Parameters which influence the operation of the aerosol generator include: air flow rate, vapor concentration and wall temperature profile. Typical wall temperature profiles at steady state, achieved after about three hours of operation, are illustrated in Figure 28. The hot zone temperature is very uniform for relatively low operating temperatures. The variation in temperature increases as the wall temperature is increased. The characteristic hot-zone temperature was defined as that measured at $z' = -20$ cm.

4.2 Aerosol Measurements

The primary instrument used to analyze aerosol generated in the laminar flow aerosol generator was the Sierra Instruments Model 268-K1 single jet cascade impactor. The characteristics of this instrument have been extensively studied, e.g., by Rao and Whitby.(22) This impactor has eight stages

Table 5. Evaporator Outlet Concentrations

T interface (°C)	x_o/x^{sat}
200	0.65
180	0.65
118	0.45
100	0.51

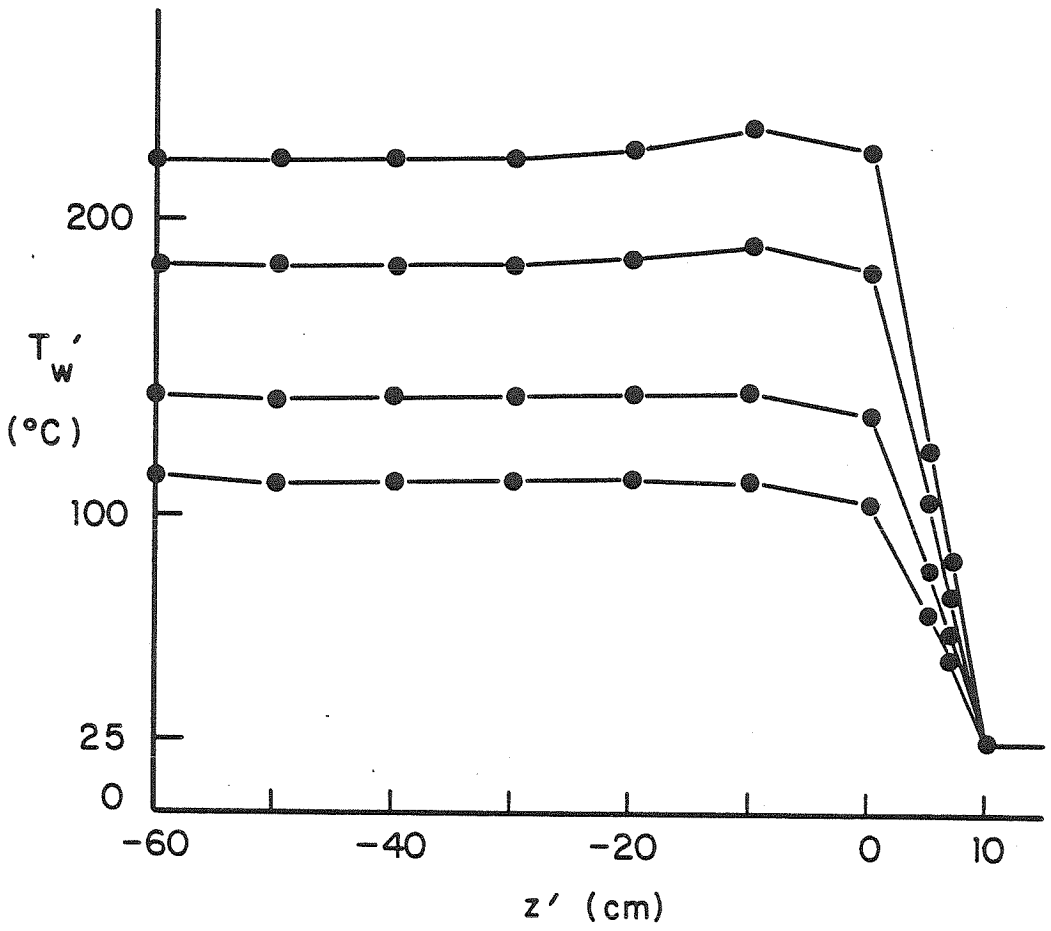

Figure 28. Typical wall temperature profiles.

and a final filter. The collection efficiency curves are sufficiently sharp to allow nearly complete separation of particles which differ by 0.1 log units in diameter. The stages of the impactor are selected to give 50 percent cut-off diameters (d_{50}) separated by approximately 0.3 log units, as illustrated in Figure 29. Collection times were chosen to obtain impactor samples sufficiently large (approximately 1 mg) for weighing, yet small enough to avoid overloading the collection surfaces. Impactor plates were weighed on a Mettler Micro Balance (accuracy of approx. ± 0.005 mg, tare wt. approx. 130 mg).

Because the size cuts are sharp, size resolution better than 0.3 log units may be achieved by collecting several samples from a constant aerosol source with the impactor operating at several different flow rates and then suitably differencing the resulting sample masses. The dilution air flow rate was varied in order to alter the impactor size cuts. Errors of a few percent in the sampling times caused proportional deviations in the total collected mass of each run. The fractional distributions of mass on the collection plates, however, are independent of sampling time. The average total mass is used to renormalize the data, and thereby remove the errors of sampling time on the shape of the measured size distribution function. The next step is to form a cumulative mass distribution function, based on fraction of total mass, from each of the impactor runs. A sample of such a cumulative distribution function from actual data is shown in Figure 30a. The data should lie on a monotonically increasing curve. Occasionally, a small inconsistency may arise in the data, such as the point at 1.0 μm on Figure 30a. All impactor data for a given constant aerosol source describe, in principle,

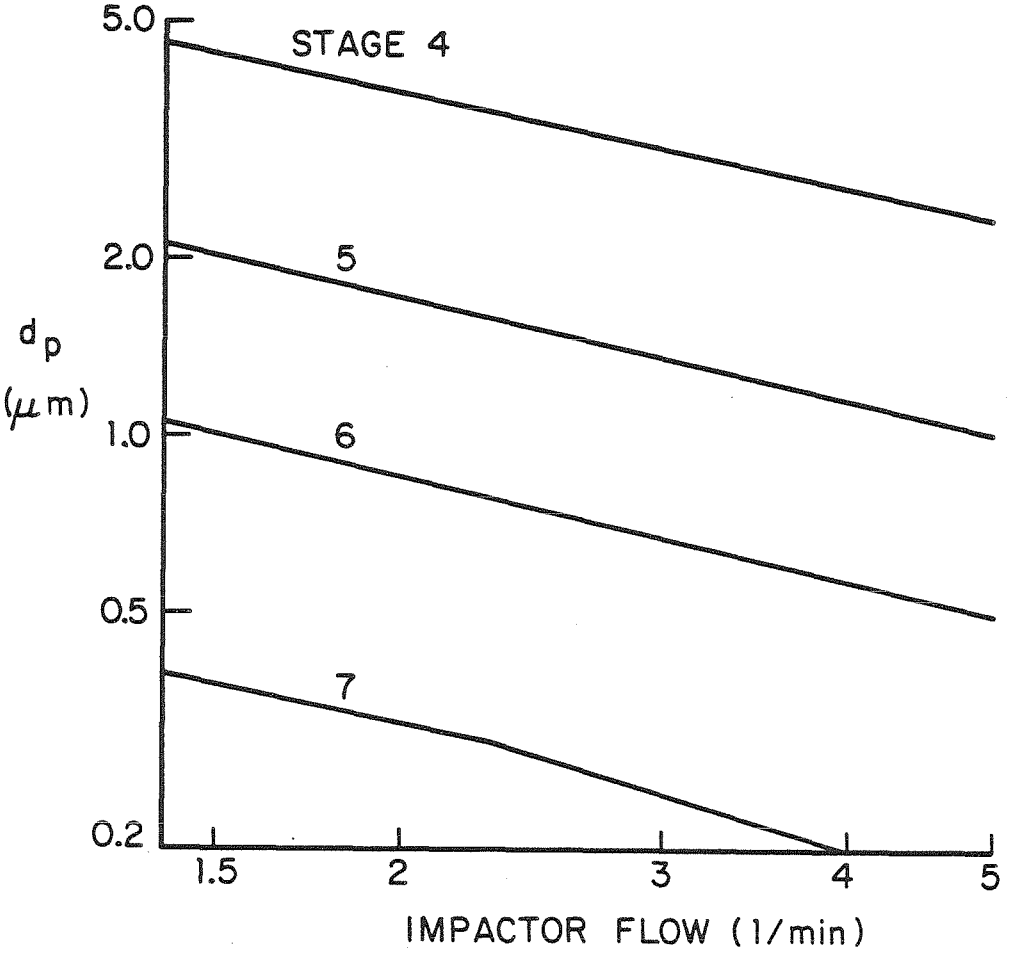

Figure 29. Fifty percent cutoff diameters for the Sierra impactor.

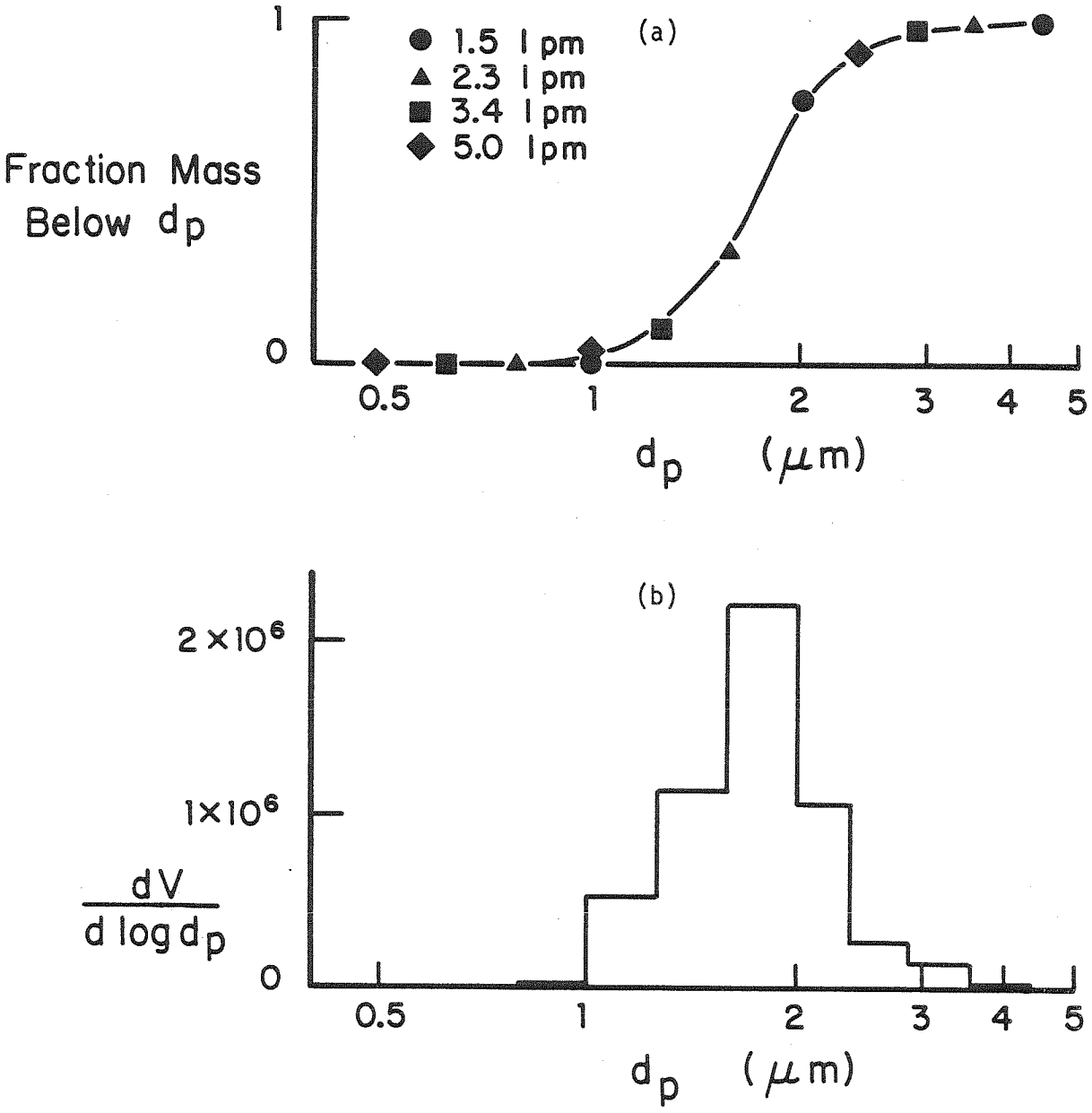

Figure 30. (a)Cumulative particle volume distribution from Sierra impactor data at four flow rates specified. Flow rate before dilution was 1.5 ℓ/min, $T_0' = 189°C$ and $x_0 = 9.35 \times 10^{-5}$.
(b)Particle volume distribution from cumulative distribution of (a).

the same cumulative distribution, as in Figure 30a. Consecutive points on this distribution are differenced and a histogram of volume distribution is constructed, as shown in Figure 30b.

In addition to the cascade impactor, a Condensation Nuclei Counter (Environment One Corporation, Model E-1033a-0016) was used to measure total number concentration of aerosol and check consistency of the impactor data.

Chapter 5

EXPERIMENTAL RESULTS

The Sierra impactor was used to measure particle volume distributions for a number of operating conditions, i.e., hot zone temperature, initial mole fraction and volumetric flow rate. Due to the large particles generated by this apparatus ($d \gtrsim 1$ μm), sizing by optical particle counter or electrical mobility analyzer was not possible.

Figure 31 shows volume distributions measured at constant initial vapor mole fraction, $x_o = 1 \times 10^{-4}$, a constant flow rate of 2.9 ℓ/min, for various hot zone temperatures. For T_o' less than approximately 210°C, the mean particle size is about 2 μm diameter. Within that range of T_o', a slight variation is detected in the shape of the distribution. The volume distributions are reproducible to within 20 percent deviation for all size ranges. The distribution at $T_o' = 162$°C is reproducibly though not greatly shifted to the left of the distributions at either $T_o' = 128$°C or 193°C. For hot zone temperatures above 210°C, the mean particle diameter shifts significantly toward smaller diameter. One anomalous channel appears in Figure 31 just above 1 μm diameter. This channel shows a consistent spike, an artifact of having chosen too small an interval (0.05 log units) for adequate particle separation. The volume indicated in this interval probably belongs to one or both of its neighboring intervals. Data collected with cutoff diameters selected as in Figure 30, with intervals not less than 0.1 log units wide, do not indicate any spurious channels. The data in Figure 31 were collected entirely on impactor stages numbered 4, 5, 6 and 7, with no aerosol of smaller diameter appearing on the afterfilter (Millipore FALP04700, 47 mm diameter, 1 μm nominal pore size). The number average particle diameter

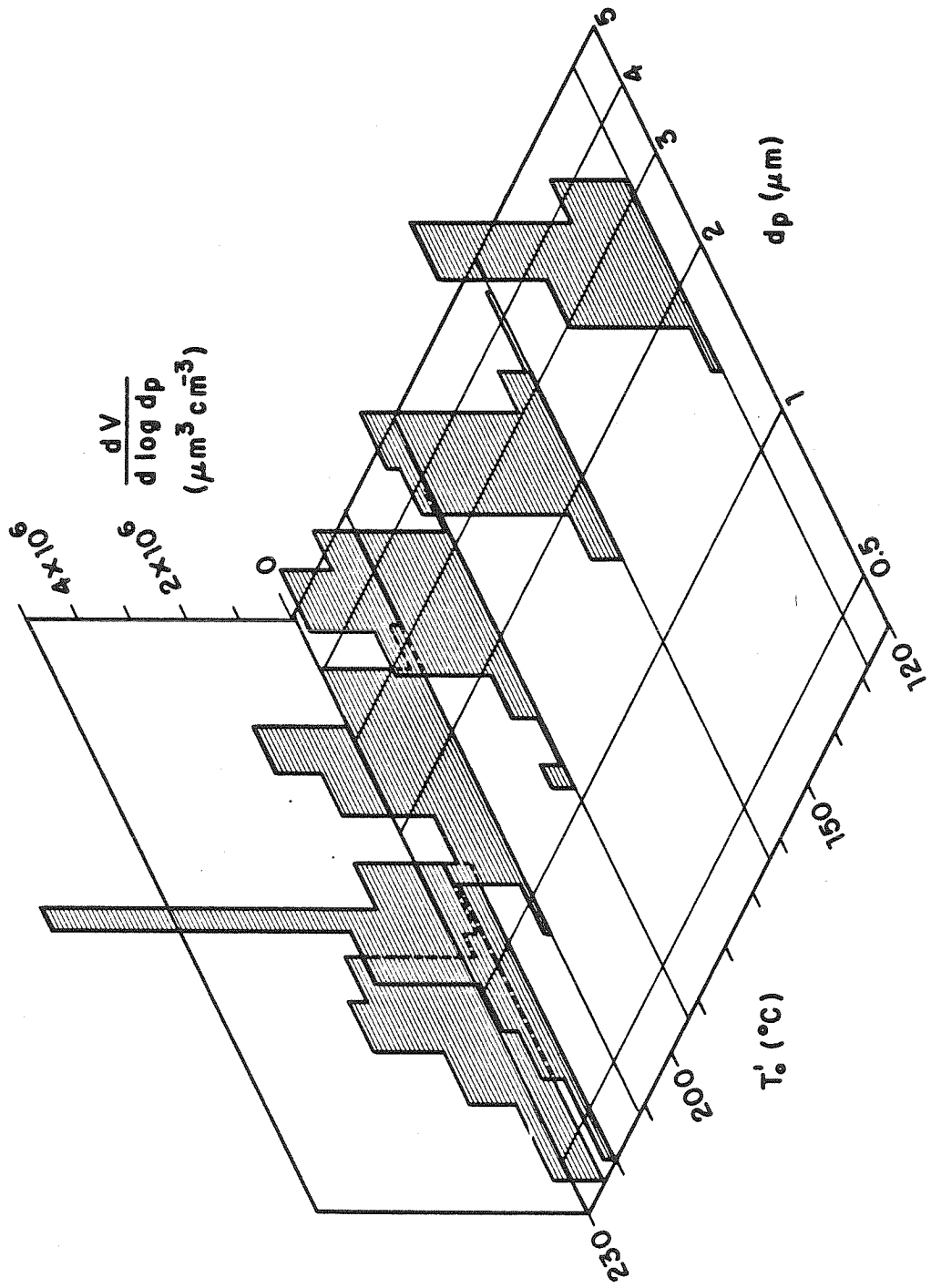

Figure 31. Measured particle volume distributions at several initial temperatures. Flow rate before dilution was 2.9 ℓ/min, $x_o = 9.1 \times 10^{-5}$ and impactor flow rates were 1.4, 2.0, 2.8, and 4.0 ℓ/min.

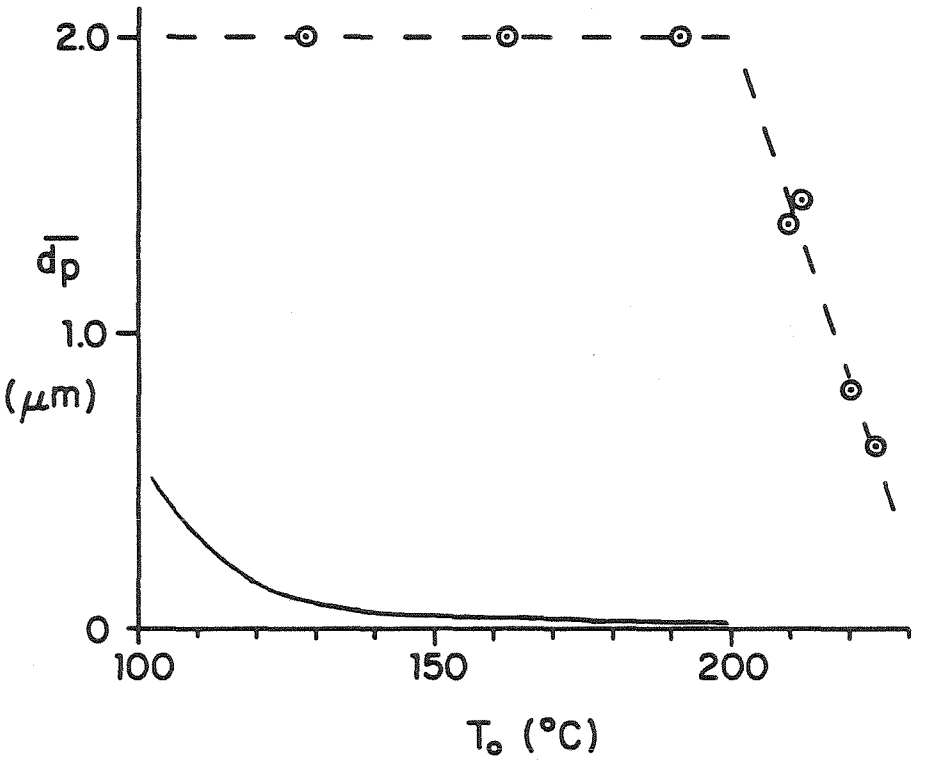

Figure 32. Number average particle diameter from ——theory, and – – – Sierra impactor data.

is shown in Figure 32 for the same data is shown in Figure 31 plus a duplicate run at 209°C. At hot zone temperatures between the dewpoint (101°C) and 200°C, the mean particle diameter was 2.0 μm. The average diameter steadily decreases with increasing temperature above 200°C. The predicted average diameter is an order of magnitude less than observed.

The dependence of aerosol volume fraction on the hot zone temperature at constant initial vapor mole fraction is plotted in Figure 33. The volume fraction of aerosol for the initial condition of $x_o = 1 \times 10^{-4}$ which would result if no vapor were lost by diffusion to the walls is 1.1×10^6 $\mu m^3\ cm^{-3}$, illustrated by the broken line. The total aerosol volume concentration varies from 60 to 90 percent of that value. The theoretical prediction (indicated by the solid curve) is approximately the same magnitude as observed. In contrast to the data, the predicted volume concentration decreases with increasing temperature. The higher-temperature data may reflect some influences of incomplete cooling and growth occurring for higher initial temperatures, possibly resulting in some collection of vapor directly by the impactor. The theory, however, predicts that approximately ten percent of the initial vapor remains uncondensed at the entrance to the dilutor. Figure 34 shows the theoretically predicted profiles of uncondensed vapor mole fraction for several values of the hot zone temperature.

The theory predicts an average particle concentration of about 10^9 cm^{-3} at submicron mean diameter, with most of the initial vapor converted to aerosol. The data show a similar fraction vapor converted to aerosol, but an average diameter ten times greater, and an average number concentration of only $10^5\ cm^{-3}$. Theory also predicts that if the concentration of particles were much less than the simulated $10^8\ cm^{-3}$ in the wall

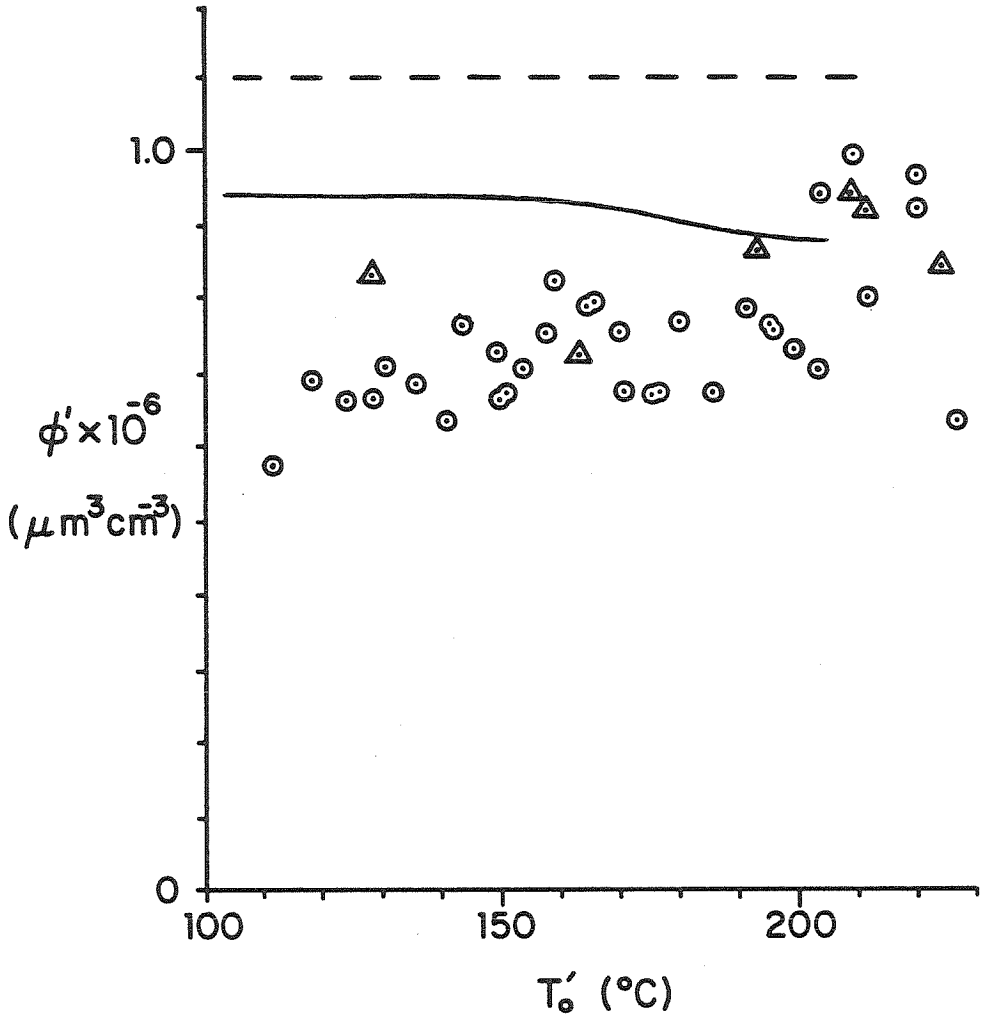

Figure 33. Average total aerosol volume fraction from theory and Sierra impactor data. — — — Maximum, corresponding to initial vapor, ———theory, △ data of Figure 32 and ⊙ other data.

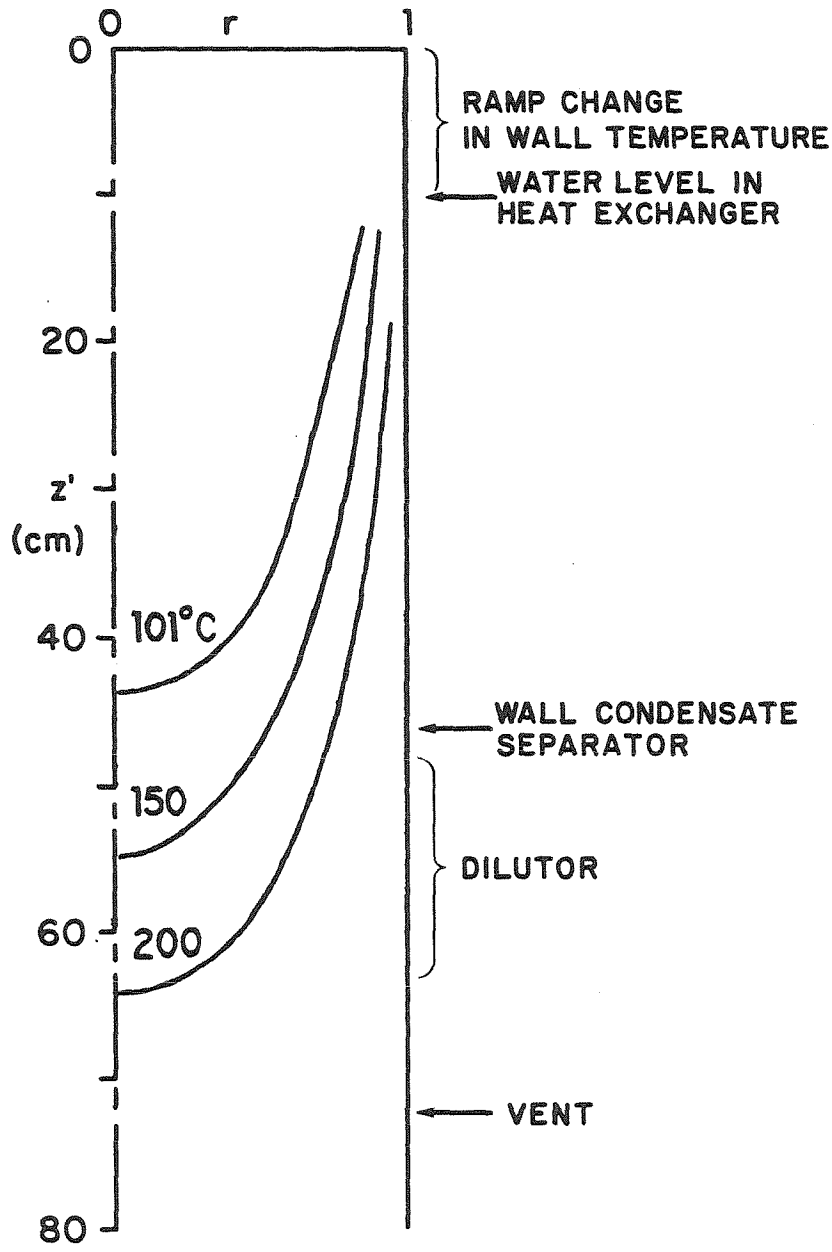

Figure 34. Theoretical profiles of uncondensed vapor in the experimental apparatus. For the indicated values of T_0', isopleths are given for $x = 0.10\, x_0$.

region of the flow, less than ten percent of the initial vapor would be found as aerosol. Wall losses of vapor would then account for the greater portion of the initial vapor. It appears, therefore, that the observed aerosol characteristics must be due to some significant coagulation effects in either the flow tube system or the Sierra impactor, or both, although Brownian coagulation has been shown to be insignificant (Appendix B). Coagulation could not be important very early in the cooled section of the tube or the lack of a dense layer of particles of 10^8 cm^{-3} concentration along the wall would result in increased wall condensation. The vapor-consuming effect of this cloud must prevail for most of the length of the cool zone, while vapor in the tube core condenses onto particles. The effects of thermophoretic diffusion have been calculated by the method of Hirschfelder, et al., (29), and have been shown to be negligible (Appendix E).

Figures 35a and b show experimentally measured aerosol volume distributions at different initial mole fractions. Figure 35b is plotted on 10^2 smaller vertical scale than Figure 35a, showing a 100-fold decrease in aerosol volume for a ten-fold decrease in initial mole fraction. In Figure 36, total aerosol volume fraction is normalized by initial mole fraction equivalent to show the fraction of inlet mass converted to aerosol, at constant hot zone temperature. The data fall generally above the theoretical prediction, but have the same general trend with initial mole fraction.

Figure 37 shows aerosol volume distributions collected at nominal flow rate of 2.9 ℓ/min, and 1.5 ℓ/min. The distributions are similar in form, but the aerosol volume fraction from the 1.5 ℓ/min experiment is smaller. The average diameter is only slightly less for the aerosol from the case of

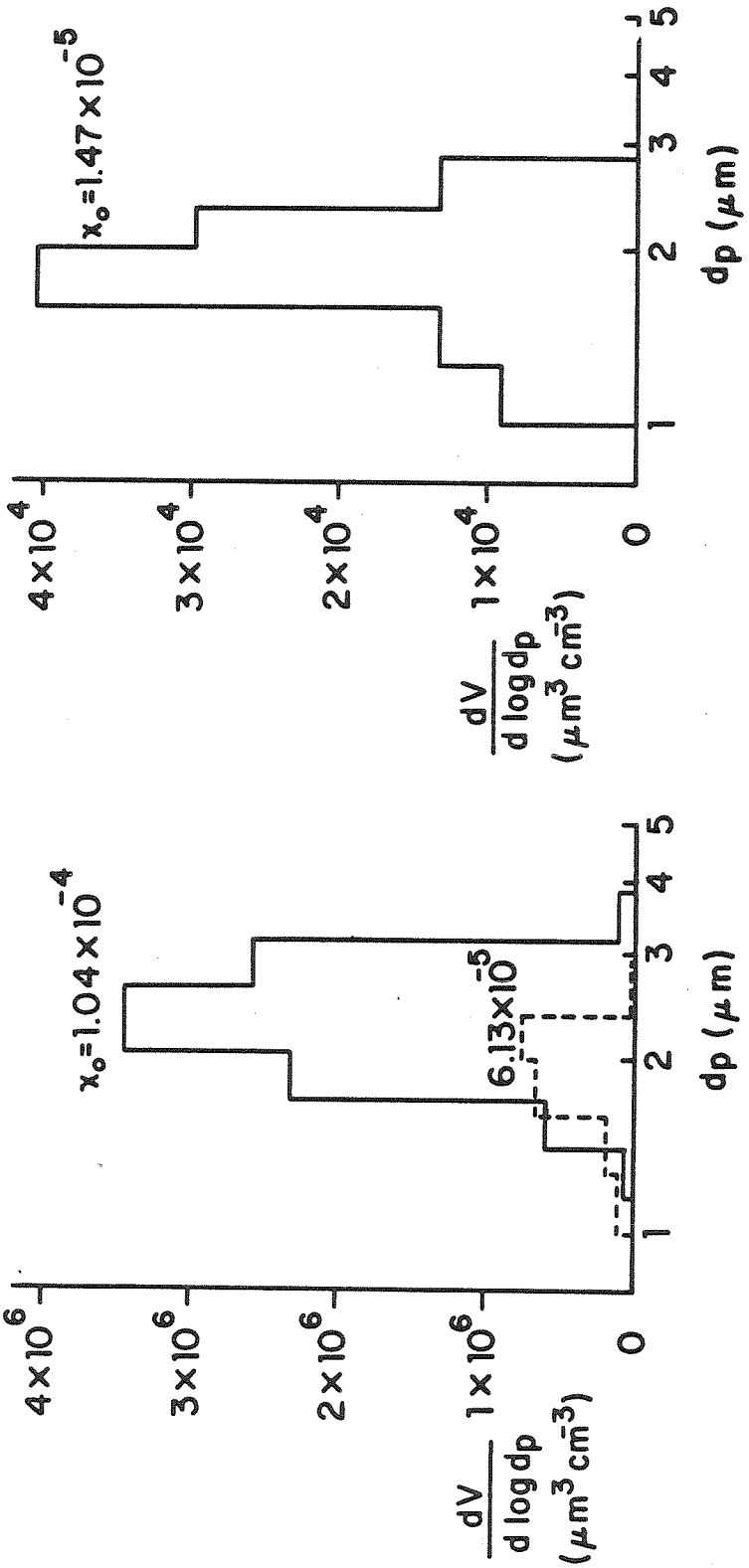

Figure 35. Average particle volume distributions from Sierra impactor data at several initial mole fractions.

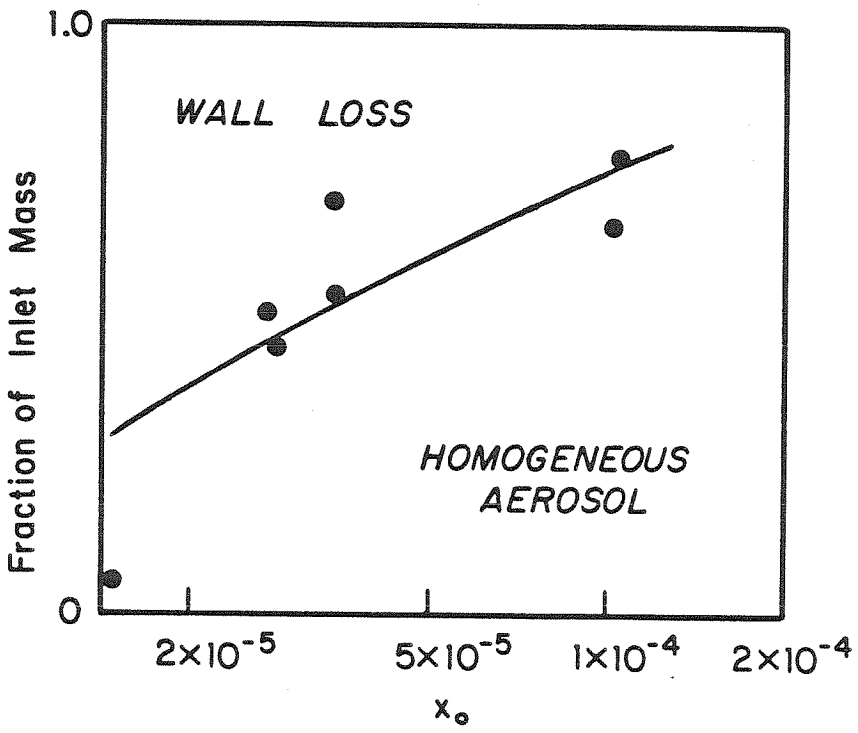

Figure 36. Dibutyl phthalate mass balance from theory and Sierra impactor data, $T_0' = 192°C$.

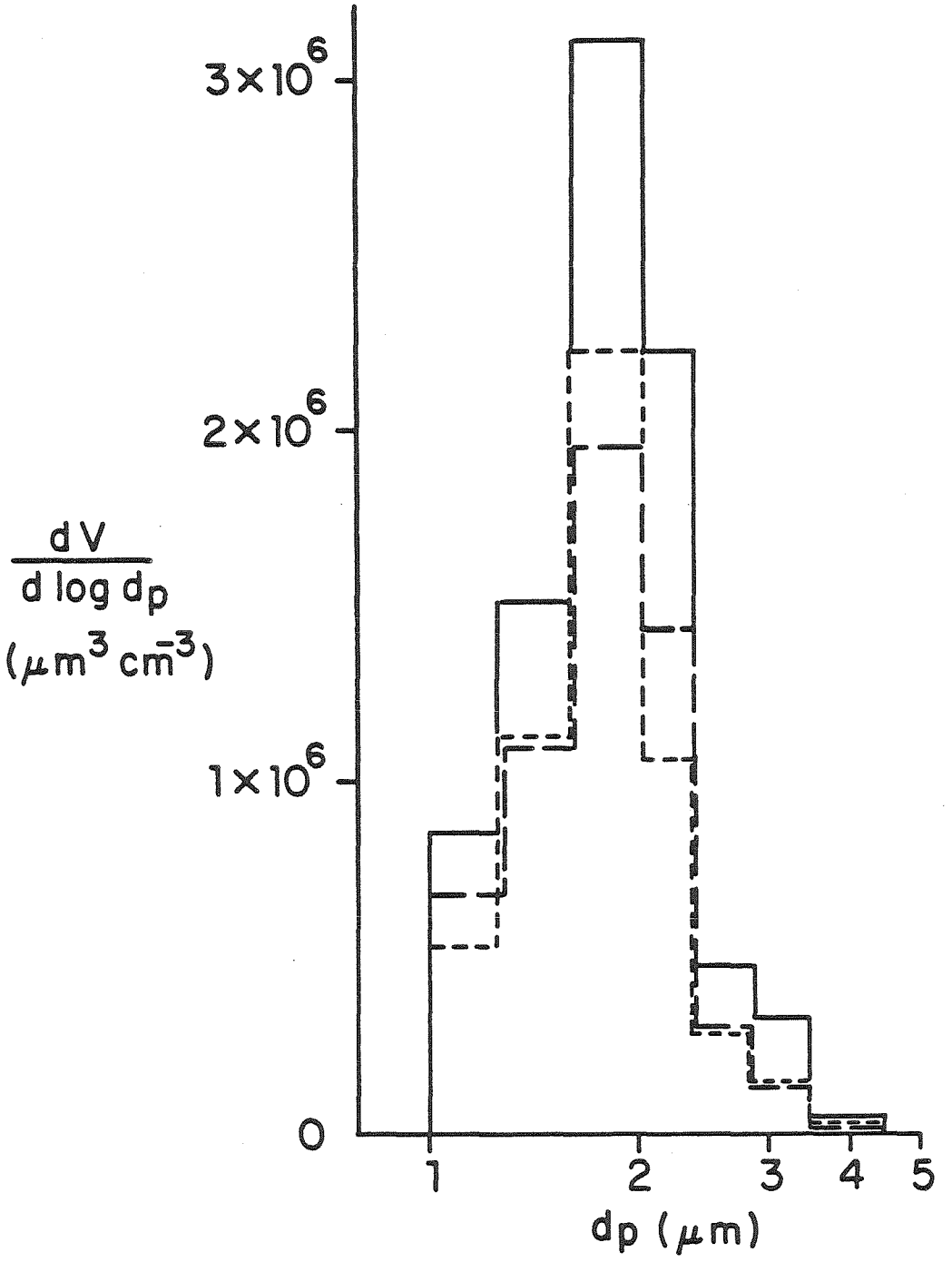

Figure 37. Dependence of aerosol volume fraction on flow rate. Flow rates before dilution: ——— 2.9 ℓ/min, — — — 1.5 ℓ/min, ----- 1.5 ℓ/min.

lower flow rate. This is consistent with the model prediction of greater vapor losses due to fewer particles created by the lower cooling rate at the lower flow rate.

As a consistency check of the cascade impactor data, the Condensation Nuclei Counter (CNC) was used to measure total aerosol number concentration at several nominal operating conditions. The CNC measured number concentrations of the same order of magnitude as those of the impactor, with a typical negative deviation of about a factor of two or three. This deviation is likely to be due to the losses of aerosol in the sampling tube of the CNC.

Chapter 6

DISCUSSION AND CONCLUSIONS

Partial agreement is shown between experimental data and theory incorporating the Lothe-Pound nucleation model. The overall mass balance on the dibutyl phthalate shows fair agreement between experiment and theory, but the outflowing aerosol mean particle diameter is underpredicted by theory by an order of magnitude, with a corresponding overprediction of number concentration by four orders of magnitude. The discrepancy cannot be explained by Brownian coagulation effects (Appendix B) or by thermophoretic diffusional effects (Appendix E).

The model prediction of aerosol size and number concentration at the cooling site within the tube is well supported by the experimental data on the overall mass balance of dibutyl phthalate. The only mechanism which can be responsible for the low wall losses observed is the large sink of vapor near the wall. This sink is adequate to account for the mass balance data only if the particle concentration in the vicinity of the wall exceeds 10^8 cm^{-3}. Therefore, simulations with a different nucleation theory, giving lower nucleation rates and agreement with the observed output average aerosol number concentration, will predict very high wall losses of vapor. Also, because vapor losses to the wall and particle growth are diffusional processes competing for available vapor, uncertainty in the mass diffusivity could not account for observed particle volumes which are four orders of magnitude greater than the predicted particle volumes. A reduction in the mass diffusivity of 20 percent, for example, has the following effects on the model predictions: (i) diffusional vapor loss decreases relative to

conductive cooling, increasing the nucleation rate and producing an order of magnitude increase in the aerosol number concentration near the wall; (ii) the loss of vapor to the wall is reduced from 16 percent to 9 percent due to the greater sink of vapor near the wall; (iii) the average particle diameter is reduced from 0.06 μm to 0.04 μm. In comparison, increasing the mass diffusivity parameter results in a smaller number of larger particles. At the same time the aerosol volume fraction decreases due to increased wall losses of vapor. An adjustment in the mean free path parameter affects only the particle diameter at which the slower, kinetic-limiting growth rate undergoes transition to the faster, diffusion-controlled growth law where most dibutyl phthalate particle growth occurs. A ten percent correction to the mean free path in the model causes the ultimate aerosol mean diameter to change about ten percent.

The discrepancies described above have not been resolved with the experiments on dibutyl phthalate. While the accuracy of the Lothe-Pound nucleation theory is well supported by the mass balance data, some unknown process may be occurring downstream of the initial nucleation zone. The dibutyl phthalate could be partially oxydizing or polymerizing in the hot zone, although such observations have not been reported in the literature. Nitrogen or other inert carrier gases may be used to prevent oxidation. Other esters have been used for studies in condensation aerosol generators (dioctyl phthalate (16), diethylhexylsebacate (23)), and organic acids (octenoic acid (6), linolenic acid (9)). These substances may be studied in the laminar flow aerosol generator. Other high boiling point organic solvents (24) are potentially suitable for this study: terpineol, B.P. =

220°C, melting point 40°C, tetrahydronaphthalene, B.P. = 208°C, butyl carbitol, B.P. = 231°C.

In understanding the unexplained discrepancies between theory and experimental observations of dibutyl phthalate aerosol, it would be advantageous to observe and characterize aerosol as it forms within the laminar flow aerosol generator. Viewing windows may be added to the tube walls to facilitate optical particle measurements on freshly nucleated aerosol, particles still small enough in diameter for optical characterization. Upgrading the vapor source to provide a more uniform evaporation rate would improve the constancy of the particle generator. A heated oil bath around the evaporator flask and air preheater coils, set within the electric furnace, would increase the heat capacity of the flask assembly and permit thermostatic control of the furnace.

APPENDIX A. BUOYANCY EFFECTS ON THE VELOCITY PROFILE

In the worst-case evaluation of the velocity profile, buoyancy is more important than the inconstant viscosity. Therefore we will assume a constant viscosity and transform Equation [1] to dimensionless variables using the transformed variables and coordinates introduced in section 3.2, and others given below. The dimensionless equation for velocity v(r) is

$$0 = -\frac{1}{2Sc}\frac{\partial p}{\partial z} + \frac{1}{r}\frac{\partial}{\partial r}\left\{r\frac{\partial v(r)}{\partial r}\right\} - \frac{Gr}{4Re}(T - \bar{T}) \qquad [A.1]$$

with boundary conditions

$$v(r) = 0 \qquad r = 1$$

$$\frac{\partial v(r)}{\partial r} = 0 \qquad r = 0$$

and dimensionless quantities defined by

$$p = (p' - p_o')/\rho_g \bar{v}^2$$

$$v(r) = v_z/\bar{v}$$

$$Re = 2R\rho_g \bar{v}/\mu$$

$$Sc = \mu/\rho_g D$$

$$Gr = (2R)^3 \rho_g{}^2 g(T_o' - T_{w_f}')/T_o'\mu^2$$

By neglecting inertial terms we will assume that the pressure gradient depends only on z and the velocity depends only on r. Also, the pressure gradient is chosen such that

$$2\int_0^1 v(r)rdr = 1 \qquad [A.2]$$

Equation [A.1] may be integrated to give

$$v(r) = 2(1 - r^2)\left[1 - \frac{Gr}{2Re}\int_0^1 r' \int_{r'}^1 \frac{1}{r''} \int_0^{r''} T(r''')r'''dr'''dr''dr' \right] + \frac{Gr}{4Re}\int_r^1 \frac{1}{r'} \int_0^{r'} T(r'')r''dr''dr' \qquad [A.3]$$

For a worst-case calculation with buoyancy, we choose to represent T(r) as the lowest-order polynomial satisfying

$$\left.\begin{aligned} T &= 0 \\ T &= 1 \\ \frac{\partial T}{\partial r} &= 0 \end{aligned}\right\} \qquad \begin{aligned} r &= 1 \\ r &= 0 \end{aligned}$$

We choose

$$T = 1 - r^2 \qquad [A.4]$$

and calculate v(r) from Equation [A.3],

$$v(r) = 2(1 - r^2)\left[1 - \frac{Gr}{384Re}(1 - 3r^2) \right] \qquad [A.5]$$

For sample operating parameters of $T_o' = 150°C$ with flowrate of 3 ℓ/min, we find Re = 230, Gr = 5.6×10^4 and the velocity profile is

$$v(r) = 2(1 - r^2)\left[1 - 0.63(1 - 3r^2) \right] \qquad [A.6]$$

Figure A.1 shows the velocity profile of Eq. [A.6] and compares it to the standard parabolic velocity profile. The conditions chosen for this calculation correspond to an early stage of cooling, where diffusional and aerosol processes have reached only half the distance from the wall to the centerline of the tube. The prarbolic velocity profile is sufficiently accurate for the purpose of modeling the aerosol production of the system.

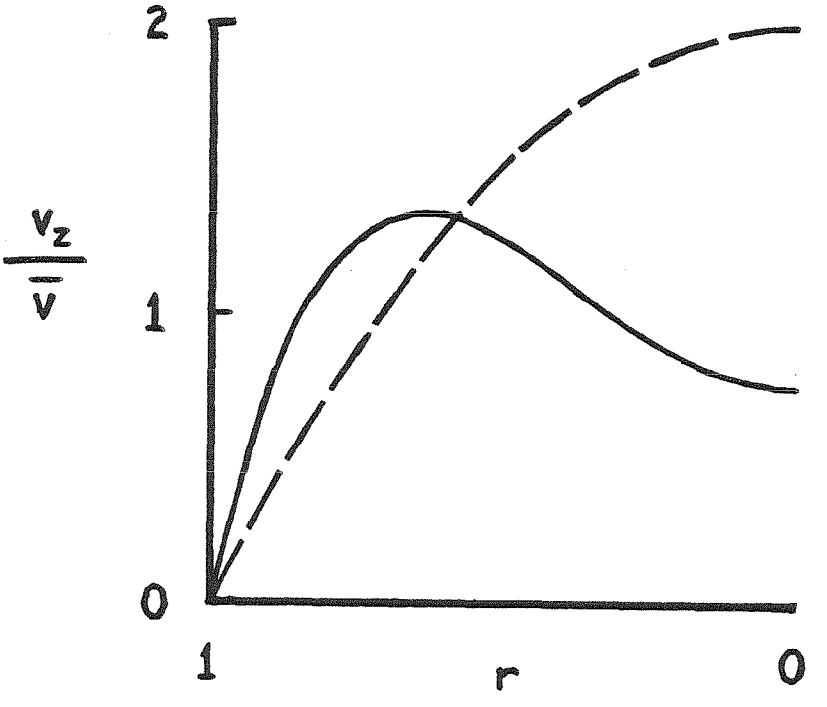

Figure A.1 Velocity profile in cooled tube. Profiles are shown for: – – – No buoyancy forces, and ——— Buoyancy induced by temperature profile of $T = 1-r^2$ with $T'_o = 150°C$, $T'_{w_f} = 25°C$, flow rate = 3 ℓ/min and Gr/Re = 243.

APPENDIX B. THE EFFECT OF COAGULATION

The maximum effect of coagulation on the number concentration of aerosol can be estimated by assuming that all the aerosol that will form along a streamline forms suddenly at one point. This assumption permits a maximum coagulation rate to apply for the maximum time for a streamline parcel of gas.

We desire to estimate a maximum particle number density that can proceed along a streamline for an axial distance of $z = 0.05$, at some radial position r, and not decrease in number by more than half. The coagulation coefficient may be taken as constant and independent of particle size, because the local particle distribution along a given streamline is predicted by the simulations to be fairly monodisperse. For particles of order 0.1 μm diameter, the coagulation coefficient is approximately $K = 1.5 \times 10^{-10}$ cm^3 sec^{-1} (25). The time needed to reach half of the initial number density is given by (25),

$$t'_{\frac{1}{2}} = \frac{2}{KN'_o} \qquad [B.1]$$

Time along a flowing streamline in laminar tube flow is given by

$$t' = \frac{R^2}{D} \frac{z}{1-r^2} \qquad [B.2]$$

Combining Eqs. [B.1] and [B.2] at $z = 0.05$ gives

$$N'_o = \frac{40D}{R^2K} (1-r^2) \qquad [\ .3]$$

Table B.1 shows the number density on various streamlines at which coagulation becomes important for 0.1 μm diameter particles after $z = 0.05$ beyond particle formation. Even for the streamline nearest the wall in the numerical simulations, a particle number density of 10^9 cm^{-3} may be taken approximately constant and unaffected by coagulation.

Table B.1 Limiting Number Density at Several Radial Positions

r	N'_o, cm^{-3}
0	$1x10^{10}$
0.50	$7x10^{9}$
0.80	$3x10^{9}$
0.90	$2x10^{9}$
0.95	$1x10^{9}$

APPENDIX C. THE ROLE OF THE KELVIN EFFECT

The driving force for the growth law of Eq. [17] including the Kelvin effect is

$$x - x_p = x \left[1 - S^{(d_p^*/d_p - 1)}\right] \qquad [C.1]$$

The Kelvin effect is negligible when the term in the square brackets of Eq. [C.1] is of order unity. If the size distribution of an aerosol lies well above the particle diameter at which the Kelvin effect is important, then the entire growth process of most particles can be adequately modeled without the Kelvin effect. The condition at which the Kelvin effect is unimportant is given by the relation

$$S^{(d_p^*/d_p - 1)} \ll 1 \qquad [C.2]$$

If we choose a cutoff condition of 0.2 for the numerical value of Eq. [C.2] at which we define, d_p^t, a transition diameter above which the Kelvin effect is negligible, we can calculate the dependence of d_p^t on the saturation ratio. Table C.1 shows this dependence for $\lambda = 5.04 \times 10^{-6}$ cm and $Kn^* = 10$. Through the entire radial cross section, the saturation ratio in the region of homogeneous nucleation (Lothe-Pound theory) is greater than 15, for $x_o = 1 \times 10^{-4}$. The distribution resulting from the simulation, shown in Figure 12, indicates that virtually all of the aerosol is much larger in diameter than the transition diameters given in Table C.1. This shows that the Kelvin effect is negligible for that case. Figure 19 shows average diameters sufficiently above the transition diameter for other initial temperatures, and Figure 23 shows the same relationship for all values of initial vapor mole fraction.

Table C.1. Transition Diameter for the Kelvin Effect

S	d_p^t/d_p^*	d_p^t, μm
45	1.73	0.0059
30	1.90	0.0065
15	2.46	0.0084

APPENDIX D. PARTICLE MASS FLUX EXPRESSION

The growth law expression of Eq. [17] arises from considering the mass balance on a growing particle of volume v' with mass flux J_m,

$$M_i c_d \frac{dv'}{dt'} = \pi d_p^2 J_m \qquad [D.1]$$

where M_i and c_d are the molecular weight and molecular density of the condensing species. We rewrite Eq. [D.1] as

$$\frac{dv'}{dt'} = \pi E_i \frac{c}{c_d} x\lambda\mathcal{D}\left(\frac{\lambda\bar{c}_i}{\mathcal{D}}\right)\left(\frac{d_p}{2\lambda}\right)^2\left(\frac{J_m}{J_k}\right) \qquad [D.2]$$

where E_i is the evaporation coefficient, c is the molar density of the gas phase, $\bar{c}_i$ is the mean molecular speed of the condensing species, and J_k is the mass flux obtained from kinetic theory, given by

$$J_k = \frac{1}{4} E_i M_i c x \bar{c}_i \qquad [D.3]$$

Next, we obtain an expression for the ratio J_m/J_k.

Davis and co-workers (26,27) have shown that a modified form of the Sitarski-Nowakowski mass flux equation is accurate for large molecular weight ratio $Z = M_i/M_j$ (20),

$$\frac{J_m}{J_k} = \frac{Kn\left[1 + \frac{3\beta_e(1+Z)^2}{4(3+5Z)} Kn\right]}{\left\{\frac{8\Omega_{ij}^{(1,1)*}}{3\pi(1+Z)} + \left[\frac{\beta_e(1+2Z)}{\pi(3+5Z)} + \frac{1}{2\beta_e}\right] Kn + \frac{9(1+Z)^2}{8(3+5Z)} Kn^2\right\}} \qquad [D.4]$$

where j refers to the carrier gas, and the Knudsen number is defined $Kn = 2\lambda_i/d_p$. The mean free path of species i is (28)

$$\frac{1}{\lambda_i} = \pi \left[\hat{n}_i \sigma_{ii}^2 \sqrt{2} + \hat{n}_j \sigma_{ij}^2 (1 + Z)^{\frac{1}{2}} \right] \qquad [D.5]$$

and β_e is related to the evaporation coefficient E_i by $\beta_e = E_i/(2 - E_i)$. $\Omega_{ij}^{(1,1)*}$ is the tabulated collision integral for molecular diffusion (29). The number concentrations of the gaseous species are given by $\hat{n}_i$ and $\hat{n}_j$. At 125°C for dibutyl phthalate, Eq. [D.5] gives $\lambda_{DBP} = 1.18 \times 10^{-2}$ μm.

The flux relation Eq. [D.4] fails to converge to the kinetic limit for Kn $\gtrsim$ 0.5. For numerical computations, the Fuchs-Sutugin formulation of the flux expression (20)

$$\frac{J_m}{J_k} = \frac{1.333\ Kn(1 + Kn)}{1 + 1.71\ Kn + 1.333\ Kn^2} \qquad [D.6]$$

yields proper limits for Kn >> 1 and Kn << 1 and approximates Eq. [D.4] provided that we choose $\lambda_i = 3D/\bar{c}_i$. For an evaporation coefficient of unity, Figure D.1 compares the flux expressions at 125°C for dibutyl phthalate in air. We see that $\lambda = 5.04 \times 10^{-2}$ μm in Eq. [D.6] provides a good expression for the growth law over the whole range of Knudsen numbers.

Equation [D.6] is used in Eq. [D.2] to calculate the growth rate, yielding Eq. [17] with F defined by

$$F(Kn) = \frac{1 + Kn}{1 + 1.71\ Kn + 1.333\ Kn^2} \qquad [D.7]$$

with the Knudsen number defined with $\lambda = 5.04 \times 10^{-2}$ μm.

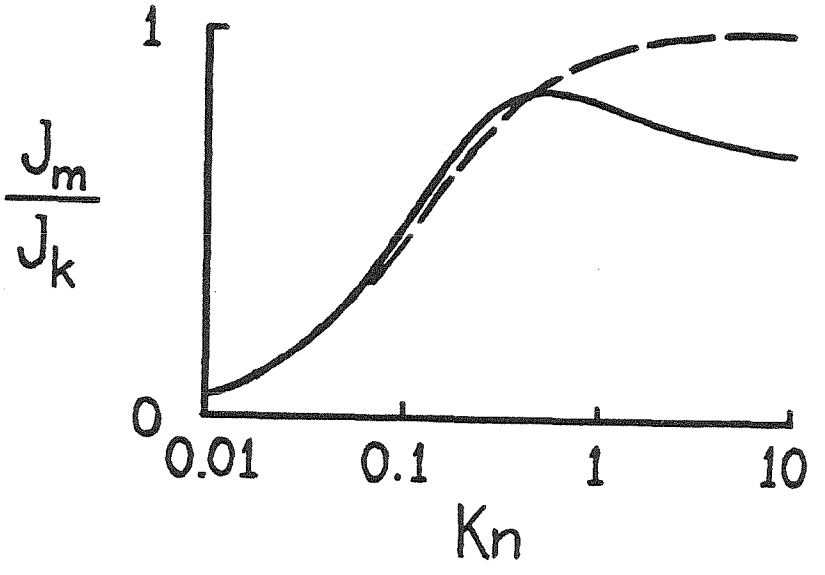

Figure D.1 Particle growth mass flux for dibutyl phthalate at 125°C normalized by flux obtained from kinetic theory. Shown are: ——— Modified Sitarski-Nowakowski expression with $\lambda = 1.18 \times 10^{-2}$ μm (Eq. [D.4]), and — — — Fuchs-Sutugin interpolation formula with $\lambda = 5.04 \times 10^{-2}$ μm (Eq. [D.6])

APPENDIX E. THE EFFECT OF THERMAL DIFFUSION

Following Hirschfelder (29), the thermal diffusion coefficient, first-order approximation from kinetic theory, is

$$[k_T]_1 = \frac{x_1 x_2}{6[\lambda_{12}]_1} \frac{S^{(1)}x_1 - S^{(2)}x_2}{X_\lambda + Y_\lambda} (6C^*_{12} - 5) \qquad [E.1]$$

where the subscripted square brackets denote first-order approximations and

$$S^{(1)} = \frac{M_1+M_2}{2M_2} \frac{[\lambda_{12}]_1}{[\lambda_1]_1} - \frac{15}{4A^*_{12}} \left(\frac{M_2-M_1}{2M_1}\right) - 1 \qquad [E.2]$$

$$S^{(2)} = \frac{M_2+M_1}{2M_1} \frac{[\lambda_{12}]_1}{[\lambda_2]_1} - \frac{15}{4A^*_{12}} \left(\frac{M_1-M_2}{2M_2}\right) - 1 \qquad [E.3]$$

and the thermal conductivity in cal cm^{-1} sec^{-1} $°K^{-1}$ for pure component is

$$[\lambda_i] \times 10^7 = 1989.1 \frac{\sqrt{T/M_i}}{\sigma_i^2 \Omega(2,2)^*(T^*)}$$

$$= \frac{15}{4} \frac{R_g}{M_i} [\eta_i]_1 \times 10^7 \qquad [E.4]$$

with [=] Å and

$$T^* = \frac{kT}{\varepsilon} \qquad [E.5]$$

For the binary mixture,

$$[\lambda_{12}]_1 = \frac{25}{32}\left[\frac{\sqrt{(m_1+m_2)\pi kT/2m_1m_2}}{\pi\sigma_{12}^2\Omega_{12}^{(2,2)*}(T_{12}^*)}\right]\left(\frac{3}{2}\,k\right)$$

$$= \frac{15}{4}\,k\left[\frac{m_1+m_2}{2m_1m_2}\right][\eta_{12}]_1 \qquad [E.6]$$

with

$$T_{12}^* = \frac{kT}{\varepsilon_{12}} \qquad [E.7]$$

$$[\eta_{12}]_1 \times 10^7 = 266.93\,\frac{\sqrt{2M_1M_2T/(M_1+M_2)}}{\sigma_{12}^2\Omega_{12}^{(2,2)*}(T_{12}^*)} \qquad [E.8]$$

The functions A*B* and C* are of order unity and are functions of T_{12}^* through tabulated collision integrals,

$$A^* = \frac{\Omega^{(2,2)*}}{\Omega^{(1,1)*}} \qquad [E.9]$$

$$B^* = \frac{5\Omega^{(1,2)*} - 4\Omega^{(1,3)*}}{\Omega^{(1,1)*}} \qquad [E.10]$$

$$C^* = \frac{\Omega^{(1,2)*}}{\Omega^{(1,1)*}} \qquad [E.11]$$

In Equation [E.1], the functions X_λ and Y_λ are

$$X_\lambda = \frac{x_1^2}{[\lambda_1]_1} + \frac{2x_1x_2}{[\lambda_{12}]_1} + \frac{x_2^2}{[\lambda_2]_1} \qquad [E.12]$$

$$Y_\lambda = \frac{x_1^2}{[\lambda_1]_1}\,U^{(1)} + \frac{2x_1x_2}{[\lambda_{12}]_1}\,U^{(Y)} + \frac{x_2^2}{[\lambda_2]_1}\,U^{(2)} \qquad [E.13]$$

with

$$U^{(1)} = \frac{4}{15} A^*_{12} - \frac{1}{12}\left(\frac{12}{5} B^*_{12} + 1\right) \frac{M_1}{M_2} + \frac{1}{2} \frac{(M_1-M_2)^2}{M_1M_2} \qquad [E.14]$$

$$U^{(2)} = \frac{4}{15} A^*_{12} - \frac{1}{12}\left(\frac{12}{5} B^*_{12} + 1\right) \frac{M_2}{M_1} + \frac{1}{2} \frac{(M_2-M_1)^2}{M_1M_2} \qquad [E.15]$$

$$U^{(Y)} = \frac{4}{15} A^*_{12}\left[\frac{(M_1+M_2)^2}{4M_1M_2}\right]\frac{[\lambda_{12}]^2_1}{[\lambda_1]_1[\lambda_2]_1} - \frac{1}{12}\left(\frac{12}{5} B^*_{12} + 1\right)$$

$$- \frac{5}{32A^*_{12}}\left(\frac{12}{5} B^*_{12} - 5\right) \frac{(M_1-M_2)^2}{M_1M_2} \qquad [E.16]$$

Table E.1 shows the thermal diffusion coefficient for dibutyl phthalate in air at 300°K and 400°K. The expression for mass flux with thermal diffusion is

$$\text{Mass Flux} \propto - D[\nabla x + k_T \nabla \ell n T'] \qquad [E.17]$$

From the numerical simulations, the gradients near the wall are approximately given by

$$\frac{\partial x/\partial r}{\partial T/\partial r} \sim O(1) \qquad [E.18]$$

Then Equation [E.17] is approximately,

$$\text{Mass Flux} \propto - D\nabla x\left[1 + k_T\left(\frac{T'_o/T'_{w_f}-1}{x_o-x_{w_f}}\right)\right] \qquad [E.19]$$

$$\propto - D\nabla x\left[1 + 3x10^{-5}\left(\frac{0.4}{10^{-4}}\right)\right] \qquad [E.20]$$

$$\propto - D\nabla x\,[1 + O(0.1)] \qquad [E.21]$$

Under simulation conditions, therefore, the thermal diffusion effect is small.

Table E.1 Thermal Diffusion Coefficient for Dibutyl Phthalate in Air

$x_1 = 10^{-4}$ dibutyl phthalate mole fraction

T (°K)	$S^{(1)}$	$S^{(2)}$	X_λ	Y_λ	$[k_T]_1$
300	35.80	- 15.51	2.11×10^4	8.66×10^4	1.64×10^{-5}
400	35.73	- 15.57	1.71×10^4	7.01×10^4	4.32×10^{-5}

APPENDIX F. FORTRAN SOURCE CODE AND SAMPLE OUTPUT

F.1 Documentation

Symbols Used In Program TUBE

VARIABLE	*	TYPE	DESCRIPTION
CRATIO	*	REAL	C/Cd, 'C RATIO' ratio of molar densities of gas, liq.
D		R	Dummy for DELX in statement function definition of RAD
DELX	*	R	Dimensionless radial interval, Eqs.[18], [19]
DELZ	*	R	Dimensionless axial interval, Eqs.[18], [19]
DIFF	*	R	Mass DIFFusivity of monomer vapor, cm**(2)/sec
E		R	Dummy for radial coordinate in statement function definition of VEL
FIL		INT.	Dummy FILe number designator
FXL		R	\
FXN		R	> Iteration scheme functions (APPENDIX)
FXU		R	/
GREEN( )	*	R	GREEN's function
ITER		I	ITERation counter in main program loop
KCYCLE	*	I	Declared for compatability with plotting program, neccesitated by use of common data file: PARAM
KNCRIT	*	R	'CRITical KNudsen number' used as initial size for seed and new particles in growth calculation
KNS	*	R	Seed KNudsen number, during growth
L		R	Dummy for X in statement function definition of RAD
LAMBDA	*	R	Mean free path of monomer, cm
LSNKFL		I	'Large SINK FLag' set by conditions after line 250, used to indicate * on output file: TABLE
N		I	Dummy
NFLX	*	I	Printout interval on X (radial)
NFLZ	*	I	Printout interval on Z (axial)
NO	*	R	Dimensional seed concentration, cm**(-3)
NSEED	*	R	Dimensionless SEED concentration
NSTEP	*	I	Axial length of wall temperature ramp in Z units
NX	*	I	Number of (radial) X - intervals
NV( )		R	Number distribution DN/DLOG(dp), cm**(-3)
NZ	*	I	Limiting number for NZZ, equal to Z - dimension specifiers
NZZ	*	I	Number of (axial) Z - intervals
PHIS		R	Seed volume fraction, microns**(3)/cm**(3)
PHIT		R	Total volume fraction, microns**(3)/cm**(3)
PHI2		R	Dimensionless sink, 'Upper-Case Phi' in theory
PI		R	PI = 3.1415927
PLTFLG	*	I	FLaG to control output to file: STORE, for PLoTting
RAD( )		REAL	statement function; Dimensionless radial coordinate ; RAD(N) = 1 - N*DELX
SIGMA	*	R	Reference surface tension, at T = 300 K, g/sec**(2)
SINK		R	last term of eq. [39], PHI2*DELZ/VEL
TMP( )	*	R	Dimensionless TeMPerature
TO	*	R	Initial wall Temperature, degrees Kelvin
TOTN		R	Homogeneous aerosol number concentration, cm**(-3)
TRUBFL		I	Incorrect-convergence FLag, informs of TROUBle
TSCALE	*	R	Ratio of Time SCALEs, 'upper-case lambda' in theory
TST(,0)	*	I	Lower limit of Z - integrals, to speed program exec.
TST(,1)	*	I	Flag, set when TST(X,0) is determined
TW	*	R	Final Wall Temperature, degrees Kelvin
V( )		R	Particle diameter, microns
VEL( )		REAL	statement function; Dimensionless VELocity profile
VL( )		R	VoLume distribution, DV/DLOG(dp), microns**(3)/cm**(3)
X		I	Integer distance from wall in units of DELX. X=1,...NX
XA( )	*	R	Dimensionless mole fraction of monomer
XAO	*	R	Initial mole fraction of monomer
XAW	*	R	Final Wall mole fraction
XBF		R	BuFfer in iteration scheme (APPENDIX)
XH		R	Homogeneous part of mole fraction solution, first two terms of right side of eq. [39]
XJ		R	Dimensionless nucleation rate, J in theory
XL	*	R	Tube radius, characteristic Length, cm
XLEWIS	*	R	LEWIS number, (thermal diffusivity)/(mass diffusivity)
XP		I	Dummy X, 'X Prime'
XU		R	Iteration scheme function (APPENDIX)
XXL		R	Iteration scheme function (APPENDIX)
Z		I	Integer axial coordinate, in dimensionless DELZ units
ZP		I	Dummy Z, 'Z Prime'

* Denotes use in COMMON blocks

DESCRIPTION OF SUBROUTINES

```
HOMOG(X,Z,XHH,TMMP)
     Calculates forst two terms of Eqs. [38] and [39] and assigns them
     to TMMP AND XHH, respectively
```

```
SBPHI2(X,Z,PHI2,VN,VL,V,PHIT,PHIS)
     Calculates PHI2,        dimensionless sink
                NV, VL, V    aerosol size distribution
                             DN/DLOG(dp), DV/DLOG(dp)  v.s. dp (microns)
                 PHIT        total aerosol volume fraction,
                             microns**(3)/cm**(3)
                 PHIS        seed volume fraction, microns**(3)/cm**(3)
```

```
TAUF(X,Z,TAUV)                                  Z
                                               /
     Calculates TAUV(delz) = TSCALE*integ. (XA - XSAT)----------dZ
     (particle growth time)                   /                (1-r**2)
                                          Z - delz
```

```
JJ(X,Z,ZZ,XJ,FLAGXJ,TOTN)
     If  Z < ZZ, recalls XJ = JJJ(X,Z), storage array for XJ
                 (Option for Z < ZZ not used by TUBE)
     If  Z = ZZ, calculates XJ at X, Z
     If  FLAGXJ = 1, calculates TOTN, TOTal Number concentration of
                             homogeneously formed aerosol by logarithmic
                             interpolated integration of JJJ
```

```
GD(DTAU,KNCRIT,GDTAU,KNAPRX)
     DTAU   = Left side of Eq. [27]
     KNCRIT = Kn* of Eq. [27]
     KNAPRX = Kn of Eq. [27]
     GDTAU  = Kn**(-1)*F(Kn)  grouping from Eqs. [28] and [30]
                 (Option for GDTAU not used by TUBE)
```

```
WALLT(Z,TWALL)
     Calculates wall temperature, TWALL, dimensionless
```

```
WALLXA(Z,XAWALL)
     Calculates wall mole fraction, XAWALL, dimensionless
```

```
XSAT(DT)   <-----REAL FUNCTION
     DT = Dummy Temperature, degrees Kelvin
```

```
GREENE(GREEN,GRNFLG)
     Calculates GREEN's function
     If DELZ is too coarse, cannot calculate, sets GRNFLG = 0
```

```
INIT
     Initialization
     Reads data from file: PARAM
     Checks to see if GRNFLG is zero ---> terminates program if GRNFLG=0
```

```
PNTPM(F)
     PrINTs ParaMeters on file number F
```

```
WRTE(X,Z,NV,VL,V,PHI2,PHIT,PHIS,TOTN,XJ,TRUBFL,LSNKFL)
     WRITEs output
     Calculates cup-mix averages
```

```
INTERP(XY,X,XO,TERP)
     Linear INTERPolation program for cup-mix averaging of aerosol
          distributions.
```

```
TRUBLE(XRF,XAXZ,X,Z,XHXZ,SINK,FXU,FXL,XU,XXL)
     If iteration scheme overworks, TRUBLE prints out diagnostic
          variables and terminates the execution.
```

APPENDIX: MODIFIED REGULA FALSI ITERATION SCHEME

Solve $X = F(X)$ $\quad 0 \le X \le 1$

The function F used here is a dummy for (XH - SINK) of TUBE.

F is large for $X \approx 0$ for some conditions.
Therefore truncate:

$$FXL = \min[1, F(XXL)]$$
$$FXU = \max[0, F(XU)]$$

Truncation of F is the only modification to REGULA FALSI

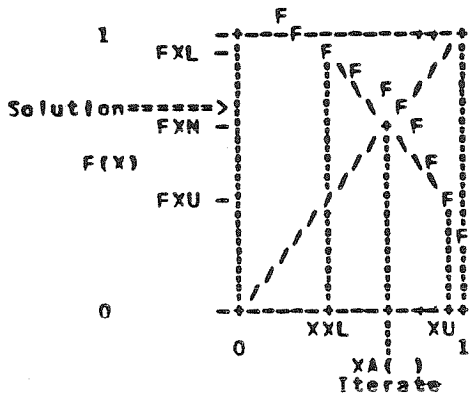

XBF is buffer for
last XA iterate.
Iteration completed when
Norm[XA-XBF] < epsilon

F.2 Fortran Code

```
      PROGRAM TUBE
C-----------------------------------------------------------------------
C
C               Marching Solution to Cooled Tube Flow
C                 .--
C                 | TW + (TO-TW)*(1 - Z/NSTEP)     0 < Z < NSTEP
C   TMP(WALL) =   |
C                 | TW             Z > NSTEP
C                 '--
C
C   XA(WALL)  =  XASAT(TMP(WALL))        wherever  XASAT < XAO
C-----------------------------------------------------------------------
      INTEGER X,Z,XP,ZP,FIL,PLTFLG,TRUBFL
      INTEGER TST(1:20,0:1)
C             TST(X,0) is the lower limit for aerosol Z-integrals
C               and set where vapor sink first appears.
C             TST(X,1) is flag, set when TST(X,0) is determined.
      REAL LAMBDA,KNCRIT,KNS,NC,NSEED
      REAL XA(0:20,0:749),TMP(0:20,0:749),
     :     NV(0:749),VL(0:749),V(0:749)
      REAL GREEN(0:20,0:20,1:2)
      COMMON /ARR/ TST
      COMMON /PLT/ PLTFLG,NZZ,KCYCLE
      COMMON /GRN/ GREEN
      COMMON /FUN/ XA,TMP,KNS
      COMMON /PR1/ PI,DELX,DELZ,LAMBDA,XL,TSCALE,KNCRIT,NSEED,NO
      COMMON /PR2/ SIGMA,DIFF,XAW,XAO,TW,TO,CRATIO
      COMMON /PR3/ NX,NZ,NFLX,NFLZ,XLEWIS,NSTEP
      RAD(L,D)=1.-D*REAL(L)   ! Dimensionless radial coordinate
      VEL(E)=1.-E*E           ! Dimensionless velocity distribution
      PI=3.1415927
      NX=20   ! Must correspond to all X-dimension declarations
      NZ=749 ! Must correspond to all Z-dimension declarations
C             Form:  NZ = 10*N - 1, any N, for output compatability
      DO 50 N=1,NX
      TST(N,0)=0 !Array of starting values for ZP (Z Prime)
      TST(N,1)=0 !Flags initially clear
   50 CONTINUE
      CALL INIT
      OPEN(12,FILE='DISTR',STATUS='NEW')
C       For detailed aerosol DISTRibutions
      OPEN(13,FILE='TABLE',STATUS='NEW')
C       For radial profiles of functions and cup-mixed averages
      IF (PLTFLG.EQ.1) OPEN(14,FILE='STORE',STATUS='NEW')
C                              For plot-program readable aerosol distrib.
C Write headings on files TABLE & DISTR
      DO 100 FIL=12,13
      WRITE (FIL,'(T2,A)') 'MARCHING SOLUTION TO COOLED TUBE FLOW'
      WRITE (FIL,'(T2,A,G10.4,A)')
     : 'Z STEPS ARE ',(DELZ*XL*XL/DIFF),' *V(MAX)'
      WRITE (FIL,'(T2,A,G10.4,A/)')
     : 'Z STEPS ARE (',2CO.*DELZ/(6.*PI*DIFF),' *Q(LPM) ) ==CM'
      CALL PNTPM(FIL)
  100 CONTINUE
C
C                ***  MAIN  PROGRAM  LOOP  ***
C
        DO 300 Z=1,NZZ
        IF (MOD(Z,10).EQ.0) WRITE (6,'(T2,A,I3)') ' Z = ',Z
          DO 300 X=1,NX
            ITER=100 !Iteration counter
            CALL HCMOG(X,Z,XH,TMP(X,Z))
            XU=1.      ! Set up iteration procedure
            XA(X,Z)=XU
            CALL SBPHI2(X,Z,PHI2,NV,VL,V,PHIT,PHIS)
            SINK=PHI2*DELZ/VEL(RAD(X,DELX))
            FXU=XH-SINK
            IF (FXU.LT.0.) FXU=0.
            IF (FXU.GT.1.) THEN    !Set incorrect convergence flag
              TRUBFL=1
            ELSE                   ! Clear incorrect convergence flag
              TRUBFL=0
            ENDIF
            XXL=0.
            XA(X,Z)=XXL
            CALL SBPHI2(X,Z,PHI2,NV,VL,V,PHIT,PHIS)
            SINK=PHI2*DELZ/VEL(RAD(X,DELX))
            FXL=XH-SINK
            IF (FXL.GT.1.) FXL=1.
            IF (FXL.LT.0.) FXL=0.
C           First-guess for XA at new Z
            XA(X,Z)=XA(X,Z-1)
            XBF=1.1
```

```
  200           CONTINUE  !       ***  Iteration Loop  ***
                ITER=ITER-1
                CALL SBPHI2(X,Z,PHI2,NV,VL,V,PHIT,PHIS)
                SINK=PHI2*DELZ/VEL(RAD(X,DELX))
                FXN=XH-SINK
C               Find zero of  (FXN-XA)
                IF (FXN.GT.1.) FXN=1.
                IF (FXN.LT.0.) FXN=0.
                IF (ABS(XBF-XA(X,Z)).GT.1.E-5) THEN
                   IF (FXN.GT.XA(X,Z)) THEN
                      XXL=XA(X,Z)
                      FXL=FXN
                   ELSE
                      XU=XA(X,Z)
                      FXU=FXN
                   ENDIF
                   XBF=XA(X,Z)
                  IF (XU-XXL*FXL-FXU.GT.0.) THEN ! Normal interpolation
                   XA(X,Z)=(XU*FXL-XXL*FXU)/(XU-XXL+FXL-FXU)
                  ELSE !Nonunique solution--   XXL < XA < XU
                   IF (XU-XXL.LT.1.E-2) THEN !Adequate solution(?) & warn
                    XA(X,Z)=(XU+XXL)/2.
                    WRITE(6,'(T2,A,I3,A,I3,A,G9.3)') 'AT X=',X,', Z=',Z,
     :                    ', XA IS +/- ',(FXU-FXL)/2.
                   ELSE  ! Write out details and terminate
                    CALL TRUBLE(XBF,XA(X,Z),X,Z,XH,SINK,FXU,FXL,XU,XXL)
                    STOP
                   ENDIF
                  ENDIF
                   IF (XA(X,Z).LT.0.) XA(X,Z)=0.
                   IF (ABS(FXL-FXU).LT.1.E-6) XA(X,Z)=(FXL+FXU)/2.
                   IF (ITER.LE.0) THEN
                     CALL TRUBLE(XBF,XA(X,Z),X,Z,XH,SINK,FXU,FXL,XU,XXL)
                     GO TO 250
                   ENDIF
                   IF (XA(X,Z).GT.1.) XA(X,Z)=1.
                   IF (XA(X,Z).LT.0.) XA(X,Z)=0.
                   GO TO 200                          ! Reiterate
                ENDIF
  250        CONTINUE
             IF (SINK.GT.XA(X,Z-1)-XA(X,Z)) THEN
                LSNKFL=1
             ELSE
                LSNKFL=0
             ENDIF
             CALL SBPHI2(X,Z,PHI2,NV,VL,V,PHIT,PHIS)
C Check for vapor sink: No--March TST(X,0).  Yes--Fix TST(X,0).
             IF (TST(X,1).EQ.0) THEN !Move starting ZP
                TST(X,0)=MAX(0,Z-2)
                IF (PHI2.GT.0.) TST(X,1)=1 !Flag set
             ENDIF
             IF ((MOD(X,NFLX)+MOD(Z,NFLZ)).EQ.0.OR.
     :           (MOD(X,NFLX)+MOD(Z,NZZ )).EQ.0) THEN  ! Print results
C               Calculate distribution parameters
                CALL SBPHI2(X,Z,PHI2,NV,VL,V,PHIT,PHIS)
                CALL JJ(X,Z,Z,XJ,1,TOTN)
                CALL WRTE(X,Z,NV,VL,V,PHI2,PHIT,PHIS,TOTN,XJ,TRUBFL,
     :                    LSNKFL)
             ENDIF
  300     CONTINUE
      CLOSE(12,STATUS='KEEP')
      CLOSE(13,STATUS='KEEP')
      IF (PLTFLG.EQ.1) CLOSE(14,STATUS='KEEP')
      WRITE(6,'(T2,A/,T2,20I4)')'STARTING ZP ARRAY:',(TST(N,0),N=1,NX)
      STOP
      END
C-----------------------------------------------------------------------
C
C                 Homogeneous Solution Routine
C
C-----------------------------------------------------------------------
      SUBROUTINE HOMOG(X,Z,XHH,TMMP)
      INTEGER X,XP,Z
      REAL XA(0:20,0:749),TMP(0:20,0:749)
      REAL GREEN(0:20,0:20,1:2)
      COMMON /GRN/ GREEN
      COMMON /FUN/ XA,TMP
      COMMON /PR1/ PI,DELX
      COMMON /PR3/ NX
      RAD(L,D)=1.-D*REAL(L)
      VEL(E)=1.-E*E
      CALL WALLXA(Z,XAWALL)
      CALL WALLT(Z,TWALL)
      XHH=XAWALL
      TMMP=TWALL
```

```
      DO 100 XP=1,NX
      XHH =XHH +( XA(XP,Z-1)-XAWALL)*VEL(R AD(XP,DELX))*GREEN(X,XP,1)
      THHP=THHP+(THP(XP,Z-1)-TWALL )*VEL(RAD(XP,DELX))*GREEN(X,XP,2)
  100 CONTINUE
      END
C-----------------------------------------------------------------------
C
C                     Aerosol Routines
C
C-----------------------------------------------------------------------
      SUBROUTINE SBPHI2(X,Z,PHI2,NV,VL,V,PHIT,PHIS)
      INTEGER X,Z,ZP
      INTEGER TST(1:20,0:1)  ! Aerosol start times
      REAL INT,LAMBDA,KNCRIT,KNAPRX,KNS,NO,NSEED
      REAL XA(0:20,0:749),TMP(0:20,0:749),TPHI(1:20,0:749)
      REAL TAUV(0:749),NV(0:749),VL(0:749),V(0:749)
      COMMON /AAA/ TST
      COMMON /FUN/ XA,TMP,KNS
      COMMON /PR1/ PI,DELX,DELZ,LAMBDA,XL,TSCALE,KNCRIT,NSEED,NO
      COMMON /PR2/ SIGMA,DIFF,XAW,XAO,TW,TO,CRATIO
      COMMON /PR3/ NX,NZ,NFLX,NFLZ
      SAVE M,TPHI,PHIF
      RAD(N,0)=1.-0*REAL(N)
      VEL(E)=1.-E*E
      DATA M /0/
      IF (M.EQ.0) THEN  ! Initialize
         DO 10 N=1,NX
         TPHI(N,0)=0.
   10    CONTINUE
         PHIF=CRATIO*(XAO-XAW)*1.E12  ! Characteristic vol. fraction
         M=1
      ENDIF
      CALL TAUF(X,Z,TAUV)
      PHIH=0.
         DO 100 ZP=0,Z-TST(X,0)  ! "Particle birth time" is Z-ZP
         CALL GD(TAUV(Z-ZP),KNCRIT,GDTAU,KNAPRX)
         CALL JJ(X,Z-ZP,Z,XJ,0,TOTN)  ! XJ = Nondim. homog. nucl. rate
            V(ZP)=2.E4*LAMBDA/KNAPRX  ! Diam., microns
            IF (  XJ.GT.0.  .AND.       ZP.GT.0.  .AND.
     :          V(ZP).GT.0.  .AND.  V(ZP-1).GT.0.) THEN
C              Calculate DN/DLOG(DP)   /cc.
               NV(ZP)=XJ*(DELZ/VEL(RAD(X,DELX)))/
     :                   (LOG10(V(ZP)/V(ZP-1)))*LAMBDA*XL*XL)
C              Calculate volume, DV/DLOG(DP), cu.microns/cc.
               DELPHI=XJ*(DELZ/VEL(RAD(X,DELX)))*(PI/6.)*V(ZP)**3.
     :                        /(LAMBDA*XL*XL)
               PHIH=PHIH + DELPHI
               VL(ZP)=DELPHI/LOG10(V(ZP)/V(ZP-1))
            ELSE
               NV(ZP)=0.
               VL(ZP)=0.
            ENDIF
  100    CONTINUE
      KNS=KNAPRX
      IF (TST(X,0).GT.0) THEN  ! Rezero remaining array elements
         DO 150 ZP=Z-TST(X,0)+1,Z
            NV(ZP)=0.
            VL(ZP)=0.
             V(ZP)=0.
  150    CONTINUE
      ENDIF
      PHIS=(4.*PI/3.)*(1.E4*LAMBDA/KNS)**3.*NO  ! Seed vol. frac.
      TPHI(X,Z)=PHIH + PHIS
      PHIT=TPHI(X,Z)
      PHI2=(TPHI(X,Z)-TPHI(X,Z-1))*VEL(RAD(X,DELX))/(DELZ*PHIF)
      END
C
C
      SUBROUTINE TAUF(X,Z,TAUV)
C     Calculates delta tau(X,Z,ZO) for ZO = TST(X,0) to Z
C     TAUV(ZZ)=TSCALE*(DELZ/VEL)*Integral(Z-ZZ TO Z)(XA-XASAT)*dZ
      INTEGER X,Z,ZP
      INTEGER TST(1:20,0:1)
      REAL XA(0:20,0:749),TMP(0:20,0:749),TAUV(0:749)
      REAL LAMBDA,KNCRIT,INT
      COMMON /AAA/ TST
      COMMON /FUN/ XA,TMP
      COMMON /PR1/ PI,DELX,DELZ,LAMBDA,XL,TSCALE,KNCRIT
      COMMON /PR2/ SIGMA,DIFF,XAW,XAO,TW,TO
      COMMON /PR3/ NX,NZ
      RAD(N,0)=1.-0*REAL(N)
      VEL(E)=1.-E*E
         ZP=Z
         INT=0.
  100    CONTINUE
```

```
            IF (ZP.LT.TST(X,0)) GO TO 199
            IF (ZP.LT.Z) THEN
               DXERLR=XA(X, ZP )
     :            -(XSAT(TW+(TO-TW)*TMP(X, ZP ))-XAW)/(XAO-XAW)
               DXLATR=XA(X,ZP+1)
     :            -(XSAT(TW+(TO-TW)*TMP(X,XP+1))-XAW)/(XAO-XAW)
C              Running integral of positive trapazoidal function
               ADD=0.  ! Unless...
               IF (DXLATR.GT.0..AND.DXERLR.LT.0.)
     :            ADD=.5*DXLATR**2./(DXLATR-DXERLR)
               IF (DXLATR.LT.0..AND.DXERLR.GT.0.)
     :            ADD=.5*DXERLR**2./(DXERLR-DXLATR)
               IF (DXLATR.GE.0..AND.DXERLR.GE.0.)
     :            ADD=.5*(DXLATR+DXERLR)
               INT=INT+ADD
            ENDIF
            TAUV(ZP)=INT*TSCALE*DELZ/VEL(RAD(X,DELX))
            ZP=ZP-1
            GO TO 100
  199       CONTINUE
         END
C
C
         SUBROUTINE JJ(X,Z,ZZ,XJ,FLAGXJ,TOTN)
C                  XJ=-Dimensionless homogeneous nucleation rate
C                  TOTN=-Total number concentration, cm**(-3)
         INTEGER X,Z,ZZ,A,B,FLAGXJ
         INTEGER TST(1:20,0:1)
         REAL JJJ(0:20,0:749),XA(0:20,0:749),TMP(0:20,0:749)
         REAL LAMBDA,KSG
         COMMON /ABB/ TST
         COMMON /FUN/ XA,TMP
         COMMON /PR1/ PI,CELX,DELZ,LAMBDA,XL
         COMMON /PR2/ SIGMA,DIFF,XAW,XAO,TW,TO
         COMMON /PR3/ NX,NZ,NFLX,NFLZ
         SAVE JJJ,KSG,INITM
         RAD(N,0)=1.-0*REAL(N)
         VEL(F)=1.-E*E
         DATA    KSG,    INITM/
     :    -0.0027039,   0/
         IF (FLAGXJ.EQ.1) GO TO 20
         IF (INITM.EQ.0) THEN  ! Initialize
            DO 10 A=0,NX
            DO 10 B=0,NZ
            JJJ(A,B)=0.
   10       CONTINUE
            INITM=1
         ENDIF
         IF (Z.EQ.ZZ) THEN   ! Calculate J
            DXA=XAW+(XAO-XAW)*XA(X,Z)
            DTMP=TW+(TO-TW)*TMP(X,Z)
            SR=DXA/XSAT(DTMP)   ! Saturation ratio
            IF (SR.GT.1.) THEN
C - - - - - - - - - - - - - - - - - - - - - - - - - - - - - - - - - - - - -
CCC
CCC         Dimensional nucleation expression in this box.
CCC           JJJ = Function of mole fraction == DXA
CCC                               temperature == DTMP
CCC                          saturation ratio == SR
CCC                        and other parameters as needed.
CCC
C           Lothe-Pound nucleation theory for dibutyl phthalate:
               SIGT=SIGMA*EXP(KSG*(DTMP-300.))  ! Surface tension at DTMP
            RSTR=2.*SIGT*3.203E-06/(DTMP*LOG(SR))  ! Critical radius
            RSTRLP=RSTR
            DO 12 I5=1,5
               RSTRLP=RSTR*(1.-3.*1.38E-16*DTMP/(2.*PI*SIGT*RSTRLP**2.))
   12       CONTINUE
            JJJ(X,Z)=SQRT(1.-9.*1.38E-16*DTMP/(2.*PI*SIGT*RSTRLP**2.))
     :     *EXP( LOG(4.*PI*DXA) - .5*LOG(2.*PI*4.618E-22*1.38E-16*DTMP)
     :        +.5*LOG(SIGT/(1.38E-16*DTMP)) + LOG(4.42E-22/(2.*PI))
     :        -3.124 + 3.*LOG(1.027*1.38E-16*DTMP) + 12.*LOG(RSTRLP)
     :        +361.675 - 4.*PI*RSTRLP**2.*SIGT/(3.*1.38E-16*DTMP)+13.848)
C
C - - - - - - - - - - - - - - - - - - - - - - - - - - - - - - - - - - - - -
               IF (JJJ(X,Z).LT.1.) JJJ(X,Z)=0. !Significance threshold
C              Nondimensionalize:
               JJJ(X,Z)=JJJ(X,Z)*(LAMBDA*XL**4.)/DIFF
            ELSE
               JJJ(X,Z)=0.
            ENDIF
         ENDIF
   20    CONTINUE
         XJ=JJJ(X,Z)
         IF (FLAGXJ.EQ.1) THEN  !Calculate total number
```

```
C Integration of JJJ*dZ/VEL with logarithmic interpolation of JJJ
         TOTN=0.
         DO 30 N=MIN(MAX(1,TST(X,0)),Z),Z
         IF (JJJ(X,N-1).EQ.JJJ(X,N)) THEN
            TOTN=TOTN+JJJ(X,N)
         ELSEIF (JJJ(X,N-1).NE.0..AND.JJJ(X,N).NE.0.) THEN
            TOTN=TOTN+(JJJ(X,N-1)-JJJ(X,N))/
     :           (LOG(JJJ(X,N-1)/JJJ(X,N)))     ! Log mean
         ELSE     !Arithmetic mean
            TOTN=TOTN+(JJJ(X,N-1)+JJJ(X,N))/2.
         ENDIF
   30    CONTINUE
         TOTN=TOTN*(DELZ/VEL(RAD(X,DELX)))/(LAMBDA*XL*XL) ! Dimensional
      ENDIF
      END
C
C
      SUBROUTINE GD(DTAU,KNCRIT,GDTAU,KNAPRX)
C                   DTAU==Growth time interval from SUBROUTINE TAUF
C                   KNCRIT==Initial Knudsen number before growth
C                   GDTAU==Kn**(-1)*F(Kn)  Fuchs-Sutugin growth rate
C                   KNAPRX==Knudsen number of particle grown for
C                           DTAU time interval from initial KNCRIT size
      REAL KNCRIT,KNAPRX
C Accurate approximate formula for GDTAU:
      D=2.*DTAU+(2.666+1./KNCRIT)/KNCRIT
      KNAPRX=(1.333+SQRT(1.776889+D))/D
      GDTAU=(1.+KNAPRX)/(KNAPRX*(1.+KNAPRX*(1.2+1.333*KNAPRX)))
        DO 10 I=1,3
C Second-order Newton method iterated thrice for Knudsen number:
        F0=((1.333*KNAPRX+1.71)*KNAPRX+1.)*KNAPRX*GDTAU-KNAPRX-1.
        F1=((4.999*KNAPRX+3.42)*KNAPRX+1.)*GDTAU-1.
        F2= (9.998*KNAPRX+3.42)*GDTAU
        KNAPRX=KNAPRX-(F1/F2)*(1.-SQRT(1.-2.*F0*F2/(F1*F1)))
   10   CONTINUE
      END
C-----------------------------------------------------------------------
C
C       Boundary Condition and Saturation Pressure Routines
C
C-----------------------------------------------------------------------
      SUBROUTINE WALLT(Z,TWALL)
      INTEGER Z
      COMMON /PR3/ NX,NZ,NFLX,NFLZ,XLEWIS,NSTEP
      TWALL=0.
      IF (Z.LT.NSTEP) TWALL=1.-REAL(Z)/REAL(NSTEP)
      END
C
C
      SUBROUTINE WALLXA(Z,XAWALL)
      INTEGER Z
      COMMON /PR2/ SIGMA,DIFF,XAW,XAO,TW,TO
      COMMON /PR3/ NX,NZ,NFLX,NFLZ,XLEWIS,NSTEP
      XAWALL=0.
      IF (Z.LT.NSTEP) THEN
          CALL WALLT(Z,TWALL)
          XAWALL=(XSAT(TW+(TO-TW)*TWALL)-XAW)/(XAO-XAW)
      ENDIF
      IF (XAWALL.GT.1.) XAWALL=1.
      END
C
C
      REAL FUNCTION XSAT(DT)
C Saturation mole fraction for dibutyl phthalate
      IF (DT.GT.399.74) THEN
         XSAT=EXP( 8925.*(1./613. -1./DT))
      ELSE
         XSAT=EXP(10778.*(1./561.5-1./DT))
      ENDIF
      END
C-----------------------------------------------------------------------
C
C             Green's functions for laminar tube flow
C
C             Finite-difference solutions to diffusion equations
C             at Z - ZP = DELZ and DELZ/Le
C             with homogeneous boundary conditions and
C             input unit mass (and heat) per unit time per unit length
C             of circle of radius r'.
C
C-----------------------------------------------------------------------
      SUBROUTINE GREENE(GREEN,GRNFLG)
      INTEGER X,Z,XP,A,B,GRNFLG
      REAL GREEN(0:20,0:20,1:2),C(0:20,0:294)
      COMMON /PR3/ NX,NZ,NFLX,NFLZ,XLEWIS
```

```
      COMMON /PR1/ PI,DELX,DELZ
      RAD(A,D)=1.-D*REAL(A)
      VEL(E)=1.-E*E              ! Velocity profile
      PRINT*,'CALCULATING GREEN FUNCTION'
C   'MICRO' DELZ = DELZ/MICRO
      MICRO=MIN(294,INT(MAX(1.,.12*DELZ/(DELX)**3.))*INT(10.*XLEWIS))
      BETA=DELZ*XLEWIS/(REAL(MICRO)*DELX*DELX)
C   Grn fncn with >50% in central spike ==> DELZ < -ln(.5)*DELX**3
C   For computationally coarse limit,       DELZ <    MICRO*DELX**3
      IF (DELZ.GT.REAL(MICRO)*DELX**3./XLEWIS) THEN
         PRINT*,'DELZ TOO LARGE'
         GO TO 300
      ENDIF
      IF (DELZ.GT..69*DELX**3.) PRINT*,
     : '>50% LOSS IN GREEN FUNCTION CENTRAL SPIKE IN WALLSIDE INTERVAL'
C   Calculate Green's functions
      DO 100 XP=1,NX
      DO  10  A=0,NX
      DO  10 R=0,MICRO
        C(A,R)=0.
   10 CONTINUE
        C(XP,0)=1./VEL(RAD(XP,DELX))
      DO  40  Z=1,MICRO
      C(1,Z)=C( 1, Z-1)*(1.-2.*BETA/VEL(RAD(1,DELX)))
     :       +C( 2, Z-1)*((RAD(1,DELX)+RAD(2,DELX))/(2.*RAD(1,DELX)))
     :                  *BETA/VEL(RAD(1,DELX))
      DO  20  X=2,NX-1
      C(X,Z)=C( X, Z-1)*(1.-2.*BETA/VEL(RAD(X,DELX)))
     :   + ( C(X-1,Z-1)*(RAD(X,DELX)+RAD(X-1,DELX))/(2.*RAD(X,DELX))
     :       +C(X+1,Z-1)*(RAD(X,DELX)+RAD(X+1,DELX))/(2.*RAD(X,DELX)) )
     :                  *BETA/VEL(RAD(X,DELX))
   20 CONTINUE
      C(NX,Z)=C( NX, Z-1)*(1.-4.*BETA/VEL(RAD(NX,DELX)))
     :       +C(NX-1,Z-1)*4.*BETA/VEL(RAD(NX,DELX))
      IF (Z.EQ.NINT(MICRO/XLEWIS)) THEN
         DO 30 A=1,NX
           GREEN(A,XP,1)=C(A,Z) ! For mass diffusion
   30    CONTINUE
      ENDIF
   40 CONTINUE
      DO  50  A=0,NX
        GREEN(A,XP,2)=C(A,MICRO)  ! For heat diffusion
   50 CONTINUE
  100 CONTINUE
      DO 200  A=0,NX
        GREEN(A,0,1)=0.
        GREEN(A,0,2)=0.
  200 CONTINUE
      GRNFLG=0  ! Clear flag iff Green's function was calculated
  300 CONTINUE
      END
C-----------------------------------------------------------------------
C
C                   Input/Output Routines
C
C-----------------------------------------------------------------------
      SUBROUTINE INIT
      INTEGER X,Z,A,B,GRNFLG,PLTFLG
      REAL XA(0:20,0:749),TMP(0:20,0:749)
      REAL GREEN(0:20,0:20,1:2)
      REAL LAMBDA,KNCRIT,KNS,NO,NSEED
      CHARACTER PM*4
      COMMON /GRN/ GREEN
      COMMON /FUN/ XA,TMP,KNS
      COMMON /PR1/ PI,DELX,DELZ,LAMBDA,XL,TSCALE,KNCRIT,NSEED,NO
      COMMON /PR2/ SIGMA,DIFF,XAW,XAO,TW,TO,CRATIO
      COMMON /PR3/ NX,NZ,NFLX,NFLZ,XLEWIS,NSTEP
      COMMON /PLT/ PLTFLG,NZZ,KCYCLE
      DATA GRNFLG /1/
      OPEN(15,FILE='PARAM',STATUS='OLD')
      READ(15,'(F7.5/,I3/,F6.4/,E8.2/,F5.3/,F5.3/,3(F5.2/),
     :  E9.3/,F6.2/,F6.2/,F8.2/,3(I3/),A/,I3)')
     :  DELZ,NSTEP,XL,LAMBDA,DIFF,CRATIO,KNCRIT,SIGMA,XLEWIS,
     :  XAO,TW,TO,NO,NFLX,NFLZ,NZZ,PM,KCYCLE
      CLOSE(15,STATUS='KEEP')
      TSCALE=(XL/LAMBDA)**2.*CRATIO*(XAO-XAW)
      XAW=XSAT(TW)
      DELX=1./NX
      NSEED=LAMBDA*XL*XL*NO
      WRITE(6,'(A)') ' INITIAL PARAMETERS'
      CALL PNTPM(6)
      WRITE(6,'(T2,A,A)') 'PLOT DECISION = ',PM
      IF (PM.EQ.'YES') PLTFLG=1  ! Set 'PLoT FLaG'
      DO 50 A=0,NX
      XA(A,0)=1.
```

```
      TMP(A,0)=1.
   50 CONTINUE
      DO 60 A=1,NZ
      XA(0,A)=0.
   60 CONTINUE
      IF (GRNFLG.EQ.1) CALL GREENE(GREEN,GRNFLG)
      IF (GRNFLG.EQ.1) STOP  ! Green's function not calculable
      END
C
C
      SUBROUTINE PNTPM(F)
      INTEGER F
      REAL LAMBDA,KNCRIT,NO,NSEED
      COMMON /PR1/ PI,DELX,DELZ,LAMBDA,XL,TSCALE,KNCRIT,NSEED,NO
      COMMON /PR2/ SIGMA,DIFF,XAW,XAO,TW,TO,CRATIO
      COMMON /PR3/ NX,NZ,NFLX,NFLZ,XLEWIS,NSTEP
      WRITE (F,'(/,T3, A , T12, A , T20, A , T32, A/
     :           T2,F6.4,T11,F7.5,T2C,G9.3,T34,I3)')
     :             'DELX','DELZ','TSCALE','WALL RAMP',
     :              DELX,  DELZ,  TSCALE,  NSTEP
      WRITE (F,'(/,T2,A,T11,A,T20,A/,T2,F5.3,T11,E7.1,T20,F6.3)')
     :     'XL (CM)','LAMBDA','DIFFUSIVITY',XL,LAMBDA,DIFF
      WRITE (F,'(/,T2, A , T11, A , T20, A , T31, A/
     :           T2,F5.3,T11,F5.2,T2C,F5.2,T35,F4.2)')
     :           'C/CO','KNCRIT','SIGMA','LEWIS NUMBER',
     :           CRATIO, KNCRIT,  SIGMA, XLEWIS
      WRITE (F,'(/,T7,A,T1F,A/,T4,G9.3,T15,G9.3,T28,A)')
     :     'XAW','XAO',XAW,XAO,'DN/DLCG(DP),      /CC'
      WRITE (F,'(T28,A)') 'DV/DLCG(DP), CU.MICRONS/CC'
      WRITE (F,'(T8,A,T17,A,T28,A/,T6,F6.2,T15,F6.2)')
     :     'TW','TO','DP, MICRONS',TW,TO
      WRITE (F,'(/,T2,A,G1C.4,A)') ' SEED CONC. = ',NO,' /CC'
      WRITE (F,'(/,T2,A,T15,A,I3,A,I3)')
     :       'PRINT FREQ.:','NFLX = ',NFLX,' NFLZ = ',NFLZ
      WRITE (F,'(/,T2,A,I3,A,I3)') ' DIMENSIONS-- X:',NX,' BY Z:',NZ
      END
C
C
      SUBROUTINE WRTE(X,Z,NV,VL,V,PHI2,PHIT,PHIS,TOTN,XJ,TRUBFL,
     :                LSNKFL)
      INTEGER X,Z,A,B,TRUBFL,HDGFLG,PLTFLG
      REAL XA(0:20,0:749),TMP(0:20,0:749)
      REAL NV(0:749),VL(0:749),V(0:749)
      REAL AVGDP(1:60),AVENV(1:60),AVEVL(1:60)
      REAL LAMBDA,KNCRIT,KNS,NO,NSEED,INTNV,INTVNV,INTVL
      COMMON /FUN/ XA,TMP,KNS
      COMMON /PR1/ PI,DELX,DELZ,LAMBDA,XL,TSCALE,KNCRIT,NSEED,NO
      COMMON /PR2/ SIGMA,DIFF,XAW,XAO,TW,TO,CRATIO
      COMMON /PR3/ NX,NZ,NFLX
      COMMON /PLT/ PLTFLG,NZZ,KCYCLE
      SAVE HDGFLG ! 'HeaDinG FLaG' detects need to print table headings
      SAVE SUMRVR,SUMRVRN,AVGDP,AVENV,AVEVL
      SAVE AVEXA,AVETMP,AVENUM,AVEVOL,AVEDP,AVESDP,AVSDVL
      DATA HDGFLG /500/
      RAD(N,D)=1.-D*REAL(N)
      VEL(E)=1.-E*E
C        Dimensionaleze nucleation rate
      XXJ=XJ*DIFF/(LAMBDA*XL**4.)
      SDIA=2.E4*LAMBDA/KNS  ! Seed diameter, microns
      INTNV=0.
      INTVNV=0.
      INTVL=0.
      DPAVE=0.
      IF (XJ.EQ.C..AND.PHIT.EQ.0.) GO TO 10
C Draw marker lines if needed
      IF (X.LT.HDGFLG) WRITE (12,'(/,T40,A,T83,A/)')
     :   '0------------','0------------'
      IF (TRUBFL.EQ.1) WRITE (12,'(T2,A)') 'INCORRECT CONVERGENCE'
      WRITE (12,'(T52,     A,    I3, A,    I3)')
     :     ' COORDINATES  X = ',X,' Z = ',Z
      DO 10 R=0,INT(Z/(10*KCYCLE))
         SUMNV=0.
         DO 5 N=10*R*KCYCLE,(10*R+9)*KCYCLE,KCYCLE
         IF (V(N+1).GT.0..AND.V(N).GT.C.) THEN ! Trapazoidal integration
          INTNV=INTNV+(NV(N)+NV(N+1))*LOG1C(V(N+1)/V(N))/2.
          INTVNV=INTVNV+(NV(N)+NV(N+1))*(V(N)+V(N+1))
     :                 *LOG10(V(N+1)/V(N))/4.
          INTVL=INTVL+(VL(N)+VL(N+1))*LOG1C(V(N+1)/V(N))/2.
         ENDIF
            SUMNV=SUMNV+NV(N)
    5    CONTINUE
         IF (SUMNV.NE.0.) WRITE (12,'(3(T2,10E12.3,/))')
     :      (NV(N*KCYCLE),N=10*R,10*R+9),
     :      (VL(N*KCYCLE),N=10*R,10*R+9),
     :       (V(N*KCYCLE),N=10*R,10*R+9)
```

```
   10 CONTINUE
      IF (INTNV.NE.0.) THEN
        DPAVE=INTVNV/INTNV
      ELSE
        DPAVE=C.
      ENDIF
      IF(PLTFLG.EQ.1.AND.Z.EQ.NZZ) THEN ! Write on plot file:'STORE.DAT'
        WRITE(14,'(I3,I3,I3)') X,Z,(1+NZZ)/KCYCLE
        DO 15 B=0,NZZ,KCYCLE
          WRITE (14,'(3E12.6)') NV(B),VL(B),V(B)
   15   CONTINUE
      ENDIF
      IF (X.LT.HOGFLG) THEN  ! Write table headings
        WRITE (13,'(//,T2,A,I3,T89,A,G10.4,A/)')
     :          'Z = ',Z,' SEED N = ',NC,' /CC.'
      WRITE(13,'(T4,A,T11,A,T17,A,T27,A,T36,A,T49,A,T59,A,T68,A,T79,A,
     :  T90,A,T107,A/,T23,A,T36,A,T47,A,T66,A,T77,A,T92,A,T105,A/,
     :  T2,A,T10,A,T17,A,T25,A,T36,A,T47,A,T58,A,T69,A,T80,A,T91,A,
     :  T99,A,T108,A)') 'X','XA','TEMP','J','INT.J','N','PHI2',
     :  'INT.PHI2','HOMO PHI','AVE E SEED DIA','SEED PHI',
     :  '(/CC.SEC.)','(/CC.)','(/CC.)','(CU.MIC/CC)','(CU.MIC/CC)',
     :  '(MICRONS)','(CU.MIC/CC)','------','------','------','------',
     :'------','------','------','------','------','------'
      CALL WALLT(Z,TWALL)
      CALL WALLXA(Z,XAWALL)
      WRITE (13,'(T2,I3,T9,F6.4,T16,F6.4)') 0,XAWALL,TWALL
      ENDIF
C        TOTN == TOTal homogeneous aerosol Number concentration from
CCC             integral of nucleation rate (log. interpolation of JJJ).
         INTNV== Total homogeneous aerosol number concentration from
CCC             INTegral of aerosol number distribution
CCC             (log. interpolation of NV).
         PHIT == Total volume fraction of aerosol from rect. integration
CCC             of volume distribution, plus seed volume.
         INTVL==Total volume fraction of homogeneously formed aerosol
C               from INTegration of volume distribution
C               (log. interpolation of VL).
      WRITE (13,'(T2,I3,T9,F6.4,T16,F6.4,T23,G10.4,T34,G10.4,T45,G10.4,
     :   T56,G10.4,T67,G10.4,T78,G10.4,T90,F6.4,T98,F6.4,T106,G10.4)')
     :X,XA(X,Z),TMP(X,Z),XXJ,TOTN,INTNV,PHI2,PHIT,INTVL,DPAVE,SDIA,PHIS
      IF (LSNKFL.EQ.1) THEN  ! Indicate Large SINK,  '*'
        WRITE (13,'(A)') '+      *'
        LSNKFL=0  ! Reset Large-SINK FLag
      ENDIF
C Calculate cup-mixed averages
      IF (X.EQ.NFLX) THEN  ! Initialize
        SUMRVR=0.
        SUMRVRN=0.
        DO 20 I=1,NX-1
        SUMRVR=SUMRVR+RAD(I,DELX)*VEL(RAD(I,DELX))
   20   CONTINUE
        SUMRVR=SUMRVR+DELX/8.
C       AVGDP array is C.C05 to 5.0 microns in range
        DO 30 I=1,60
        AVGDP(I)=10.**((I-46.)/20.)
        AVENV(I)=0.
        AVEVL(I)=0.
   30   CONTINUE
        AVEXA=0.    ! Mole fraction
        AVETMP=0.   ! Temperature
        AVENUM=0.   ! Total N from distribution
        AVEVOL=0.   ! Total V from distribution
        AVEDP=0.    ! Average DP from distribution
        AVESDP=0.   ! Seed DP
        AVSDVL=0.   ! Seed volume
      ENDIF
      IF (X.EQ.NX) THEN
        WEIGHT=DELX/(8.*SUMRVR)
        WEIGHTN=WEIGHT*INTNV
      ELSE
        WEIGHT=RAD(X,DELX)*VEL(RAD(X,DELX))/SUMRVR
        WEIGHTN=WEIGHT*INTNV
      ENDIF
      DO 40 I=1,60
      CALL INTERP(NV,V,AVGDP(I),TERP)
      AVENV(I)=AVENV(I) + TERP*WEIGHT
      CALL INTERP(VL,V,AVGDP(I),TERP)
      AVEVL(I)=AVEVL(I) + TERP*WEIGHT
   40 CONTINUE
      AVEXA =AVEXA +  XA(X,Z)*WEIGHT
      AVETMP=AVETMP+ TMP(X,Z)*WEIGHT
      AVENUM=AVENUM+   INTNV *WEIGHT
      AVEVOL=AVEVOL+   INTVL *WEIGHT
      AVEDP =AVEDP +   DPAVE *WEIGHTN
      AVESDP=AVESDP+    SDIA *WEIGHT
```

```
      AVSDVL=AVSDVL+    PHIS *WEIGHT
C  Accumulate sum of 'Numbered' weights
      SUMRVRN=SUMRVRN + WEIGHTN
      IF (X.EQ.NX) THEN  ! Print cup-mix quantities
      IF (SUMRVRN.GT.0.) AVEDP=AVEDP/SUMRVRN
      WRITE (13,'(/,A/,T9,F6.4,T16,F6.4,T45,G10.4,T78,G10.4,T90,F6.4,
     :  T98,F6.4,T106,G10.4)') ' CUP-MIX AVERAGES:',
     :  AVEXA,AVETMP,AVENUM,AVEVOL,AVEDP,AVESDP,AVSDVL
      WRITE(13,'(/,A,F5.1,A,F5.1,A,F5.1,A,F5.1,A)')
     :  ' VAPOR: ',100.*AVEXA,' %, AEROSOL: ',
     :  1.E-10*AVEVOL/(CRATIO*XAO),' % HOMOG., ',
     :  1.E-10*AVSDVL/(CRATIO*XAO),' % SEED.  WALL LOSS = ',
     :  100.*(1.-AVEXA-1.E-12*(AVEVOL+AVSDVL)/(CRATIO*XAO)),' %'
      WRITE (13,'(/,A)') ' DISTRIBUTIONS:'
      DO 50 IFIL=13,14
C  Write on 'STORE' if PLTFLG=1 and N=NZZ
      IF ((IFIL.EQ.14.AND.PLTFLG.NE.1).OR.
     :    (IFIL.EQ.14.AND.      Z.NE.NZZ)  ) GO TO 50
        DO 49 IN=0,5
        WRITE(IFIL,'(3(T2,10E12.4/))')
     :       (AVENV(I),I=10*IN+1,10*(IN+1)),
     :       (AVEVL(I),I=10*IN+1,10*(IN+1)),
     :       (AVGDP(I),I=10*IN+1,10*(IN+1))
   49   CONTINUE
   50 CONTINUE
      ENDIF
      HOGFLG=X
      END
C
C
      SUBROUTINE INTERP(YX,X,XO,TERP)
C                       YX==Function to be interpolated
C                       X ==Array of independent variable
C                       XO==Value of X for which to find interpolated YX
C                       TERP==Interpolated value of YX
      REAL YX(0:749),X(0:749)
C  Assume that values of X(N) ascend in N
      COMMON /PR3/ NX,NZ
      TERP=0.
      DO 10 N=0,NZ
      IF (X(N).GE.XO) THEN
         TERP=YX(N-1) + (XO-X(N-1))*(YX(N)-YX(N-1))/(X(N)-X(N-1))
         GO TO 20
      ENDIF
   10 CONTINUE
   20 CONTINUE
      END
C
C
      SUBROUTINE TROUBLE(XBF,XAXZ,X,Z,XHXZ,SINK,FXU,FXL,XU,XXL)
C Diagnostic information printed out
      INTEGER X,Z
      PRINT*,'ITERATION LIMIT REACHED AT X =',X,', Z =',Z
      PRINT*,'XA = ',XXL,' GIVES ',FXL
      PRINT*,'XA = ',XU,' GIVES ',FXU
      PRINT*,'LAST XA WAS ',XBF,', GIVING XH-SINK = ',(XHXZ-SINK)
      PRINT*,'NEXT XA = ',XAXZ
      END
```

F.3 Parameter Data File

```
0.000500   DELZ                                   F8.6
  16       WALL                                    I3
0.8636     XL    Tube radius, cm                   F6.4
1.71E-06   LAMBDA,  cm                            E8.2
0.052      DIFFusivity,  cm**2 sec**(-1)          F5.3
0.011      c/cd                                    F5.3
10.00      KNCRIT                                  F5.2
33.00      SIGMA at 298 K                          F5.2
 4.20      Lewis number                            F5.2
0.100E-03  XA0                                     E9.3
298.00     TW,        Degrees Kelvin               F6.2
423.00     T0,        4 2 3 == Nominal             F6.2
0.00E+00   Seed concentration,  cm**(-3)           E8.2
  1        NFLX                                    I3
 20        NFLZ                                    I3
239        N77 <=749, 2 3 9 = Nominal              I3
NO         Plots?              Left-justified A
  1        KCYCLE for DISTR. output & plotting.    I3
 20        NX     Read by plotting program.        I3
```

F.4 Fortran Plotting Program

```
C-----------------------------------------------------------------------
C
C     Plotting program for local aerosol distributions, Z=NZZ
C
C-----------------------------------------------------------------------
      INTEGER IMESS(1:2),X,Z
      REAL MAXNV,MAXVL
      REAL NV(1:500),VL(1:500),V(1:500)
      REAL AVENV(1:60),AVEVL(1:60),AVGDP(1:60)
      DATA IMESS /'R = ','Z = '/
      OPEN(21,FILE='PARAM',STATUS='OLD')
      READ(21,'(F8.6,18(/),I3)') DELZ,NX
      CLOSE(21,STATUS='KEEP')
       XLEFT=-1.5    ! LOG(DP) at left
       XRIGHT=.5     ! LOG(DP) at right
       XSCALE=(XRIGHT-XLEFT)/8.
C     XZERDP=-Position of 1 micron point on 8" wide plot, before scaling
       XZERDP=-XLEFT/XSCALE
      PRINT*,'NUMBER OF PLOTS?'
      READ*,NPLOTS
      IF (NPLOTS.LE.0) STOP
C    Plot at every NCYCLE-th value of X, starting with X=NSTART
      PRINT*,'X COORDINATE OF FIRST PLOT?'
      READ*,NSTART
      PRINT*,'X-INTERVAL SPACING BETWEEN PLOTS?'
      READ*,NCYCLE
      IF (NSTART+(NPLOTS-1)*NCYCLE.GT.NX) THEN
         PRINT*,'INCOMPATABLE, TOO MANY PLOTS REQUESTED'
         STOP
      ENDIF
      PRINT*,'PLOT SPEED (1-20):'
      READ*,NSP ! 1=Slowest,   20=Fastest
C    Read entire file 'STORE', and draw appropriate plots
      OPEN(14,FILE='STORE',STATUS='OLD')
      CALL PLOTS(53,0,8)
C    Reduce an 8" wide plot to 6" wide
      CALL FACTOR(0.75)
      DO 100 M=1,NX+1
C        Find maximum values and scale to round units
         MAXNV=0.
         MAXVL=0.
         IF (M.NE.NX+1) THEN  ! Read local distributions
            READ(14,'(I3,I3,I3)') X,Z,NPTS
            DO 10 N=1,NPTS
               READ (14,'(3E12.6)') NV(N),VL(N),V(N)
               MAXNV=MAX(MAXNV,NV(N))
               MAXVL=MAX(MAXVL,VL(N))
               V(N)=LOG10(MAX(1.E-3,V(N)))/XSCALE
               IF (V(N).LT.XLEFT/XSCALE) V(N)=XLEFT/XSCALE
               IF (V(N).GT.XRIGHT/XSCALE) V(N)=XRIGHT/XSCALE
   10          CONTINUE
         ELSE  ! Read averaged distribution
            DO 11 IN=0,5
               READ(14,'(3(T2,10E12.4/))')
     :         (AVENV(I),I=10*IN+1,10*(IN+1)),
     :         (AVEVL(I),I=10*IN+1,10*(IN+1)),
     :         (AVGDP(I),I=10*IN+1,10*(IN+1))
   11       CONTINUE
            DO 12 I=1,60
               MAXNV=MAX(MAXNV,AVENV(I))
               MAXVL=MAX(MAXVL,AVEVL(I))
               AVGDP(I)=LOG10(MAX(1.E-3,AVGDP(I)))/XSCALE
             IF (AVGDP(I).LT. XLEFT/XSCALE) AVGDP(I)= XLEFT/XSCALE
             IF (AVGDP(I).GT.XRIGHT/XSCALE) AVGDP(I)=XRIGHT/XSCALE
   12          CONTINUE
         ENDIF
C     If plot is not to be drawn, skip on to 100
         IF (M.LT.NSTART.OR.
     :   (M.GT.NSTART+(NPLOTS-1)*NCYCLE.AND.M.LT.NX+1)) GO TO 100
         IF (MOD(M-NSTART,NCYCLE).NE.0.AND.M.NE.NX+1) GO TO 100
         IF (MAXNV.EQ.0.) GO TO 100
C  Find appropriate scaling for vertical axis
         YMAGN=INT(LOG10(1.E10*MAXNV)-10.)
         YSCN=MAXNV*10.**(-YMAGN)
         IF (YSCN.LT.2.) THEN
            YSCLN=2.*10.**YMAGN
         ELSEIF (YSCN.LT.5.) THEN
            YSCLN=5.*10.**YMAGN
         ELSE
            YSCLN=10.**(YMAGN+1)
         ENDIF
         YMAGV=INT(LOG10(1.E10*MAXVL)-10.)
         YSCV=MAXVL*10.**(-YMAGV)
         IF (YSCV.LT.2.) THEN
            YSCLV=2.*10.**YMAGV
```

```
      ELSEIF (YSCV.LT.5.) THEN
         YSCLV=5.*10.**YMAGV
      ELSE
         YSCLV=10.**(YMAGV+1)
      ENDIF
C  Scale distributions for plotting
C  Scaling for 5" high plot, before rescaling by 'FACTOR' statement
      YSCLN=YSCLN/5.
      YSCLV=YSCLV/5.
      IF (M.NE.NX+1) THEN  ! Scale local distributions
         DO 20 N=1,NPTS
            NV(N)=NV(N)/YSCLN
            VL(N)=VL(N)/YSCLV
20       CONTINUE
      ELSE !               Scale averaged distributions
         DO 21 N=1,60
            AVENV(N)=AVENV(N)/YSCLN
            AVEVL(N)=AVEVL(N)/YSCLV
21       CONTINUE
      ENDIF
C  Draw axis, labels, box around volume distribution plot
      CALL ORIGIN(2.,1.333,1)
      CALL SPEED(NSP)
      CALL AXIS(0.,0.,7HLOG(DP),-7,8.,0.,XLEFT,XSCALE)
      CALL AXIS(0.,0.,11HDV/DLOG(DP),11,5.,90.,0.,YSCLV)
      CALL SPEED(20)
      CALL PLOT(8.,0.,3)
      CALL SPEED(NSP)
      CALL PLOT(8.,5.,2)
      CALL PLOT(0.,5.,2)
      CALL SPEED(20)
      CALL ORIGIN(XZEROP,0.,1)
C  Draw volume distribution
      IF (M.NE.NX+1) THEN  ! Local distribution
         CALL PLOT(V(1),VL(1),3)
         CALL SPEED(NSP)
         DO 30 N=2,NPTS
            CALL PLOT(V(N),VL(N),2)
30       CONTINUE
      ELSE  ! Plot average distribution
         CALL PLOT(AVGDP(1),AVEVL(1),3)
         CALL SPEED(NSP)
         DO 31 N=2,60
            CALL PLOT(AVGDP(N),AVEVL(N),2)
31       CONTINUE
      ENDIF
C  Draw axis, labels, box around number distribution plot
      CALL ORIGIN(-XZEROP,6.667,1)
      CALL AXIS(0.,0.,7HLOG(DP),-7,8.,0.,XLEFT,XSCALE)
      CALL AXIS(0.,0.,11HDN/DLOG(DP),11,5.,90.,0.,YSCLN)
      CALL SPEED(20)
      CALL PLOT(8.,0.,3)
      CALL SPEED(NSP)
      CALL PLOT(8.,5.,2)
      CALL PLOT(0.,5.,2)
      CALL ORIGIN(XZEROP,0.,1)
C  Draw number distribution
      CALL SPEED(20)
      IF (M.NE.NX+1) THEN  ! Local distribution
         CALL PLOT(V(1),NV(1),3)
         CALL SPEED(NSP)
         DO 40 N=2,NPTS
            CALL PLOT(V(N),NV(N),2)
40       CONTINUE
         CALL ORIGIN(-XZEROP,0.,1)
C  Draw title
         CALL SYMBOL(2.,-1.,.25,IMESS(1),0.,4)
         CALL NUMBER(999.,999.,.25,(1.-REAL(X)/NX),0.,2)
         CALL SYMBOL(4.5,-1.,.25,IMESS(2),0.,4)
         CALL NUMBER(999.,999.,.25,DELZ*REAL(Z),0.,3)
      ELSE  ! Plot average distribution
         CALL PLOT(AVGDP(1),AVENV(1),3)
         CALL SPEED(NSP)
         DO 50 N=2,60
            CALL PLOT(AVGDP(N),AVENV(N),2)
50       CONTINUE
         CALL ORIGIN(-XZEROP,0.,1)
C  Draw title 'AVERAGE'
         CALL SYMBOL(3.2,-1.,.25,7HAVERAGE,0.,7)
      ENDIF
      CALL ORIGIN(28./3.,-8.,1)
100 CONTINUE
    CALL SPEED(20)
    CALL PLOT(0.,0.,999)
    CLOSE(14,STATUS='KEEP')
    END
```

F.5 Parameter Data File for Plotting Programs

```
1.00        SC, SCaling parameter
 20         NSTEP,  Axial length of wall temperature ramp
423.00      TO
298.00      TW
0.100E-03   XAO
Data file to supply parameters for STREAM, STREAM3D AND STREAMG.
Maintain (TO-TW)/(423-298) = SC  to preserve sat'n curve location
```

F.6 Fortran Plotting Programs

```
C-----------------------------------------------------------------------
C
C       Plotting Program to Visualize Streamlines
C          on Temperature-Mole Fraction Space
C
C         Cooling and Diffusion Without Aerosol
C
C-----------------------------------------------------------------------
      REAL XA(0:50,0:200),TMP(0:50,0:200),GREEN(0:50,0:50,1:2)
      INTEGER X,Z
      COMMON /GRN/ GREEN
      COMMON /FUN/ XA,TMP
      COMMON /PAR/ PI,DELX,DELZ
      COMMON /XRA/ NX,XLEWIS,NSTEP
      COMMON /PJ/ XAW,XAO,TW,TO
      NX=50
      NZZ=200
      DELX=1./NX
      DELZ=.0005
      XLEWIS=4.2  ! For dibutyl phthalate
      OPEN(10,FILE='TAO',STATUS='OLD')
      READ(10,'(F5.2)') SC
      READ(10,'(I3)') NSTEP
      READ(10,'(F6.2)') TO
      READ(10,'(F6.2)') TW
      READ(10,'(E9.3)') XAO
      CLOSE(10,STATUS='KEEP')
      XAW=XSAT(TW)
      DO 5 N=1,NX
       TMP(N,0)=1.
       XA(N,0)=1.
    5 CONTINUE
C  Read Green's functions
      OPEN(11,FILE='GREN',STATUS='OLD')
      DO 73 I3=1,2
       DO 73 I2=1,NX
        DO 73 I1=1,NX
         READ(11,'(E12.6)') GREEN(I1,I2,I3)
   73 CONTINUE
      PRINT*,'GREEN READ FROM FILE: GREN.DAT'
      DO 100 Z=1,NZZ
       IF(MOD(Z,10).EQ.0) PRINT*,'Z =',Z
       DO 300 X=1,NX
        CALL HOMOG(X,Z,XA(X,Z),TMP(X,Z))
  300  CONTINUE
  100 CONTINUE
C Plot
      PRINT*,'WRITING PLOT'
      CALL PLOTS(53,0,9)
      CALL FACTOR(17./24)
      CALL ORIGIN(1.,2.,1)
      CALL SPEED(3)
      CALL PLOT(0.,0.,3)
      CALL PLOT(10.,0.,2)
      CALL PLOT(10.,10.,2)
      CALL PLOT(0.,10.,2)
      CALL PLOT(0.,0.,2)
      DO 30 X=5,NX,5   ! Draw streamlines at NX/5 radial positions
       CALL PLOT(10.*XA(X,0),10.*MIN(1.,SC*TMP(X,0)),3)
       DO 20 Z=1,NZZ
        CALL PLOT(10.*XA(X,Z),10.*MIN(1.,SC*TMP(X,Z)),2)
   20  CONTINUE
   30 CONTINUE
      DO 31 Z=0,NZZ,20  ! Draw NZZ/20 lines of constant Z
       CALL PLOT(10.*XA(1,Z),10.*MIN(1.,SC*TMP(1,Z)),3)
       DO 32 X=2,NX
        CALL PLOT(10.*XA(X,Z),10.*MIN(1.,SC*TMP(X,Z)),2)
   32  CONTINUE
   31 CONTINUE
C Assign saturation curve
      DO 87 N=0,NX
       TMP(N,0)=1.-REAL(N)/NX
       XA(N,0)=MIN(1.,(XSAT(TW+(TO-TW)*TMP(N,0))-XAW)/(XAO-XAW))
   87 CONTINUE
      CALL PLOT(10.*XA(0,0),10.*MIN(1.,SC*TMP(0,0)),3)
      DO 89 N=1,NX
       CALL PLOT(10.*XA(N,0),10.*MIN(1.,SC*TMP(N,0)),2)
   89 CONTINUE
      CALL PLOT(11.,-2.,999)
      END
```

```
C-----------------------------------------------------------------------
C
C                    Integration Routines
C
C-----------------------------------------------------------------------

      SUBROUTINE HOMOG(X,Z,XHH,TMMP)
      INTEGER X,XP,Z
      REAL XA(0:50,0:200),TMP(0:50,0:200)
      REAL GREEN(0:50,0:50,1:2)
      COMMON /GRN/ GREEN
      COMMON /FUN/ XA,TMP
      COMMON /PAR/ PI,DELX,DELZ
      COMMON /XRA/ NX
      RAD(L,D)=1.-D*REAL(L)
      VEL(E)=1.-E*E
      CALL WALLXA(Z,XAWALL)
      CALL WALLT(Z,TWALL)
      XHH=XAWALL
      TMMP=TWALL
      DO 100 XP=1,NX
      XHH =XHH +( XA(XP,Z-1)-XAWALL)*VEL(RAD(XP,DELX))*GREEN(X,XP,1)
      TMMP=TMMP+(TMP(XP,Z-1)-TWALL )*VEL(RAD(XP,DELX))*GREEN(X,XP,2)
  100 CONTINUE
      END
C-----------------------------------------------------------------------
C
C       Boundary Condition and Saturation Pressure Routines
C
C-----------------------------------------------------------------------
      SUBROUTINE WALLT(Z,TWALL)
      INTEGER Z
      COMMON /XRA/ NX,XLEWIS,NSTEP
      TWALL=0.
      IF (Z.LT.NSTEP) TWALL=1.-REAL(Z)/REAL(NSTEP)
      END
C
C
      SUBROUTINE WALLXA(Z,XAWALL)
      INTEGER Z
      COMMON /PJ/ XAW,XAO,TW,TO
      COMMON /XRA/ NX,XLEWIS,NSTEP
      XAWALL=0.
      IF (Z.LT.NSTEP) THEN
          CALL WALLT(Z,TWALL)
          XAWALL=(XSAT(TW+(TO-TW)*TWALL)-XAW)/(XAO-XAW)
      ENDIF
      IF (XAWALL.GT.1.) XAWALL=1.
      END
C
C
      REAL FUNCTION XSAT(DT)
C  Saturation mole fraction for dibutyl phthalate
      IF (DT.GT.399.74) THEN
         XSAT=EXP( 8925.*(1./613. -1./DT))
      ELSE
         XSAT=EXP(10778.*(1./561.5-1./DT))
      ENDIF
      END
```

```
C-----------------------------------------------------------------------
C
C     Plotting Program for Three-Dimensional Visualization
C       of Streamlines on Temperature-Mole Fraction Space
C
C            Cooling and Diffusion Without Aerosol
C
C-----------------------------------------------------------------------
      REAL XA(0:50,0:200),TMP(0:50,0:200),GREEN(0:50,0:50,1:2)
      INTEGER X,Z
      COMMON /GRN/ GREEN
      COMMON /FUN/ XA,TMP
      COMMON /PAR/ PI,DELX,DELZ
      COMMON /XRA/ NX,XLEWIS,NSTEP
      COMMON /PJ/ XAW,XAO,TW,TO
      NX=50
      NZZ=200
      DELX=1./NX
      DELZ=.0005
      XLEWIS=4.2  ! For dibutyl phthalate
      OPEN(10,FILE='TAD',STATUS='OLD')
      READ(10,'(F5.2)') SC
      READ(10,'(I3)') NSTEP
      READ(10,'(F6.2)') TO
      READ(10,'(F6.2)') TW
      READ(10,'(E9.3)') XAO
      CLOSE(10,STATUS='KEEP')
      XAW=XSAT(TW)
      DO 5 N=1,NX
       TMP(N,0)=1.
       XA(N,0)=1.
    5 CONTINUE
C  Read Green's functions
      OPEN(11,FILE='GREN',STATUS='OLD')
      DO 73 I3=1,2
       DO 73 I2=1,NX
        DO 73 I1=1,NX
         READ(11,'(E12.6)') GREEN(I1,I2,I3)
   73 CONTINUE
      CLOSE(11,STATUS='KEEP')
      DO 100 Z=1,NZZ
       IF(MOD(Z,10).EQ.0) PRINT*,'Z =',Z
       DO 300 X=1,NX
        CALL HOMOG(X,Z,XA(X,Z),TMP(X,Z))
  300  CONTINUE
  100 CONTINUE
C Plot
      PRINT*,'WRITING PLOT'
      CALL PLOTS(53,0,10)
      CALL FACTOR(11./16.)
      CALL ORIGIN(6.,4.,1)
      CALL SPEED(3)
      CALL PLOT(0.,0.,3)
      CALL PLOT(-5.,0.,2)
      CALL PLOT(-3.,-3.,2)
      CALL PLOT(2.,-3.,2)
      CALL PLOT(0.,0.,2)
      CALL PLOT(2.,10.,2)
      CALL PLOT(-3.,10.,2)
      CALL PLOT(-5.,0.,2)
      CALL PLOT(2.,-3.,3)
      CALL PLOT(4.,7.,2)
      CALL PLOT(2.,10.,2)
      DO 30 X=5,NX,5
       XPLOT=-5.*MIN(1.,SC*TMP(X,0))
       YPLOT=0.
       CALL PLOT(XPLOT,YPLOT,3)
       DO 20 Z=1,NZZ
        XPLOT=-5.*MIN(1.,SC*TMP(X,Z))+2.*(1.-XA(X,Z)+REAL(Z)/NZZ)
        YPLOT=10.*REAL(Z)/NZZ-3.*(1.-XA(X,Z))
        CALL PLOT(XPLOT,YPLOT,2)
   20  CONTINUE
   30 CONTINUE
      DO 31 Z=0,NZZ,20
       XPLOT=-5.*MIN(1.,SC*TMP(1,Z))+2.*(1.-XA(1,Z)+REAL(Z)/NZZ)
       YPLOT=10.*REAL(Z)/NZZ-3.*(1.-XA(1,Z))
       CALL PLOT(XPLOT,YPLOT,3)
       DO 32 X=2,NX
        XPLOT=-5.*MIN(1.,SC*TMP(X,Z))+2.*(1.-XA(X,Z)+REAL(Z)/NZZ)
        YPLOT=10.*REAL(Z)/NZZ-3.*(1.-XA(X,Z))
        CALL PLOT(XPLOT,YPLOT,2)
   32  CONTINUE
   31 CONTINUE
C Assign Saturation Curve
      DO 87 N=0,NX
```

```
      TMP(N,0)=1.-REAL(N)/NX
      XA(N,0)=MIN(1.,(XSAT(TW+(TO-TW)*TMP(N,0))-XAW)/(XAO-XAW))
   87 CONTINUE
      XPLOT=-5.*MIN(1.,SC*TMP(0,0))+2.*(1.-XA(0,0))
      YPLOT=-3.*(1.-XA(0,0))
      CALL PLOT(XPLOT,YPLOT,3)
      DO 89 N=1,NX
       XPLOT=-5*MIN(1.,SC*TMP(N,0))+2.*(1.-XA(N,0))
       YPLOT=-3.*(1.-XA(N,0))
       CALL PLOT(XPLOT,YPLOT,2)
   89 CONTINUE
C Draw wall streamline
      XPLOT=-5.*MIN(1.,SC*TMP(0,0))+2.*(1.-XA(0,0))
      YPLOT=-3.*(1.-XA(0,0))
      CALL PLOT(XPLOT,YPLOT,3)
      DO 93 N=1,NX
       XPLOT=-5.*MIN(1.,SC*TMP(N,0))
     :       +2.*(1.-XA(N,0)+REAL(N*NSTEP)/REAL(NX*NZZ))
       YPLOT=10.*N*NSTEP/(NX*NZZ)+3.*(1.-XA(N,0))
       CALL PLOT(XPLOT,YPLOT,2)
   93 CONTINUE
      CALL PLOT(70./11.,-4.,999)
      END
C-------------------------------------------------------------------------
CC
CC                    Integration Routines
CC
C-------------------------------------------------------------------------
      SUBROUTINE HOMOG(X,Z,XHH,TMMP)
      INTEGER X,XP,Z
      REAL XA(0:50,0:200),TMP(0:50,0:200)
      REAL GREEN(0:50,0:50,1:2)
      COMMON /GRN/ GREEN
      COMMON /FUN/ XA,TMP
      COMMON /PAR/ PI,DELX,DELZ
      COMMON /XRA/ NX
      RAD(L,D)=1.-D*REAL(L)
      VEL(E)=1.-E*E
      CALL WALLXA(Z,XAWALL)
      CALL WALLT(Z,TWALL)
      XHH=XAWALL
      TMMP=TWALL
      DO 100 XP=1,NX
      XHH =XHH +( XA(XP,Z-1)-XAWALL)*VEL(RAD(XP,DELX))*GREEN(X,XP,1)
      TMMP=TMMP+(TMP(XP,Z-1)-TWALL )*VEL(RAD(XP,DELX))*GREEN(X,XP,2)
  100 CONTINUE
      END
C-------------------------------------------------------------------------
C
C      Boundary Condition and Saturation Pressure Routines
C
C-------------------------------------------------------------------------
      SUBROUTINE WALLT(Z,TWALL)
      INTEGER Z
      COMMON /XRA/ NX,XLEWIS,NSTEP
      TWALL=0.
      IF (Z.LT.NSTEP) TWALL=1.-REAL(Z)/REAL(NSTEP)
      END
C
C
      SUBROUTINE WALLXA(Z,XAWALL)
      INTEGER Z
      COMMON /PJ/ XAW,XAO,TW,TO
      COMMON /XRA/ NX,XLEWIS,NSTEP
      XAWALL=0.
      IF (Z.LT.NSTEP) THEN
          CALL WALLT(Z,TWALL)
          XAWALL=(XSAT(TW+(TO-TW)*TWALL)-XAW)/(XAO-XAW)
      ENDIF
      IF (XAWALL.GT.1.) XAWALL=1.
      END
C
C
      REAL FUNCTION XSAT(DT)
C  Saturation mole fraction for dibutyl phthalate
      IF (DT.GT.399.74) THEN
         XSAT=EXP( 8925.*(1./613. -1./DT))
      ELSE
         XSAT=EXP(10778.*(1./561.5-1./DT))
      ENDIF
      END
```

```
C-----------------------------------------------------------------
C
C       GREEN'S FUNCTION CALCULATION FOR STREAM PROGRAMS
C
C-----------------------------------------------------------------
      REAL GREEN(0:50,0:50,1:2)
      INTEGER X,Z
      COMMON /PAR/ DELX,DELZ
      COMMON /XRA/ NX,XLEWIS,NSTEP
      NX=50
      NZZ=200
      DELX=1./NX
      DELZ=.0005
      XLEWIS=4.2   ! FOR DIBUTYL PHTHALATE
      OPEN(10,FILE='TAD',STATUS='OLD')
      READ(10,'(F5.2)') SC
      READ(10,'(I3)') NSTEP
      READ(10,'(F6.2)') TO
      READ(10,'(F6.2)') TW
      READ(10,'(E9.3)') XAC
      CLOSE(10,STATUS='KEEP')
      CALL GREENE(GREEN)
C STORE GREEN FUNCTION
      OPEN(11,FILE='GREN',STATUS='NEW')
      DO 73 I3=1,2
       DO 73 I2=1,NX
        DO 73 I1=1,NX
         WRITE(11,'(E12.6)') GREEN(I1,I2,I3)
   73 CONTINUE
      CLOSE(11,STATUS='KEEP')
      END
C-----------------------------------------------------------------
C
C                 GREEN FUNCTION FOR TUBE FLOW
C
C-----------------------------------------------------------------
      SUBROUTINE GREENE(GREEN)
      INTEGER X,Z,XP,A,B
      REAL GREEN(0:50,0:50,1:2),C(0:50,0:294)
      COMMON /XRA/ NX,XLEWIS,NSTEP
      COMMON /PAR/ DELX,DELZ
      RAD(A,B)=1.-B*REAL(A)
      VEL(B)=1.-B*B          !VELOCITY PROFILE
      PRINT*,'CALCULATING GREEN FUNCTION'
C   "MICRO" DELZ = DELZ/MICRO
      MICRO=294
      BETA=DELZ*XLEWIS/(REAL(MICRO)*DELX*DELX)
C   GRN FNCN WITH >50Z IN CENTRAL SPIKE ==> DELZ < -LN(.5)*DELX**3
C   FOR COMPUTATIONALLY COARSE LIMIT,       DELZ <    MICRO*DELX**3
      IF (DELZ.GT.REAL(MICRO)*DELX**3./XLEWIS) THEN
         PRINT*,'DELZ TOO LARGE'
         GO TO 300
      ENDIF
      IF (DELZ.GT..69*DELX**3.) PRINT*,
     : '>50Z LOSS IN GREEN FUNCTION CENTRAL SPIKE IN WALLSIDE INTERVAL'
C   CALCULATE GREEN FUNCTION
      DO 100 XP=1,NX
      DO  10  A=0,NX
      DO  10 B=0,MICRO
        C(A,B)=0.
   10 CONTINUE
        C(XP,0)=1./VEL(RAD(XP,DELX))
      DO  40  Z=1,MICRO
      C(1,Z)=C( 1, Z-1)*(1.-2.*BETA/VEL(RAD(1,DELX)))
     :       +C( 2, Z-1)*((RAD(1,DELX)+RAD(2,DELX))/(2.*RAD(1,DELX)))
     :                  *BETA/VEL(RAD(1,DELX))
      DO  20  X=2,NX-1
      C(X,Z)=C( X, Z-1)*(1.-2.*BETA/VEL(RAD(X,DELX)))
     :    + ( C(X-1,Z-1)*(RAD(X,DELX)+RAD(X-1,DELX))/(2.*RAD(X,DELX))
     :      +C(X+1,Z-1)*(RAD(X,DELX)+RAD(X+1,DELX))/(2.*RAD(X,DELX)) )
     :                  *BETA/VEL(RAD(X,DELX))
   20 CONTINUE
      C(NX,Z)=C( NX, Z-1)*(1.-4.*BETA/VEL(RAD(NX,DELX)))
     :       +C(NX-1,Z-1)*4.*BETA/VEL(RAD(NX,DELX))
      IF (Z.EQ.NINT(MICRO/XLEWIS)) THEN
         DO 30 A=1,NX
           GREEN(A,XP,1)=C(A,Z) !MOLE FRACTION
   30    CONTINUE
      ENDIF
   40 CONTINUE
      DO  50  A=0,NX
        GREEN(A,XP,2)=C(A,MICRO)  !TEMPERATURE
   50 CONTINUE
  100 CONTINUE
      DO 200  A=0,NX


        GREEN(A,C,1)=0.
        GREEN(A,0,2)=0.
  200 CONTINUE
  300 CONTINUE
      END
```

F.7 Sample Output

```
REV1 SOLUTION TC COOLED TUBE FLOW
Z STEPS ARE C.3196E-02 *V(MAX)
Z STEPS ARE (0.4547E-01 *C(LPM) ) ==CM

  DELX       DELZ      TSCALE        WALL RAMP
C.0500     0.00012   C.281E+06          64

XL (CM)   LAMBDA    DIFFUSIVITY
0.864     0.2E-05     0.028

C/CD      KNCRIT    SIGMA         LEWIS NUMBER
0.011     10.00     33.00              7.74

      XAW          XAC
   C.381E-07   0.1C0E-03     DN/DLOG(DP),       /CC
                             DV/DLOG(DP), CU.MICRONS/CC
      TW           TC        DP, MICRONS
    298.00     423.00

 SEED CONC. = C.COCOE+00 /CC

PRINT FREQ.: NFLX =    1 NFLZ =   40

 DIMENSIONS-- X: 20 BY Z:749
```

Z = 40

SEED N = 0.0000E+00 /CC.

X	XA	TEMP	J (/CC.SEC.)	INT.J (/CC.)	N (/CC.)	PHI2	INT.PHI2 (CU.MIC/CC)	HOMO PHI (CU.MIC/CC)	AVE & SEED DIA (MICRONS)		SEED PHI (CU.MIC/CC)
0	0.0718	0.3750									
1	0.3523	0.4473	0.0000E+00	0.0000E+00	0.0000E+00	0.0000E+00	0.0000E+00	0.0000E+00	0.0000	0.0107	0.0000E+00
2	0.6166	0.5221	0.0000E+00	0.0000E+00	0.0000E+00	0.0000E+00	0.0000E+00	0.0000E+00	0.0000	0.0071	0.0000E+00
3	0.8153	0.5962	0.0000E+00	0.0000E+00	0.0000E+00	0.0000E+00	0.0000E+00	0.0000E+00	0.0000	0.0035	0.0000E+00
4	0.9299	0.6660	0.0000E+00	0.0000E+00	0.0000E+00	0.0000E+00	0.0000E+00	0.0000E+00	0.0000	0.0035	0.0000E+00
5	0.9793	0.7294	0.0000E+00	0.0000E+00	0.0000E+00	0.0000E+00	0.0000E+00	0.0000E+00	0.0000	0.0035	0.0000E+00
6	0.9952	0.7853	0.0000E+00	0.0000E+00	0.0000E+00	0.0000E+00	0.0000E+00	0.0000E+00	0.0000	0.0035	0.0000E+00
7	0.9991	0.8332	0.0000E+00	0.0000E+00	0.0000E+00	0.0000E+00	0.0000E+00	0.0000E+00	0.0000	0.0035	0.0000E+00
8	0.9999	0.8732	0.0000E+00	0.0000E+00	0.0000E+00	0.0000E+00	0.0000E+00	0.0000E+00	0.0000	0.0035	0.0000E+00
9	1.0000	0.9057	0.0000E+00	0.0000E+00	0.0000E+00	0.0000E+00	0.0000E+00	0.0000E+00	0.0000	0.0035	0.0000E+00
10	1.0000	0.9313	0.0000E+00	0.0000E+00	0.0000E+00	0.0000E+00	0.0000E+00	0.0000E+00	0.0000	0.0035	0.0000E+00
11	1.0000	0.9511	0.0000E+00	0.0000E+00	0.0000E+00	0.0000E+00	0.0000E+00	0.0000E+00	0.0000	0.0035	0.0000E+00
12	1.0000	0.9658	0.0000E+00	0.0000E+00	0.0000E+00	0.0000E+00	0.0000E+00	0.0000E+00	0.0000	0.0035	0.0000E+00
13	1.0000	0.9766	0.0000E+00	0.0000E+00	0.0000E+00	0.0000E+00	0.0000E+00	0.0000E+00	0.0000	0.0035	0.0000E+00
14	1.0000	0.9842	0.0000E+00	0.0000E+00	0.0000E+00	0.0000E+00	0.0000E+00	0.0000E+00	0.0000	0.0035	0.0000E+00
15	1.0000	0.9894	0.0000E+00	0.0000E+00	0.0000E+00	0.0000E+00	0.0000E+00	0.0000E+00	0.0000	0.0035	0.0000E+00
16	1.0000	0.9930	0.0000E+00	0.0000E+00	0.0000E+00	0.0000E+00	0.0000E+00	0.0000E+00	0.0000	0.0035	0.0000E+00
17	1.0000	0.9952	0.0000E+00	0.0000E+00	0.0000E+00	0.0000E+00	0.0000E+00	0.0000E+00	0.0000	0.0035	0.0000E+00
18	1.0000	0.9966	0.0000E+00	0.0000E+00	0.0000E+00	0.0000E+00	0.0000E+00	0.0000E+00	0.0000	0.0035	0.0000E+00
19	1.0000	0.9973	0.0000E+00	0.0000E+00	0.0000E+00	0.0000E+00	0.0000E+00	0.0000E+00	0.0000	0.0035	0.0000E+00
20	1.0000	0.9976	0.0000E+00	0.0000E+00	0.0000E+00	0.0000E+00	0.0000E+00	0.0000E+00	0.0000	0.0035	0.0000E+00
CUP-MIX AVERAGES:											
	0.9603	0.8581			0.0000E+00			0.0000E+00	0.0000	0.0037	0.0000E+00

VAPOR: 96.0 %, AEROSOL: 0.0 % HOMOG., 0.0 % SEED. WALL LOSS = 4.0 %

DISTRIBUTIONS:

0.0000E+00	0.0000E+00	0.0000E+00	0.0000E+00	0.0000E+00	0.0000E+00	0.0000E+00	0.0000E+00	0.0000E+00	0.0000E+00
0.0000E+00	0.0000E+00	0.0000E+00	0.0000E+00	0.0000E+00	0.0000E+00	0.0000E+00	0.0000E+00	0.0000E+00	0.0000E+00
0.5623E-02	0.6310E-02	0.7079E-02	0.7943E-02	0.8913E-02	0.1000E-01	0.1122E-01	0.1259E-01	0.1413E-01	0.1585E-01
0.0000E+00	0.0000E+00	0.0000E+00	0.0000E+00	0.0000E+00	0.0000E+00	0.0000E+00	0.0000E+00	0.0000E+00	0.0000E+00
0.0000E+00	0.0000E+00	0.0000E+00	0.0000E+00	0.0000E+00	0.0000E+00	0.0000E+00	0.0000E+00	0.0000E+00	0.0000E+00
0.1778E-01	0.1995E-01	0.2239E-01	0.2512E-01	0.2818E-01	0.3162E-01	0.3548E-01	0.3981E-01	0.4467E-01	0.5012E-01
0.0000E+00	0.0000E+00	0.0000E+00	0.0000E+00	0.0000E+00	0.0000E+00	0.0000E+00	0.0000E+00	0.0000E+00	0.0000E+00
0.0000E+00	0.0000E+00	0.0000E+00	0.0000E+00	0.0000E+00	0.0000E+00	0.0000E+00	0.0000E+00	0.0000E+00	0.0000E+00
0.5623E-01	0.6310E-01	0.7079E-01	0.7943E-01	0.8913E-01	0.1000E+00	0.1122E+00	0.1259E+00	0.1413E+00	0.1585E+00
0.0000E+00	0.0000E+00	0.0000E+00	0.0000E+00	0.0000E+00	0.0000E+00	0.0000E+00	0.0000E+00	0.0000E+00	0.0000E+00
0.0000E+00	0.0000E+00	0.0000E+00	0.0000E+00	0.0000E+00	0.0000E+00	0.0000E+00	0.0000E+00	0.0000E+00	0.0000E+00
0.1778E+00	0.1995E+00	0.2239E+00	0.2512E+00	0.2818E+00	0.3162E+00	0.3548E+00	0.3981E+00	0.4467E+00	0.5012E+00
0.0000E+00	0.0000E+00	0.0000E+00	0.0000E+00	0.0000E+00	0.0000E+00	0.0000E+00	0.0000E+00	0.0000E+00	0.0000E+00
0.0000E+00	0.0000E+00	0.0000E+00	0.0000E+00	0.0000E+00	0.0000E+00	0.0000E+00	0.0000E+00	0.0000E+00	0.0000E+00
0.5623E+00	0.6310E+00	0.7079E+00	0.7943E+00	0.8913E+00	0.1000E+01	0.1122E+01	0.1259E+01	0.1413E+01	0.1585E+01
0.0000E+00	0.0000E+00	0.0000E+00	0.0000E+00	0.0000E+00	0.0000E+00	0.0000E+00	0.0000E+00	0.0000E+00	0.0000E+00
0.0000E+00	0.0000E+00	0.0000E+00	0.0000E+00	0.0000E+00	0.0000E+00	0.0000E+00	0.0000E+00	0.0000E+00	0.0000E+00
0.1778E+01	0.1995E+01	0.2239E+01	0.2512E+01	0.2818E+01	0.3162E+01	0.3548E+01	0.3981E+01	0.4467E+01	0.5012E+01

Z = 80 SEED N = 0.0000E+00 /CC.

	X	XA	TEMP	J (/CC.SEC.)	INT.J (/CC.)	N (/CC.)	PHI2	INT.PHI2 (CU.MIC/CC)	HOMO PHI (CU.MIC/CC)	AVE & SEED DIA (MICRONS)		SEED PHI (CU.MIC/CC)
0		0.0000	0.0000									
1	*	0.0522	0.0669	0.0000E+00	0.6529E+11	0.1101E+12	18.74	0.5911E+06	0.5408E+06	0.0209	0.0459	0.0000E+00
2	*	0.1591	0.1372	0.1018E+06	0.1009E+11	0.1051E+11	50.44	0.5063E+06	0.4787E+06	0.0436	0.0793	0.0000E+00
3		0.4041	0.2104	0.8490E+09	0.2920E+08	0.2047E+08	0.2440	355.3	327.2	0.0239	0.1017	0.0000E+00
4		0.6037	0.2859	3613.	25.51	9.145	0.1070E-06	0.5137E-04	0.4052E-04	0.0158	0.0568	0.0000E+00
5		0.7570	0.3623	0.0000E+00	0.0000E+00	0.0000E+00	0.0000E+00	0.0000E+00	0.0000E+00	0.0000	0.0270	0.0000E+00
6		0.8629	0.4382	0.0000E+00	0.0000E+00	0.0000E+00	0.0000E+00	0.0000E+00	0.0000E+00	0.0000	0.0243	0.0000E+00
7		0.9298	0.5119	0.0000E+00	0.0000E+00	0.0000E+00	0.0000E+00	0.0000E+00	0.0000E+00	0.0000	0.0154	0.0000E+00
8		0.9678	0.5817	0.0000E+00	0.0000E+00	0.0000E+00	0.0000E+00	0.0000E+00	0.0000E+00	0.0000	0.0044	0.0000E+00
9		0.9868	0.6463	0.0000E+00	0.0000E+00	0.0000E+00	0.0000E+00	0.0000E+00	0.0000E+00	0.0000	0.0035	0.0000E+00
10		0.9952	0.7045	0.0000E+00	0.0000E+00	0.0000E+00	0.0000E+00	0.0000E+00	0.0000E+00	0.0000	0.0035	0.0000E+00
11		0.9984	0.7558	0.0000E+00	0.0000E+00	0.0000E+00	0.0000E+00	0.0000E+00	0.0000E+00	0.0000	0.0035	0.0000E+00
12		0.9995	0.7999	0.0000E+00	0.0000E+00	0.0000E+00	0.0000E+00	0.0000E+00	0.0000E+00	0.0000	0.0035	0.0000E+00
13		0.9999	0.8369	0.0000E+00	0.0000E+00	0.0000E+00	0.0000E+00	0.0000E+00	0.0000E+00	0.0000	0.0035	0.0000E+00
14		1.0000	0.8672	0.0000E+00	0.0000E+00	0.0000E+00	0.0000E+00	0.0000E+00	0.0000E+00	0.0000	0.0035	0.0000E+00
15		1.0000	0.8915	0.0000E+00	0.0000E+00	0.0000E+00	0.0000E+00	0.0000E+00	0.0000E+00	0.0000	0.0035	0.0000E+00
16		1.0000	0.9103	0.0000E+00	0.0000E+00	0.0000E+00	0.0000E+00	0.0000E+00	0.0000E+00	0.0000	0.0035	0.0000E+00
17		1.0000	0.9242	0.0000E+00	0.0000E+00	0.0000E+00	0.0000E+00	0.0000E+00	0.0000E+00	0.0000	0.0035	0.0000E+00
18		1.0000	0.9338	0.0000E+00	0.0000E+00	0.0000E+00	0.0000E+00	0.0000E+00	0.0000E+00	0.0000	0.0035	0.0000E+00
19		1.0000	0.9393	0.0000E+00	0.0000E+00	0.0000E+00	0.0000E+00	0.0000E+00	0.0000E+00	0.0000	0.0035	0.0000E+00
20		1.0000	0.9412	0.0000E+00	0.0000E+00	0.0000E+00	0.0000E+00	0.0000E+00	0.0000E+00	0.0000	0.0035	0.0000E+00
CUP-MIX AVERAGES:		0.8676	0.6133			0.2403E+10			0.2644E+05	0.0243	0.0186	0.0000E+00

VAPOR: 86.8 %, AEROSOL: 2.4 % HOMOG., 0.0 % SEED. WALL LOSS = 10.8 %

DISTRIBUTIONS:

0.2211E+06	0.2919E+06	0.3712E+06	0.4604E+06	0.5606E+06	0.6754E+06	0.8040E+06	0.1100E+07	0.3552E+07	0.2830E+09
0.1317E+00	0.1739E+00	0.2213E+00	0.2745E+00	0.3343E+00	0.4032E+00	0.7654E+00	0.1536E+01	0.5898E+01	0.7388E+03
0.5623E-02	0.6310E-02	0.7079E-02	0.7943E-02	0.8913E-02	0.1000E-01	0.1122E-01	0.1259E-01	0.1413E-01	0.1585E-01
0.4676E+10	0.1781E+11	0.1517E+11	0.1299E+10	0.1760E+09	0.2054E+09	0.7401E+09	0.1876E+10	0.2772E+10	0.1512E+10
0.2151E+05	0.8519E+05	0.7455E+05	0.1032E+05	0.1739E+04	0.4076E+04	0.2027E+05	0.6330E+05	0.1300E+06	0.9913E+05
0.1778E-01	0.1995E-01	0.2239E-01	0.2512E-01	0.2818E-01	0.3162E-01	0.3548E-01	0.3981E-01	0.4467E-01	0.5012E-01
0.2138E+09	0.2955E+07	0.7726E+05	0.9818E+04	0.1471E+03	0.2341E-01	0.0000E+00	0.0000E+00	0.0000E+00	0.0000E+00
0.1916E+05	0.3477E+03	0.1414E+02	0.2363E+01	0.5037E-01	0.1112E-04	0.0000E+00	0.0000E+00	0.0000E+00	0.0000E+00
0.5623E-01	0.6310E-01	0.7079E-01	0.7943E-01	0.8913E-01	0.1000E+00	0.1122E+00	0.1259E+00	0.1413E+00	0.1585E+00
0.0000E+00	0.0000E+00	0.0000E+00	0.0000E+00	0.0000E+00	0.0000E+00	0.0000E+00	0.0000E+00	0.0000E+00	0.0000E+00
0.0000E+00	0.0000E+00	0.0000E+00	0.0000E+00	0.0000E+00	0.0000E+00	0.0000E+00	0.0000E+00	0.0000E+00	0.0000E+00
0.1778E+00	0.1995E+00	0.2239E+00	0.2512E+00	0.2818E+00	0.3162E+00	0.3548E+00	0.3981E+00	0.4467E+00	0.5012E+00
0.0000E+00	0.0000E+00	0.0000E+00	0.0000E+00	0.0000E+00	0.0000E+00	0.0000E+00	0.0000E+00	0.0000E+00	0.0000E+00
0.0000E+00	0.0000E+00	0.0000E+00	0.0000E+00	0.0000E+00	0.0000E+00	0.0000E+00	0.0000E+00	0.0000E+00	0.0000E+00
0.5623E+00	0.6310E+00	0.7079E+00	0.7943E+00	0.8913E+00	0.1000E+01	0.1122E+01	0.1259E+01	0.1413E+01	0.1585E+01
0.0000E+00	0.0000E+00	0.0000E+00	0.0000E+00	0.0000E+00	0.0000E+00	0.0000E+00	0.0000E+00	0.0000E+00	0.0000E+00
0.0000E+00	0.0000E+00	0.0000E+00	0.0000E+00	0.0000E+00	0.0000E+00	0.0000E+00	0.0000E+00	0.0000E+00	0.0000E+00
0.1778E+01	0.1995E+01	0.2239E+01	0.2512E+01	0.2818E+01	0.3162E+01	0.3548E+01	0.3981E+01	0.4467E+01	0.5012E+01

Z = 120

SEED N = 0.0000E+00 /CC.

	X	XA	TEMP	J (/CC.SEC.)	INT.J (/CC.)	N (/CC.)	PHI?	INT.PHI2 (CU.MIC/CC)	HOMO PHI (CU.MIC/CC)	AVE & SEED DIA (MICRONS)		SEED PHI (CU.MIC/CC)
0		0.0000	0.0000									
1	*	0.0285	0.0443	0.0000E+00	0.6529E+11	0.1131E+12	8.573	0.1292E+07	0.1214E+07	0.0272	0.0507	0.0000E+00
2	*	0.0827	0.0910	40.18	0.1009E+11	0.1089E+11	23.49	0.1527E+07	0.1497E+07	0.0638	0.0941	0.0000E+00
3	*	0.1982	0.1399	0.1179E+09	0.2391E+10	0.2348E+10	22.91	0.2595E+06	0.2557E+06	0.0544	0.1504	0.0000E+00
4	*	0.3517	0.1908	0.3396E+10	0.1546E+10	0.1441E+10	31.46	0.9672E+05	0.9324E+05	0.0429	0.1626	0.0000E+00
5		0.5455	0.2435	0.8852E+09	0.1960E+08	0.1362E+08	0.3066	273.6	250.2	0.0250	0.1385	0.0000E+00
6		0.6936	0.2974	0.1996E+05	151.7	73.03	0.1520E-05	0.6558E-03	0.5527E-03	0.0186	0.0751	0.0000E+00
7		0.8046	0.3519	0.0000E+00	0.0000E+00	0.0000E+00	0.0000E+00	0.0000E+00	0.0000E+00	0.0000	0.0245	0.0000E+00
8		0.8833	0.4062	0.0000E+00	0.0000E+00	0.0000E+00	0.0000E+00	0.0000E+00	0.0000E+00	0.0000	0.0238	0.0000E+00
9		0.9350	0.4595	0.0000E+00	0.0000E+00	0.0000E+00	0.0000E+00	0.0000E+00	0.0000E+00	0.0000	0.0204	0.0000E+00
10		0.9664	0.5110	0.0000E+00	0.0000E+00	0.0000E+00	0.0000E+00	0.0000E+00	0.0000E+00	0.0000	0.0146	0.0000E+00
11		0.9839	0.5599	0.0000E+00	0.0000E+00	0.0000E+00	0.0000E+00	0.0000E+00	0.0000E+00	0.0000	0.0074	0.0000E+00
12		0.9928	0.6054	0.0000E+00	0.0000E+00	0.0000E+00	0.0000E+00	0.0000E+00	0.0000E+00	0.0000	0.0035	0.0000E+00
13		0.9970	0.6468	0.0000E+00	0.0000E+00	0.0000E+00	0.0000E+00	0.0000E+00	0.0000E+00	0.0000	0.0035	0.0000E+00
14		0.9988	0.6836	0.0000E+00	0.0000E+00	0.0000E+00	0.0000E+00	0.0000E+00	0.0000E+00	0.0000	0.0035	0.0000E+00
15		0.9996	0.7153	0.0000E+00	0.0000E+00	0.0000E+00	0.0000E+00	0.0000E+00	0.0000E+00	0.0000	0.0035	0.0000E+00
16		0.9999	0.7415	0.0000E+00	0.0000E+00	0.0000E+00	0.0000E+00	0.0000E+00	0.0000E+00	0.0000	0.0035	0.0000E+00
17		1.0000	0.7621	0.0000E+00	0.0000E+00	0.0000E+00	0.0000E+00	0.0000E+00	0.0000E+00	0.0000	0.0035	0.0000E+00
18		1.0000	0.7769	0.0000E+00	0.0000E+00	0.0000E+00	0.0000E+00	0.0000E+00	0.0000E+00	0.0000	0.0035	0.0000E+00
19		1.0000	0.7858	0.0000E+00	0.0000E+00	0.0000E+00	0.0000E+00	0.0000E+00	0.0000E+00	0.0000	0.0035	0.0000E+00
20		1.0000	0.7888	0.0000E+00	0.0000E+00	0.0000E+00	0.0000E+00	0.0000E+00	0.0000E+00	0.0000	0.0035	0.0000E+00
CUP-MIX AVERAGES:		0.7904	0.4570			0.2665E+10			0.9125E+05	0.0340	0.0431	0.0000E+00

VAPOR: 79.0 %, AEROSOL: 8.3 % HOMOG., 0.0 % SEED. WALL LOSS = 12.7 %

DISTRIBUTIONS:

0.4127E+07	0.5429E+07	0.6856E+07	0.8794E+07	0.1120E+08	0.1408E+08	0.1742E+08	0.2207E+08	0.2819E+08	0.3558E+08
0.9708E+00	0.1312E+01	0.1701E+01	0.3028E+01	0.5908E+01	0.9521E+01	0.1398E+02	0.2679E+02	0.4770E+02	0.7600E+02
0.5623E-02	0.6310E-02	0.7079E-02	0.7943E-02	0.8913E-02	0.1000E-01	0.1122E-01	0.1259E-01	0.1413E-01	0.1585E-01
0.4650E+08	0.6137E+08	0.4656E+09	0.1445E+11	0.2584E+11	0.1683E+10	0.2841E+09	0.3212E+09	0.4091E+09	0.5147E+09
0.1500E+03	0.2608E+03	0.3174E+04	0.1508E+06	0.2760E+06	0.2601E+05	0.6569E+04	0.1064E+05	0.1920E+05	0.3419E+05
0.1778E-01	0.1995E-01	0.2239E-01	0.2512E-01	0.2818E-01	0.3162E-01	0.3548E-01	0.3981E-01	0.4467E-01	0.5012E-01
0.1437E+10	0.5069E+10	0.2066E+10	0.1988E+09	0.8117E+08	0.2527E+08	0.5784E+07	0.6169E+06	0.7896E+03	0.2876E+00
0.1342E+06	0.6783E+06	0.3669E+06	0.5190E+05	0.3006E+05	0.1320E+05	0.4266E+04	0.6386E+03	0.1138E+01	0.5845E-03
0.5623E-01	0.6310E-01	0.7079E-01	0.7943E-01	0.8913E-01	0.1000E+00	0.1122E+00	0.1259E+00	0.1413E+00	0.1585E+00
0.0000E+00	0.0000E+00	0.0000E+00	0.0000E+00	0.0000E+00	0.0000E+00	0.0000E+00	0.0000E+00	0.0000E+00	0.0000E+00
0.0000E+00	0.0000E+00	0.0000E+00	0.0000E+00	0.0000E+00	0.0000E+00	0.0000E+00	0.0000E+00	0.0000E+00	0.0000E+00
0.1778E+00	0.1995E+00	0.2239E+00	0.2512E+00	0.2818E+00	0.3162E+00	0.3548E+00	0.3981E+00	0.4467E+00	0.5012E+00
0.0000E+00	0.0000E+00	0.0000E+00	0.0000E+00	0.0000E+00	0.0000E+00	0.0000E+00	0.0000E+00	0.0000E+00	0.0000E+00
0.0000E+00	0.0000E+00	0.0000E+00	0.0000E+00	0.0000E+00	0.0000E+00	0.0000E+00	0.0000E+00	0.0000E+00	0.0000E+00
0.5623E+00	0.6310E+00	0.7079E+00	0.7943E+00	0.8913E+00	0.1000E+01	0.1122E+01	0.1259E+01	0.1413E+01	0.1585E+01
0.0000E+00	0.0000E+00	0.0000E+00	0.0000E+00	0.0000E+00	0.0000E+00	0.0000E+00	0.0000E+00	0.0000E+00	0.0000E+00
0.0000E+00	0.0000E+00	0.0000E+00	0.0000E+00	0.0000E+00	0.0000E+00	0.0000E+00	0.0000E+00	0.0000E+00	0.0000E+00
0.1778E+01	0.1995E+01	0.2239E+01	0.2512E+01	0.2818E+01	0.3162E+01	0.3548E+01	0.3981E+01	0.4467E+01	0.5012E+01

Z = 160

SEED N = 0.0000E+00 /CC.

X		YA	TEMP	J (/CC.SEC.)	INT.J (/CC.)	N (/CC.)	PHI2	INT.PHI2 (CU.MIC/CC)	HOMO PHI (CU.MIC/CC)	AVE & SEED DIA (MICRONS)		SEED PHI (CU.MIC/CC)
0		0.0000	0.0000									
1	*	0.0186	0.0327	0.0C0CE+0C	0.6529E+11	0.1138E+12	4.077	0.1607E+07	0.1520E+07	0.0293	0.0523	0.0000E+00
2	*	0.0503	0.0671	0.0C00E+00	0.1009E+11	0.1095E+11	9.616	0.1940E+07	0.1914E+07	0.0692	*0.0983	0.0000E+00
3	*	0.1073	0.1032	0.1C55E+05	0.2396E+10	0.2386E+10	10.07	0.5551E+06	0.5519E+06	0.0735	0.1602	0.0000E+00
4	*	0.1825	0.1410	0.4501E+07	0.1690E+10	0.1680E+10	24.05	0.5727E+06	0.5674E+06	0.0838	0.1834	*0.0000E+00
5	*	0.3043	0.1801	0.7002E+05	0.1325E+10	0.1290E+10	34.34	0.2232E+06	0.2194E+06	0.0614	0.1880	0.0000E+00
6		0.4760	0.2204	0.1122E+11	0.1010E+10	0.8857E+09	28.38	0.4713E+05	0.4510E+05	0.0370	0.1757	0.0000E+00
7		0.6492	0.2615	0.1501E+10	0.2224E+08	0.1492E+08	0.4643	299.9	273.0	0.0248	0.1470	0.0000E+00
8		0.7707	0.3028	0.3251E+0E	218*.	1116.	0.3153E-04	0.1170E-01	0.1001E-01	0.0196	0.0925	0.0000E+00
9		0.8557	0.3439	0.0000E+0C	0.0C00E+00	0.0000E+00	0.0000E+00	0.0000E+00	0.0000E+00	0.0000	0.0236	0.0000E+00
10		0.9132	0.3842	0.0C00E+00	0.0000E+00	0.0000E+00	0.0000E+00	0.0000E+00	0.0000E+00	0.0000	0.0234	0.0000E+00
11		0.9503	0.4230	0.0C00E+0C	0.0000E+00	0.0000E+00	0.0000E+00	0.0000E+00	0.0000E+00	0.0000	0.0218	0.0000E+00
12		0.9730	0.4598	0.0000E+00	0.0000E+00	0.0000E+00	0.0000E+00	0.0000E+00	0.0000E+00	0.0000	0.0191	0.0000E+00
13		0.9860	0.4940	0.0000E+0C	0.0000E+00	0.0000E+00	0.0000E+00	0.0000E+00	0.0000E+00	0.0000	0.0157	0.0000E+00
14		0.9931	0.5249	0.000CE+0C	0.0000E+00	0.0000E+00	0.0000E+00	0.0000E+00	0.0000E+00	0.0000	0.0118	0.0000E+00
15		0.9968	0.5520	0.0C00E+0C	0.0000E+00	0.0000E+00	0.0000E+00	0.0000E+0C	0.0000E+00	0.0000	0.0082	0.0000E+00
16		0.9985	0.5749	0.0000E+0C	0.0000E+00	0.0000E+00	0.0000E+00	0.0000E+00	0.0000E+00	0.0000	0.0054	0.0000E+00
17		0.9993	0.5931	0.0C00E+00	0.0000E+00	0.0000E+00	0.0000E+00	0.0000E+0C	0.0000E+00	0.0000	0.0038	0.0000E+00
18		0.9997	0.6063	0.0C00E+00	0.0000E+00	0.0000E+00	0.0000E+00	0.0000E+00	0.0000E+00	0.0000	0.0035	0.0000E+00
19		0.9998	0.6143	0.0C0CE+0C	0.0C00E+00	0.0000E+00	0.0000E+00	0.0000E+00	0.0000E+00	0.0000	0.0035	0.0000E+00
20		0.9999	0.6170	0.0000E+0C	0.0000E+00	0.0000E+00	0.0000E+00	0.0000E+00	0.0000E+00	0.0000	0.0035	0.0000E+00

CUP-MIX AVERAGES:

0.7083	0.3465	0.2845E+10			0.1702E+06	0.0393	0.0744	0.0000E+00

VAPOR: 70.8 %, AEROSOL: 15.5 % HOMOG., 0.0 % SEED. WALL LOSS = 13.7 %

DISTRIBUTIONS:

0.7412E+07	0.9748E+07	0.1232E+C8	0.1521E+08	0.1861E+08	0.2294E+08	0.2783E+08	0.3352E+08	0.4012E+08	0.4822E+08
0.2322E+01	0.3139E+01	0.4165E+01	0.5320E+01	0.8211E+01	0.1711E+02	0.2726E+02	0.4092E+02	0.6417E+02	0.1159E+03
C.5623E-02	0.6310E-02	C.7079E-02	C.7943E-02	0.8913E-02	0.1000E-01	C.1122E-01	0.1259E-01	0.1413E-01	0.1585E-01
0.5773E+08	0.6897E+08	0.8458E+08	0.7324E+09	0.2672E+11	0.1416E+11	0.6426E+09	0.2097E+09	0.2683E+09	0.3618E+09
0.1812E+03	0.3084E+03	0.52C2E+C3	C.6589E+04	0.3442E+06	0.1947E+06	0.1307E+05	0.6980E+04	0.1255E+05	0.2390E+05
0.1778E-01	0.1995E-01	0.2239E+01	0.2512E-01	0.2818E-01	0.3162E-01	0.3548E-01	0.3981E-01	0.4467E-01	0.5012E-01
0.5441E+09	0.2728E+10	0.64C6E+10	0.1588E+10	0.1019E+10	0.5280E+09	0.1592E+09	0.2464E+08	0.1194E+07	0.1015E+05
C.5094E+05	0.3754E+06	0.1176E+07	0.4134E+06	0.3772E+06	0.2757E+06	0.1176E+06	0.2565E+05	0.1751E+04	0.2106E+02
0.5623E-01	C.6310E-01	0.7079E-C1	0.7943E-01	0.8913E-01	C.1000E+00	0.1122E+00	0.1259E+00	0.1413E+00	0.1585E+00
0.6649E+01	0.0000E+00	0.00C0E+00	0.0000E+00	0.0000E+00	0.0000E+00	C.0000E+00	0.0000E+00	0.0000E+00	0.0000E+00
0.1947E-C1	C.0000E+00	C.00C0E+CC	0.0000E+00	0.0000E+00	0.0000E+00	C.0000E+00	0.0000E+00	0.0000E+00	0.0000E+00
0.1778E+00	0.1995E+00	0.2239E+CC	0.2512E+00	0.2818E+00	0.3162E+00	0.3548E+00	0.3981E+00	0.4467E+00	0.5012E+00
0.0000E+C0	C.0000E+C0	C.00C0E+C0	0.0000E+00	0.0000E+00	0.0000E+00	0.0000E+00	0.0000E+00	0.0000E+00	0.0000E+00
C.0000E+00	0.0000E+00	0.00C0E+C0	0.0000E+00	0.0000E+00	0.0000E+00	0.0000E+00	0.0000E+00	0.0000E+00	0.0000E+00
0.5623E+00	0.6310E+00	C.7079E+00	0.7943E+00	C.8913E+00	C.1000E+01	C.1122E+01	0.1259E+01	0.1413E+01	0.1585E+01
0.0000E+00	0.0000E+00	0.0000E+CC	0.0000E+00	0.0000E+00	0.0000E+00	0.0000E+00	0.0000E+00	0.0000E+00	0.0000E+00
C.00C0E+CC	C.00C0E+00	C.0000E+C0	0.00C0E+C0	0.0000E+00	C.0000E+00	C.0000E+00	0.0000E+00	0.0000E+00	0.0000E+00
0.1778E+01	C.1995E+01	C.2239E+C1	C.2512E+01	0.2818E+01	0.3162E+01	0.3548E+01	0.3981E+01	0.4467E+01	0.5012E+01

Z = 200 SEED N = 0.0000E+00 /CC.

X		XA	TEMP	J (/CC.SEC.)	INT.J (/CC.)	N (/CC.)	PHI2	INT.PHI2 (CU.MIC/CC)	HOMO PHI (CU.MIC/CC)	AVE & SEED DIA (MICRONS)		SEED PHI (CU.MIC/CC)
0		0.0000	0.0000									
1	*	0.0130	0.0247	0.0000E+00	0.6529E+11	0.1141E+12	2.113	0.1768E+07	0.1676E+07	0.0303	0.0530	0.0000E+00
2	*	0.0332	0.0507	0.0000E+00	0.1009E+11	0.1097E+11	4.367	0.2123E+07	0.2099E+07	0.0713	0.0999	0.0000E+00
3	*	0.0648	0.0780	0.0000E+00	0.2396E+10	0.2392E+10	4.047	0.6798E+06	0.6773E+06	0.0792	0.1633	0.0000E+00
4	*	0.1028	0.1066	478.1	0.1690E+10	0.1687E+10	8.897	0.7953E+06	0.7911E+06	0.0944	0.1892	0.0000E+00
5	*	0.1556	0.1363	0.5979E+05	0.1350E+10	0.1342E+10	14.37	0.5144E+06	0.5108E+06	0.0860	0.1997	0.0000E+00
6	*	0.2254	0.1668	0.1124E+07	0.1404E+10	0.1390E+10	29.95	0.4756E+06	0.4701E+06	0.0831	0.1997	0.0000E+00
7	*	0.3335	0.1980	0.4885E+08	0.1222E+10	0.1201E+10	49.44	0.3143E+06	0.3088E+06	0.0745	0.1968	0.0000E+00
8	*	0.4937	0.2295	0.2286E+10	0.1177E+10	0.1114E+10	64.97	0.1345E+06	0.1300E+06	0.0536	0.1849	0.0000E+00
9		0.6936	0.2610	0.2014E+11	0.4171E+09	0.3144E+09	15.44	0.1042E+05	9658.	0.0301	0.1661	0.0000E+00
10		0.8199	0.2919	0.3729E+09	0.2852E+07	0.1655E+07	0.6906E-01	26.06	22.93	0.0226	0.1298	0.0000E+00
11		0.8926	0.3218	0.1054E+06	470.5	214.9	0.7215E-05	0.1915E-02	0.1598E-02	0.0185	0.0854	0.0000E+00
12		0.9366	0.3502	0.0000E+00	0.0000E+00	0.0000E+00	0.0000E+00	0.0000E+00	0.0000E+00	0.0000	0.0235	0.0000E+00
13		0.9634	0.3768	0.0000E+00	0.0000E+00	0.0000E+00	0.0000E+00	0.0000E+00	0.0000E+00	0.0000	0.0229	0.0000E+00
14		0.9795	0.4009	0.0000E+00	0.0000E+00	0.0000E+00	0.0000E+00	0.0000E+00	0.0000E+00	0.0000	0.0219	0.0000E+00
15		0.9888	0.4221	0.0000E+00	0.0000E+00	0.0000E+00	0.0000E+00	0.0000E+00	0.0000E+00	0.0000	0.0207	0.0000E+00
16		0.9940	0.4401	0.0000E+00	0.0000E+00	0.0000E+00	0.0000E+00	0.0000E+00	0.0000E+00	0.0000	0.0194	0.0000E+00
17		0.9968	0.4545	0.0000E+00	0.0000E+00	0.0000E+00	0.0000E+00	0.0000E+00	0.0000E+00	0.0000	0.0183	0.0000E+00
18		0.9982	0.4650	0.0000E+00	0.0000E+00	0.0000E+00	0.0000E+00	0.0000E+00	0.0000E+00	0.0000	0.0173	0.0000E+00
19		0.9989	0.4713	0.0000E+00	0.0000E+00	0.0000E+00	0.0000E+00	0.0000E+00	0.0000E+00	0.0000	0.0168	0.0000E+00
20		0.9991	0.4735	0.0000E+00	0.0000E+00	0.0000E+00	0.0000E+00	0.0000E+00	0.0000E+00	0.0000	0.0165	0.0000E+00
CUP-MIX AVERAGES:												
		0.5995	0.2638			0.3090E+10			0.2817E+06	0.0443	0.1151	0.0000E+00

VAPOR: 59.9 %, AEROSOL: 25.6 % HOMOG., 0.0 % SEED. WALL LOSS = 14.4 %

DISTRIBUTIONS:

0.5038E+07	0.6650E+07	0.8458E+07	0.1049E+08	0.1310E+08	0.1606E+08	0.1941E+08	0.2345E+08	0.2884E+08	0.3497E+08
0.2995E+01	0.3964E+01	0.5054E+01	0.6279E+01	0.8998E+01	0.1215E+02	0.1579E+02	0.3214E+02	0.5902E+02	0.8978E+02
0.5623E-02	0.6310E-02	0.7079E-02	0.7943E-02	0.8913E-02	0.1000E-01	0.1122E-01	0.1259E-01	0.1413E-01	0.1585E-01
0.4266E+08	0.5162E+08	0.6251E+08	0.3483E+09	0.1635E+11	0.2511E+11	0.1228E+10	0.2192E+09	0.2865E+09	0.4162E+09
0.1379E+03	0.2360E+03	0.4057E+03	0.3390E+04	0.2345E+06	0.3696E+06	0.2541E+05	0.7298E+04	0.1355E+05	0.2757E+05
0.1778E-01	0.1995E-01	0.2239E-01	0.2512E-01	0.2818E-01	0.3162E-01	0.3548E-01	0.3981E-01	0.4467E-01	0.5012E-01
0.6362E+09	0.1768E+10	0.7203E+10	0.3208E+10	0.2294E+10	0.1691E+10	0.7262E+09	0.1656E+09	0.1663E+08	0.4649E+06
0.5959E+05	0.2376E+06	0.1353E+07	0.8250E+06	0.8504E+06	0.8837E+06	0.5357E+06	0.1725E+06	0.2443E+05	0.9628E+03
0.5623E-01	0.6310E-01	0.7079E-01	0.7943E-01	0.8913E-01	0.1000E+00	0.1122E+00	0.1259E+00	0.1413E+00	0.1585E+00
0.1713E+04	0.3513E-01	0.0000E+00	0.0000E+00	0.0000E+00	0.0000E+00	0.0000E+00	0.0000E+00	0.0000E+00	0.0000E+00
0.5020E+01	0.1411E-03	0.0000E+00	0.0000E+00	0.0000E+00	0.0000E+00	0.0000E+00	0.0000E+00	0.0000E+00	0.0000E+00
0.1778E+00	0.1995E+00	0.2239E+00	0.2512E+00	0.2818E+00	0.3162E+00	0.3548E+00	0.3981E+00	0.4467E+00	0.5012E+00
0.0000E+00	0.0000E+00	0.0000E+00	0.0000E+00	0.0000E+00	0.0000E+00	0.0000E+00	0.0000E+00	0.0000E+00	0.0000E+00
0.0000E+00	0.0000E+00	0.0000E+00	0.0000E+00	0.0000E+00	0.0000E+00	0.0000E+00	0.0000E+00	0.0000E+00	0.0000E+00
0.5623E+00	0.6310E+00	0.7079E+00	0.7943E+00	0.8913E+00	0.1000E+01	0.1122E+01	0.1259E+01	0.1413E+01	0.1585E+01
0.0000E+00	0.0000E+00	0.0000E+00	0.0000E+00	0.0000E+00	0.0000E+00	0.0000E+00	0.0000E+00	0.0000E+00	0.0000E+00
0.0000E+00	0.0000E+00	0.0000E+00	0.0000E+00	0.0000E+00	0.0000E+00	0.0000E+00	0.0000E+00	0.0000E+00	0.0000E+00
0.1778E+01	0.1995E+01	0.2239E+01	0.2512E+01	0.2818E+01	0.3162E+01	0.3548E+01	0.3981E+01	0.4467E+01	0.5012E+01

Z = 240 SEED N = 0.0000E+00 /CC.

X		XA	TEMP	J (/CC.SEC.)	INT.J (/CC.)	N (/CC.)	PHI2	INT.PHI2 (CU.MIC/CC)	HOMO PHI (CU.MIC/CC)	AVE & SEED DIA (MICRONS)		SEED PHI (CU.MIC/CC)
0		0.0000	0.0000									
1	*	0.0094	0.0188	0.0000E+00	0.6529E+11	0.1143E+12	1.136	0.1852E+07	0.1758E+07	0.0307	0.0534	0.0000E+00
2	*	0.0229	0.0386	0.0000E+00	0.1009E+11	0.1098E+11	2.108	0.2208E+07	0.2185E+07	0.0722	0.1007	0.0000E+00
3	*	0.0419	0.0594	0.0000E+00	0.2396E+10	0.2394E+10	1.744	0.7308E+06	0.7287E+06	0.0813	0.1645	0.0000E+00
4	*	0.0634	0.0811	0.0000E+00	0.1690E+10	0.1689E+10	3.522	0.8785E+06	0.8748E+06	0.0978	0.1911	0.0000E+00
5	*	0.0900	0.1037	5.285	0.1350E+10	0.1345E+10	5.242	0.6212E+06	0.6180E+06	0.0924	0.2030	0.0000E+00
6	*	0.1210	0.1270	75.71	0.1404E+10	0.1397E+10	10.05	0.6608E+06	0.6558E+06	0.0939	0.2052	0.0000E+00
7	*	0.1617	0.1507	790.1	0.1223E+10	0.1216E+10	15.73	0.5851E+06	0.5797E+06	0.0944	0.2065	0.0000E+00
8	*	0.2136	0.1747	5377.	0.1215E+10	0.1205E+10	26.42	0.5406E+06	0.5343E+06	0.0920	0.2032	0.0000E+00
9	*	0.2828	0.1987	0.4002E+05	0.1243E+10	0.1229E+10	45.01	0.4905E+06	0.4829E+06	0.0882	0.2016	0.0000E+00
10	*	0.3807	0.2223	0.1226E+07	0.1269E+10	0.1247E+10	75.20	0.4001E+06	0.3915E+06	0.0813	0.1944	0.0000E+00
11	*	0.5227	0.2452	0.9690E+08	0.1326E+10	0.1284E+10	116.6	0.2609E+06	0.2524E+06	0.0680	0.1877	0.0000E+00
12		0.7212	0.2670	0.1230E+11	0.1333E+10	0.1185E+10	111.0	0.8694E+05	0.8176E+05	0.0436	0.1720	0.0000E+00
13		0.8837	0.2873	0.3180E+11	0.2941E+09	0.1911E+09	12.03	4451.	3980.	0.0262	0.1500	0.0000E+00
14		0.9450	0.3058	0.8485E+09	0.4374E+07	0.2313E+07	0.1156	31.44	27.04	0.0214	0.1253	0.0000E+00
15		0.9706	0.3221	0.5333E+07	0.2051E+05	9427.	0.3849E-03	0.8743E-01	0.7300E-01	0.0187	0.0982	0.0000E+00
16		0.9834	0.3359	0.2383E+05	73.57	29.77	0.1004E-05	0.2002E-03	0.1628E-03	0.0168	0.0695	0.0000E+00
17		0.9903	0.3470	144.4	0.3729	0.1319	0.3474E-08	0.5830E-06	0.4529E-06	0.0149	0.0386	0.0000E+00
18		0.9940	0.3550	2.141	0.3456E-02	0.0000E+00	0.0000E+00	0.0000E+00	0.0000E+00	0.0000	0.0226	0.0000E+00
19		0.9958	0.3599	0.0000E+00	0.0000E+00	0.0000E+00	0.0000E+00	0.0000E+00	0.0000E+00	0.0000	0.0225	0.0000E+00
20		0.9964	0.3616	0.0000E+00	0.0000E+00	0.0000E+00	0.0000E+00	0.0000E+00	0.0000E+00	0.0000	0.0224	0.0000E+00
CUP-MIX AVERAGES:												
		0.4355	0.2010			0.3450E+10			0.4548E+06	0.0498	0.1627	0.0000E+00

VAPOR: 43.5 %, AEROSOL: 41.3 % HOMOG., 0.0 % SEED. WALL LOSS = 15.1 %

DISTRIBUTIONS:

0.4939E+07	0.6520E+07	0.8294E+07	0.1030E+08	0.1257E+08	0.1512E+08	0.1879E+08	0.2433E+08	0.3053E+08	0.3741E+08
0.4333E+01	0.5720E+01	0.7276E+01	0.9050E+01	0.1108E+02	0.1337E+02	0.2132E+02	0.3963E+02	0.6697E+02	0.1044E+03
0.5623E-02	0.6310E-02	0.7079E-02	0.7943E-02	0.8913E-02	0.1000E-01	0.1122E-01	0.1259E-01	0.1413E-01	0.1585E-01
0.4555E+08	0.5804E+08	0.7283E+08	0.1600E+09	0.1097E+11	0.3106E+11	0.1570E+10	0.2483E+09	0.3040E+09	0.4359E+09
0.1520E+03	0.2998E+03	0.4800E+03	0.1540E+04	0.1633E+06	0.4760E+06	0.3350E+05	0.8356E+04	0.1445E+05	0.2885E+05
0.1778E-01	0.1995E-01	0.2239E-01	0.2512E-01	0.2818E-01	0.3162E-01	0.3548E-01	0.3981E-01	0.4467E-01	0.5012E-01
0.6850E+09	0.1616E+10	0.7304E+10	0.4799E+10	0.4106E+10	0.3694E+10	0.1895E+10	0.5030E+09	0.6003E+08	0.2196E+07
0.6433E+05	0.2177E+06	0.1375E+07	0.1236E+07	0.1523E+07	0.1932E+07	0.1399E+07	0.5239E+06	0.8828E+05	0.4567E+04
0.5623E-01	0.6310E-01	0.7079E-01	0.7943E-01	0.8913E-01	0.1000E+00	0.1122E+00	0.1259E+00	0.1413E+00	0.1585E+00
0.1338E+05	0.3559E+01	0.0000E+00	0.0000E+00	0.0000E+00	0.0000E+00	0.0000E+00	0.0000E+00	0.0000E+00	0.0000E+00
0.3917E+02	0.1471E-01	0.0000E+00	0.0000E+00	0.0000E+00	0.0000E+00	0.0000E+00	0.0000E+00	0.0000E+00	0.0000E+00
0.1778E+00	0.1995E+00	0.2239E+00	0.2512E+00	0.2818E+00	0.3162E+00	0.3548E+00	0.3981E+00	0.4467E+00	0.5012E+00
0.0000E+00	0.0000E+00	0.0000E+00	0.0000E+00	0.0000E+00	0.0000E+00	0.0000E+00	0.0000E+00	0.0000E+00	0.0000E+00
0.0000E+00	0.0000E+00	0.0000E+00	0.0000E+00	0.0000E+00	0.0000E+00	0.0000E+00	0.0000E+00	0.0000E+00	0.0000E+00
0.5623E+00	0.6310E+00	0.7079E+00	0.7943E+00	0.8913E+00	0.1000E+01	0.1122E+01	0.1259E+01	0.1413E+01	0.1585E+01
0.0000E+00	0.0000E+00	0.0000E+00	0.0000E+00	0.0000E+00	0.0000E+00	0.0000E+00	0.0000E+00	0.0000E+00	0.0000E+00
0.0000E+00	0.0000E+00	0.0000E+00	0.0000E+00	0.0000E+00	0.0000E+00	0.0000E+00	0.0000E+00	0.0000E+00	0.0000E+00
0.1778E+01	0.1995E+01	0.2239E+01	0.2512E+01	0.2818E+01	0.3162E+01	0.3548E+01	0.3981E+01	0.4467E+01	0.5012E+01

Z = 280 SEED N = 0.0000E+00 /CC.

X		XA	TEMP	J (/CC.SEC.)	INT.J (/CC.)	N (/CC.)	PHI2	INT.PHI2 (CU.MIC/CC)	HOMO PHI (CU.MIC/CC)	AVE & SEED DIA (MICRONS)		SEED PHI (CU.MIC/CC)
0		0.0000	C.0000									
1	*	0.0070	0.0143	0.0000E+00	0.6529E+11	0.1143E+12	0.6415	0.1898E+07	0.1803E+07	0.0310	0.0536	0.0000E+00
2	*	0.0165	0.0294	0.0000E+00	0.1009E+11	0.1099E+11	1.099	0.2250E+07	0.2228E+07	0.0727	0.1010	0.0000E+00
3	*	0.02RR	0.0452	0.0C00E+0C	0.2396E+10	0.2395E+10	0.8361	0.7539E+06	0.7519E+06	0.0823	0.1651	0.0000E+00
4	*	0.0423	C.0618	0.0C00E+0C	0.1690E+10	0.1690E+10	1.590	0.9134E+06	0.9099E+06	0.0992	0.1919	0.0000E+00
5	*	0.0577	0.0790	0.0000E+0C	0.1350E+10	0.1346E+10	2.218	0.6626E+06	0.6596E+06	0.0946	0.2042	0.0000E+00
6	*	0.0743	0.0967	0.0C00E+0C	C.14C4E+10	0.1399E+10	3.948	0.7265E+06	0.7218E+06	0.0972	0.2069	0.0000E+00
7	*	0.0536	C.1149	0.0000E+0C	0.1223E+10	0.1218E+10	5.583	0.6716E+06	0.6666E+06	0.0992	0.2091	0.0000E+00
8	*	0.1148	0.1332	0.0000E+0C	0.1215E+10	0.1209E+10	R.32R	0.6649E+06	0.6588E+06	0.0992	0.2070	0.0000E+00
9	*	0.1385	0.1515	0.0000E+00	0.1243E+10	0.1235E+10	12.34	0.6735E+06	0.6661E+06	0.0990	0.2072	0.0000E+00
10	*	0.1654	0.1694	0.0C00E+00	0.1269E+10	0.1259E+10	17.76	0.6700E+06	0.6612E+06	0.0981	0.2031	0.0000E+00
11	*	0.1960	0.1869	0.0000E+0C	0.1327E+10	0.1314E+10	25.50	0.6629E+06	0.6526E+06	0.0963	0.2018	0.0000E+00
12	*	0.2311	0.2035	0.0000E+0C	0.1420E+10	0.1404E+10	36.63	0.6516E+06	0.6395E+06	0.0936	0.1965	0.0000E+00
13	*	0.2715	0.2190	0.0000E+00	0.1548E+10	0.1527E+10	52.61	0.6324E+06	0.6184E+06	0.0899	0.1920	0.0000E+00
14		0.3183	C.2331	1.700	0.1716E+10	0.1687E+10	75.58	0.6038E+06	0.5878E+06	0.0854	0.1887	0.0000E+00
15		0.3725	0.2456	13.50	0.1931E+10	0.1891E+10	108.4	0.5649E+06	0.5470E+06	0.0800	0.1845	0.0000E+00
16		0.4345	0.2562	234.R	0.2199E+10	0.2142E+10	153.7	0.5159E+06	0.4963E+06	0.0740	0.1795	0.0000E+00
17		0.5023	0.2646	6697.	0.2514E+10	0.2432E+10	211.8	0.4591E+06	0.4383E+06	0.0676	0.1739	0.0000E+00
18		0.5692	C.2708	0.175RE+06	0.2852E+10	0.2737E+10	274.9	0.4019E+06	0.3805E+06	0.0615	0.1708	0.0000E+00
19		0.6210	0.2745	0.1964E+07	0.3141E+10	0.2991E+10	325.0	0.3575E+06	0.3361E+06	0.0568	0.1681	0.0000E+00
20		0.6402	C.2758	0.455RE+07	0.3278E+10	0.3111E+10	344.9	0.3420E+06	0.3205E+06	0.0550	0.1663	0.0000E+00
CUP-MIX AVERAGES:												
		0.1835	C.1533			0.3976E+10			0.7233E+06	0.0565	0.1901	0.0000E+00

VAPOR: 18.3 %, AEROSOL: 65.8 % HOMOG., 0.0 % SEED. WALL LOSS = 15.9 %

DISTRIBUTIONS:

0.9454E+03	0.1248E+04	C.1599E+C4	0.22C4E+C4	0.5189E+04	0.1103E+05	0.1779E+05	0.2808E+05	0.5719E+05	0.1380E+06
0.2863E-03	C.3782E-03	0.4883E-C3	C.8284E-03	0.4585E-02	0.1274E-01	0.2223E-01	0.4059E-01	0.1315E+00	0.4517E+00
0.5623E-02	0.6310E-02	0.7079E-02	0.7943E-02	0.8913E-02	0.1000E-01	0.1122E-01	0.1259E-01	0.1413E-01	0.1585E-01
0.2634E+06	0.5657E+C6	C.1457E+07	C.8598E+07	0.7839E+10	0.3425E+11	0.1616E+10	0.1272E+09	0.2214E+09	0.4708E+09
0.1031E+01	0.3137E+01	C.1135E+C2	0.7428E+02	0.1184E+06	0.5365E+06	0.3476E+05	0.4409E+04	0.1071E+05	0.3176E+05
C.1778E-01	C.1995E-01	0.2239E-C1	C.2512E-01	0.2818E-01	0.3162E-01	0.3548E-01	0.3981E-01	0.4467E-01	0.5012E-01
0.9210E+09	0.1985E+10	0.8065E+10	0.6701E+10	0.6735E+10	0.6741E+10	0.3778E+10	0.1054E+10	0.1298E+09	0.5067E+07
0.8709E+05	0.2660E+C6	C.1516E+C7	C.1736E+07	0.2497E+07	0.3526E+07	0.2788E+07	0.1098E+07	0.1908E+06	0.1051E+05
C.5623E-C1	C.6310E-01	0.7079E-C1	0.7943E-01	0.8913E-01	0.1000E+00	0.1122E+00	0.1259E+00	0.1413E+00	0.1585E+00
0.3454E+05	0.1190E+02	0.0000E+C0	0.00C0E+00	0.0000E+00	0.0000E+00	0.0000E+00	0.0000E+00	0.0000E+00	0.0000E+00
0.1011E+C3	0.4917E-01	C.0000E+C0	0.00C0E+00	0.0000E+00	C.0000E+00	0.0000E+00	0.0000E+00	0.0000E+00	0.0000E+00
0.1778E+00	0.1995E+00	C.2239E+C0	C.2512E+C0	0.2818E+00	0.3162E+00	0.3548E+00	0.3981E+00	0.4467E+00	0.5012E+00
C.0000E+00	0.0000E+00	C.00C0E+00	0.00C0E+00	0.0000E+00	0.0000E+00	0.0000E+00	0.0000E+00	0.0000E+00	0.0000E+00
C.00C0E+C0	C.00C0E+C0	C.00C0E+C0	0.0000E+00	0.0000E+00	0.0000E+00	0.0000E+00	0.0000E+00	0.0000E+00	0.0000E+00
0.5623E+00	C.6310E+00	0.7079E+CC	0.7943E+00	0.8913E+00	0.1000E+01	0.1122E+01	0.1259E+01	0.1413E+01	0.1585E+01
0.00C0E+0C	C.0000E+00	C.00C0E+C0	0.00C0E+00	0.0000E+00	0.0000E+00	C.0000E+00	0.0000E+00	0.0000E+00	0.0000E+00
C.0000E+00	0.0000E+00	C.0000E+00	0.00C0E+00	0.0000E+00	0.0000E+00	0.0000E+00	0.0000E+00	0.0000E+00	0.0000E+00
C.1778E+C1	C.1995E+C1	C.2239E+C1	C.2512E+01	0.2818E+01	C.3162E+01	C.3548E+01	0.3981E+01	0.4467E+01	0.5012E+01

Z = 320

SEED N = 0.0000E+00 /CC.

	X	XA	TEMP	J (/CC.SEC.)	INT.J (/CC.)	N (/CC.)	PHI2	INT.PHI2 (CU.MIC/CC)	HOMO PHI (CU.MIC/CC)	AVE & SEED DIA (MICRONS)		SEED PHI (CU.MIC/CC)
0		0.0000	0.0000									
1	*	0.0054	0.0109	0.0000E+00	0.6529E+11	0.1144E+12	0.3838	0.1925E+07	0.1830E+07	0.0312	0.0537	0.0000E+00
2	*	0.0123	0.0224	0.0000E+00	0.1009E+11	0.1099E+11	0.6206	0.2273E+07	0.2251E+07	0.0730	0.1012	0.0000E+00
3	*	0.0209	0.0345	0.0000E+00	0.2396E+10	0.2395E+10	0.4440	0.7655E+06	0.7636E+06	0.0827	0.1653	0.0000E+00
4	*	0.0301	0.0471	0.0000E+00	0.1690E+10	0.1690E+10	0.8125	0.9301E+06	0.9267E+06	0.0998	0.1923	0.0000E+00
5		0.0402	0.0602	0.0000E+00	0.1350E+10	0.1347E+10	1.089	0.6813E+06	0.6785E+06	0.0956	0.2047	0.0000E+00
6		0.0506	0.0738	0.0000E+00	0.1404E+10	0.1399E+10	1.859	0.7545E+06	0.7500E+06	0.0986	0.2076	0.0000E+00
7		0.0618	0.0876	0.0000E+00	0.1223E+10	0.1219E+10	2.484	0.7057E+06	0.7008E+06	0.1010	0.2100	0.0000E+00
8		0.0732	0.1015	0.0000E+00	0.1215E+10	0.1210E+10	3.473	0.7092E+06	0.7034E+06	0.1015	0.2083	0.0000E+00
9		0.0845	0.1155	0.0000E+00	0.1243E+10	0.1237E+10	4.760	0.7315E+06	0.7243E+06	0.1019	0.2088	0.0000E+00
10		0.0959	0.1292	0.0000E+00	0.1269E+10	0.1262E+10	6.229	0.7441E+06	0.7354E+06	0.1019	0.2052	0.0000E+00
11		0.1069	0.1425	0.0000E+00	0.1327E+10	0.1317E+10	7.979	0.7574E+06	0.7472E+06	0.1010	0.2044	0.0000E+00
12		0.1172	0.1552	0.0000E+00	0.1420E+10	0.1409E+10	10.02	0.7722E+06	0.7601E+06	0.0994	0.1997	0.0000E+00
13		0.1263	0.1670	0.0000E+00	0.1548E+10	0.1534E+10	12.28	0.7858E+06	0.7715E+06	0.0971	0.1959	0.0000E+00
14		0.1340	0.1778	0.0000E+00	0.1716E+10	0.1698E+10	14.70	0.7981E+06	0.7813E+06	0.0943	0.1935	0.0000E+00
15		0.1398	0.1873	0.0000E+00	0.1931E+10	0.1908E+10	17.15	0.8098E+06	0.7902E+06	0.0910	0.1903	0.0000E+00
16		0.1436	0.1953	0.0000E+00	0.2199E+10	0.2168E+10	19.49	0.8214E+06	0.7987E+06	0.0874	0.1864	0.0000E+00
17		0.1453	0.2017	0.0000E+00	0.2514E+10	0.2475E+10	21.56	0.8330E+06	0.8070E+06	0.0839	0.1822	0.0000E+00
18		0.1455	0.2065	0.0000E+00	0.2852E+10	0.2805E+10	23.23	0.8445E+06	0.8154E+06	0.0807	0.1803	0.0000E+00
19	*	0.1449	0.2093	0.0000E+00	0.3141E+10	0.3086E+10	24.35	0.8543E+06	0.8226E+06	0.0783	0.1785	0.0000E+00
20	*	0.1445	0.2103	0.0000E+00	0.3278E+10	0.3220E+10	24.86	0.8611E+06	0.8282E+06	0.0774	0.1771	0.0000E+00
CUP-MIX AVERAGES:		0.0850	0.1168			0.3984E+10			0.8283E+06	0.0589	0.1927	0.0000E+00

VAPOR: 8.5 %, AEROSOL: 75.3 % HOMOG., 0.0 % SEED. WALL LOSS = 16.2 %

DISTRIBUTIONS:

0.0000E+00	0.0000E+00	0.0000E+00	0.0000E+00	0.0000E+00	0.1165E+00	0.7746E+00	0.3310E+01	0.1392E+02	0.5912E+02
0.0000E+00	0.0000E+00	0.0000E+00	0.0000E+00	0.0000E+00	0.6183E-07	0.5734E-06	0.3466E-05	0.2059E-04	0.1235E-03
0.5623E-02	0.6310E-02	0.7079E-02	0.7943E-02	0.8913E-02	0.1000E-01	0.1122E-01	0.1259E-01	0.1413E-01	0.1585E-01
0.2490E+03	0.1041E+04	0.3534E+05	0.5242E+07	0.6056E+10	0.3617E+11	0.1677E+10	0.3148E+08	0.7920E+07	0.3423E+08
0.7349E-03	0.4347E-02	0.2110E+00	0.4480E+02	0.9170E+05	0.5739E+06	0.3625E+05	0.9094E+03	0.3717E+03	0.2284E+04
0.1778E-01	0.1995E-01	0.2239E-01	0.2512E-01	0.2818E-01	0.3162E-01	0.3548E-01	0.3981E-01	0.4467E-01	0.5012E-01
0.1494E+09	0.8084E+09	0.6957E+10	0.6538E+10	0.7535E+10	0.8416E+10	0.5051E+10	0.1456E+10	0.1815E+09	0.7257E+07
0.1417E+05	0.1095E+06	0.1311E+07	0.1699E+07	0.2799E+07	0.4404E+07	0.3724E+07	0.1517E+07	0.2671E+06	0.1506E+05
0.5623E-01	0.6310E-01	0.7079E-01	0.7943E-01	0.8913E-01	0.1000E+00	0.1122E+00	0.1259E+00	0.1413E+00	0.1585E+00
0.5044E+05	0.1969E+02	0.0000E+00	0.0000E+00	0.0000E+00	0.0000E+00	0.0000E+00	0.0000E+00	0.0000E+00	0.0000E+00
0.1480E+03	0.8137E-01	0.0000E+00	0.0000E+00	0.0000E+00	0.0000E+00	0.0000E+00	0.0000E+00	0.0000E+00	0.0000E+00
0.1778E+00	0.1995E+00	0.2239E+00	0.2512E+00	0.2818E+00	0.3162E+00	0.3548E+00	0.3981E+00	0.4467E+00	0.5012E+00
0.0000E+00	0.0000E+00	0.0000E+00	0.0000E+00	0.0000E+00	0.0000E+00	0.0000E+00	0.0000E+00	0.0000E+00	0.0000E+00
0.0000E+00	0.0000E+00	0.0000E+00	0.0000E+00	0.0000E+00	0.0000E+00	0.0000E+00	0.0000E+00	0.0000E+00	0.0000E+00
0.5623E+00	0.6310E+00	0.7079E+00	0.7943E+00	0.8913E+00	0.1000E+01	0.1122E+01	0.1259E+01	0.1413E+01	0.1585E+01
0.0000E+00	0.0000E+00	0.0000E+00	0.0000E+00	0.0000E+00	0.0000E+00	0.0000E+00	0.0000E+00	0.0000E+00	0.0000E+00
0.0000E+00	0.0000E+00	0.0000E+00	0.0000E+00	0.0000E+00	0.0000E+00	0.0000E+00	0.0000E+00	0.0000E+00	0.0000E+00
0.1778E+01	0.1995E+01	0.2239E+01	0.2512E+01	0.2818E+01	0.3162E+01	0.3548E+01	0.3981E+01	0.4467E+01	0.5012E+01

Z = 359 SEED N = 0.0000E+00 /CC.

X		XA	TEMP	J (/CC.SEC.)	INT.J (/CC.)	N (/CC.)	PHIZ	INT.PHIZ (CU.MIC/CC)	HOMO PHI (CU.MIC/CC)	AVE & SEED DIA (MICRONS)		SEED PHI (CU.MIC/CC)
0		0.0000	0.0000									
1	*	0.0043	0.0084	0.0000E+00	0.6529E+11	0.1144E+12	0.2444	0.1941E+07	0.1845E+07	0.0312	0.0538	0.0000E+00
2	*	0.0096	0.0172	0.0000E+00	0.1009E+11	0.1099E+11	0.3791	0.2286E+07	0.2265E+07	0.0731	0.1013	0.0000E+00
3	*	0.0160	0.0265	0.0000E+00	0.2396E+10	0.2395E+10	0.2612	0.7718E+06	0.7699E+06	0.0830	0.1655	0.0000E+00
4	*	0.0228	0.0362	0.0000E+00	0.1690E+10	0.1690E+10	0.4650	0.9388E+06	0.9356E+06	0.1002	0.1925	0.0000E+00
5		0.0300	0.0462	0.0000E+00	0.1350E+10	0.1347E+10	0.6090	0.6909E+06	0.6881E+06	0.0961	0.2050	0.0000E+00
6		0.0373	0.0566	0.0000E+00	0.1404E+10	0.1399E+10	1.016	0.7684E+06	0.7639E+06	0.0992	0.2080	0.0000E+00
7		0.0448	0.0672	0.0000E+00	0.1223E+10	0.1219E+10	1.319	0.7218E+06	0.7170E+06	0.1018	0.2105	0.0000E+00
8		0.0521	0.0779	0.0000E+00	0.1215E+10	0.1210E+10	1.789	0.7292E+06	0.7234E+06	0.1025	0.2088	0.0000E+00
9		0.0591	0.0886	0.0000E+00	0.1243E+10	0.1237E+10	2.362	0.7561E+06	0.7490E+06	0.1031	0.2095	0.0000E+00
10		0.0656	0.0992	0.0000E+00	0.1269E+10	0.1262E+10	2.968	0.7734E+06	0.7649E+06	0.1033	0.2060	0.0000E+00
11		0.0714	0.1094	0.0000E+00	0.1327E+10	0.1318E+10	3.634	0.7920E+06	0.7818E+06	0.1026	0.2053	0.0000E+00
12		0.0762	0.1191	0.0000E+00	0.1420E+10	0.1410E+10	4.346	0.8124E+06	0.8003E+06	0.1012	0.2007	0.0000E+00
13		0.0800	0.1282	0.0000E+00	0.1548E+10	0.1535E+10	5.063	0.8317E+06	0.8174E+06	0.0991	0.1970	0.0000E+00
14		0.0826	0.1364	0.0000E+00	0.1716E+10	0.1700E+10	5.759	0.8497E+06	0.8328E+06	0.0964	0.1947	0.0000E+00
15		0.0841	0.1437	0.0000E+00	0.1931E+10	0.1910E+10	6.402	0.8667E+06	0.8468E+06	0.0932	0.1915	0.0000E+00
16		0.0845	0.1499	0.0000E+00	0.2199E+10	0.2172E+10	6.970	0.8831E+06	0.8600E+06	0.0897	0.1877	0.0000E+00
17		0.0840	0.1549	0.0000E+00	0.2514E+10	0.2480E+10	7.452	0.8987E+06	0.8722E+06	0.0862	0.1834	0.0000E+00
18	*	0.0830	0.1585	0.0000E+00	0.2852E+10	0.2810E+10	7.846	0.9135E+06	0.8836E+06	0.0830	0.1815	0.0000E+00
19	*	0.0821	0.1607	0.0000E+00	0.3141E+10	0.3093E+10	8.120	0.9255E+06	0.8929E+06	0.0806	0.1797	0.0000E+00
20	*	0.0818	0.1614	0.0000E+00	0.3278E+10	0.3227E+10	8.261	0.9335E+06	0.8997E+06	0.0796	0.1782	0.0000E+00
CUP-MIX AVERAGES:												
		0.0559	0.0897			0.3986E+10			0.8582E+06	0.0595	0.1934	0.0000E+00

VAPOR: 5.6 %, AEROSOL: 78.0 % HOMOG., 0.0 % SEED, WALL LOSS = 16.4 %

DISTRIBUTIONS:

0.0000E+00	0.0000E+00	0.0000E+00	0.0000E+00	0.0000E+00	0.0000E+00	0.4777E-01	0.1052E+01	0.5618E+01	0.2838E+02
0.0000E+00	0.0000E+00	0.0000E+00	0.0000E+00	0.0000E+00	0.0000E+00	0.3597E-07	0.1101E-05	0.8310E-05	0.5928E-04
0.5623E-02	0.6310E-02	0.7079E-02	0.7943E-02	0.8913E-02	0.1000E-01	0.1122E-01	0.1259E-01	0.1413E-01	0.1585E-01
0.1376E+03	0.6372E+03	0.3111E+05	0.4920E+07	0.4981E+10	0.3734E+11	0.1740E+10	0.3296E+08	0.6575E+07	0.2753E+08
0.4063E-03	0.2654E-02	0.1878E+00	0.4246E+02	0.7521E+05	0.5970E+06	0.3786E+05	0.9549E+03	0.3082E+03	0.1825E+04
0.1778E-01	0.1995E-01	0.2239E-01	0.2512E-01	0.2818E-01	0.3162E-01	0.3548E-01	0.3981E-01	0.4467E-01	0.5012E-01
0.1119E+09	0.6190E+09	0.6561E+10	0.6186E+10	0.7384E+10	0.8824E+10	0.5566E+10	0.1652E+10	0.2100E+09	0.8399E+07
0.1047E+05	0.8325E+05	0.1235E+07	0.1607E+07	0.2742E+07	0.4618E+07	0.4108E+07	0.1720E+07	0.3086E+06	0.1747E+05
0.5623E-01	0.6310E-01	0.7079E-01	0.7943E-01	0.8913E-01	0.1000E+00	0.1122E+00	0.1259E+00	0.1413E+00	0.1585E+00
0.6085E+05	0.2459E+02	0.0000E+00	0.0000E+00	0.0000E+00	0.0000E+00	0.0000E+00	0.0000E+00	0.0000E+00	0.0000E+00
0.1784E+03	0.1017E+00	0.0000E+00	0.0000E+00	0.0000E+00	0.0000E+00	0.0000E+00	0.0000E+00	0.0000E+00	0.0000E+00
0.1778E+00	0.1995E+00	0.2239E+00	0.2512E+00	0.2818E+00	0.3162E+00	0.3548E+00	0.3981E+00	0.4467E+00	0.5012E+00
0.0000E+00	0.0000E+00	0.0000E+00	0.0000E+00	0.0000E+00	0.0000E+00	0.0000E+00	0.0000E+00	0.0000E+00	0.0000E+00
0.0000E+00	0.0000E+00	0.0000E+00	0.0000E+00	0.0000E+00	0.0000E+00	0.0000E+00	0.0000E+00	0.0000E+00	0.0000E+00
0.5623E+00	0.6310E+00	0.7079E+00	0.7943E+00	0.8913E+00	0.1000E+01	0.1122E+01	0.1259E+01	0.1413E+01	0.1585E+01
0.0000E+00	0.0000E+00	0.0000E+00	0.0000E+00	0.0000E+00	0.0000E+00	0.0000E+00	0.0000E+00	0.0000E+00	0.0000E+00
0.0000E+00	0.0000E+00	0.0000E+00	0.0000E+00	0.0000E+00	0.0000E+00	0.0000E+00	0.0000E+00	0.0000E+00	0.0000E+00
0.1778E+01	0.1995E+01	0.2239E+01	0.2512E+01	0.2818E+01	0.3162E+01	0.3548E+01	0.3981E+01	0.4467E+01	0.5012E+01

APPENDIX G. THE EFFECT OF A GROWING AEROSOL ON THE RATE OF HOMOGENEOUS NUCLEATION OF A VAPOR

The Effect of a Growing Aerosol on the Rate of Homogeneous Nucleation of a Vapor

ANDREW J. PESTHY, RICHARD C. FLAGAN,[1] AND JOHN H. SEINFELD

Department of Chemical Engineering, California Institute of Technology, Pasadena, California 91125

Received October 20, 1980; accepted December 15, 1980

Growing particles in a supersaturated vapor act as sources of latent heat and sinks for vapor, altering the vapor concentration and gas temperature near the particles, and, consequently, decreasing the homogeneous nucleation rate in the vicinity of the particles. Solutions for the vapor concentration and temperature profiles around a growing particle are obtained, and the solutions are used to predict the average nucleation rate per unit volume of fluid as a function of time. The average nucleation rate is shown to be proportional to the initially undisturbed rate and proportional to a term dependent largely on the total volume fraction of growing aerosol present. Under a wide range of conditions, the nucleation rate for dibutyl phthalate is calculated to quench gradually at the time when the fraction of available vapor condensed into aerosol approaches 5 to 9%.

1. INTRODUCTION

The classical approach to predicting the rate of formation of new, stable particles by homogeneous nucleation neglects the effect of existing particles on the nucleation rate (1). Even in the absence of foreign particles, those formed via nucleation, and present during the continuing nucleation process, may be expected to influence the rate of formation of fresh particles through the scavenging of vapor molecules that might otherwise be available for cluster growth and nucleation. To describe the effect of an existing aerosol on the rate of homogeneous nucleation, it is necessary to consider the effect of growing particles on the vapor (monomer) concentration and temperature fields in the vicinity of a growing particle.

Since particle growth occurs by condensation of monomer from the gas phase, a spherically symmetric radial distribution of monomer partial pressure develops in time about a growing particle. The accompanying release of latent heat of condensation at the particle surface also leads to the development of a nonuniform temperature profile about the growing particle. The rate of formation of new particles by homogeneous nucleation is a strong function of temperature and saturation ratio. Consequently, the local perturbations in the monomer and temperature fields caused by growing particles may have a significant effect on the nucleation rate, and the resulting actual average nucleation rate per unit volume of air may thus deviate substantially from the intrinsically predicted value.

An elementary analysis is developed for the case in which stationary nucleation theory is applicable to the region in the vicinity of nucleated and growing particles, a case simplified by the unidirectional coupling between homogeneous nucleation rate and monomer depletion due to particle growth. The case of "catastrophic nucleation," in which monomer depletion by nucleating particles causes a significant influence in the nucleation rate, represents a mutual coupling of nucleation rate and monomer depletion, and is not included in the analysis.

[1] Department of Environmental Engineering Science.

0021-9797/81/080465-15$02.00/0

In this paper, conditions are developed for assessing the importance of the effect of growing particles on the rate of homogeneous nucleation of a vapor in a given situation. Section 2 is devoted to a consideration of the effect of growing particles on the average nucleation rate. In Section 3 solutions for the concentration and temperature profiles around growing particles are obtained. In Section 4 these profiles are used to calculate the average nucleation rate in the presence of a growing aerosol. Section 5 presents a sample calculation for dibutyl phthalate in air.

2. AVERAGE NUCLEATION RATE AROUND A GROWING PARTICLE

Consider a single growing particle, the radius of which, at time t, is r_0. If J_∞ denotes the "intrinsic" nucleation rate based on conditions (monomer concentration and temperature) far from the particle, and if $J(r)$ is the nucleation rate at radial position r from the particle center, then the deviation from the intrinsic nucleation rate is $\Delta J(r) = J(r) - J_\infty$. If we select a radius r_a, arbitrary at this point, but characteristic of the distance from the particle at which background conditions are reached, the average nucleation rate over the volume within r_a is

$$\bar{J} = \frac{\int_0^{r_a} J(r) r^2 dr}{\int_0^{r_a} r^2 dr}. \qquad [1]$$

Equation [1] may be rewritten as

$$\frac{\bar{J}}{J_\infty} = 1 - \frac{3}{r_a^3} \int_0^{r_a} \frac{-\Delta J(r)}{J_\infty} r^2 dr. \qquad [2]$$

It is useful to introduce the notion of a "clearance volume" around the particle, defined by that radius, ρr_0, for which the nucleation rate from 0 to ρr_0 is zero, and that beyond ρr_0 is J_∞, such that over the entire volume of radius r_a the average nucleation rate is $\bar{J}$. Thus,

$$\frac{\bar{J}}{J_\infty} = 1 - \rho^3 \left(\frac{r_0}{r_a}\right)^3. \qquad [3]$$

Comparison of Eqs. [2] and [3] gives the expression for the dimensionless clearance volume ρ^3,

$$\rho^3 = 3 \int_0^{r_a/r_0} \frac{-\Delta J(y, t)}{J_\infty} y^2 dy. \qquad [4]$$

In general, ρ^3 may be a function of particle size and time. During the initial phase of nucleation and condensational growth, the region of influence on the nucleation rate by the particles is localized within the averaging volume such that we can effectively let $r_a/r_0 \to \infty$, and

$$\rho^3 = 3 \int_0^{\infty} \frac{-\Delta J(y, t)}{J_\infty} y^2 dy. \qquad [5]$$

After the regions of influence of adjacent particles overlap, the averaging volume must be chosen as some characteristic volume associated with each particle.

The coefficient of ρ^3 in Eq. [3] is the volume fraction of the particle within the sphere of radius r_a. By averaging over all particles in a distribution, the resulting average nucleation rate is

$$\frac{\bar{J}}{J_\infty} = 1 - \int_0^{\infty} \rho^3 v n_v(v, t) dv, \qquad [6]$$

where $n_v(v, t)$ is the aerosol volume distribution, defined such that $n_v dv$ is the number of particles per unit volume of gas having volumes in the range $[v, v + dv]$.

The radius of the averaging volume may depend on particle size, with the restriction that the averaging over all particles is performed over the whole volume of gas. That is,

$$\int_0^{\infty} \left(\frac{r_a}{r_0}\right)^3 v n_v dv = 1. \qquad [7]$$

A reasonable choice is to assign averaging volumes proportional to particle volumes,

$$\frac{r_a}{r_0} = \phi^{-1/3}, \qquad [8]$$

where $\phi = \int_0^\infty n_v v dv$ is the volume fraction of the existing aerosol.

A convenient condition indicating a significant decrease in the average nucleation rate may be specified as the onset of overlap of clearance volumes defined by Eq. [5]. This occurrence corresponds to

$$\int_0^\infty \rho^3 v n_v(v, t) dv \cong 1, \qquad [9]$$

where ρ^3 is the clearance volume averaged as in Eq. [5].

3. CONCENTRATION AND TEMPERATURE PROFILES AROUND A GROWING PARTICLE

Expressions for the monomer concentration and temperature profiles around a growing particle can be obtained by solution of the appropriate mass and energy conservation equations. Typical aerosol volume distributions reveal that most of the aerosol volume is associated with the large particles. An assumption that may be invoked, and one that can later be tested, is that the particle clearance volume is proportional to the particle volume. Consequently, most of the clearance volume is associated with the larger particles, and the mass and energy conservation equations can be based on continuum theory ($Kn \ll 1$) with only small errors expected for those small ($Kn \gtrsim 1$) particles for which continuum transport theory is invalid.

Before writing the conservation equations it is useful to compare the relative rates of the significant processes occurring. Table I summarizes the characteristic time scales for the processes of vapor diffusion, heat transport in the gas phase, heat conduction in the particle, and growth of the particle. The time scales were calculated from continuum theory assuming particle growth rate is negligible compared to the rate of the other processes, an assumption that is later shown to be correct. The time scales for the diffusion processes in the gas phase are much shorter than that for particle growth. The time scales for heat conduction in aqueous or organic particles is less than or comparable to that for particle growth. For metallic particles, the time scale for internal heat conduction is much less than that for particle growth, but still greater than that for heat conduction in air.

In light of these differing time scales, a physical picture of the nucleation and subsequent growth processes emerges. The entire process is initiated by the formation of a new particle by homogeneous nucleation. At critical nucleus size, the equilibrium partial pressure at the particle surface equals the partial pressure far from the particle. Therefore we may assume that the nucleation process does not disturb the background monomer vapor concentration field. It is this assumption that limits the present model to homogeneous nucleation processes that are slow enough to allow for definition of an "intrinsic" nucleation rate based on stationary nucleation theory.

Due to the Kelvin effect, the equilibrium vapor concentration at the particle surface is dependent on particle size. As the particle grows to a diameter of only a few times the critical size, the Kelvin effect becomes unimportant and the equilibrium vapor pressure at the particle surface approaches a constant value equal to the saturation pressure. The condition corresponding to particle radius r_0 for which the Kelvin effect is unimportant in a vapor of saturation ratio S is

$$S^{(1-r^*/r_0)} \gg 1. \qquad [10]$$

Since the critical saturation ratio in most processes is much greater than unity, the Kelvin effect becomes unimportant for even a modest increase in particle radius. In this work, we will neglect the Kelvin effect and assume that the equilibrium vapor pressure at the particle surface is the saturation pressure for all particles greater than the critical size. The consequence of this assumption is that the particle growth rate is not accurately represented in the initial stage of

TABLE I

Characteristic Times for Growing Particle Processes

	Heat conduction in air r_p^2/α	Heat conduction in particle r_p^2/α_d	Vapor diffusion $r_p^2/\mathcal{D}$	Particle growth $c_d r_p^2/\mathcal{D} x_{A_\infty}$
τ/τ_{cond}	1	α/α_d	$\alpha/\mathcal{D} = \mathrm{Le}$	$c_d\,\mathrm{Le}/c x_{A_\infty}$
Typical values in air				
Dibutyl phthalate (DBP)	1	310	4.2	$380/x_{A_\infty} > 10^3$
Organics	1	200	2–4	$(10-100)/x_{A_\infty} > 10^2$
Water	1	90	0.86	$20/x_{A_\infty} > 10^2$
Metals	1	~5	1.5	$5000/x_{A_\infty} > 10^4$

growth. It will be shown later, however, that the monomer concentration and temperature profiles around a growing particle large enough for neglecting the Kelvin effect are not dependent on the initial conditions, but only on the instantaneous particle size.

As growth begins, vapor diffusion proceeds on a much faster time scale than growth. Even before significant growth occurs, vapor diffusion evolves through hundreds of time constants. Consequently, the vapor concentration profile within tens of radii from the particle is at steady state, whereas the more distant part of the profile is still changing.

The growth rate is determined by the diffusional flux of monomer vapor. Since the vapor concentration profile near the particle approaches steady state before appreciable growth occurs, the steady state diffusional flux may be used to calculate the particle growth rate. As growth proceeds hundreds of times slower than diffusion, the profile near the particle remains close to its steady-state value at all times, whereas the region of transience propagates farther from the particle.

An energy balance describes the effects of latent heat release by condensation at the particle surface. Heat conduction occurs both in the particle interior and in the exterior gas phase. The ratio of the characteristic time for conduction in a particle to that for outward conduction in the vapor is of the order of 100 for most nonmetals in air, and the order of 10 for metals. The high value of this ratio suggests that the latent heat is primarily conducted outward. As vapor condensation begins, the particle surface temperature rises until the rate of outward heat conduction balances the rate of latent heat generation. The formation of the external temperature and the monomer concentration profiles occurs simultaneously on approximately the same time scales. Consequently, the steady-state fluxes of heat and vapor may be related by a steady-state energy balance to determine the steady-state surface temperature at all times during the particle growth.

For most systems the surface temperature is elevated by only a few degrees Kelvin, and as a result, the total molar density of the gas c may be assumed constant. The saturation pressure at the particle surface is elevated to the thermodynamic value at the surface temperature, providing the surface boundary condition for the vapor diffusion process.

An additional consequence of the diffusion of monomer to the particle is Stefan flow, a net flow of gas toward the particle. The particle growth rate and the Stefan flow velocity at the surface are related by a mass balance. The Stefan flow is several orders of magnitude faster than the particle growth rate. Therefore, the convective velocity induced by the outward motion of the growing particle surface is negligible.

It is evident that all processes except par-

ticle growth reach steady state in the vicinity of the particle well before the onset of significant growth. This physical picture suggests that we seek steady-state solutions to the conservation equations for a particle of fixed radius, from which to calculate expressions for the velocity profile and the particle growth rate. These expressions will then be used in the full conservation equations applying to a growing particle, describing the monomer vapor concentration and temperature profiles on a time scale relating to particle growth.

The steady-state conservation equations for total molar density of the gas, monomer concentration, and temperature are (2)

$$\frac{1}{r^2}\frac{d}{dr}(cr^2V_r^*) = 0 \qquad [11]$$

$$V_r^*\frac{dc_A}{dr} = c\mathcal{D}\frac{1}{r^2}\left(r^2\frac{dx_A}{dr}\right), \qquad [12]$$

$$V_r\frac{dT}{dr} = \alpha\frac{1}{r^2}\frac{d}{dr}\left(r^2\frac{dT}{dr}\right). \qquad [13]$$

The mass balances are written in molar units since the constant total molar density c provides an immediate simplification in solving for the molar average velocity, V_r^*.

The particle mass balance is[2]

$$cV_{r_0}^*(4\pi r_0^2) + c_d\frac{d}{dt}\left(\frac{4}{3}\pi r_0^3\right) = 0. \qquad [14]$$

The particle energy balance assuming outward conduction only is

$$cV_{r_0}^*\Delta H_v(4\pi r_0^2) - k_T\left.\frac{dT}{dr}\right|_{r_0}(4\pi r_0^2) = 0. \qquad [15]$$

The terms containing $cV_{r_0}^*$ represent the molar flow rate of monomer contributing to the total moles and latent heat energy of the particle. The second term of Eq. [14] is the rate of change of the number of moles of monomer in the particle. The second term of Eq. [15] is the rate of heat conduction away from the particle.

We can solve Eq. [11] for V_r^* and then solve Eq. [12] with the boundary conditions

$$x_A = x_{A_0}, \quad r = r_0,$$
$$x_A = x_{A_\infty}, \quad r \to \infty. \qquad [16]$$

The concentration profile becomes (2)

$$\frac{1 - x_A}{1 - x_{A_\infty}} = \left(\frac{1 - x_{A_0}}{1 - x_{A_\infty}}\right)^{r_0/r} \qquad [17]$$

and the molar average velocity at any radial position r is

$$V_r^* = -\left(\frac{r_0}{r}\right)^2\frac{\mathcal{D}}{r_0}\ln\left[\frac{1 - x_{A_0}}{1 - x_{A_\infty}}\right]. \qquad [18]$$

From the particle mass balance (Eq. [14]) and Eq. [18], the particle growth rate is obtained as

$$r_0\frac{dr_0}{dt} = \frac{c\mathcal{D}}{c_d}\ln\left[\frac{1 - x_{A_0}}{1 - x_{A_\infty}}\right]. \qquad [19]$$

The initial condition for the particle radius corresponds to the critical size nucleus, r^*,

$$r_0 = r^*, \quad t = 0. \qquad [20]$$

Note that $r_0(dr_0/dt)$ is constant in time (3).

The steady state temperature profile must be calculated from Eq. [13] and used in the particle energy balance, Eq. [15], to evaluate the surface temperature. That is, we solve Eq. [13] subject to

$$T = T_0, \quad r = r_0,$$
$$T = T_\infty, \quad r \to \infty. \qquad [21]$$

In a binary system of dilute monomer A, the mass average velocity is related to the molar average velocity by

$$V_r \cong V_r^*\frac{M_A}{M_B} \qquad [22]$$

This relation may be used with Eq. [18] in Eq. [13] and solved to get

[2] In a binary system, the total molar flux is $N_{Ar} + N_{Br} = cV_r^*$. At all times at the surface, $N_{Br} = 0$. Thus the surface molar flux of A is $N_{Ar_0} = cV_{r_0}^*$.

$$\frac{T - T_\infty}{T_0 - T_\infty} = \frac{\left(\frac{1 - x_{A_0}}{1 - x_{A_\infty}}\right)^{Le^{-1}(M_A/M_B)(r_0/r)} - 1}{\left(\frac{1 - x_{A_0}}{1 - x_{A_\infty}}\right)^{Le^{-1}(M_A/M_B)} - 1}, \quad [23]$$

where the Lewis number, $Le = \alpha/\mathcal{D}$. As long as the factor $Le^{-1}(M_A/M_B) \ln [1 - x_{A_0}/1 - x_{A_\infty}]$ is much less than unity, the convective term of Eq. [13] is negligible when compared with the conductive term, and Eq. [23] simplifies to the well-known result for pure conduction,

$$\frac{T - T_\infty}{T_0 - T_\infty} = \frac{r_0}{r}. \quad [24]$$

The appropriate expression for T, Eq. [23] or [24], may be used with Eq. [18] in Eq. [15] to solve for T_0. Equation [24] applies for dilute vapor, and we get

$$k_T(T_0 - T_\infty) = \Delta H_r c \mathcal{D} \ln \left[\frac{1 - x_{A_0}}{1 - x_{A_\infty}}\right]. \quad [25]$$

The boundary condition on mole fraction is

$$x_A = x_{A_0} = x_A^{sat}(T_0), \quad r = r_0. \quad [26]$$

Therefore, Eq. [25] becomes implicit for T_0,

$$k_T(T_0 - T_\infty) = \Delta H_r c \mathcal{D} \ln \left[\frac{1 - x_A^{sat}(T_0)}{1 - x_{A_\infty}}\right]. \quad [27]$$

For dilute monomer A, one can approximate Eq. [27] by

$$k_T(T_0 - T_\infty) = \Delta H_r c \mathcal{D}[x_{A_\infty} - x_A^{sat}(T_0)]. \quad [28]$$

Equation [28] will be solved later for the boundary condition T_0.

Now that expressions for the particle growth rate, Stefan flow velocity, and boundary conditions have been derived from the steady-state conservation equations, the full conservation equations for the time-dependent monomer concentration and temperature profiles can be solved for all r on the time scale of particle growth. In the vicinity of the growing particle the solutions will be expected to match the pseudo-steady-state solutions derived above for any instant during the growth. The conservation equations are

$$\frac{\partial c_A}{\partial t} + V_r^* \frac{\partial c_A}{\partial r} = c\mathcal{D} \frac{1}{r^2} \frac{\partial}{\partial r}\left(r^2 \frac{\partial x_A}{\partial r}\right), \quad [29]$$

$$\frac{\partial T}{\partial t} + V_r \frac{\partial T}{\partial r} = \alpha \frac{1}{r^2} \frac{\partial}{\partial r}\left(r^2 \frac{\partial T}{\partial r}\right) \quad [30]$$

subject to boundary conditions,

$$x_A = x_A^{sat}(T_0), \quad T = T_0, \quad r = r_0(t), \quad [31]$$

$$x_A = x_{A_\infty}, \quad T = T_\infty, \quad r \to \infty, \quad [32]$$

and initial conditions,

$$x_A = x_{A_\infty}, \quad T = T_\infty, \quad t = 0, r > r^*. \quad [33]$$

The boundary conditions at r_0 are constant on the time scale of particle growth, but the boundary itself moves in time. This complication is readily simplified by transformation to a rescaled radial coordinate defined by $y = r/r_0(t)$. The conservation equations with the velocity distribution from Eqs. [18] and [22] and growth rate from Eq. [19] become

$$\frac{\partial x_A}{\partial \theta} - \left[2Ay + \frac{B}{y^2}\right]\frac{\partial x_A}{\partial y} = \frac{1}{y^2}\frac{\partial}{\partial y}\left(y^2 \frac{\partial x_A}{\partial y}\right) \quad [34]$$

$$\frac{\partial T}{\partial \theta} - \left[2Ay + \frac{BM_A}{M_B}\frac{1}{y^2}\right]\frac{\partial T}{\partial y} = Le \frac{1}{y^2}\frac{\partial}{\partial y}\left(y^2 \frac{\partial T}{\partial y}\right) \quad [35]$$

with boundary conditions

$$x_A = x_A^{sat}(T_0), \quad T = T_0, \qquad y = 1; \qquad [36]$$

$$x_A = x_{A_\infty}, \quad T = T_\infty, \qquad x \to \infty; \qquad [37]$$

and initial conditions

$$x_A = x_{A_\infty}, \quad T = T_\infty, \qquad \theta = 0, y > 1, \qquad [38]$$

where

$$A = \frac{1}{2}\frac{c}{c_d} \ln\left[\frac{1 - x_{A_0}}{1 - x_{A_\infty}}\right], \qquad [39]$$

$$B = \ln\left[\frac{1 - x_{A_0}}{1 - x_{A_\infty}}\right], \qquad [40]$$

$$\theta = \frac{1}{4A} \ln\left\{1 + 4A\frac{\mathcal{D}t}{r^{*2}}\right\}. \qquad [41]$$

The terms containing the factor A arise from the coordinate transformation, and those containing the factor B arise from the Stefan flow. It is apparent by comparison to Eq. [19] that A is a dimensionless growth rate parameter, and $A > 0$. (The case of $A < 0$ corresponds to an evaporating particle and is not of interest here.) Typically, A is less than 10^{-3} and $B \ll 1$. Therefore the terms in A play a significant role for large y, and the terms in B contribute a small part only for $y \cong 1$.

Viewed in the (y, θ) coordinate system, Eqs. [34] and [35], with the boundary conditions and initial conditions given by Eqs. [36]–[38], describe diffusional processes about a fixed sphere in a fluid of infinite extent with uniform initial concentration and temperature. At time $\theta = 0$, a step change in concentration and temperature occurs at the surface of the sphere while the fluid flows radially toward the sphere at a velocity, constant in time, given by the quantities in the square brackets in Eqs. [34] and [35]. Because the parameters A and B are small, the induced convection in the (y, θ) system is not significant near the sphere and the equations are approximated by

$$\frac{\partial x_A}{\partial \theta} = \frac{1}{y^2}\frac{\partial}{\partial y}\left(y^2 \frac{\partial x_A}{\partial y}\right), \qquad [42]$$

$$\frac{\partial T}{\partial \theta} = \mathrm{Le}\,\frac{1}{y^2}\frac{\partial}{\partial y}\left(y^2 \frac{\partial T}{\partial y}\right) \qquad [43]$$

with well-known solutions,

$$\frac{x_A - x_{A_0}}{x_{A_\infty} - x_{A_0}} = 1 - \frac{1}{y}\,\mathrm{erfc}\left[\frac{y - 1}{(4\theta)^{1/2}}\right], \qquad [44]$$

$$\frac{T - T_\infty}{T_0 - T_\infty} = \frac{1}{y}\,\mathrm{erfc}\left[\frac{y - 1}{(4\,\mathrm{Le}\,\theta)^{1/2}}\right]. \qquad [45]$$

These solutions apply only until the concentration and temperature begin to change beyond $y > 1/2A$, where the velocity term becomes important. This interval of time corresponds to the time before significant particle growth occurs in the true physical picture, and while the time coordinates θ and $\mathcal{D}t/r^{*2}$ are about equal,

$$4A\theta < 1. \qquad [46]$$

During this initial phase of time, the solutions, Eqs. [44] and [45], reduce to the pseudo-steady-state expressions in the limit of dilute monomer vapor, Eqs. [17] and [24].

For longer times the diffusive processes proceed outward from the particle against a negative radial velocity, ultimately establishing a steady state in the (y, θ) coordinates. The approach to steady state requires solution of Eqs. [34] and [35] and is done elsewhere (4). The proper boundary and initial conditions accounting for the transient influence of the Kelvin effect in the first stages of particle growth need not be imposed because such short transience in the initial conditions does not alter the ultimate steady state. For practical limits of y, steady state is approached relatively quickly on the time scale of growth so we proceed to solve and interpret the steady state.

The steady-state solution to Eqs. [34] and [35] is only apparent in the transformed coordinate $y = r/r_0(t)$. The corresponding picture in the physical (r, t) coordinates is that of a growing particle with the diffusion profile transients evolving outward in a scale

proportional to the growing particle radius. That is, the transient profiles at any two times are mappable into each other by a simple scaling of the r coordinate.

For this part we seek solutions to

$$-\left[2Ay + \frac{B}{y^2}\right]\frac{\partial x_A}{\partial y} = \frac{1}{y^2}\frac{\partial}{\partial y}\left(y^2\frac{\partial x_A}{\partial y}\right), \quad [47]$$

$$-\left[2Ay + \frac{BM_A}{M_B}\frac{1}{y^2}\right]\frac{\partial T}{\partial y} = \mathrm{Le}\,\frac{1}{y^2}\frac{\partial}{\partial y}\left(y^2\frac{\partial T}{\partial y}\right) \quad [48]$$

subject to boundary conditions of Eqs. [36] and [37]. The solutions are

$$\frac{x_A(y) - x_{A_0}}{x_{A_\infty} - x_{A_0}} = 1 - F(y; A, B), \quad [49]$$

$$\frac{T(y) - T_\infty}{T_0 - T_\infty} = F\left(y; \frac{A}{\mathrm{Le}}, \frac{BM_A}{\mathrm{Le}\,M_B}\right), \quad [50]$$

where

$$F(y; A, B) = \frac{\int_y^\infty (1/z^2)\exp(-Az^2 + B/z)dz}{\int_1^\infty (1/z^2)\exp(-Az^2 + B/z)dz}. \quad [51]$$

Note that if the growth rate parameter A were set equal to zero, we recover the steady-state solutions of Eqs. [17] and [23]. Most systems are sufficiently dilute that $B \ll 1$ and the function F simplifies to

$$F(y; A) = \frac{(1/y)\exp(-Ay^2) - (\pi A)^{1/2}\,\mathrm{erfc}\,(A^{1/2}y)}{\exp(-A) - (\pi A)^{1/2}\,\mathrm{erfc}\,(A^{1/2})}. \quad [52]$$

Asymptotic expansions for both cases $Ay^2 \ll 1$ and $Ay^2 \gg 1$ may be combined to form a computationally simpler expression for F,

$$F(y; A) \equiv \frac{(1/y)\exp(-Ay^2)}{2Ay^2 + (2A)^{1/2}y + 1}. \quad [53]$$

This expression is within a few percent equal to Eq. [52] for $A \lesssim 10^{-4}$. The function F is illustrated in Fig. 1. For the case of no growth, $A = 0$, and F reduces to the classical steady-state diffusion profile without convection. For $A > 0$, the F profiles drop off sharply at some distance y from the particle characteristic of the growth rate A.

Now we need to apply the relations in Eqs. [26] and [28] to incorporate the boundary conditions. For convenience, the energy balance, Eq. [28], can be solved in terms of a dimensionless thermal difference, $\Delta T \equiv (T_0 - T_\infty)/T_\infty$, and the Lewis number

$$\Delta_T = \left(\frac{\Delta H_v}{RT_\infty}\right)\left(\frac{R}{M_B C_p}\right) \times \mathrm{Le}^{-1}\,[x_{A_\infty} - x_A^{\mathrm{sat}}(T_0)]. \quad [54]$$

The saturation mole fraction may be replaced by the integrated Clausius–Clapeyron expression which yields the implicit equation for Δ_T,

$$\Delta_T = \left(\frac{\Delta H_v}{RT_\infty}\right)\left(\frac{R}{M_B C_p}\right)\mathrm{Le}^{-1}\left\{x_{A_\infty} - x_A^{\mathrm{sat}}(T_\infty) \times \exp\left[\frac{\Delta H_v}{RT_\infty}\left(\frac{\Delta_T}{1 + \Delta_T}\right)\right]\right\}. \quad [55]$$

Under conditions typical for homogeneous nucleation for many vapors, supersaturation is high enough that $x_{A_\infty} \gg x_A^{\mathrm{sat}}(T_0)$ and Eq. [54] becomes explicit for Δ_T,

$$\Delta_T \equiv \left(\frac{\Delta H_v}{RT_\infty}\right)\left(\frac{R}{M_B C_p}\right)\mathrm{Le}^{-1}\,x_{A_\infty}. \quad [56]$$

The boundary condition in Eq. [31] is similarly rewritten in terms of T_∞ and used to express a dimensionless mole fraction difference, $\Delta_x \equiv (x_{A_\infty} - x_{A_0})/x_{A_\infty}$,

$$\Delta_x = 1 - \frac{x_A^{sat}(T_\infty)}{x_{A_\infty}} \times \exp\left[\frac{\Delta H_v}{RT_\infty}\left(\frac{\Delta_T}{1+\Delta_T}\right)\right]. \quad [57]$$

For dilute vapor, the mole fraction and temperature profiles can be expressed in these parameters as

$$X(y) \equiv \frac{x_A(y)}{x_{A_\infty}} = 1 - \Delta_x F\left(y; \frac{1}{2}\frac{c}{c_d}\Delta_x x_{A_\infty}, \Delta_x x_{A_\infty}\right), \quad [58]$$

$$\Gamma(y) \equiv \frac{T(y)}{T_\infty} = 1 + \Delta_T F\left(y; \frac{1}{2}\mathrm{Le}^{-1}\frac{c}{c_d}\Delta_x x_{A_\infty}, \mathrm{Le}^{-1}\frac{M_A}{M_B}\Delta_x x_{A_\infty}\right). \quad [59]$$

From the concentration and temperature profiles, the saturation ratio profile may be calculated directly. From the definition of the saturation ratio, we get

$$S(y) = X(y)\frac{x_{A_\infty}}{x_A^{sat}(T(y))}. \quad [60]$$

Applying the integrated Clausius–Clapeyron equation for the saturation concentration gives

$$\frac{S(y)}{S_\infty} = X(y)\exp\left[\frac{-\Delta H_v}{RT_\infty}\left(1 - \frac{1}{\Gamma(y)}\right)\right], \quad [61]$$

where $S_\infty = x_{A_\infty}/x_A^{sat}(T_\infty)$ is the saturation ratio far from the particle.

The above results describe the spatial variations of mole fraction, temperature, and saturation ratio with which to calculate the clearance volume from Eq. [5]. For the later profiles during the aerosol growth process, applicable to calculating the clearance volume from Eq. [4], we note that Reiss (5, 6) has shown that for $r_a \gg r_0$, the mass and energy balances are well approximated by the pseudo-steady-state approximation even though the background conditions may change slowly in time. Neglecting Stefan flow, the conservation equations are

$$\frac{1}{r^2}\frac{\partial}{\partial r}\left(r^2\frac{\partial x_A}{\partial r}\right) = 0, \quad [62]$$

$$\frac{1}{r^2}\frac{\partial}{\partial r}\left(r^2\frac{\partial T}{\partial r}\right) = 0. \quad [63]$$

Note that x_A and T are still functions of time. The background conditions provide boundary conditions which change only slowly with time,

$$x_A = x_{A_0}, \quad T = T_0, \quad r = r_0; \quad [64]$$

$$x_A = x_{Ab}, \quad T = T_b, \quad r = r_a\ (r_a \gg r_0). \quad [65]$$

The solutions to Eqs. [62] and [63] with these boundary conditions are

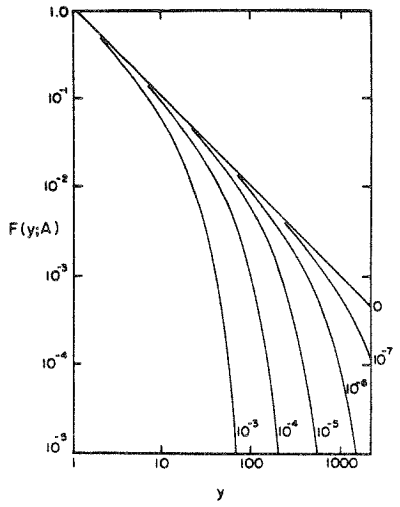

FIG. 1. Dimensionless diffusion profiles around a growing particle. Parameter A is the particle growth rate $r_0(dr_0/dt)$ nondimensionalized by mass diffusivity $\mathcal{D}$ to express $F(y) = (x_{A_\infty} - x_A(y))/(x_{A_\infty} - x_{A_0})$ or by thermal diffusivity α to express $F(y) = (T(y) - T_\infty)/(T_0 - T_\infty)$.

$$x_A(y) = x_{Ab}\left[\frac{r_a}{r_a - r_0}\right]\left(1 - \frac{1}{y}\right) + x_{A_0}\left[\frac{r_a}{r_a - r_0}\right]\left(\frac{1}{y} - \frac{r_0}{r_a}\right), \quad [66]$$

$$T(y) = T_b\left[\frac{r_a}{r_a - r_0}\right]\left(1 - \frac{1}{y}\right) + T_0\left[\frac{r_a}{r_a - r_0}\right]\left(\frac{1}{y} - \frac{r_0}{r_a}\right), \quad [67]$$

where $y = r/r_0$ and $1 \le y \le r_a/r_0$. The background conditions change with time according to restrictions based on overall mass and energy conservation. With no loss of generality, we can assume that the initial volume fraction of aerosol is zero. For any time later during the aerosol growth, we can write the monomer component mass balance averaged over a volume containing a representative sample of growing particles. The initial mole fraction of monomer x_{A_∞} is set equal to the sum of the average vapor mole fraction calculated over the whole aerosol distribution and the effective mole fraction of monomer in the condensed phase,

$$x_{A_\infty} = \int_0^\infty \left[3\int_0^{r_a/r_0} x_A(y)y^2dy\right] \times vn_v(v)dv + \phi\frac{c_d}{c}. \quad [68]$$

Similarly the latent heat generated per unit volume of gas by vapor condensation is equal to the average increase in the thermal energy of the system. Neglecting the thermal mass of the particles,

$$\Delta H_v\phi\frac{c_d}{c} = M_B C_p \int_0^\infty \left[3\int_0^{r_a/r_0} [T(y) - T_\infty]y^2dy\right] \times vn_v(v)dv. \quad [69]$$

If we define the final aerosol volume fraction after the vapor condenses to form aerosol as

$$\phi_f = \frac{c}{c_d}(x_{A_\infty} - x_{A_0}) \quad [70]$$

then Eqs. [68] and [69] become

$$x_A = \int_0^\infty \left[3\int_0^{r_a/r_0} x_A(y)y^2dy\right] \times vn_v(v)dv + (x_{A_\infty} - x_{A_0})\frac{\phi}{\phi_f}, \quad [71]$$

$$T_\infty = \int_0^\infty \left[3\int_0^{r_a/r_0} T(y)y^2dy\right]vn_v(v)dv - \left(\frac{\Delta H_v}{R}\right)\left(\frac{R}{M_B C_p}\right)(x_{A_\infty} - x_{A_0})\frac{\phi}{\phi_f}. \quad [72]$$

Employing Eq. [8] for the averaging volumes, we get

$$x_A = x_{A_0} + (x_{A_\infty} - x_{A_0})\left[\frac{1 - \phi/\phi_f}{1 - (3/2)\phi^{1/3}}\right]\left(1 - \frac{1}{y}\right), \quad [73]$$

$$T(y) = T_0 - \left[\frac{T_0 - T_\infty}{1 - (3/2)\phi^{1/3}} - \left(\frac{\Delta H_v}{R}\right)\left(\frac{R}{M_B C_p}\right) \times \frac{x_{A_\infty} - x_{A_0}}{1 - (3/2)\phi^{1/3}}\left(\frac{\phi}{\phi_f}\right)\right]\left(1 - \frac{1}{y}\right). \quad [74]$$

An additional restriction comes from the particle energy balance, Eq. [15], determining the surface temperature of the particle, T_0. The form of the energy balance for dilute vapor is

$$-\left.\frac{\partial T}{\partial y}\right|_{y=1} = \left(\frac{\Delta H_v}{R}\right)\left(\frac{R}{M_B C_p}\right)\mathrm{Le}^{-1}\left.\frac{\partial x_A}{\partial y}\right|_{y=1}. \quad [75]$$

Evaluation of the surface gradients from Eqs. [73] and [74] yields

$$T_0 - T_\infty = \left(\frac{\Delta H_v}{R}\right)\left(\frac{R}{M_B C_p}\right)\mathrm{Le}^{-1} \times (x_{A_\infty} - x_{A_0})\left[1 + (\mathrm{Le} - 1)\frac{\phi}{\phi_f}\right]. \quad [76]$$

Equation [74] for temperature now becomes

$$T(y) = T_\infty + \left(\frac{\Delta H_v}{R}\right)\left(\frac{R}{M_B C_p}\right) \times \mathrm{Le}^{-1}(x_{A_\infty} - x_{A_0})\left\{1 + (\mathrm{Le} - 1)\frac{\phi}{\phi_f} - \left(\frac{1 - \phi/\phi_f}{1 - (3/2)\phi^{1/3}}\right)\left(1 - \frac{1}{y}\right)\right\} . \quad [77]$$

As the volume fraction ϕ approaches ϕ_f, Eq. [77] predicts a spatially uniform maximum gas temperature attained from latent heat release,

$$T_{max} = T_\infty + \left(\frac{\Delta H_v}{R}\right)\left(\frac{R}{M_B C_p}\right)(x_{A_\infty} - x_{A_0}). \quad [78]$$

We can now write expressions for the rescaled mole fraction and temperature analogous to Eqs. [58] and [59],

$$X(y) = 1 - \Delta_x\left\{1 - \left[\frac{1 - \phi/\phi_f}{1 - (3/2)\phi^{1/3}}\right]\left(1 - \frac{1}{y}\right)\right\} , \quad [79]$$

$$\Gamma(y) = 1 + \Delta_T\left\{1 + (\mathrm{Le} - 1)\frac{\phi}{\phi_f} - \left[\frac{1 - \phi/\phi_f}{1 - (3/2)\phi^{1/3}}\right]\left(1 - \frac{1}{y}\right)\right\} , \quad [80]$$

where

$$\Delta_x \equiv \frac{x_{A_\infty} - x_{A_0}}{x_{A_\infty}} ,$$

and

$$\Delta_T \equiv \left(\frac{\Delta H_v}{RT_\infty}\right)\left(\frac{R}{M_B C_p}\right)\mathrm{Le}^{-1}(x_{A_\infty} - x_{A_0}).$$

Throughout Eqs. [64]–[80] the quantities x_{A_∞} and T_∞ refer to the initial background conditions at the time the aerosol growth begins, while x_{A_0} and T_0 are related at all times by the energy balance, Eq. [76], and by thermodynamics, Eq. [26]. Equation [61] still expresses the saturation ratio, where S_∞ is understood to represent the initial background conditions. We see that the time dependence of the diffusion profiles above enters through the aerosol volume fraction, as well as the normalized radial coordinate, $y = r/r_0(t)$. Note also that for this phase of the aerosol growth process, the particle growth rate expression, Eq. [19], is generalized to

$$r_0\frac{dr_0}{dt} = \frac{c\mathscr{D}}{c_d}\left.\frac{\partial x_A}{\partial y}\right|_{y=1} = \frac{c\mathscr{D}}{c_d}(x_A - x_{A_0})\left[\frac{1 - \phi/\phi_f}{1 - (3/2)\phi^{1/3}}\right] . \quad [81]$$

4. CALCULATION OF THE AVERAGE NUCLEATION RATE

In order to combine the results of Sections 2 and 3, we need to employ the elementary theory of homogeneous nucleation for an expression for the nucleation rate (7),

$$J = \frac{2P_A}{(2\pi m k_B T)^{1/2}}\left(\frac{P_A V_m^{2/3}}{k_B T}\right)\left(\frac{\sigma V_m^{2/3}}{k_B T}\right)^{1/2} \times \exp\left[-\frac{16\pi\sigma^3 V_m^2}{3(k_B T)^3(\ln S)^2}\right] . \quad [82]$$

Early in the aerosol growth process, the relative change of nucleation rate from some point y near a particle to the region outside its influence is given by

$$\frac{-\Delta J(y)}{J_\infty} = 1 - \left(\frac{X(y)}{\Gamma(y)}\right)^2 \times \exp\left\{-\frac{16\pi}{3(\ln S_\infty)^2}\left(\frac{\sigma V_m^{2/3}}{k_B T_\infty}\right)^3 \times \left(\Gamma(y)^{-3}\left[\frac{\ln S_\infty}{\ln S(y)}\right]^2 - 1\right)\right\} . \quad [83]$$

This quantity does not rely on the accuracy of the nucleation rate expression, only on the form of that expression. Applied to stable, growing particles, this relation is a function only of y, and not of time or particle size. Therefore, when Eq. [83] is integrated in Eq. [5], ρ^3 is independent of particle size. The expression for average nucleation rate, Eq. [6], then simplifies to

$$\bar{J} = J_\infty(1 - \rho^3\phi). \qquad [84]$$

The assumption made in Section 3 that the particle clearance volume is proportional to the particle volume is verified.

We find that ρ^3 is a function only of T_∞, x_{A_∞}, $x_A^{sat}(T_\infty)$, c/c_d, Le, $\sigma V_m^{2/3}$, $\Delta H_v/R$, $R/M_B C_p$, and M_A/M_B. The first two parameters are dependent on the conditions causing nucleation, and the remaining parameters are material properties. Since typically $x_{A_\infty} \gg x_A^{sat}(T_\infty)$, the dependence of ρ^3 on x_A^{sat} is very weak. Also, the dependence of ρ^3 on M_A/M_B is very weak when Stefan flow is negligible.

Late in the growth process, the diffusion profiles of Eqs. [79] and [80] are functions not only of y, but also of the aerosol volume fraction ϕ. Therefore the integrand of Eq. [4] and ρ^3 itself will be functions of the aerosol volume fraction, and of the final aerosol volume fraction, ϕ_f. The average nucleation rate is then calculated by Eq. [6].

In the next section, we calculate the clearance volume for dibutyl phthalate only for the initial phase of aerosol nucleation and growth, while ρ^3 is a function only of T_∞ and x_{A_∞}, and not a function of the aerosol distribution. We will then use the initial clearance volume to develop the criterion presented in Eq. [9] for significant quenching of the homogeneous nucleation process.

5. CLEARANCE VOLUME FOR DIBUTYL PHTHALATE

Sample calculations for ρ^3 have been carried out for dibutyl phthalate (bp 340°C) in air for a range of values of T_∞ and x_{A_∞}. Dibutyl phthalate was chosen for sample calculations due to its application in aerosol studies (8). For most practical conditions, ρ^3 was found to be weakly dependent on T_∞ because the long range effect of monomer depletion dominated the difference function of Eq. [83]. The parameters used in the calculation are

$$c/c_d = 0.011, \quad \Delta H_v/R = 8930°K,$$

$$\text{Le} = 4.2, \quad R/M_B C_p = 0.274,$$

$$\sigma V_m^{2/3} = 2.18 \times 10^{-13} \text{ ergs}, \quad M_A/M_B = 9.61.$$

Figure 2 shows the dimensionless clearance volume ρ^3 as a function of initial monomer partial pressure for $T_\infty = 25°C$. The range of dibutyl phthalate partial pressure shown corresponds to saturation pressure in the temperature range 120–160°C. Some values of the intrinsic nucleation rate are indicated, ranging from 10^2 to 10^{10} cm^{-3} sec^{-1}. We see that the dimensionless clearance volume varies over an order of magnitude. The observed variation of the clearance volume is mostly due to the variation of the dimensionless particle growth rate, A, over the range of monomer partial pressure. At high partial pressure, the particle growth rate is high, and the extent of the transient monomer concentration profile remains small, resulting in low clearance volume. At low partial pressure, low growth rate results, and the influence of the particle on the monomer depletion extends farther, exhibiting a high clearance volume. The variation of the clearance volume with partial pressure is also dependent on the sensitivity of the homogeneous nucleation rate, Eq. [82], to the local changes of vapor concentration near a particle.

To construct a meaningful picture of the dependence of ρ^3 on monomer partial pressure and its consequences, we can rearrange the expression for the average nucleation rate, Eq. [84], to get

$$\frac{\bar{J}}{J_\infty} = 1 - (\rho^3\phi_f)\frac{\phi}{\phi_f}, \qquad [85]$$

where ϕ_f is the final aerosol volume fraction if all available monomer vapor grows to form aerosol and is related to the initial mole fraction by Eq. [70]. Note that under practical conditions of $x_{A_0} \ll x_{A_\infty} \ll 1$, the final aerosol volume fraction is related to the dimensionless growth rate parameter by

$$\phi_f \equiv 2A. \qquad [86]$$

The criterion for significant overlap of the clearance volumes of neighboring particles, Eq. [9], can be interpreted as a homogeneous nucleation quenching condition and expressed as

$$\frac{\phi}{\phi_f} \cong (\rho^3\phi_f)^{-1}. \qquad [87]$$

Physically, $(\rho^3\phi_f)^{-1}$ is the fraction of monomer vapor condensed into aerosol at the time that the homogeneous nucleation rate quenches. The function $(\rho^3\phi_f)^{-1}$ for dibutyl phthalate is shown in Fig. 3 with isopleths of homogeneous nucleation rate, and we see its variation with partial pressure and temperature is relatively minor. The region of Fig. 3 corresponding to conditions causing an intrinsic homogeneous nucleation rate of up to 10^6 cm^{-3} sec^{-1} indicates a fairly constant value of $(\rho^3\phi_f)^{-1}$ at about 5 to 9%. Conditions for $(\rho^3\phi_f)^{-1}$ in excess of 10% can be reached only in systems having a characteristic cooling time short enough such that the system attains the given temperature before the aerosol volume fraction grows to the limit for homogeneous nucleation quenching.

6. DISCUSSION

Because the analysis is based on continuum transport theory, the results are exact for systems in which the critical nucleus size is large compared to the mean free path of the gas, such as high-molecular-weight organics. Even if the critical nucleus size is outside of the continuum regime, the present results are expected to be accurate as long as the particle grows into the continuum size regime. For a system in which particles never grow into the continuum size regime, an extension of this work to the free molecule or transition regime is required. A model for particle growth applicable to an ensemble of particles smaller than the mean free path of the surrounding gas has been given by other authors (9–11).

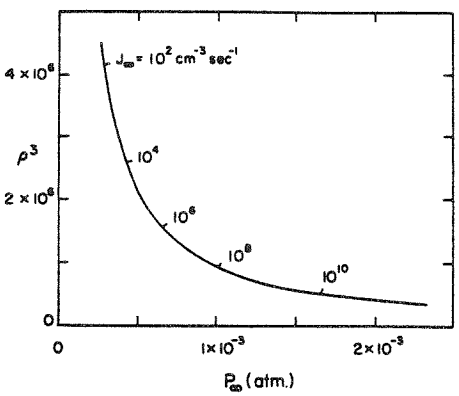

FIG. 2. Dimensionless clearance volume for dibutyl phthalate in air at 25°C. The intrinsic nucleation rate J_∞ is indicated for the range of monomer partial pressure given.

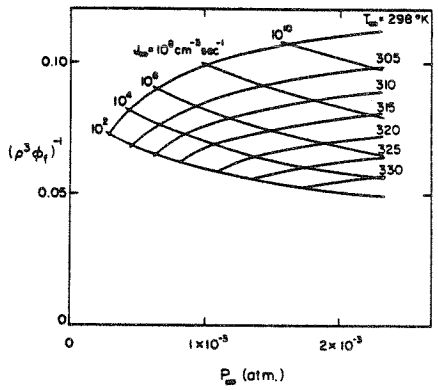

FIG. 3. Fraction of dibutyl phthalate vapor condensed into aerosol at time of homogeneous nucleation quenching. The intrinsic nucleation rate J_∞ is indicated for the range of temperature and monomer partial pressure given.

From the continuum theory, we have found that homogeneous nucleation occurs initially at the intrinsic rate corrected by an amount proportional to the aerosol volume fraction at any instant. As the fraction of condensed monomer vapor approaches a critical level, the homogeneous nucleation rate drops significantly below the intrinsic rate. The subsequent phase of aerosol growth and coagulation is not expected to be influenced by a significant rate of formation of new particles relative to the initial rate. The critical fraction of condensed monomer is only weakly dependent on the amount of vapor initially present or on the

temperature achieved at the time of aerosol formation. This critical fraction is 5 to 9% for dibutyl phthalate in air and is in general a function of the monomer/carrier-gas system.

Preliminary calculations for a self-nucleated growing dibutyl phthalate aerosol in a LaMer generator suggest that the conditions at Eq. [87] are reached at about the same time that coagulation becomes significant. Thus a growing self-nucleated aerosol appears to evolve through three stages of description: An initial phase of homogeneous nucleation and growth, a transition when homogeneous nucleation slows significantly and coagulation begins to occur, and the final phase of growth with coagulation. Dobbins (12) presents an interpretation of such "nucleation pulses" from which the nucleation rate may be calculated from detailed temperature and pressure histories, and total particle concentration produced by the pulse. His semi-theoretical model is applied to cloud chambers in which the dominant nucleation cutoff mechanism is latent heat release, and the background vapor concentration is constant and known through the duration of the nucleation pulse. The present model allows calculation of nucleation rate when either or both nucleation cutoff mechanisms, monomer depletion and latent heating, are important.

For a vapor cooled to supersaturation in the presence of foreign nuclei, the growth process may reach the quenching condition of Eq. [87] before sufficient supersaturation occurs to produce a significant number of new particles. Such conditions are ensured by choosing condensable monomer, carrier gas, initial concentration and cooling conditions, in order to minimize $(\rho^3\phi_t)^{-1}$ and maintain nucleation at a minimum rate and quenched as early as possible.

APPENDIX: NOTATION

A	Dimensionless growth rate parameter defined by Eq. [39]
B	Parameter defined in Eq. [40]
c	Total molar concentration of gas, mole cm^{-3}
c_A	Molar concentration of monomer vapor, cx_A, mole cm^{-3}
c_d	Molar concentration of particle, mole cm^{-3}
C_p	Specific heat of gas at constant pressure, cal g^{-1} °K^{-1}
$\mathcal{D}$	Diffusivity of monomer in gas, cm^2 sec^{-1}
F	Function defined by Eq. [51]
ΔH_v	Latent heat of vaporization of monomer, cal mole^{-1}
J_∞	Intrinsic nucleation rate far from particle, cm^{-3} sec^{-1}
$\bar{J}$	Average nucleation rate, cm^{-3} sec^{-1}
k_B	Boltzmann's constant, 1.38×10^{-16} erg °K^{-1}
k_T	Thermal conductivity of gas, cal sec^{-1} cm^{-1} °K^{-1}
Le	Lewis number, $\alpha/\mathcal{D}$
M	Molecular weight, g mole^{-1}
n_v	Aerosol number distribution in particle volume, cm^{-6}
P_∞	Partial pressure of monomer far from particle, atm
r	Radial coordinate measured from particle center, cm
r^*	Radius of particle of critical size, cm
r_a	Radius of averaging volume, cm
r_0	Radius of particle, cm
R	Gas law constant, 1.987 cal mol^{-1} °K^{-1}
S	Saturation ratio
t	Time, sec
T	Temperature, °K
v	Particle volume variable, cm^3
v^*	Volume of particle of critical size, cm^3
V_m	Molecular volume of monomer, cm^3
V_r	Radial velocity, cm sec^{-1}
x_A	Mole fraction of monomer in gas
X	Rescaled mole fraction of monomer defined by Eq. [58]
y	Dimensionless radial coordinate, $r/r_0(t)$

α	Thermal diffusivity of gas, $k_T/\rho_g C_p$, $cm^2\ sec^{-1}$
Γ	Dimensionless temperature defined by Eq. [59]
Δ_T	Temperature difference, $T_0 - T_\infty/T_\infty$
Δ_x	Mole fraction difference, $x_{A_\infty} - x_{A_0}/x_{A_\infty}$
θ	Dimensionless time defined by Eq. [41]
ρ	Dimensionless radius of the clearance volume
ρ_g	Gas density, $g\ cm^{-3}$
σ	Surface tension of condensed monomer, $erg\ cm^{-2}$
ϕ	Aerosol volume fraction
ϕ_f	Final aerosol volume fraction

Superscripts and Subscripts

sat	Saturation
*	Molar average
A	Monomer
B	Carrier gas
b	Background
0	Particle surface
∞	Far from particle

ACKNOWLEDGMENT

This work was supported by National Science Foundation Grant PFR76-04179.

REFERENCES

1. Springer, G. S., *in* "Advances in Heat Transfer" (T. F. Irvine and J. P. Hartnett, Eds.), Vol. 14, pp. 281–346. Academic Press, New York, 1978.
2. Bird, R. B., Stewart, W. E., and Lightfoot, E. N., "Transport Phenomena." Wiley, New York, 1960.
3. Ham, F. S., *Phys. Chem. Solids* **6**, 335 (1958).
4. Vrentas, J. S., and Shin, D., *Chem. Eng. Sci.* **35**, 1687 (1980).
5. Reiss, H., *J. Chem. Phys.* **19**, 482 (1951).
6. Reiss, H., Patel, J. R., and Jackson, K. A., *J. Appl. Phys.* **48**, 5274 (1977).
7. Friedlander, S. K., "Smoke, Dust and Haze." Wiley, New York, 1977.
8. LaMer, V. K., Inn, E. C. Y., and Wilson, I. B., *J. Colloid Interface Sci.* **5**, 471 (1950).
9. Frisch, H. L., and Collins, F. C., *J. Chem. Phys.* **20**, 1797 (1952).
10. Collins, F. C., and Frisch, H. L., *J. Chem. Phys.* **21**, 1116 (1953).
11. Frisch, H. L., and Collins, F. C., *J. Chem. Phys.* **21**, 2158 (1953).
12. Dobbins, R. A., and Eklund, T. I., *Aerosol Sci.* **5**, 497 (1974).

SYMBOLS USED

c	Total molar concentration of gas, mole cm^{-3}
c_d	Molar concentration of particle, mole cm^{-3}
c^*	Nucleation function defined by Eq. [40], sec^{-1}
$\bar{c}_i$	Mean molecular speed of species i, cm sec^{-1}
C_p	Specific heat of gas at constant pressure, cal g^{-1} $°K^{-1}$
D	Diffusivity of monomer in gas, cm^2 sec^{-1}
d_p	Particle diameter, μm
d_p^t	Particle diameter at Kelvin effect transition, μm
E_i	Evaporation coefficient
f	Distribution function defined by Eq. [45]
F	Fuchs-Sutugin growth law function
g	Gravitational acceleration, 980 cm sec^{-2}
G	Green's function
G_1, G_2	Finite-difference Green's functions
h	Planck's constant, 6.62×10^{-27} erg sec
ΔH_v	Latent heat of vaporization of monomer, cal $mole^{-1}$
I	Growth law function, dv'/dt', μm^3 sec^{-1}
J'	Nucleation rate function, cm^{-3} sec^{-1}
J	Dimensionless nucleation rate, $\frac{\gamma R^5}{D} J'$
ΔJ	Nucleation rate deviation, $J_\infty - J$, cm^{-3} sec^{-1}
J_m	Mass flux to particle, g cm^{-2} sec^{-1}
J_k	Mass flux obtained from kinetic limit, Eq. [D.3], g $cm^{-2} sec^{-1}$
k	Boltzmann's constant, 1.38×10^{-16} erg $°K^{-1}$
K	Particle coagulation rate constant, cm^3 sec^{-1}
Kn	Knudsen number, $2\lambda/d_p$

Le	Lewis number, α/D
M_A	Molecular weight of species A, g $mole^{-1}$
n'	Aerosol number distribution in particle volume, μm^{-3} cm^{-3}
n	Dimensionless aerosol number distribution, $\gamma\lambda^3 R^3 n'$
$\hat{n}_A$	Number density of gaseous species A, cm^{-3}
N'	Total aerosol number concentration, cm^{-3}
N	Dimensionless total aerosol number concentration, $\gamma R^3 N'$
N*	Nucleation function defined by Eq. [40], cm^{-3}
N_r	Summation limit in radial discretization
N_z	Summation limit in axial discretization
p'	Total gas pressure, g cm^{-1} sec^{-2}
p	Dimensionless gas pressure, $(p'-p'_o)/\rho_g \bar{v}^2$
Pe	Péclet number, $2R\bar{v}/D$
r'	Radial coordinate in tube, cm
r	Dimensionless radial coordinate in tube, r'/R
Δr	Radial discretization step size
R	Radius of tube, cm
Re	Reynolds number, $2R\rho_g \bar{v}/\mu$
S	Saturation ratio, x/x^{sat}
S_v	Vapor sink function, sec^{-1}
t'	Time, sec
t	Dimensionless time, Dt'/R^2
T'	Temperature, °K
T	Dimensionless temperature, $(T'-T'_{w_f})/(T'_o-T'_{w_f})$
U	Unit step function
v'	Particle volume variable, μm^3

v	Dimensionless particle volume, v'/λ^3
v'^*	Volume of particle of critical size, μm^3
v^*	Dimensionless volume of particle of critical size, v'^*/λ^3
$\bar{v}$	Average axial velocity, cm sec^{-1}
v_z	Axial velocity, cm sec^{-1}
$v(r)$	Dimensionless axial velocity, $v_z/\bar{v}$
V_ℓ	Volume of monomer molecule in liquid, cm^3
x	Mole fraction of monomer in gas
$\dot{X}$	Rescaled mole fraction, $(x-x_{w_f})/(x_o-x_{w_f})$
z'	Axial coordinate, cm
z	Dimensionless axial coordinate, $z'/(R\ Pe)$
$\hat{z}$	Axial position of particle nucleation, defined by Eq. [27]
Δz	Axial discretization step size
Z	Molecular weight ratio, M_i/M_j
α	Thermal diffusivity of gas, $cm^2\ sec^{-1}$
β	Latent heating parameter, $\frac{\Delta H_v}{C_p}\left(\frac{x_o-x_{w_f}}{T'_o-T'_{w_f}}\right)$
β_e	Function of evaporation coefficient, Appendix D.
γ	Length scaling parameter, λ/R
δ	Dirac delta function
δ_{ij}	Kronecker delta function
ζ	Axial coordinate
ζ_c	Sticking coefficient
θ	Growth law function defined by Eq. [16]
κ	Nucleation function defined by Eq. [40]

λ Mean free path of monomer, defined in Appendix D, μm

Λ Time scaling parameter, $(c/c_d)(x_o-x_{w_f})\gamma^{-2}$

μ Viscosity of gas, g cm^{-1} sec^{-1}

ν Growth law function defined by Eq. [16]

ξ Radial coordinate around particle

ρ Radial coordinate in tube

ρ_g Mass density of gas, g cm^{-3}

ρ_ℓ Mass density of liquid phase, g cm^{-3}

σ Surface tension, g sec^{-2}

σ_A Lennard-Jones collision diameter, Å

ϕ' Aerosol volume fraction, μm^3 cm^{-3}

ϕ Dimensionless aerosol volume fraction, $\gamma\lambda^{-3}R^3\phi'$

$\hat{\phi}$ Dimensionless aerosol volume fraction, $10^{-12}\phi'$ cm^3 μm^{-3}

ϕ Dimensionless vapor sink function, $\frac{R^2}{D}\frac{S_v}{x_o-x_{w_f}}$

ψ Eigenfunction defined by Eqs. [34]-[36]

$\Omega_{ij}^{(1,1)*}$ Collision integral for molecular diffusion (29)

Superscripts and Subscripts

b	Background
f	Final
FS	Fuchs-Sutugin theory
i,j,m,n	Integer subscripts
LP	Lothe-Pound theory
o	Initial
p	Particle
s	Seed
sat	Saturation
w	Wall
$\overline{\ }$	Average
∞	Far from the particle
*	Value at nucleation or initial seed

REFERENCES

1. McMurry, P. H., Friedlander, S. K., J. Colloid Interface Sci. 64, 248 (1978).

2. McMurry, P. H., J. Colloid Interface Sci. 78, 513 (1980).

3. Gelbard, F. M., Seinfeld, J. H., J. Colloid Interface Sci. 68, 363 (1979).

4. McMurry, P. H., Friedlander, S. K., Atmospheric Environment 13, 1635 (1979).

5. La Mer, V. K., Inn, E. C, Y., and Wilson, I. B., J. Colloid Interface Sci. 5, 471 (1950).

6. Matijević, E., Schulz, K. F., and Kerker, M., J. Colloid Interface Sci. 17, 26 (1962).

7. Matijević, E., Kitani, S., and Kerker, M., J. Colloid Interface Sci. 19, 223 (1964).

8. Okada, T., Ishibashi, H., and Kitani, S., J. Colloid Interface Sci. 29, 613 (1969).

9. Huang, C. M., Kerker, M., Matijević, E., and Cooke, D. D., J. Colloid Interface Sci. 33, 244 (1970).

10. Shahriari, S., Goodrich, F. C., J. Colloid Interface Sci. 39, 312 (1972).

11. Nicolaon,G., Cooke, D. D., Kerker, M., and Matijević, E., J. Colloid Interface Sci. 34, 534 (1970).

12. Nicolaon, G., Cooke, D. D., Davis, E. J., Kerker, M. and Matijević, E., J. Colloid Interface Sci. 35, 490 (1971).

13. Nicolaon, G., Kerker, M., Cooke, D. D., and Matijević, E, J. Colloid Interface Sci. 38, 460 (1972).

14. Nicolaon, G., and Kerker, M., J. Colloid Interface Sci. 43, 246 (1973).

15. Davis, E. J. and Liao, S. C., J. Colloid Interface Sci. 50, 488 (1975).

16. Chang, R., and Davis, E. J., J. Colloid Interface Sci. 54, 352 (1976).

17. Carroz, J. W., Odencrantz, F. K., and Finnegan, W. G., "Generation of Fumes Simulating Particle Air Pollutants." EPA-600/2-77-132, July 1977.

18. Springer, G. S., in "Advances in Heat Transfer" (T. F. Irvine and J. P. Hartnett, Eds.), Vol. 14, pp. 281-346. Academic Press, New York 1978.

19. Pesthy, A. J., Flagan, R. C., and Seinfeld, J. H., J. Colloid Interface Sci. 82, 465 (1981).

20. Davis, E. J., Ravindran, P., and Ray, A. K., Adv. Colloid Interface Sci. 15, 1 (1981).

21. Ray, A. K., Davis, E. J., and Ravindran, P., J. Chem. Phys. 71, 582 (1979).

22. Rao, A. K., and Whitby, K. T., Am. Ind. Hyg. Assoc. J. 38, 174 (1977).

23. Chatterjee, A., Kerker, M., and Cooke, D. D., J. Colloid Interface Sci. 53, 71 (1975).

24. Gardner, G. S., and Brewer, J. E., Ind. Eng. Chem. 29, 179 (1937).

25. Friedlander, S. K., "Smoke, Dust and Haze." Wiley, New York, 1977.

26. Davis, E. J. and Ray, A. K., J. Aerosol Sci. 9, 411 (1978).

27. Davis, E. J., Ravindran, P., and Ray, A. K., Chem. Eng. Commun. 5, 251 (1980).

28. Jeans, J., "The Dynamical Theory of Gases." Dover Publications, New York, 1954.

29. Hirschfelder, J. O., Curtiss, C. F., and Bird, R. B., "Molecular Theory of Gases and Liquids." Wiley, New York, 1964.